The Role of CtIP in BRCA1-Mediated Tumor Suppression

Colleen R. Reczek

Submitted in partial fulfillment of the requirements for

the degree of Doctor of Philosophy under the

Executive Committee of the Graduate School of Arts and Sciences

COLUMBIA UNIVERSITY

2012

ABSTRACT

The Role of CtIP in BRCA1-Mediated Tumor Suppression

Colleen R. Reczek

Familial cases of breast and ovarian cancer are often attributed to germline mutations of the BRCA1 tumor suppressor gene. Although the mechanisms of *BRCA1* tumor suppression are poorly understood, its protein product has been implicated in multiple aspects of the DNA damage response. As such, BRCA1 may suppress tumor development through its role in the maintenance of genomic integrity. The C-terminus of BRCA1 contains two tandem BRCT motifs that form a single phosphoprotein binding motif that mediates the interaction of BRCA1 with at least three distinct phospho-ligands; Abraxas, BACH1, and CtIP. We recently reported that the tumor suppression activity of BRCA1 is dependent on the phospho-recognition function of its BRCT motifs. Of the three known phospho-ligands, the CtIP repair protein is intriguing because its interaction with BRCA1 is ablated by tumor-associated missense mutations in the BRCT domain. Accordingly, CtIP may be a critical mediator of the genome maintenance and tumor suppression functions of BRCA1. Here we evaluate the role of CtIP in these BRCA1-dependent processes using murine cells expressing Ctip polypeptides (Ctip-S326A) that fail to interact with Brca1. Surprisingly, we demonstrate that the BRCA1-CtIP interaction is dispensable for mammalian cell viability, critical aspects of BRCA1 function in genome stability, and BRCA1-mediated tumor suppression.

Given that CtIP plays a diverse role in maintaining genome integrity, we also assessed whether CtIP has functions relevant to tumor suppression independent of its interaction with BRCA1. To test this hypothesis, we generated mice carrying a conditional-null Ctip (*Ctip*^{Co}) allele and used Cre recombination to inactivate the gene specifically in mammary epithelial cells. Unexpectedly, we found that mammary-specific inactivation of Ctip does not induce breast carcinogenesis. Additionally, when we examined the effects of mammary-specific Ctip loss in a tumor-prone setting, we found that p53-deficient mammary tumorigenesis was dramatically inhibited by Ctip inactivation. This result indicates not only that Ctip inactivation fails to potentiate p53-induced mammary tumor formation, but that Ctip loss actually provides a protective effect against tumorigenesis in this setting.

Furthermore, since we recently demonstrated that the genome maintenance and tumor suppression functions of BRCA1 do not depend on its individual interaction with the BRCT phospho-ligands Abraxas, BACH1, or CtIP, we examined whether the interaction of BRCA1 with two or more of these phospho-ligands mediates these functions. Strikingly, the genome maintenance functions of BRCA1 are grossly perturbed only when the interaction of BRCA1 with its three known BRCT phospho-ligands are simultaneously ablated. Thus, the major BRCA1 supercomplexes assembled from these interactions (complexes A, B, and C) have the potential to act in a compensatory manner with respect to one another. In light of these results, it will be important to ascertain whether tumor suppression is dependent on BRCA1 association with these three known BRCT phospho-ligands.

LIST OF TABLES AND FIGURES

CHAPTER I

INTRODUCTION

A. BRCA1 in hereditary breast cancer

Breast cancer is among the most common malignancies in the United States, affecting more than one in eight women. Moreover, women with a family history of breast cancer are at an increased (2-fold) risk of developing the disease. These women often carry inherited mutations in the breast cancer susceptibility genes *BRCA1* or *BRCA2*. Women with a mutated allele of either *BRCA1* or *BRCA2* face a lifetime risk of 60-85% for breast cancer, as well as an overall increased risk for ovarian cancer (Wooster and Weber, 2003). The tumors that arise in women with germline *BRCA1* or *BRCA2* mutations show loss or mutation of the corresponding wildtype allele, thus rendering both copies of the gene nonfunctional. Therefore, *BRCA1* and *BRCA2* behave as classic tumor suppressor genes in accord with Knudson's "two-hit" model (Knudson, 1971).

In its role as a tumor suppressor, BRCA1 behaves as a caretaker that maintains the integrity of the genome. Its protein product has been implicated in a rather diverse set of cellular processes that include ubiquitination, cell cycle checkpoint control, DNA repair, centrosome duplication, and transcriptional regulation (reviewed in Deng, C.-X., 2006; Nagaraju and Scully, 2007; Greenberg, R. A., 2008; Huen et al., 2010; Moynahan and Jasin, 2010; Roy et al., 2011). Although the exact mechanism of tumor suppression by BRCA1 remains elusive, it is conceivable that loss of BRCA1 destabilizes the genome, triggering mutations in other tumor suppressors and oncogenes, ultimately leading to tumor formation (Deng, C.-X., 2001; Simon and Zhang, 2008).

B. The BRCA1 protein

The *BRCA1* gene encodes a large nuclear protein of 1863 amino acids in humans and 1812 amino acids in mice (Miki et al., 1994; Bennett et al., 1995). It contains two recognizable amino acid motifs, an N-terminal RING domain and two tandem copies of the BRCT domain at its C-terminus (Miki et al., 1994) (Figure 1). The RING domain contains a metal-binding core that coordinates two atoms of zinc (Freemont, P.S., 1993). This domain can be found in a large and diverse family of eukaryotic proteins that possess E3 ubiquitin ligase activity (Joazeiro and Weissman, 2000). The BRCA1 carboxy-terminal (BRCT) domain was first identified as an ~80-100 amino acid motif that exists in two tandem copies at the C-terminus of BRCA1; subsequently, this domain was identified in an array of proteins which function in the cellular response to DNA damage (Koonin et al., 1996; Bork et al., 1997; Callebaut, I. and Mornon, J.-P., 1997). The paired BRCT repeats of BRCA1 form a characteristic globular structure that can act as a phosphopeptide binding domain (Manke et al., 2003; Yu et al., 2003). While most cancer-predisposing BRCA1 mutations cause gross truncations that eliminate one or both of the BRCT repeats, single amino acid substitutions in the RING or BRCT domains have also been found in some familial patients (Miyake et al., 2000). Therefore, these domains are critical for the tumor suppression activity of BRCA1.

The steady-state protein levels of BRCA1 fluctuate with the cell cycle. In particular, these levels remain low in resting G_0 cells and early cycling G_1 cells; however, as cells traverse the G_1/S boundary, the expression of BRCA1 increases dramatically and remains high throughout the S and G_2/M phases (Chen et al., 1996). Localization of BRCA1 to discrete nuclear bodies coincides with peak expression, forming what are referred to as

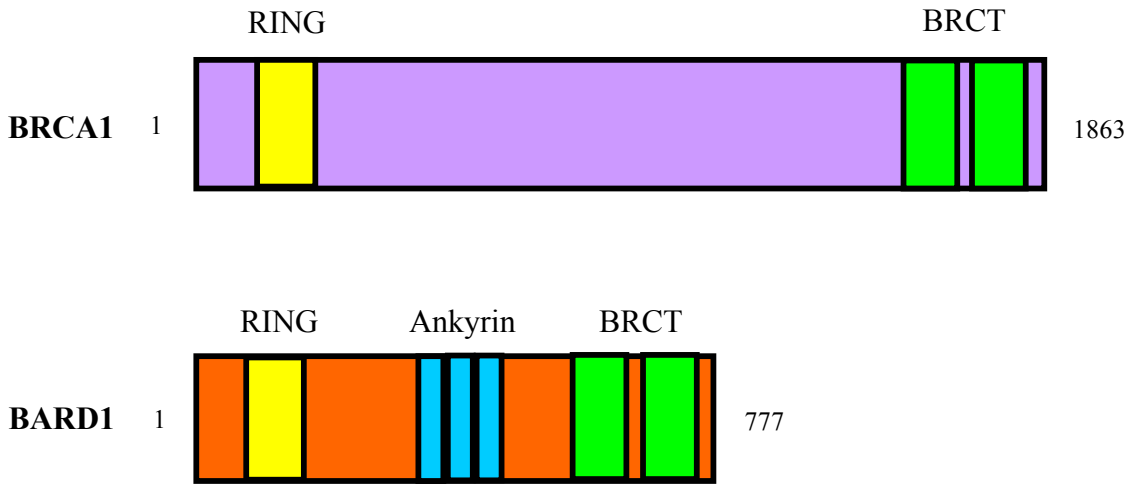

Figure 1. Domain structures of BRCA1 and BARD1. Both proteins harbor an amino-terminal RING domain (yellow) and two carboxy-terminal BRCT repeats (green). In addition, BARD1 contains three tandem ankyrin repeats (blue).

S-phase foci (Scully et al., 1997a). This is in contrast to the diffuse distribution of BRCA1 polypeptides observed throughout the nucleoplasm of resting cells and G_1 cycling cells (Scully et al., 1997a). When cells experience a genotoxic insult, the S-phase BRCA1 foci disperse and BRCA1 polypeptides relocate and accumulate at sites of DNA damage along with other DNA damage response proteins (Scully et al., 1997b). This dynamic change in the localization of BRCA1 in response to DNA damage further supports an important role for BRCA1 in the maintenance of genomic integrity.

C. The functions of BRCA1

The integrity of the genome is maintained in part by BRCA1's broad spectrum of cellular functions. Some of these include cell cycle checkpoint control, DNA repair, and centrosome duplication (reviewed in Deng, C.-X., 2006; Nagaraju and Scully, 2007; Greenberg, R. A., 2008; Huen et al., 2010; Moynahan and Jasin, 2010; Roy et al., 2011). In response to genotoxic stress, cell cycle checkpoints preserve genome integrity by halting cell cycle progression and allowing for proper repair of the damaged DNA. If damage is too extensive, cells may undergo growth arrest and apoptosis. In contrast, if the checkpoint is not functional, then cell cycle progression may proceed in the face of DNA damage, promoting genomic instability and ultimately tumorigenesis (Xu, X. et al., 1999; reviewed in Deng, C.-X., 2006).

BRCA1 has been implicated in a number of cell cycle checkpoints induced by ionizing radiation (IR), including two distinct G_2/M checkpoints: the IR-induced transient G_2/M checkpoint and the IR-induced G_2 accumulation checkpoint (Xu, B. et al., 2002).

These checkpoints prevent cells from entering mitosis with damaged DNA. The transient G_2/M and G_2 accumulation checkpoints are both defective in HCC1937 cells, a human breast cancer line that expresses a C-terminally-truncated BRCA1 polypeptide lacking one of the tandem BRCT motifs. Moreover, both checkpoints can be restored by reconstitution of HCC1937 cells with wild-type BRCA1 (Xu, B. et al., 2001; Yarden et al., 2002; Yu et al., 2003). A defective G_2/M checkpoint has also been observed in *Brca1*$^{\Delta 11/\Delta 11}$ mouse embryonic fibroblasts (MEFs), which carry a targeted deletion of exon 11 (Xu, X. et al., 1999). Therefore, BRCA1, and more specifically, the BRCT domains of BRCA1 are important for proper activation of these cell cycle checkpoints. Interestingly, the checkpoint functions of BRCA1 are determined in part by proteins that bind in a phosphorylation-dependent manner to its BRCT motifs (Yu et al., 2003; Yu and Chen, 2004; reviewed in Huen et al., 2010). For example, the interaction between BRCA1 and a phosphorylated isoform of the BACH1 protein is required for activation of the G_2 accumulation checkpoint (Yu et al., 2003), while the interaction of BRCA1 with phosphorylated CtIP mediates the transient G_2/M checkpoint (Yu and Chen, 2004). The importance of these interactions with respect to the genome stability and tumor suppression functions of BRCA1 will be discussed in more detail later.

BRCA1 also contributes to genome stability through its role in homology-directed repair (HDR) of DNA double-strand breaks (DSBs). Chromosomal DSBs can arise from both endogenous and exogenous threats, including ionizing radiation (IR). Since these DSBs can induce aberrant chromosomal rearrangements and ultimately cell death, proper DSB repair is vital to the integrity of the genome (Moynahan et al., 2001; reviewed in Moynahan and Jasin, 2010). A function for BRCA1 in HDR emerged from early studies

in which BRCA1 was shown to disperse from S-phase foci following DNA damage and re-emerge as IR-induced foci (IRIFs) along with the Rad51 protein, a central component of the HDR pathway (Scully et al., 1997b). Additional evidence suggestive of a role for BRCA1 emerged from studies of genomic stability in various BRCA1-deficient settings. For example, the HCC1937 human breast cancer cell line, expressing a C-terminally truncated form of BRCA1, is aneuploidy and harbors a high number of chromosomal aberrations (Tomlinson et al., 1998). In addition, MEFs derived from *Brca1*$^{\Delta 11/\Delta 11}$ mice exhibit extensive spontaneous chromosomal instability, resulting in aneuploidy, chromosome breaks, and translocations (Xu, X. et al., 1999). Similarly, the Brca1-deficient mouse embryonic stem (ES) cell line 236.44 accumulates high levels of chromosomal rearrangements, even in the absence of overt genotoxic stress (Moynahan et al., 2001). Brca1-deficient cells are also hypersensitive to genotoxic agents, such as IR and DNA-crosslinking drugs, that cause DSB formation, further suggesting a key role for BRCA1 in DSB repair (Shen et al., 1998; Abbott et al., 1999; Moynahan et al., 1999).

Compelling evidence implicating BRCA1 in the HDR pathway of DSB repair arose when Moynahan et al. (1999) used an *in vivo* assay to measure the efficiency of HDR in *Brca1*$^{\Delta 223\text{-}763/\Delta 223\text{-}763}$ ES cells (Brca1-null ES cell line 236.44). Notably, they observed that these cells are unable to efficiently repair an enzymatically-induced chromosomal break by HDR (Moynahan et al., 1999). Moreover, the HDR defect of *Brca1*$^{\Delta 223\text{-}763/\Delta 223\text{-}763}$ ES cells was partially ameliorated following complementation with wild-type Brca1 (Moynahan et al., 2001). These findings specifically implicate BRCA1 in the HDR pathway of DSB repair.

The regulation of centrosome duplication is another potential caretaker function of BRCA1. Mammalian cells normally contain one or two centrosomes depending on the cell cycle phase. In mitosis, the duplicated centrosomes reside at opposite poles to form the vertices of the bipolar spindle, which is critical for proper chromosome segregation. Thus, aberrant replication of centrosomes can result in chromosomal aneuploidy and ultimately lead to tumorigenesis (Deng, C.-X., 2002). The aneuploidy often observed in BRCA1-deficient cells, as mentioned above, suggests a role for BRCA1 in maintaining the fidelity of chromosome segregation. This is supported by the observation that centrosome amplification occurs in approximately 25% of interphase and M phase *Brca1*$^{\Delta 11/\Delta 11}$ MEFs, leading to formation of multipolar spindles and missegregation of chromosomes (Xu, X. et al., 1999). Additionally, abnormal centrosomes and chromosome numbers were reported in high-grade human breast tumors (Lingle et al., 1998; Pihan et al., 1998). These results suggest that dysregulation of centrosome duplication in the absence of BRCA1 may directly contribute to genetic instability in cancer.

D. The BRCA1/BARD1 heterodimer

BRCA1 exerts its pleiotropic functions by interacting with a diverse set of proteins. The BRCA1-associated RING domain protein BARD1 is an obligate binding partner of BRCA1 and a central mediator of BRCA1 function (Wu et al., 1996; reviewed in Baer and Ludwig, 2002; Irminger-Finger and Jefford, 2006; Huen et al., 2010). Like BRCA1, BARD1 contains an N-terminal RING domain and two C-terminal BRCT repeats (Wu et al., 1996). Additionally, BARD1 has three central ankyrin (ANK) repeats, a common

amino acid motif that may serve to mediate protein-protein interactions (Figure 1) (Wu et al., 1996; Mosavi et al., 2004). Most, if not all, of the cellular pool of endogenous BRCA1 polypeptides associates with BARD1 to form the BRCA1/BARD1 heterodimeric complex *in vivo* (Yu and Baer, 2000). This association is mediated by sequences encompassing their respective RING domains (Wu et al., 1996). In particular, the two alpha-helices that flank the RING domains of both proteins combine to form a four-helix bundle, stabilizing the BRCA1/BARD1 heterodimer (Brzovic et al., 2001).

As a heterodimer, BRCA1/BARD1 acts as a potent ubiquitin E3 ligase (Hashizume et al., 2001) that catalyzes the formation of K6-linked polyubiquitin chains, a novel linkage not associated with proteasomal degradation (Wu-Baer et al., 2003; Nishikawa et al., 2004). Tumorigenic missense mutations in the RING domain of BRCA1 inactivate the E3 ligase activity of the heterodimer (Ruffner et al., 2001). Therefore, insight into the molecular underpinnings of BRCA1-mediated tumor suppression may be attained by studying the ubiquitination targets of BRCA1/BARD1 (Baer and Ludwig, 2002). It is important to note that CtIP is a *bona fide* ubiquitination substrate of BRCA1/BARD1 (Yu et al., 2006) and, as will be discussed below, may play a role in BRCA1-mediated tumor suppression.

E. BRCA1/BARD1 in tumor suppression

Mouse models have been employed to examine the role of BRCA1 in tumor suppression. In contrast to human BRCA1 mutation carriers, mice bearing either null or hypomorphic *Brca1* alleles in a heterozygous setting are not susceptible to tumor

formation (reviewed in Deng and Scott, 2000; Evers and Jonkers, 2006). Homozygous *Brca1*-null mice, on the other hand, are embryonic lethal (E6.5-E7.5) and suffer from a severe defect in cellular proliferation (Hakem et al., 1996; Liu et al., 1996; Ludwig et al., 1997; reviewed in Evers and Jonkers, 2006). On the surface, this appears contradictory to the unrestrained cell proliferation associated with BRCA1-mutated cancers. However, close examination revealed increased expression of the cyclin-dependent kinase inhibitor p21 in *Brca1*-null embryos, suggesting that the impaired cellular proliferation could be the result of p53-dependent G_1 cell cycle arrest (Hakem et al., 1996). This notion is supported by the fact that concomitant loss of *Brca1* and *p53* prolongs survival of mutant embryos to ~E8.5-E9.5 (Hakem et al., 1997; Ludwig et al., 1997). In this regard, it is intriguing that most breast tumors of human BRCA1 mutation carriers also harbor somatic mutations of the *p53* gene (Crook et al., 1997).

To circumvent the embryonic lethality associated with Brca1 nullizygosity, mouse models using a conditional *Brca1*-null allele and the Cre-loxP recombination system have been developed to study BRCA1-associated breast cancer (Xu et al., 1999a; Liu, X. et al., 2007; McCarthy et al., 2007; Shakya et al., 2008). Indeed, several groups have shown that mammary-specific loss of Brca1 in mice leads to the development of mammary tumors, albeit with long latency, that closely resemble the basal-like mammary carcinomas that arise in human BRCA1 mutation carriers (McCarthy et al., 2007; Liu, X. et al., 2007; Shakya et al., 2008). These tumors typically display a basal-like histopathology, including positive staining for the cytoskeletal markers CK5 and CK14, and display the "triple-negative" phenotype which reflects lack of expression of the estrogen receptor (ER), progesterone receptor (PR) and HER2/neu surface marker

(McCarthy et al., 2007; Liu, X. et al., 2007; Shakya et al., 2008). Additionally, cells from Brca1-mutant mammary tumors display extensive chromosomal instability characterized by aneuploidy and elevated levels of gross chromosomal rearrangements (Xu et al., 1999a; Shakya et al., 2008). Presumably, the genomic instability that results from Brca1 loss triggers genetic alterations in other genes that eventually lead to tumor formation. To ascertain whether p53 mutations represent one of the genetic changes that promote BRCA1-associated tumorigenesis, Brca1 conditional mice were bred to have only one functional copy of p53 (Donehower et al., 1992; Xu et al., 1999a). If p53 deficiency does promote BRCA1 tumorigenesis, then tumor formation in these mice may be accelerated since only the single wildtype p53 allele needs to be mutated (Xu et al., 1999a; Deng and Scott, 2000). Indeed, Xu et al. (1999a) reported that loss of p53 accelerates the formation of mammary tumors in these mice and thus, Brca1 and p53 cooperate in mammary tumorigenesis.

The study of BRCA1-mediated tumor suppression is greatly facilitated by animal models that accurately recapitulate the responsible genetic lesion(s) and consequent tumor phenotype of human BRCA1-associated carcinogenesis. For example, a mouse model was employed to determine whether the tumor suppression activity of Brca1 is mediated by the Brca1/Bard1 heterodimeric complex or through a Bard1-independent aspect of Brca1 function. Since *Bard1*-null mice suffer an early embryonic death similar to *Brca1*-null animals (McCarthy et al., 2003), tumor suppression was examined in a mammary-specific fashion using a conditional *Bard1*-null allele (Shakya et al., 2008). Significantly, mammary-specific inactivation of *Bard1* induced breast tumors in mice that were indistinguishable from those that arise in conditional *Brca1*-null females in all

measurable respects, including the kinetics of tumor formation, histopathology, and gene expression profiles (Shakya et al., 2008). These results implied that BARD1 itself serves as a tumor suppressor in mammary epithelial cells. Indeed, cancer-predisposing lesions of BARD1, although rare, were subsequently implicated in hereditary breast cancer (De Brakeleer et al., 2010; Sabatier et al., 2010; Ratajska et al., 2012). Furthermore, double conditional *Brca1/Bard1*-mutant mice develop mammary tumors with kinetics that are indistinguishable from those of the single *Brca1*- and *Bard1*-mutant animals (Shakya et al., 2008). The epistatic behavior of the *Brca1* and *Bard1* genes implies that their protein products mediate tumor suppression through a common functional pathway involving the Brca1/Bard1 heterodimer (Shakya et al., 2008).

F. The BRCT domains of BRCA1

Apart from the RING domain, the only other identifiable structural domain of BRCA1 is the C-terminal BRCT motif, which mediates phospho-dependent protein-protein interactions. The BRCT domain is an evolutionarily conserved amino acid motif found in more than forty non-orthologous eukaryotic proteins, either as an isolated domain or as multiple tandem repeats comprised of two or more BRCT units (Bork et al., 1997; Huyton et al., 2000). The two tandem BRCT repeats of BRCA1 fold in a head-to-tail fashion through a large hydrophobic interface with a deep surface cleft (Williams et al., 2001) (Figure 2). Most tumor-associated mutations in BRCA1 result in the partial truncation or complete loss of one or both BRCT motifs (Williams et al., 2003; Wooster and Weber, 2003). For example, the HCC1937 human breast cancer cell line, established

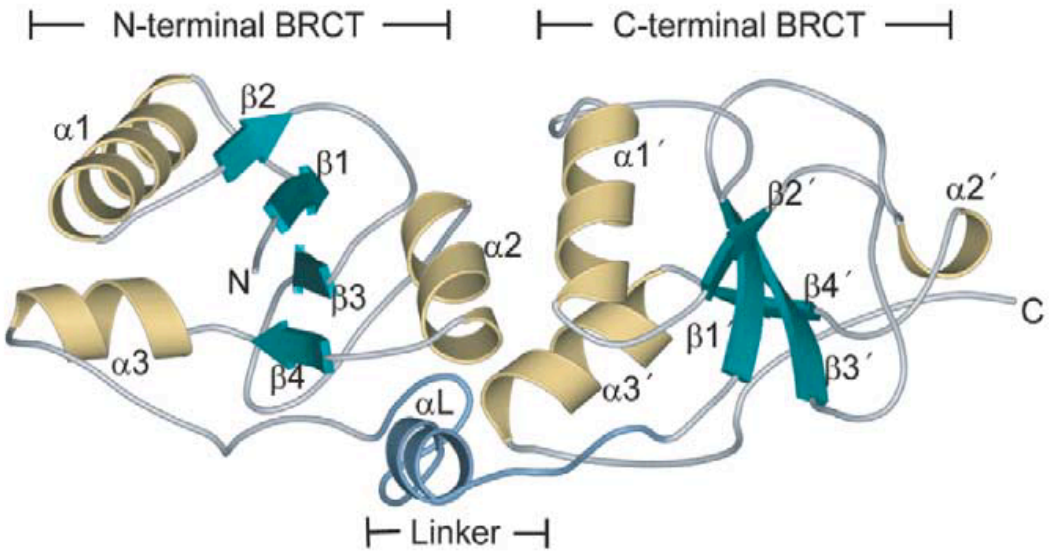

Figure 2. Structure of the tandem BRCT repeats of BRCA1. The N- and C-terminal BRCT repeats of BRCA1 are joined by a linker (αL, blue) and pack in a head-to-tail manner involving a large hydrophobic interface. Each single repeat consists of a parallel four-stranded β-sheet (green), which is flanked on one side by a pair of α-helices (α1 and α3, gold) and on the other side by a single α-helix (α2, gold). In the second BRCT repeat, the corresponding structural elements are indicated by primes (e.g., α1', β1', etc.). (Adapted from Glover et al., 2004)

from a germline BRCA1 mutation carrier, expresses a truncated BRCA1 protein product lacking the C-terminal BRCT domain (Tomlinson et al., 1998). Additionally, mice that express a truncated Brca1 polypeptide lacking both BRCT domains are highly tumor prone (Ludwig et al., 2001). Therefore, the BRCT repeats play an important role in mediating the tumor suppressor function of BRCA1.

Further insight into the function of the BRCT domains emerged with the realization that two tandem BRCT motifs can fold into a globular domain that serves as a phospho-protein interaction surface (Manke et al., 2003; Yu et al., 2003). The tandem BRCT repeats of BRCA1 preferentially recognize a pSer-x-x-Phe motif in partner proteins (Manke et al., 2003; Rodriguez et al., 2003). The phosphoserine (pSer) residue of the phospho-ligand binds to a basic pocket in the N-terminal BRCT repeat while the phenylalanine (Phe) residue fits into a hydrophobic pocket at the N- and C-terminal BRCT interface (Clapperton et al., 2004; Shiozaki et al., 2004; Williams et al., 2004) (Figure 3). Tumor susceptibility in some breast cancer families can be ascribed to missense mutations in conserved residues of the BRCT repeats (e.g. S1655F and M1775R) (Williams et al., 2001). These single amino acid substitutions prevent the interaction of BRCA1 with its BRCT phospho-ligands by perturbing the integrity of either the phosphoserine or phenylalanine binding pockets (Clapperton et al., 2004; Shiozaki et al., 2004; Williams et al., 2004). For example, the serine to phenylalanine mutation at position 1655 (S1655F) disrupts hydrogen bond formation between S1655 of BRCA1 and the pSer residue of the phospho-ligand. Furthermore, the methionine to arginine mutation at position 1775 (M1775R) results in a severe steric clash between the arginine side chain and the Phe (+3) residue of the phospho-ligand (Clapperton et al.,

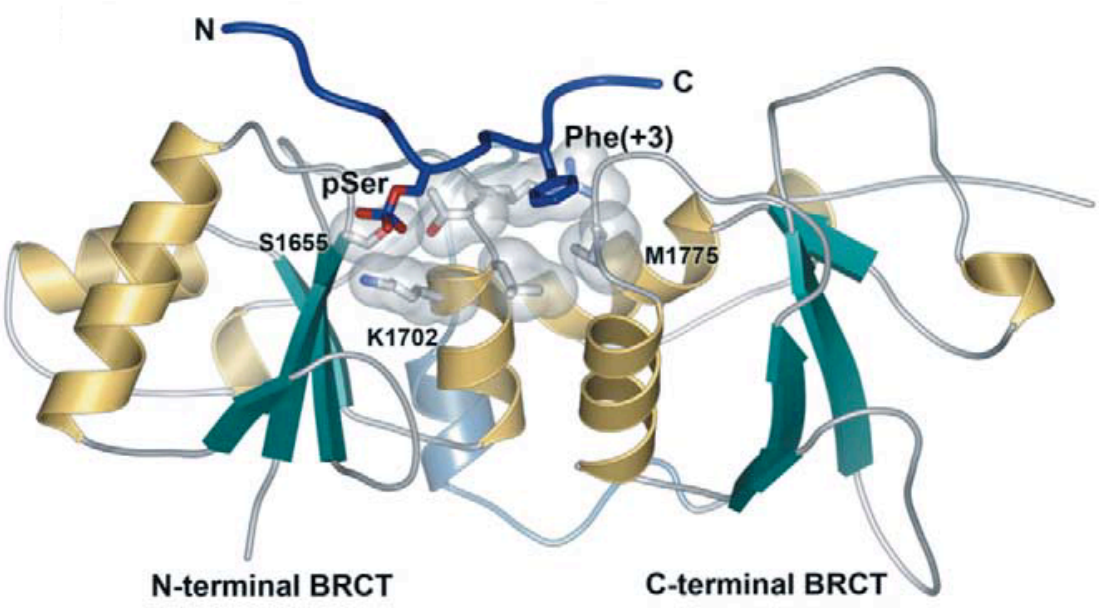

Figure 3. Phosphopeptide recognition by the BRCT repeats of BRCA1. The BRCT repeats of BRCA1 act as a phosphopeptide binding module that preferentially recognizes a pSer-x-x-Phe motif in partner proteins (dark blue). The phosphoserine (pSer) residue binds to a basic pocket in the N-terminal BRCT repeat while the phenylalanine (Phe +3) residue fits into a hydrophobic pocket at the interface between the two repeats. Cancer-associated missense mutations in conserved residues of the BRCT repeats (e.g. S1655F and M1775R) prevent phosphopeptide binding. (Adapted from Glover et al., 2004)

2004; Shiozaki et al., 2004; Williams et al., 2004). Mutations which ablate phosphoprotein recognition by the BRCT repeats of BRCA1 elicit breast tumors, as seen recently in mice bearing the Brca1-S1598F mutation, corresponding to human residue S1655 (Shakya et al., 2011). Thus, the phosphopeptide binding property of the BRCT repeats is essential for BRCA1-mediated tumor suppression.

G. The BRCT-interacting phosphoproteins

The BRCT domains of BRCA1 are known to interact *in vivo* with a number of cellular proteins containing the pSer-x-x-Phe motif, including Abraxas/CCDC98, BACH1/BRIP1/FancJ, CtIP, and Acetyl-CoA carboxylase alpha or ACCA (Wong et al., 1998; Yu et al., 1998; Cantor et al., 2001; Magnard et al., 2002; Yu et al., 2003; Yu et al., 2004; Ray et al., 2006; Kim et al., 2007; Liu, Z. et al., 2007; Wang et al., 2007). Since the phospho-recognition surface of a tandem BRCT motif can only accommodate one phospho-ligand at a time, at any given moment, a single BRCA1 polypeptide will bind Abraxas, BACH1, CtIP, or ACCA in a mutually exclusive manner (Yu and Chen, 2004; Greenberg et al., 2006; Kim et al., 2007; Liu, Z. et al., 2007; Wang et al., 2007). Thus, BRCA1, in association with BARD1, forms a distinct complex with each of these BRCT-interacting phosphoproteins. Notably, three of the BRCT phospho-dependent interactions mediate unique aspects of BRCA1 function in the cellular response to DNA damage (Greenberg et al., 2006). These BRCA1 supercomplexes are often referred to as complex A, complex B or complex C, depending on BRCA1's association with the phosphoprotein Abraxas, BACH1, or CtIP, respectively (Wang et al., 2007).

Complex A: In the absence of DNA damage, Abraxas associates independently with both BRCA1 and RAP80, a protein that harbors a ubiquitin-interacting motif (UIM). While the interaction between Abraxas and the BRCT domains of BRCA1 require phosphorylation of the S406 residue of Abraxas, the Abraxas/RAP80 interaction is phosphorylation-independent. In response to DNA damage, the three proteins form a complex whereby Abraxas bridges the association between BRCA1 and RAP80. This complex also contains several additional repair proteins: NBA1/Merit40, BRCC45 and BRCC36 proteins. The resulting supercomplex targets BRCA1 to sites of DNA damage in part through the recognition of ubiquitinated histones by the UIM of RAP80. Consequently, IR-induced foci (IRIFs) of BRCA1 fail to form in cells treated with Abraxas siRNA. In contrast, Abraxas recruitment to IRIFs is unaffected by BRCA1 depletion. Therefore, Abraxas acts upstream of BRCA1 in the DNA damage response. Interestingly, although complex A is required for the damage-induced transient G_2/M checkpoint, the checkpoint defect observed in Abraxas-deficient cells is less severe than that of BRCA1-deficient cells, despite the placement of Abraxas upstream of BRCA1. This suggests that complex A mediates only part of BRCA1 function in response to DNA damage (Kim et al., 2007; Kim et al., 2007a; Liu, Z. et al., 2007; Sobhian et al., 2007; Wang et al., 2007; Yan et al., 2007).

Complex B: The BRCT repeats of BRCA1 interact with a second phospho-ligand, the BRCA1-associated carboxyl-terminal helicase (BACH1) (Cantor et al., 2001), which is equivalent to the FancJ component of the Fanconi pathway (Levitus et al., 2005; Levran et al., 2005; Litman et al., 2005). BACH1 is phosphorylated in a cell-cycle dependent manner at residue S990 at the S to M phase transition, allowing for the

phospho-dependent interaction between BACH1 and the BRCT sequences of BRCA1. Thus, formation of the BRCA1-BACH1 complex is regulated with respect to cell cycle progression (Yu et al., 2003). Following DNA damage, the checkpoint protein TopBP1 associates with BRCA1-BACH1 to form complex B. This supercomplex appears to be essential for activation of the IR-induced G_2 accumulation checkpoint since expression of siRNA-resistant BACH1-S990A mutant is not sufficient to rescue the checkpoint defect observed in BACH1 siRNA-treated cells, indicating that the phosphorylation-dependent interaction between BACH1 and BRCA1 is necessary for G_2 accumulation checkpoint control (Yu et al., 2003). More recently, this supercomplex has been shown to activate a second checkpoint, the IR-induced S-phase checkpoint as elevated levels of DNA synthesis are observed in IR-treated U2OS cells transfected with either BRCA1, BACH1 or TopBP1 siRNA (Greenberg et al., 2006). Proper activation of these checkpoints may be an important mechanism to prevent genomic instability and suppress tumor formation.

Complex C: BRCA1 function in DNA-damage induced checkpoint control is further mediated by its interaction with the BRCT-interacting phosphoprotein CtIP (Wong et al., 1998; Yu et al., 1998; Yu and Chen, 2004). CtIP associates with the BRCT sequences of BRCA1 in a cell cycle-dependent manner (Yu and Baer, 2000). This interaction requires phosphorylation of CtIP at residue S327, which occurs transiently in the late S and G_2 phases of the cell cycle (Yu and Chen, 2004). Therefore, the BRCA1-CtIP complex primarily exists in the late S and G_2 phase, in contrast to the S to M phase-specific BRCA1-BACH1 complex. Notably, the BRCT domains of BRCA1 bind to the BACH1 phosphopeptide with a 5-fold higher affinity than to the CtIP phosphopeptide, perhaps explaining the transient nature of the BRCA1-CtIP complex (Yu and Chen, 2004; Varma

et al., 2005). The difference in cell cycle-dependent regulation of these BRCA1 complexes is consistent with the distinct functions of these complexes in DNA damage-induced checkpoint control (Yu and Chen, 2004). In response to DNA damage, the BRCA1-CtIP complex associates with the proteins of the MRN complex (Mre11/Rad50/Nbs1) to form a third supercomplex, complex C (Greenberg et al., 2006). This complex is required for the IR-induced transient G_2/M checkpoint. Indeed, siRNA-mediated CtIP depletion specifically ablates the transient G_2/M checkpoint, but not the BACH1-dependent G_2 accumulation checkpoint (Yu and Chen, 2004). Furthermore, the checkpoint defect of CtIP-depleted cells could be rescued by exogenous expression of wild-type CtIP, but not a mutant CtIP (S327A) that fails to bind BRCA1 (Yu and Chen, 2004). It is important to note however, that both complex A and complex C contribute to the BRCA1-dependent transient G_2/M checkpoint (Wang et al., 2007). Perhaps these different BRCA1-containing complexes promote distinct steps to ensure efficient cell cycle arrest and checkpoint control (Wang et al., 2007). A better understanding of the role of each of these BRCA1 complexes in genome stability and tumorigenesis is necessary.

H. The CtIP protein

CtIP/RBBP8 (CtBP interacting protein/Retinoblastoma binding protein 8) is a ubiquitously expressed 897 amino acid nuclear protein (Fusco et al., 1998; Schaeper et al., 1998; Wong et al., 1998; Yu et al., 1998). In addition to binding BRCA1, CtIP has also been reported to interact with the transcriptional co-repressor CtBP (C-terminal

binding protein) (Schaeper et al., 1998) and the tumor suppressor Rb (retinoblastoma protein) (Fusco et al., 1998). CtIP contains several short sequence motifs required for interaction with these protein partners (Figure 4). As mentioned above, the BRCT sequences of BRCA1 recognize the pSer-x-x-Phe motif centered on S327 of CtIP (Yu and Chen, 2004). A conserved PLDLS motif is present in the central region of CtIP to mediate the association of CtIP with CtBP (Schaeper et al., 1998). Furthermore, Rb and its family members, p130 and p107 are reported to interact with human CtIP through an LxCxE motif that lies in the N-terminal region of the protein (Fusco et al., 1998; Stokes et al., 2007). These interactions appear to mediate the function of CtIP in transcriptional regulation, the DNA damage response, and cell cycle checkpoint control (Meloni et al., 1999; Li et al., 2000; Yu and Chen, 2004; Chen, P.-L. et al., 2005; Liu and Lee, 2006). Apart from these short sequence motifs, the only recognizable structural domain of CtIP is an N-terminal coiled-coil sequence that mediates CtIP homodimerization (Figure 4) (Dubin et al., 2004). Although the biological role of this domain has not yet been determined, it may stabilize the *in vivo* interaction of CtIP with the Rb family of proteins (Stokes et al., 2007).

Interestingly, CtIP protein expression varies with the cell cycle in parallel with BRCA1 (Yu and Baer, 2000). The steady-state levels of CtIP are low in resting and cycling G_1 cells; however, as cells traverse the G_1/S boundary, CtIP protein expression is dramatically induced, with peak expression in late S and G_2 (Yu and Baer, 2000; Yu and Chen, 2004). The cell cycle-regulated phosphorylation of CtIP on residue S327 by cyclin-dependent kinase 2 (CDK2) coincides with peak expression of CtIP (Yu and Chen, 2004; Yata and Esashi, 2009). Thus, the BRCA1-CtIP complex forms when cellular

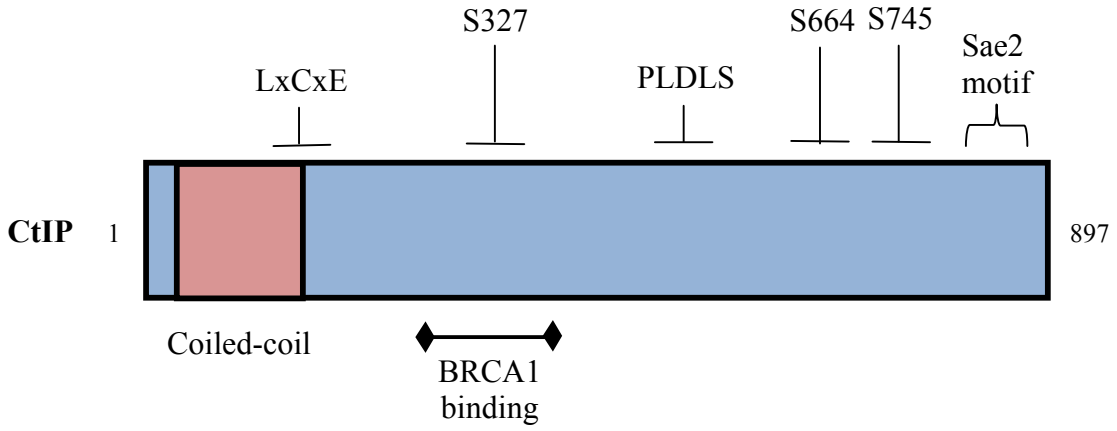

Figure 4. The human CtIP polypeptide. A schematic map of human CtIP (897 amino acids) illustrating the N-terminal coiled-coil domain (pink) that mediates CtIP homodimerization and C-terminal sequences that share homology with the yeast Sae2 protein (Sae2 motif). The S327 phosphorylation site that facilitates BRCA1 binding is also shown, as are the short sequence motifs implicated in binding the Rb tumor suppressor (LxCxE) and the CtBP transcriptional co-repressor (PLDLS). In addition, two reported ATM phosphorylation sites (S664 and S745) are depicted.

levels of both CtIP and BRCA1 proteins are maximal. Co-immunoprecipitation experiments reveal that in unsynchronized cells 10-20% of the BRCA1 polypeptide pool and 5-20% of the CtIP polypeptide pool interact to form a BRCA1-CtIP complex (Yu and Baer, 2000).

In response to DNA damage, CtIP is phosphorylated by the ATM kinase at S664 and S745 (Figure 4) (Li et al., 2000) and relocalizes from a diffuse nuclear distribution to discrete punctate foci that co-localize with γH2AX, a marker of DSBs, and BRCA1 (Yu et al., 2006). DNA damage-induced CtIP focus formation is reported to require the BRCA1-CtIP interaction, as CtIP fails to form IRIFs in HCC1937 cells, which express a truncated BRCA1 polypeptide lacking the C-terminal BRCT repeat (Yu et al., 2006). Moreover, the BRCA1-CtIP interaction is required for BRCA1/BARD1-mediated ubiquitination of CtIP following DNA damage, a modification that promotes the recruitment of CtIP to damaged sites (Yu et al., 2006). Perhaps DNA damage-induced CtIP hyperphosphorylation triggers the BRCA1/BARD1-dependent ubiquitination of CtIP and thus, the formation of CtIP foci (reviewed in Barber and Boulton, 2006). The resulting accumulation of ubiquitinated CtIP on chromatin following DNA damage may mediate the transient G_2/M checkpoint since catalytically inert BRCA1 polypeptides fail to activate this checkpoint (Yu et al., 2006). Although the precise mechanism by which CtIP ubiquitination promotes the transient G_2/M checkpoint remains unclear, these results highlight the importance of the coordinated action of the RING and BRCT domains in regulating BRCA1-dependent functions.

I. The functions of CtIP

To define the role of Ctip *in vivo*, a *Ctip*-null allele was generated using ES cell technology (Chen, P.-L. et al., 2005). Correctly identified recombinant ES cell clones were used to generate chimeric mice and subsequently heterozygous $Ctip^{+/-}$ mice. Intercrossing the $Ctip^{+/-}$ animals failed to produce $Ctip^{-/-}$ nullizygous mice, indicating that Ctip is essential for early embryonic development (Chen, P.-L. et al., 2005). The *Ctip*-null embryos died at embryonic day 4 (E4.0), as the blastocysts failed to enter S phase (Chen, P.-L. et al., 2005). Although *Ctip*- and *Brca1*-null mutations both affect cell proliferation, *Ctip*-null embryos die earlier *in utero* than *Brca1*-null embryos (E6.5-E7.5), suggesting essential Brca1-independent functions of Ctip in early embryogenesis (Hakem et al., 1996; Liu et al., 1996; Ludwig et al., 1997; Chen, P.-L. et al., 2005). Furthermore, the phenotypic defects associated with the *Ctip*-null mutation, in contrast to the *Brca1*-null mutation (Hakem et al., 1997; Ludwig et al., 1997), could not be mitigated in a *p53*-null background (unpublished data). Therefore, p53 is not required for the early lethality of *Ctip*-null embryos.

Recent studies with mice bearing the *Ctip*-null allele also suggest a direct role for Ctip in tumorigenesis (Chen, P.-L. et al., 2005). Although healthy, heterozygous $Ctip^{+/-}$ mice succumb to multiple tumors, predominantly lymphomas, at an increased rate relative to the wildtype $Ctip^{+/+}$ mice (Chen, P.-L. et al., 2005). Since the wildtype *Ctip* allele was retained in these $Ctip^{+/-}$ tumors, Chen, P.-L. et al. (2005) propose that Ctip lesions promote tumor formation by haploid insufficiency.

To date, mutations that alter both CtIP alleles in accord with the Knudson "two-hit" tumor suppressor model have not been observed in human tumors, including familial breast cancer (Wong et al., 1998; Gorringe et al., 2008). Nevertheless, a mutational screen of CtIP cDNA from 89 human tumor cell lines revealed missense variants in the human *CtIP* gene in cell lines derived from breast, ovarian, pancreas and colon carcinomas (Wong et al., 1998). Furthermore, a monoallelic one basepair deletion within the A9 repeat of the *CtIP* gene, which would result in a C-terminally truncated protein, has been observed in over 20% of mismatch repair-deficient colorectal carcinomas (Vilkki et al., 2002). Perhaps inactivation of one *CtIP* allele is sufficient for human oncogenesis given that tumorigenesis in mice has been attributed to CtIP haploinsufficiency (Chen, P.-L. et al., 2005; Chinnadurai, G., 2006).

Since CtIP is itself a candidate tumor suppressor, it may modulate the tumor suppressor function of BRCA1, its interacting partner, in part by promoting genome stability. In fact, CtIP has been implicated in at least two critical aspects of the DNA damage response; cell cycle checkpoint control (Yu and Chen, 2004) and DNA double-strand break (DSB) repair (Sartori et al., 2007). As mentioned above, CtIP is involved in the BRCA1-dependent transient G_2/M checkpoint after DNA damage (Yu and Chen, 2004). Activation of this checkpoint requires the BRCA1-CtIP interaction as well as the E3 ligase activity of the BRCA1/BARD1 heterodimer (Yu and Chen, 2004; Yu et al., 2006). Thus, checkpoint control by CtIP may be a critical mediator of the genome maintenance and tumor suppression functions of BRCA1.

Furthermore, recent studies have implicated CtIP in DNA resection, an early step in the cellular response to DNA double-strand breaks (DSBs) (Sartori et al., 2007). Chromosomal DSBs are highly toxic mutagenic lesions that must be repaired to maintain the integrity of the genome (Rouet et al., 1994; Helleday et al., 2007). Due to the tumorigenic potential of unrepaired or misrepaired DSBs, eukaryotes have evolved complex and highly conserved mechanisms to detect and repair such lesions (Khanna and Jackson, 2001; Jackson, S. P., 2002). The repair of DSBs in mammalian cells is achieved primarily through two major pathways, non-homologous end joining (NHEJ) and homology-directed repair (HDR) (Figure 5) (reviewed in Raynard et al., 2008; Huertas, P. 2010; Paull, T. T. 2010; Mimitou and Symington, 2011; Symington and Gautier, 2011). NHEJ is an error-prone process that requires little or no nucleolytic processing of the two DNA ends for ligation and repair of the DSB. In contrast, HDR requires extensive 5' to 3' resection of the DSB ends to produce 3' single-stranded DNA (ssDNA) overhangs. The resected ssDNA tail is initially coated with the RPA heterotrimer to form a ssDNA/RPA filament that activates checkpoint signaling through the ATR kinase (Zou and Elledge, 2003). Subsequently, RPA is displaced from the nucleofilament by the recombination protein Rad51 in a process facilitated by the BRCA2 polypeptide (Yang et al., 2005). The resulting ssDNA/Rad51 filament can then recognize, invade, and recombine with a homologous template, preferably a sister chromatid, to accurately restore genetic information disrupted by the DSB.

Although NHEJ occurs throughout all phases of the cell cycle, it assumes the greatest importance in the G_0 and G_1 phases, whereas HDR is largely restricted to the S and G_2 phases when sister chromatids are available as templates for homologous repair

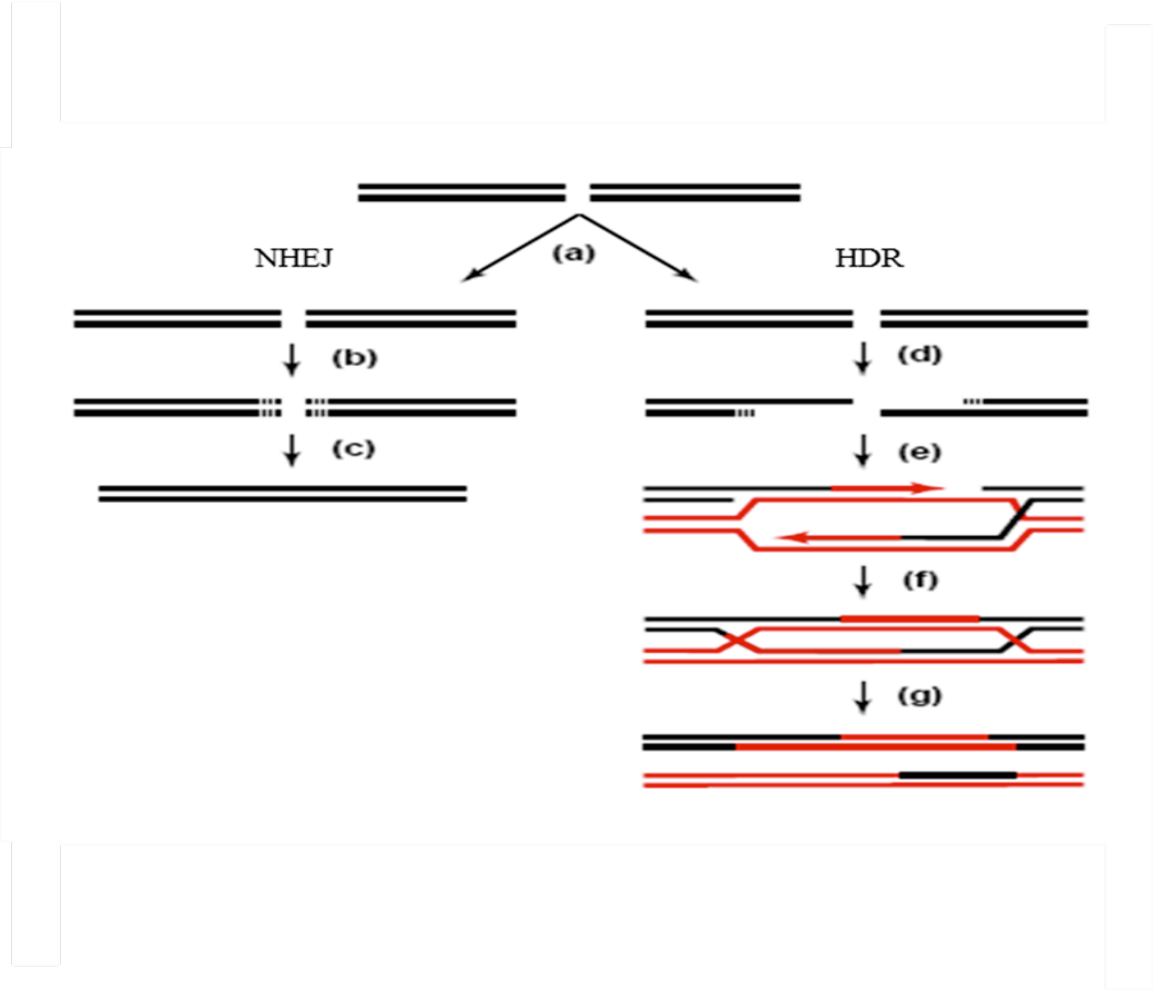

Figure 5. DNA double strand break repair pathways in eukaryotes. Left, non-homologous end joining (NHEJ) pathway. Right, homology-directed repair (HDR) pathway. DNA double strand break repair proceeds through a number of distinct steps: (a) DNA damage detection, (b) minimal DNA end processing, (c) DNA end ligation, (d) 5' to 3' DNA resection, (e) strand invasion and DNA synthesis, (f) DNA end ligation, and (g) resolution. DNA sequences of the damaged chromosome are depicted in black, while those of the template chromosome used for HDR are shown in red. (Adapted from Lisby and Rothstein, 2004)

(reviewed in Haber, J. E., 2000; Karran, P., 2000; Khanna and Jackson, 2001; Jackson, S. P., 2002; Lisby and Rothstein, 2004; Raynard et al., 2008; Huertas, P. 2010; Paull, T. T. 2010; Mimitou and Symington, 2011; Symington and Gautier, 2011). Cell cycle control of DSB repair pathway choice is an important aspect of genome maintenance, as gross chromosomal rearrangements may result if HDR occurs in the G_1 phase (Lisby and Rothstein, 2004). This coordination of the DNA repair pathway and the cell cycle is regulated by cyclin-dependent kinases (CDKs). In part, CDKs govern the choice between repair pathways by regulating 5' to 3' resection of DSBs (Figure 5d), an event that is necessary for HDR but actually inhibits NHEJ (Aylon et al., 2004; Ira et al., 2004). Given the critical role of DNA resection as both a regulator and effector of HDR, the factors that mediate resection are of keen interest.

For a long time, the MRN (Mre11/Rad50/Nbs1) complex was the only known component of the DNA resection machinery in higher eukaryotes (Jazayeri et al., 2006; Williams et al., 2007; Buis et al., 2008). The MRN complex is comprised of three polypeptides: Mre11, Rad50, and Nbs1 (Xrs2 in *S. cerevisiae*) (D'Amours and Jackson, 2002). In response to DSBs, MRN acts as a sensor that rapidly localizes to sites of DNA damage to initiate damage-induced signaling through activation of the ATM kinase (Mirzoeva and Petrini, 2001; Uziel et al., 2003; Lee and Paull, 2004; Lisby et al., 2004). ATM activation requires the DNA nuclease activity of Mre11 (Uziel et al., 2003) and results in the phosphorylation of a number of downstream substrates, including H2AX, Mre11, Nbs1, CtIP, RPA, BRCA1, and the protein kinase Chk2 (reviewed in Lavin and Khanna, 1999; Khanna et al., 2001; Shiloh, Y., 2001; D'Amours and Jackson, 2002).

Phosphorylation of these and other substrates by ATM initiates cell-cycle arrest and facilitates DNA repair.

Interestingly, the MRN complex acts as both an upstream activator and downstream target of the ATM kinase. Recent evidence indicates that DNA-damage induced phosphorylation of Mre11 and Nbs1 may stimulate the nuclease activity of Mre11, and thereby modulate the DNA resection function of the MRN complex (Costanzo et al., 2001; D'Amours and Jackson, 2002; Jazayeri et al., 2006; Buis et al., 2008). DNA resection and the consequent formation of ssDNA/RPA filaments in response to genotoxic stress can be observed cytologically by the formation of nuclear foci that stain with RPA-specific antibodies. In Mre11-deficient ataxia-telangiectasia-like disorder (ATLD) cells containing either an empty vector or a Mre11-nuclease mutant, RPA focus formation is markedly impaired following ionizing radiation, implicating the mammalian MRN complex and its nuclease activity in the initial processing of DSBs (Jazayeri et al., 2006). Furthermore, a reduction in RPA focus formation has also been observed in $Mre11^{\Delta/\Delta}$ (MRN-deficient) and $Mre11^{H129N/\Delta}$ (nuclease-deficient) MEFs (Buis et al., 2008). Using a DR-GFP assay to more definitively examine DSB repair, Buis et al. (2008) measured HDR of an I-*Sce*I endonuclease-induced DSB in $Mre11^{\Delta/+}$, $Mre11^{\Delta/\Delta}$, and $Mre11^{H129N/\Delta}$ MEFs. A pronounced defect in HDR was observed in both the $Mre11^{\Delta/\Delta}$ and $Mre11^{H129N/\Delta}$ cell lines relative to control cells ($Mre11^{\Delta/+}$), as measured by the percentage of GFP-positive cells. Overall, these data implicate the nuclease activities of the mammalian MRN complex in the DNA resection step of the HDR pathway.

In vitro, the Mre11 protein shows single-stranded endonuclease and 3' to 5' exonuclease activities (Paull and Gellert, 1998). The polarity of the exonuclease activity however is opposite from that required to generate, in a direct manner, the 3' single-stranded DNA overhangs that arise from DNA resection *in vivo*. It is possible that Mre11 functions in concert with a DNA helicase that unwinds the DNA duplex and allows the Mre11 endonuclease to resect 5' ends (Krogh et al., 2005). However, recent studies in *S. cerevisiae* demonstrate that DSB resection is a more complex process that occurs in at least two separate stages (Gravel et al., 2008; Mimitou and Symington 2008; Zhu et al., 2008; Nicolette et al., 2010; Niu et al., 2010). In this model, the 5' endonuclease activity of the MRX complex (the yeast counterpart of the MRN complex), together with the Sae2 protein, carries out the initial stage of resection to yield short ssDNA tails of roughly 100-400 nucleotides. In a subsequent extension stage, ssDNA tails greater than a kilobase in length are generated through the coordinated action of the 5' to 3' exonucleolytic activities of the Exo1 protein or the Sgs1/Dna2 helicase/exonuclease complex (Gravel et al., 2008; Mimitou and Symington, 2008; Zhu et al., 2008; Nicolette et al., 2010; Niu et al., 2010). A similar two stage DSB resection process has also been identified in mammalian cells, in which the initial stage is mediated by the MRN complex in collaboration with CtIP, which shares amino acid homology with the yeast Sae2 protein. The minimally resected DSB intermediates generated by MRN/CtIP then recruit helicases and nucleases, including BLM (Sgs1 in budding yeast), Exo1, and Dna2, to catalyze extensive and processive resection (Gravel et al., 2008; Raynard et al., 2008).

The amino acid homology between mammalian CtIP and yeast Sae2 is restricted to an approximately 100 residue region located at the C-termini of both proteins. This

homology, herein termed the "Sae2 motif", contains potential CDK and ATM/ATR phosphorylation sites that may serve to regulate DSB resection and HDR (Figures 4 and 6) (Sartori et al., 2007; Huertas et al., 2008). Notably, the Sae2 motif of CtIP contains a CDK consensus site analogous to S267 of Sae2, a phosphorylatable residue that mediates cell cycle control of DSB resection in *S. cerevisiae* (Huertas et al., 2008; Huertas and Jackson, 2009). Phosphorylation of the analogous residue of human CtIP (T847) is needed for effective ssDNA generation, RPA recruitment, and RPA phosphorylation in response to DNA damage (Huertas and Jackson, 2009). Exactly how phosphorylation of CtIP at residue T847 modulates DNA resection remains unresolved, since T847 phosphorylation is not required for the CtIP-MRN interaction (Sartori et al., 2007). Nonetheless, the mechanism by which DSB resection is controlled and the role of CtIP in the initial processing of a DSB appears to be conserved over a vast phylogenetic spectrum.

The biochemical mechanisms by which CtIP facilitates MRN-mediated DNA resection are not understood. Interestingly, the yeast Sae2 protein harbors an intrinsic endonuclease activity that acts cooperatively with MRX to cleave hairpin DNA structures *in vitro* (Lengsfeld et al., 2007). Although a corresponding enzymatic activity for CtIP has not yet been reported, recent studies indicate that CtIP promotes DNA resection by physically associating with and stimulating the endonuclease activity of the MRN complex (Sartori et al., 2007). Moreover, CtIP downregulation dramatically impairs ssDNA generation and RPA focus formation (Sartori et al., 2007), as well as ATR-dependent Chk1 phosphorylation (Yu and Chen, 2004). Furthermore, siRNA-mediated CtIP depletion reduces homology-directed repair of an I-*Sce*I-induced DSB to levels

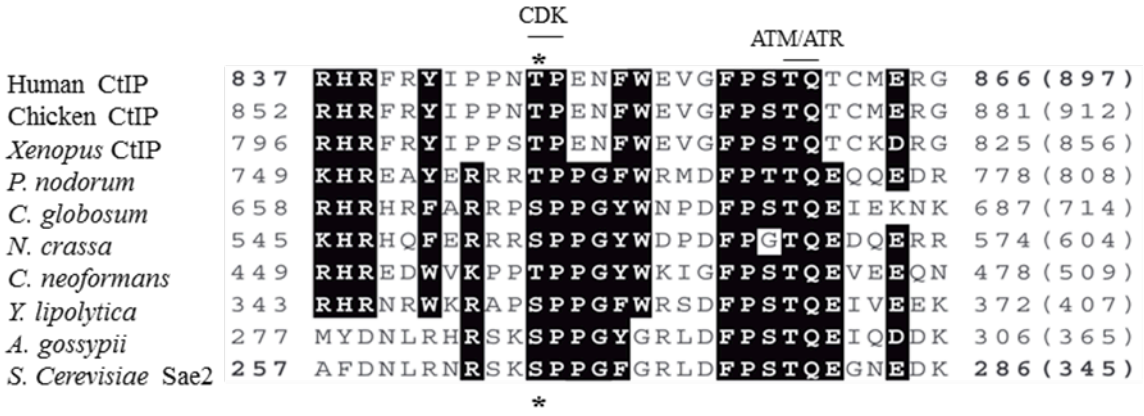

Figure 6. Alignment of the C-terminus of human CtIP with those of CtIP/Sae2 homologues from different species. Potential CDK (S/T-P) and ATM/ATR (S/T-Q) phosphorylation sites are indicated. Conserved residues are shaded black. Asterisks (*) show the position of the conserved CtIP T847 and Sae2 S267 residues. GenBank accessions: Human CtIP (AAC14371), Chicken CtIP (XP_419158), *Xenopus laevis* CtIP (AAH73395), *Phaeosphaeria nodorum* (EAT90897), *Chaetomium globosum* (XP_001224668), *Neurospora crassa* (XP_957865), *Cryptococcus neoformans* (EAL19137), *Yarrowia lipolytica* (XP_502193), *Ashbya gossypii* (NP_984048) and *Saccharomyces cerevisiae* Sae2 (NP_011340). (Adapted from Sartori et al., 2007)

comparable to those achieved by depleting Mre11 or the key homologous recombination protein Rad51 (Sartori et al., 2007). Since depletion of CtIP and Mre11 in tandem does not decrease HDR efficiency any further, the two proteins likely promote DSB repair by homologous recombination through a common mechanism (Sartori et al., 2007). Therefore, in mammalian cells, CtIP collaborates with the MRN complex to resect DSB ends and thereby initiate both checkpoint signaling and homologous recombination.

It is unclear as to whether BRCA1 is required for the DNA resection functions of CtIP. This notion is attractive as it could potentially explain how BRCA1 controls various checkpoints and HDR pathways. A requirement for BRCA1 in CtIP-mediated resection would also be consistent with genetic data that places BRCA1 upstream of BRCA2 in the HDR pathway (Stark et al., 2004). Furthermore, the BRCA1, BARD1, CtIP, and MRN polypeptides are known to form a discrete protein complex (BRCA1 complex C) in mammalian cells that could potentially mediate the resection functions ascribed to CtIP and MRN (Greenberg et al., 2006; Chen et al., 2008). If so, complex C may control the transient G_2/M checkpoint indirectly through its role in DNA end resection (reviewed in Huen et al., 2010). It has been reported by one group that RPA focus formation in response to IR is impaired in HCC1937 cells, a BRCA1-mutant human breast tumor line, but not in HCC1937 cells reconstituted with wild-type BRCA1 (Chen et al., 2008). Although this result suggests that BRCA1 is required for DNA resection, another group reported that siRNA-mediated depletion of BRCA1 in HeLa cells has no effect on IR-induced RPA focus formation (Zhao et al., 2007). The requirement for BRCA1 in CtIP-dependent DNA resection remains a critical issue, as it

may help explain the molecular mechanisms by which BRCA1 maintains genomic stability and suppresses tumor formation.

J. Goals and Rationale

Although a clear understanding of the mechanism of BRCA1-mediated tumor suppression has been obscured by the broad spectrum of cellular activities attributed to BRCA1 and the plethora of BRCA1-interacting partners, meaningful insights have recently emerged using an accurate mouse model of basal-like breast cancer. For instance, despite the importance of both the RING and BRCT domains in tumor suppression, only the phosphopeptide binding property of the BRCT repeats, and not the E3 ligase activity of the RING domain, is required for BRCA1-mediated tumor suppression (Shakya et al., 2011). Thus, mammary tumor formation in mice homozygous for the S1598F mutation (corresponding to the human mutation S1655F) is accelerated relative to wildtype mice and comparable with that of conditional *Brca1*-null mice (Shakya et al., 2011). On the other hand, tumor formation is suppressed in homozygous Brca1-I26A mutant mice expressing an enzymatically defective Brca1 (Shakya et al., 2011). This result emphasizes the importance of BRCT phosphopeptide recognition for tumor suppression. It is noteworthy that at least three different DNA damage response proteins (Abraxas, BACH1, and CtIP) interact with the BRCT repeats of BRCA1 to form distinct protein complexes (reviewed in Huen et al., 2010; Moynahan and Jasin, 2010). Since BRCA1's association with one or more of these BRCT phosphopeptides (and/or others yet to be discovered) appears to mediate its tumor suppression function (Shakya et

al., 2011), analysis of these interactions is critical and may provide novel targets for cancer therapy.

In this study, we sought to determine the role of CtIP in BRCA1-mediated tumor suppression. Among the three known BRCT-interacting phospho-ligands, CtIP seemed a likely candidate to mediate BRCA1 function in genome stability and tumor suppression. First, CtIP is the only known BRCT-interacting phosphopeptide that is also an enzymatic substrate of BRCA1/BARD1's E3 ligase activity (Yu et al., 2006). When this research began, a role for the E3 ligase activity of BRCA1 in tumor suppression was predicted based on the presence of tumor-associated mutations in the RING domain that inactivate BRCA1 enzymatic activity (Hashizume et al., 2001). Second, cancer-associated missense mutations in the BRCT domains of BRCA1 disrupt the BRCA1-CtIP interaction, highlighting the potential importance of a stable BRCA1-CtIP complex for tumor suppression (Yu et al., 1998). Third, CtIP plays a prominent role in maintaining genome stability by activating the transient G_2/M checkpoint (Yu and Chen, 2004) and promoting the DNA resection and homology-directed repair of DSBs (Sartori et al., 2007). Therefore, we hypothesized that CtIP may be a key downstream mediator of the genome maintenance and tumor suppression functions of BRCA1.

To elucidate the role of CtIP in these BRCA1-dependent processes, we examined genome stability in cells and tumor suppression in mice that express a Ctip polypeptide with a missense mutation (Ctip-S326A) that ablates its interaction with Brca1. Furthermore, we assessed if CtIP serves as a tumor suppressor in mammary epithelial cells, and, if so, whether this activity is epistatic with Brca1-mediated tumor suppression.

To this end, we tested whether mammary-specific lesions of Ctip lead to basal-like breast tumors similar to those observed in conditional *Brca1*-null mice (Shakya et al., 2008). Finally, for reasons that will be discussed, we also examined how the phospho-dependent interaction of BRCA1 with two or more of its BRCT-binding partners affects genome stability and tumor suppression.

CHAPTER II

MATERIALS AND METHODS

A. Targeted mutagenesis

A1. Ctip^{S326A}

The homology arms of the *Ctip*^{S326A} targeting construct (Figure 7B) were derived from a 6.0 kilobasepair *Eco*RI fragment of genomic DNA from strain 129-derived E14 TG2a ES cells (Warren et al., 1994). This fragment encompasses exons 10, 11, and 12 of the *Ctip* locus. The natural serine codon (TCT) for residue 326 in exon 11 was substituted with an alanine codon (GCA) by site-directed mutagenesis (Stratagene). An *Age*I restriction site was also introduced into exon 11 in this manner by converting the sequence TCCGGT to ACCGGT. In the final construct, the homology fragment was interrupted at the *Hpa*I restriction site of intron 10 by insertion of a *loxP*-flanked PGK promoter-driven neomycin selection marker cassette. A gene cassette encoding herpes simplex virus type 1 thymidine kinase (HSV-TK) was also included in the construct as a negative selection marker. For gene targeting, *Not*I-linearized targeting vector DNA was introduced into 129/Sv embryonic stem (ES) cells by electroporation (30 ug of DNA at 0.8 kV/3 μF), and after neomycin selection, drug-resistant ES cell subclones were analyzed for gene targeting by Southern blotting *Pvu*II-digested genomic DNA with a 5' flanking *Ctip* probe ("*Ctip #6*") spanning exon 9 (Figure 7A). Correctly targeted heterozygous *Ctip*$^{S326A\text{-}neo/+}$ 129/Sv ES cells were identified (Figure 7C and 9).

An identical *Ctip*^{S326A} targeting construct was generated by replacing the *loxP*-flanked neomycin resistance cassette with a *loxP*-flanked PGK promoter-driven hygromycin selection marker. The *Ctip*$^{S326A\text{-}hyg}$ targeting construct was linearized with the *Not*I restriction enzyme and electroporated into *Ctip*$^{+/-}$ ES cells (30 ug of DNA at 0.8 kV/3 μF). The functionally null *Ctip*$^{-}$ allele of these cells was generated previously by

replacing 1.2 kilobases of *Ctip* genomic DNA, including part of exon 11 and all of exon 12, with a MC1 promoter-driven neomycin expression cassette (unpublished data; Ludwig, Baer, and Efstratiadis, Columbia University). DNA was prepared from the hygromycin-resistant ES cell subclones and digested with the *Pvu*II restriction enzyme. Southern analysis using the exon 9-spanning 5' flanking *Ctip* probe ("*Ctip #6*") revealed correctly targeted $Ctip^{S326A\text{-}hyg/-}$ ES clones (Figure 8). Adeno-cre virus infection of these ES cells resulted in $Ctip^{S326A/-}$ ES subclones with the *loxP*-flanked hygromycin resistance gene cassette removed (Figure 7D). Briefly, an Adeno-cre virus stock solution was prepared by adding 3 ul of Adeno-cre virus (2.84×10^{10} pfu/mL) to 300 ul of pre-warmed Dulbecco's Modified Eagle Medium (DMEM) (Cellgro) supplemented with 2.5% heat-inactivated fetal bovine serum (FBS; HyClone ES Cell Screened, Thermo Scientific). $Ctip^{S326A\text{-}hyg/-}$ ES cells in a subconfluent well of a 12-well plate were washed twice with 1X PBS and incubated at 37°C in 300 ul of virus stock solution for 1 hour. Every 15 minutes, the 12-well plate was gently shaken by hand to distribute the virus. Following virus infection, the cells were washed twice with 1X PBS and provided fresh DMEM supplemented with 15% heat-inactivated FBS, 2 mM L-glutamine, 1% non-essential amino acids, 0.1 mM 2-mercaptoethanol, and LIF (1,000 units/mL) (Esgro; Millipore). The next day, the virus-infected cells were seeded at a 1:250 dilution onto a 10-cm layer of mitotically inactive primary embryonic fibroblasts (Feeders). DNA was prepared from individually picked ES subclones and analyzed by Southern for removal of the *loxP*-flanked hygromycin resistance gene cassette.

A2. Ctip^{Co}

The conditional-null *Ctip*$^{Co\text{-}neo}$ targeting vector consisted of a 9.7 kb fragment containing exon 1 and exon 2 of Ctip (Figure 24B). A single *loxP* site was introduced upstream of the transcriptional initiation site in the *Nhe*I restriction site of intron 1. A second *loxP* site was cloned into the *Eco*RV restriction site of intron 2, along with an *FRT*-flanked PGK-neomycin resistance cassette. The HSV-TK negative selection gene cassette was included in the construct for selection against random integration. Gene targeting was performed by electroporating *Not*I-linearized targeting vector DNA (30 ug of DNA at 0.8 kV/3 μF) into 129/Sv ES cells and selecting for neomycin-resistant ES subclones. Genomic DNA prepared from the surviving drug-resistant ES cell subclones was digested with *Spe*I and analyzed by Southern blotting with a 5' flanking *Ctip* probe ("*Ctip-2*") upstream of exon 1 (Figure 24A). Several heterozygous *Ctip*$^{Co\text{-}neo/+}$ 129/Sv ES clones were obtained (Figure 25).

B. ES cell culture

ES cells were cultured in Dulbecco's Modified Eagle Medium (DMEM) (Cellgro) supplemented with 15% heat-inactivated fetal bovine serum (FBS; HyClone ES Cell Screened, Thermo Scientific), 2 mM L-glutamine, 1% non-essential amino acids, 100 ug/mL penicillin/streptomycin, 0.1 mM 2-mercaptoethanol, 1.25 ug/mL Plasmocin (InvivoGen) and LIF (1,000 units/mL) (Esgro; Millipore) at 37°C in 5% CO_2/95% humidity. For all recombination reporter assays, ES cells were maintained in the above ES medium without penicillin/streptomycin, Plasmocin, and LIF. Unless otherwise noted, ES cells were grown on a layer of mitotically inactive primary embryonic

fibroblasts in the presence of LIF to maintain their pluripotency. For gene targeting, ES cells were selected with 250 ug/mL neomycin (G418/Geneticin; Gibco), 200 ug/mL hygromycin B (Roche), 1.5 ug/mL puromycin (Sigma), or 10 ug/mL 6-thioguanine (Sigma). ES cells targeted with the HSV-TK containing targeting vectors mentioned in Section A were simultaneously selected with 2 μM ganciclovir (Roche) for 3 days starting on day 2 of selection. All ES cells were frozen down in an equal volume of 2X freezing medium, 80% heat-inactivated FBS and 20% dimethylsulfoxide (DMSO).

C. Animals

The mice used in this study were housed in an AAALAC-accredited facility at Columbia University. All experiments involving mice were performed according to the Columbia University Institutional Animal Care and Use Committee-approved protocols. $Ctip^{S326A\text{-}neo/+}$ 129Sv ES cells were injected into C57BL/6J blastocysts to derive germline chimeric male mice, which were mated to C57BL/6J females (B6). $Ctip^{S326A\text{-}neo/+}$ mice were intercrossed to generate homozygous $Ctip^{S326A\text{-}neo/S326A\text{-}neo}$ mutants or mated with $Ctip^{+/-}$ animals to obtain $Ctip^{S326A\text{-}neo/-}$ mice. Heterozygous $Ctip^{S326A\text{-}neo/+}$ animals were also crossed to mice that ubiquitously express Cre recombinase ($Rosa^{Cre}$ animals) to produce $Ctip^{S326A/+}$ mice with the *loxP*-flanked neomycin resistance cassette removed (Figure 7D). Subsequent intercrossing of these animals yielded homozygous $Ctip^{S326A/S326A}$ mice. The $Ctip^{S326A/S326A}$ mice were also crossed with homozygous $Abx^{S404A/S404A}$ and homozygous $Bach1^{FH\text{-}S994A/FH\text{-}S994A}$ mutant mice (kindly provided by Dr. Thomas Ludwig, Columbia University) to produce heterozygous double mutant mice, which upon intercrossing, generated homozygous double mutant animals (e.g.,

Abx$^{S404A/S404A}$/*Ctip*$^{S326A/S326A}$ (AC) and *Bach1*$^{FH\text{-}S994A/FH\text{-}S994A}$/*Ctip*$^{S326A/S326A}$ (BC)). Similarly, the *Abx*$^{S404A/S404A}$ and *Bach1*$^{FH\text{-}S994A/FH\text{-}S994A}$ mice were crossed and ultimately bred to generate the *Abx*$^{S404A/S404A}$/*Bach1*$^{FH\text{-}S994A/FH\text{-}S994A}$ (AB) double mutant animals. The double mutant mice were then crossed to produce animals bearing four mutant alleles (e.g., *Abx*$^{S404A/+}$/*Bach1*$^{FH\text{-}S994A/FH\text{-}S994A}$/*Ctip*$^{S326A/+}$) and subsequently bred to generate triple homozygous (*Abx*$^{S404A/S404A}$/*Bach1*$^{FH\text{-}S994A/FH\text{-}S994A}$/*Ctip*$^{S326A/S326A}$ (ABC)) mutant mice.

The *Ctip*$^{Co\text{-}neo/+}$ 129Sv ES cells were also injected into C57BL/6J blastocysts to derive germline chimeras that mated with B6 females. *Ctip*$^{Co\text{-}neo/+}$ heterozygotes were mated with Flpe-expressing mice to produce offspring expressing the *Ctip*^{Co} allele with the *FRT*-flanked neomycin cassette removed (Figure 24D). By intercrossing these animals, homozygous *Ctip*$^{Co/Co}$ mice were obtained and used in a breeding regimen to derive experimental and control cohorts as described in Section B5a of Chapter IV. The *Wap*^{Cre} mice (Ludwig et al., 2001a) and the *p53*^{flex7} mice, hereafter referred to as the p53 conditional-null (*p53*^{Co}) mice, have been described (Chen, Z. et al., 2005; Shakya et al., 2011). Additionally, the *p53*$^{LSL\text{-}R270H}$ mouse strain (number 01XM3) (Olive et al., 2004) was obtained from the NCI-Frederick Mouse Repository. Homozygous *Ctip*$^{Co/Co}$ mice were also mated with *Rosa*^{Cre} animals (kindly provided by Dr. Thomas Ludwig, Columbia University) to generate *Ctip*$^{Co\text{-}rec/+}$ *Rosa*$^{Cre/+}$ heterozygotes, which were then intercrossed to assess the function of the Cre-recombined product of the conditional-null *Ctip*^{Co} allele. Furthermore, analysis of concomitant loss of Ctip and Ku70 was made possible with the *Ku70*$^{-/-}$ mice provided by Dr. Shan Zha (Columbia University). All mice generated in this study were maintained on a mixed 129/B6 genetic background.

C1. Whole-body IR treatment

To assess the sensitivity of various mouse genotypes to ionizing radiation (IR), mice at 2 months of age were irradiated on a rotating platform with a sublethal dose of 8 Gys using the Mark I Cesium-137 mouse irradiator (J. L. Shepard and Associates). All mice were carefully monitored for at least 6 weeks following irradiation for signs of distress or death, at which time necropsies were performed.

D. Generating MEFs

To generate primary mouse embryonic fibroblasts (MEFs), E13.5 day embryos were aseptically dissected from a pregnant mother mouse and placed in a 10-cm dish containing sterile 1X PBS. The uterine membrane was cut to free the individual embryos. The yolk sac of each embryo was collected and saved in a 1.5 mL Eppendorf tube for genotyping. Using forceps, the embryo's head, intestines and liver were removed. The remainder of the embryo was transferred to a 60 mm plate and minced using two scalpels in a sterile tissue culture hood. Each embryo was incubated at 37ºC in 500 ul of Trypsin-EDTA 1X (0.25% Trypsin, 2.21 mM EDTA in Hank's Balanced Salt Solution without sodium bicarbonate, calcium, and magnesium) (Cellgro) for 8 minutes. Following incubation, 9.5 mL of MEF media (see below, Section F) was added to each 60 mm dish and the cells/media were passed first through an 18.5 gauge needle (3 times) and then through a 21.5 gauge needle (3 times) using a 10 mL syringe. On the last needle passage, the cells/media (10 mL) were transferred to a 15 mL tube with 4 mL of MEF media. The tube was inverted three times and then left undisturbed for 5 minutes to allow the undigested tissue to settle at the bottom of the tube. Only the cells in a single-

cell suspension (~12 mL) were then plated onto a 10-cm gelatinized dish. The next day, the cells were washed twice with 1X PBS and provided fresh MEF media. When confluent, the cells were split at a 1:5 dilution and seeded onto five 10-cm gelatinized plates for freezing and maintenance. Using Lipofectamine 2000 (Invitrogen), primary MEFs at early passage were immortalized by transfection with the pMSSVLT plasmid (10 ug/10-cm plate), a vector which drives expression of the SV40 large-T antigen (Schuermann M., 1990). Cells were passaged until only the immortalized MEFs remained in culture (approximately 12 passages/4 weeks). Established immortalized MEF cell lines were then frozen down and re-genotyped.

E. Generating mammary tumor cells

Two weeks after mammary neoplasms were detected by palpation, the mouse was sacrificed and a piece of tumor tissue was collected in order to establish a primary mammary tumor cell line. The mammary tumor tissue was placed in a 60 mm dish and transferred to a sterile tissue culture hood. Using two scalpels, the mammary tumor tissue was diced and then incubated at 37ºC for 5 minutes in 500 ul of Trypsin-EDTA 1X (0.25% Trypsin, 2.21 mM EDTA in Hank's Balanced Salt Solution without sodium bicarbonate, calcium, and magnesium) (Cellgro). After trypsinization, 5 mL of MEF media was added directly to the 60 mm plate. With a 10 mL syringe, the cells/media were passed through an 18.5 gauge needle three times followed by three passages with a 21.5 gauge needle. After the final passage, the cells/media were dispensed onto a gelatinized 10-cm plate. 5 mL of MEF media was again added to the 60 mm plate to collect the remaining cells and this too was transferred to the 10-cm plate. The 10-cm

plate was then left undisturbed for 4 days in the 37ºC incubator to allow for the tumor tissue pieces to adhere before being provided fresh MEF media. Mammary tumor cells were split once the cells reached 60% confluency. By approximately the sixth passage (4 weeks), the mammary tumor cell line was established, the cells were frozen down and collected for DNA.

Ctip/p53-null mammary tumor cell lines were established from mammary carcinomas that arose in experimental females (e.g., $Ctip^{Co/-,Co/Co}/p53^{Co/+,Co/Co}/Wap^{Cre/+}$) following mammary-specific co-inactivation of Ctip and p53 (Figure 30). Mammary tumor cell lines were also established from the breast tumors that developed in $Ctip^{Co/Co}/p53^{LSL\text{-}R270H/+}/Wap^{Cre/+}$ experimental females, which underwent mammary-specific inactivation of Ctip and expression of the $p53^{R270H}$ dominant-negative mutation (Figure 31). Additionally, p53-null and $p53^{R270H}$ mutant mammary tumor cell lines were derived from the mammary tumors of control $Ctip^{Co/+,+/+}/p53^{Co/+,Co/Co}/Wap^{Cre/+}$ and $Ctip^{Co/+,+/+}/p53^{LSL\text{-}R270H/+}/Wap^{Cre/+}$ females, respectively (Figures 30 and 31).

F. MEFs and mammary tumor cell culture

Primary and immortalized MEFs and mouse mammary carcinoma cell lines were cultured in Dulbecco's Modified Eagle Medium (DMEM) (Cellgro) supplemented with 10% heat-inactivated fetal bovine serum (FBS; Tissue Culture Biologicals), 100 ug/mL penicillin/streptomycin, 2 mM L-glutamine, and 1.25 ug/mL Plasmocin (InvivoGen) and grown on tissue culture plates pre-treated with 0.1% gelatin. All cell lines were grown at 37°C and maintained in a humidified atmosphere of 5% CO_2. Primary MEFs were mitotically inactivated with 10 ug/mL mitomycin C (Sigma) in MEF media for 2 hours at

37°C to be used as feeders for ES cells. All cells were frozen in an equal volume of 2X freezing medium, 80% heat-inactivated FBS and 20% dimethylsulfoxide (DMSO).

G. Molecular analysis

G1. Southern analyses

For genotyping by Southern analysis, genomic DNA was prepared from mouse tails, embryo yolk sacs, mammary tumor tissues, mammary tumor cells, MEF cells, and ES cells by dissolving the tissue or cultured cells in 500 ul of lysis buffer (50 mM Tris-HCL, pH 8.0, 0.1 M NaCL, 2 mM EDTA, 1% SDS) containing 200 ug/mL proteinase K overnight at 56°C. Genomic DNA was precipitated with isopropanol, dissolved in 1X TE buffer (10 mM Tris-HCL, 1 mM EDTA, pH 8.0), and digested (10 ug DNA) with the appropriate restriction enzyme(s) in a volume of 30 ul with 10 units of enzyme. The digested genomic DNA was fractionated on a 0.8% agarose, 1X TAE gel, depurinated in 0.25 M HCL, denatured in 0.5 M NaOH/1.5 M NaCL and blotted onto a Biodyne B nylon membrane (Pall) via an upward capillary transfer for at least 6 hours. To permanently immobilize the DNA to the membrane, the membrane was baked at 80°C for 15 minutes and then pre-hybridized with 350 ug of sonicated denatured salmon sperm DNA in 10 mL Rapid Hybridization buffer (5X SSC, 10% polyethylene glycol MW 8000, 5% poly(sodium 4-styrenesulfonate), 0.2% cetylpyridinium chloride monohydrate) for 35 minutes at 65°C in a rotating hybridization oven. A [α^{32}P]-dCTP-labeled (Perkin Elmer) probe was prepared using the Prime-It II Random Primer Labeling Kit (Agilent Technologies). The ^{32}P-labeled probe was denatured with 250 ug of salmon sperm DNA by boiling for 10 minutes at 95°C before being placed on ice and added directly to the

blot with pre-hybridization solution for a 2 hour incubation at 65°C. Following hybridization, the membrane was washed sequentially for 12 minutes at 65°C in 500 mL of wash 1) 2X SSC, 0.5% SDS, 2) 1X SSC, 0.5% SDS, 3) 0.1X SSC, 0.1% SDS, dried on Whatman paper, wrapped in Saran wrap, and exposed to Kodak BioMax MS film with two amplifying screens at -80°C overnight.

The $Ctip^{+}$ (7.9 kb), $Ctip^{S326A}$ (7.9 kb), $Ctip^{-}$ (6 kb), $Ctip^{S326A\text{-}neo}$ (5.8 kb), and $Ctip^{S326A\text{-}hyg}$ (10.4 kb) alleles were detected by hybridizing *Pvu*II-digested genomic DNA with the 5' flanking *Ctip* probe spanning exon 9 ("*Ctip #6*") (Figure 7A). The $Ctip^{+}$ (12.7 kb) allele was also occasionally detected by hybridizing *Spe*I-digested DNA with the 5' flanking Ctip probe upstream of exon 1 ("*Ctip-2*") (Figure 24A). This "*Ctip-2*" probe also recognized the $Ctip^{Co\text{-}neo}$ (8.3 kb) allele in *Spe*I-digested DNA. Additionally, the Ctip genotype could be determined by digesting the DNA with *Bgl*II/*Nhe*I and hybridizing with a probe ("$Ctip^{Co}$-*SmaI*") spanning exon 1 (data not shown). This "$Ctip^{Co}$-*SmaI*" probe discriminates between the unrecombined $Ctip^{Co}$ (5.6 kb) allele and the recombined $Ctip^{Co\text{-}rec}$ (4.2 kb) allele lacking the transcriptional initiator methionine; however, both the $Ctip^{+}$ and $Ctip^{-}$ alleles are recognized as a 3.3 kb band. Therefore, to discriminate between these two alleles, the DNA had to be digested with *Pvu*II and hybridized with the exon 9-spanning *Ctip* probe ("*Ctip #6*") (see above, Figure 7A).

The $Rosa^{+}$ (10.5 kb) and the $Rosa^{Cre}$ (2.8 kb) alleles were detected by digesting the DNA with *Eco*RV and hybridizing with the "*Rosa*" probe. *Eco*RV-digested DNA was also hybridized with the "*Flpe*" probe to identify the presence of Flpe recombinase. The presence of Wap^{Cre} was detected by digesting the DNA with *Eco*RI and hybridizing with

the "*Wap*" probe. A 6.8 kb band represented the Wap^{+} allele, while a 3.5 kb, 8 kb or 9 kb band represented the Wap^{Cre} allele. To determine the p53 genotype of various DNA samples, the $p53^{+}$ (4.6 kb), $p53^{Co\text{-}rec}$ (4.3 kb) and $p53^{Co}$ (2.5 kb) alleles were discriminated by hybridization of *Eco*RV-digested genomic DNA with the "$p53^{Co}$" probe. Additionally, the $p53^{LSL\text{-}R270H}$ (6.8 kb) allele was detected following hybridization of *Eco*RV-digested DNA with the "*SV40*" probe. To assess amplification of c-*Met*, the DNA samples were digested with *Eco*RI and hybridized with the "*c-Met*" probe. The intensity of the bands relative to the amount of DNA loaded on the gel was compared across samples using tail DNA, which lacks c-*Met* amplification, as a control.

G2. PCR analysis

Polymerase chain reaction (PCR) genotyping was performed on genomic DNA prepared from mouse tails, embryo yolk sacs, mammary gland tissue, MEF cells, and ES cells as described above. PCRs were carried out using *Taq* DNA Polymerase (Invitrogen) with 10X PCR buffer (200 mM Tris-HCL (pH 8.4), 500 mM KCL), 50 mM $MgCl_2$, a 10 mM dNTP mix, and when necessary, 100% DMSO. Each PCR reaction occurred in a total volume of 25 ul and was run on an Eppendorf Mastercycler Gradient PCR machine. Unless otherwise noted, 1 ul of genomic DNA was amplified per sample and oligonucleotide primers were used at a 10 μM concentration.

The $Ctip^{+}$ (350 bp) and $Ctip^{S326A}$ (430 bp) alleles were amplified using 1 ul of 1:10 diluted DNA with primer 1 and primer 2 (see Table 1 below) under the following PCR conditions: 94°C 3 min (1 cycle); 94°C 30 sec, 62°C 30 sec, 72°C 30 sec (40 cycles); 72°C 3 min (1 cycle); 4°C hold. Using the same PCR conditions and primers 3 and 4, the $Ctip^{+}$ (250 bp) and $Ctip^{Co}$ (290 bp) alleles were amplified. These primers amplify across

the single *loxP* site in intron 1 of *Ctip*. The $Ctip^{Co\text{-}rec}$ (350 bp) allele was amplified in the presence of DMSO with primer 3 and primer 5 using the same PCR conditions as above except with an annealing temperature of 58°C.

To genotype the Abx^{+} and Abx^{S404A} alleles, primers 6 and 7 were used with 1 ul of 1:10 diluted DNA in the presence of DMSO under the following PCR conditions: 94°C 3 min (1 cycle); 94°C 30 sec, 54°C 30 sec, 72°C 30 sec (29 cycles); 72°C 3 min (1 cycle); 4°C hold. These primers amplify a 190 bp band for the Abx^{+} allele and a 250 bp band for the Abx^{S404A} allele. Primers 8 and 9 were used at a 100 μM concentration to amplify the $Bach1^{+}$ (520 bp) and $Bach1^{FH\text{-}S994A}$ (350 bp) alleles. The PCR conditions for this reaction were as follows: 94°C 3 min (1 cycle); 94°C 30 sec, 64°C 1 min, 72°C 1 min (34 cycles); 72°C 3 min (1 cycle); 4°C hold. Finally, the $Ku70^{+}$ (450 bp) and $Ku70^{-}$ (320 bp) alleles were amplified in the presence of DMSO using primers 10, 11, and 12 under the following conditions: 94°C 3 min (1 cycle); 94°C 30 sec, 57°C 30 sec, 72°C 1 min (34 cycles); 72°C 5 min (1 cycle); 4°C hold. All amplified fragments were separated by 2% agarose gel electrophoresis.

Table 1. PCR primers.

Primer #	Primer Name	Primer Sequence
1	Ctip-HpaI junction 5’	5’- GTCCTCAGTGGGCTTCATTTC
2	Ctip-mct2-Rev	5’- ATGTCTAAGAGAGAGGGGGAG
3	Ctip-NheI 5’	5’- GGGCTCAGTTTCTGGGTGCT
4	Ctip-NheI 3’	5’- CATGTTGGGCATGGTGACTC
5	Ctip-EcoRV 3’	5’- TTGCAGAGAACCAAAGTTCAGC
6	Abx-Ex 9 Forw	5’- CAGCAGGCACCAAGACAAGG
7	Abx-3’ UTR Rev	5’- TCTGTGTATTAATCCAGAAGGCAAAGA
8	Bach1 5’	5’- GCCAAGTGTCCCAGCTCAAA
9	Bach1 3’	5’- TCAGTGTCCCAGGCAACTAAG
10	Ku70 5’	5’- ACACGGCTTCCTTAATGTGA
11	Ku70 3’	5’- GGCTGGCTTTAGCACTGTCA
12	Ku70_Loxp1h3	5’- ACGTAAACTCCTCTTCAGACCT

H. Histological analysis

Mice were sacrificed and autopsied when they became moribund or had a palpable tumor mass. All major organs and any tumors identified were dissected, fixed overnight in 10% buffered formalin, and dehydrated prior to paraffin embedding. Paraffin blocks were sectioned at 4 μm and stained with hematoxylin and eosin for histopathological evaluation. For immunophenotyping, all specimens were labeled with antibodies against E-cadherin (BD Pharmingen), vimentin (RDI), CK5 (Covance), CK14 (Covance), ER (Santa Cruz) and PR (ABR).

I. Glutathione-agarose affinity chromatography

Rosetta(DE3)pLysS competent cells (Novagen) were transformed with <0.5 ug of the GST-containing expression plasmid and spread onto an ampicillin/chloramphenicol plate (75 ug/mL ampicillin and 38 ug/mL chloramphenicol). A single colony from the plate was inoculated in 3 mL of 1X LB Broth (Difco, BD) media containing ampicillin and chloramphenicol throughout the day at 37ºC. Half of the overday bacterial culture was then inoculated overnight at 37ºC. The next morning, two 1 L flasks were prepared with 400 mL of 2X LB media, 150 ul of 200 mg/mL ampicillin, 400 ul of 38 mg/mL chloramphenicol, and 50 mL of the overnight culture and put to shake at 37ºC until the OD_{600}= 0.5 (~ 1.5 hrs), at which point, 160 ul of 1M IPTG was added (final concentration is 0.4 mM) to each flask to induce production of the plasmid-encoded protein. The flasks were shaken at 37ºC for an additional 4 hours. The cells were pelleted by centrifugation at 5,000 rpm for 5 minutes at 4ºC and each pellet was resuspended in 8 mL of cold Buffer D (50 mM Hepes pH 7.5, 0.4 M NaCL, 0.1 mM EDTA pH 8.0, 0.1% NP40, 10% glycerol) supplemented with 1 mM dithiothreitol (DTT) and a complete protease inhibitor pellet (Roche). The resuspended pellets were stored at -80ºC overnight.

Two hours before use, the glutathione-agarose resin (Sigma) was prepared by adding 0.3 g of glutathione-agarose resin to 30 mL of cold Buffer E (50 mM Hepes pH 7.5, 0.15 M NaCL, 0.1 mM EDTA pH 8.0, 10% glycerol). The resin/buffer was mixed and stored at 4ºC until swollen. Once swollen, the glutathione-agarose resin was equilibrated by washing in 20 mL of Buffer D twice. Between each wash, the resin was centrifuged at 2,000 rpm for 2 minutes at 4ºC and the supernatant was discarded. The resin was then

washed with 10 mL of Buffer D supplemented with 1 mM DTT and a complete protease inhibitor pellet (Roche), spun down, and stored at 4ºC until needed.

To purify the GST-fusion protein, the cell suspensions were thawed on ice and sonicated 15 times with a 30-second burst followed by a 15-second rest. The culture was pelleted and the supernatant was added to the equilibrated glutathione-agarose resin to mix for 2 hours at 4ºC. After mixing, the beads were pelleted and washed two times with 20 mL of Buffer D supplemented with 1 mM DTT and a protease inhibitor pellet (Roche). Between each wash, the beads were centrifuged at 2000 rpm for 2 minutes at 4ºC and the supernatant was removed. These rounds of washes/centrifugation were repeated two more times with 20 mL of Buffer E supplemented with 1 mM DTT. Following this final spin, ~ 2 mL of the Buffer E wash was left behind. The resin was then transferred into a 5 mL Econo-Column (Bio-Rad). The GST-fusion protein was eluted in cold Elution Buffer (0.1g glutathione dissolved in 50 mL of Buffer E supplemented with 1 mM DTT, pH 8.0) made fresh and the eluents were collected in 1 mL fractions. The protein concentration was checked in each fraction using the Bio-Rad Protein Assay reagent (Bio-Rad). The eluted material was subjected to SDS-PAGE and stained with Coomassie blue (Gibco) to estimate the yield of intact fusion protein.

I1. Generation of a mouse-specific Brca1 antibody

A cDNA fragment containing amino acids 1484-1812 of murine *Brca1* (mBR-SZ) was subcloned into the GST-containing expression vector pGEX2. The glutathione S-transferase (GST)-Brca1 fusion protein was purified by glutathione-agarose affinity chromatography and sent to Covance for commercial polyclonal antibody production in rabbits.

J. Western analysis and antibodies

J1. Western blot

Cells were scraped in 5 mL of cold 1X PBS and lysed in low salt Nonidet P-40 (NP40) lysis buffer (10 mM Hepes, pH 7.6, 1 M NaCL, 0.1% NP40, 5 mM EDTA, 10% glycerol) supplemented with 1 mM dithiothreitol (DTT), 5 mM sodium fluoride, 0.1 mM sodium orthovanadate, and complete protease inhibitor (Roche). To detect Brca1 hyperphosphorylation following 1 mM hydroxyurea (Sigma) treatment for 1 hour, cells were lysed 1 hour post-drug removal in low salt Nonidet P-40 (NP40) lysis buffer supplemented with 1 mM DTT, 25 mM sodium fluoride, 10 mM sodium orthovanadate, and complete protease inhibitor (2x concentration). Lysates were cleared by high-speed centrifugation at 4ºC for 10 minutes. The protein concentration of each sample was determined by using the Bio-Rad Protein Assay reagent (Bio-Rad). Samples were prepared for SDS-PAGE by adding 5X protein loading dye (0.313 M Tris-Cl pH 6.8, 10% SDS, 50% glycerol, 25% 2-mercaptoethanol, 0.05% bromophenol blue) and boiled at 150ºC for 4 minutes to elute the proteins. Samples were fractionated on Tris-glycine polyacrylamide gels (6-10%) and transferred onto Optitran nitrocellulose membranes (Whatman) in western transfer buffer (25 mM Tris-Cl pH 7.6, 190 mM glycine, 20% methanol, 0.04% SDS) overnight at 22 V at room temperature. Membranes were blocked at room temperature for 35 minutes in 10% milk in TBS-T (20 mM Tris-Cl pH 7.6, 0.137 M NaCL, 0.1% Tween 20), washed for 5 minutes in TBS-T, and then incubated at room temperature with the desired dilution of primary antibody in 2% milk in TBS-T for 2.0-2.5 hours. The membranes were then washed in TBS-T three times for 10 minutes and incubated for 1 hour at room temperature with a 1:10,000 dilution of either HRP-

conjugated goat anti-mouse (Sigma) or donkey anti-rabbit (Amersham) secondary antibodies prepared in 2% milk in TBS-T. Following incubation and a quick rinse in TBS-T, the membranes were washed two times for 10 minutes each in TBS-T. The membranes were incubated with the SuperSignal West Pico Chemiluminescent substrate (Pierce) or the more sensitive SuperSignal West Dura Chemiluminescent substrate (Pierce) for 4 minutes before exposure of the immobilized proteins on autoradiographic film.

J2. Antibodies

Immunoblotting was performed with a rabbit polyclonal antibody raised against amino acids 1484-1812 of mouse Brca1 (mB-57J; 1:2000 dilution) (Section I1) and a monoclonal mouse anti-CtIP antibody (14-1; 1:50 dilution) (Yu and Baer, 2000). Other antibodies used include: monoclonal anti-α-tubulin (1:10000 dilution) (DM1A, Calbiochem) and polyclonal anti-Na^+/K^+ ATPase (1:5000 dilution) (RDI Division, Fitzgerald Industries).

K. Co-immunoprecipitation of Ctip with Brca1

Cells were scraped in 5 mL of cold 1X PBS and centrifuged at 1200 rpm for 2 minutes at 4°C. The cell pellet was lysed in 10 times its volume with freshly made cold Buffer A (10 mM Hepes pH 7.9, 10 mM KCl, 0.1 mM EGTA) supplemented with 1 mM dithiothreitol (DTT), 5 mM sodium fluoride, 0.1 mM sodium orthovanadate, and complete protease inhibitor (Roche). Following lysis for 15 minutes on ice, a 1/16 volume of 10% NP40 was added to each sample. The samples were vortexed vigorously

for 10 seconds, set on ice for 5 minutes, and centrifuged at 2000 rpm for 5 minutes at 4°C. The supernatant or cytoplasmic fraction was removed while the nuclear pellet was resuspended in 1.5 times its volume with freshly made cold Buffer C (20 mM Hepes pH 7.9, 10% glycerol, 0.4 M NaCL, 0.5 mM EDTA, 0.5 mM EGTA, 0.1% NP40) supplemented with 1 mM DTT, 5 mM sodium fluoride, 0.1 mM sodium orthovanadate, and complete protease inhibitor (Roche) and put at 4°C to rotate for 15 minutes. After mixing, the samples were spun down at maximum speed for 10 minutes at 4°C. The supernatant or nuclear extract was transferred to a new tube and the protein concentration was measured using the Bio-Rad Protein Assay reagent (Bio-Rad).

The nuclear extract lysate (~800 ug-1500 ug) was incubated by rotating at 4°C overnight with either the mouse-specific Brca1 polyclonal antibody (mB-56F; 1:20 dilution) or the matched pre-immune serum (mB-56Pre; 1:20 dilution) in a total volume of 300 ul. The next day, 25 ul of protein A sepharose beads (20% slurry; GE Healthcare) per sample were prepared by washing the beads four times in 500 ul of cold Buffer C supplemented with 1 mM DTT, 5 mM sodium fluoride, 0.1 mM sodium orthovanadate, and complete protease inhibitor (Roche) and spinning down at 8000 rpm for 30 seconds at 4°C between each wash. The packed protein A sepharose beads were added to each lysate/antibody sample and put to rotate at 4°C for 1 hour. After incubation, the samples were spun down (30 seconds, 8000 rpm, 4°C) and the supernatant/flow-through was collected. The lysate and antibody-bound beads were washed three times with 500 ul of cold Buffer C supplemented with 1 mM DTT, 5 mM sodium fluoride, 0.1 mM sodium orthovanadate, and complete protease inhibitor (Roche). After the final wash, as much buffer as possible was removed and 40 ul of 2X protein loading dye was added. These

samples were boiled for 4 minutes at 150ºC to elute the bound proteins and fractionated on a 6% Tris-glycine polyacrylamide gel set at 95 V. The gel was transferred overnight at 22 V at room temperature and the western blot procedure was followed as described in Section J.

L. Gene-targeting analysis

Gene-targeting efficiency at the *Pim1* locus was measured by electroporating Ctip$^{+/-}$ and Ctip$^{S326A/-}$ ES cells with the *Xho*I-linearized p59xDR-GFP6 DNA targeting vector (30 ug of DNA at 0.8 kV/3 μF) (a kind gift of Maria Jasin; Moynahan et al., 2001a), selecting for hygromycin resistance, and evaluating the drug-resistant clones for gene targeting by Southern analysis. Genomic DNA of individual hygromycin-resistant clones was prepared, digested with *Hinc*II, and hybridized with the "*P22*" probe (see Figure 3 of Moynahan et al., 2001a). A 3.6 kb fragment represents the wildtype *Pim1* allele while a 2.4 kb fragment represents the targeted *Pim1* allele. The p59xDR-GFP6 plasmid contains a promoterless hygromycin-resistance marker flanked by targeting arms comprised of *Pim1* genomic DNA. Thus, most hygromycin-resistant clones are correctly targeted by homologous recombination because hygromycin expression is dependent on the *Pim1* promoter. However, hygromycin-resistant clones can also arise upon random integration of the p59xDR-GFP6 construct adjacent to transcriptional promoters at other genomic sites.

For assessing the gene-targeting efficiency of Ctip$^{+/-}$ and Ctip$^{S326A/-}$ ES cells at the *Rb* locus, ES cells were electroporated with the *Hpa*I-linearized Rb-G (Rb-pgkhyg) targeting vector (30 ug of DNA at 0.8 kV/3 μF). The Rb-G vector was derived by

inserting a PGK-hyg cassette into the *Bgl*II site within exon 19 of Rb (see Figure 1d of te Riele et al., 1992). ES cells were selected with hygromycin and genomic DNA was prepared from the surviving clones. The gene-targeting efficiency of the ES cells was revealed following an *Eco*RI digest of the genomic DNA and Southern blot hybridization analysis with the "*p153*" probe (same as probe B in Figure 1a of te Riele et al., 1992). The wildtype and targeted *Rb* alleles are 9.7 and 4.9 kb, respectively. The Rb-pgkhyg targeting vector contains the mouse *pgk1* (phosphoglycerate kinase) promoter to drive expression of the hygromycin-resistance gene. Therefore, in contrast to the p59xDR-GFP6 vector, a greater proportion of the hygromycin-resistant clones result from random integration of the Rb-G vector and thus, the targeting efficiency with this vector is lower overall.

M. Recombination reporter assays

To measure repair of I-*Sce*I-induced chromosomal DNA breaks, each ES clone carrying a specific chromosomally integrated GFP recombination reporter was trypsinized and seeded in 6-wells of a 12-well gelatinized plate in the absence of a feeder layer (~1 x 10^6 cells/well). The next day, ES cells (~50% confluent) were provided fresh media (ES media minus penicillin/streptomycin, Plasmocin, and LIF) and transfected with 2.5 ug of either empty vector (pCAGGS) or the I-*Sce*I expression vector (pCβASce) using Lipofectamine 2000 (Invitrogen). Following a 24 hour incubation, each well of transfected cells was washed twice with 1X PBS, trypsinized, and replated in a well of a 6-well gelatinized plate. 48 hours after replating and 72 hours post-transfection, the cells were washed with PBS and trypsinized prior to resuspension in cold 1% FCS/PBS.

Samples were placed on ice and protected from light before flow cytometric analysis on the FACSCalibur using the CellQuest software (BD Biosciences). The proportion of GFP positive events (at least 70,000 events were scored per sample) provided a measure of DSB repair.

M1. Homology-directed repair (HDR)

By assessing the gene-targeting efficiency of *Ctip*$^{+/-}$ and *Ctip*$^{S326A/-}$ ES cells at the *Pim1* locus, DR-GFP reporter ES cell lines of each genotype were obtained (Section L). These correctly targeted *Ctip*$^{+/-}$ *DR-GFP* and *Ctip*$^{S326A/-}$ *DR-GFP* ES clones were examined as described above for their ability to repair chromosomal DSBs by HDR.

M2. Single-strand annealing (SSA)

Ctip$^{+/-}$ and *Ctip*$^{S326A/-}$ ES cells were electroporated with the *Sac*I/*Kpn*I-linearized hprtSAGFP targeting vector (30 ug of DNA at 0.8 kV/3 μF) (a kind gift of Jeremy Stark; JS #125; Stark et al., 2004) and plated onto gelatinized-only 10-cm plates. This targeting construct has homology to the *Hprt* locus and contains a puromycin resistance marker as well as the SSA reporter substrate, SA-GFP. Upon proper integration, the *Hprt* gene is inactivated, rendering the cells resistant to the nucleotide analog 6-thioguanine (6-TG) (Pierce et al., 2001; Stark et al., 2004). Therefore, only correctly targeted clones should be resistant to both puromycin and 6-TG. The ES cells were selected with 1.5 ug/mL puromycin for 5 days followed by 10 ug/mL of 6-TG for 4 days (from a stock of 10 mg/mL in 1N NaOH). For Southern analysis, genomic DNA was prepared from the doubly-resistant ES clones, digested with *Pst*I, and hybridized with the "*HPRT-SSA*" probe, an 800bp iGFP *Hind*III fragment from the DR-GFP plasmid (a kind gift from Jeremy Stark; JS #65). Since the Southern blot probe ("*HPRT-SSA*") was part of the

targeting construct, only the two GFP repeats were recognized, as 7.5 kb and 3.3 kb bands. Multiple *Ctip*$^{+/-}$ *SA-GFP* and *Ctip*$^{S326A/-}$ *SA-GFP* reporter ES clones were obtained and used to compare the SSA repair efficiency among genotypes.

M3. Alternative non-homologous end joining (alt-NHEJ)

To assess the efficiency of DSB repair by alt-NHEJ, *Ctip*$^{+/-}$ and *Ctip*$^{S326A/-}$ ES cells were electroporated with the *Xho*I-linearized pim-EJ2-GFP-hyg targeting vector (30 ug of DNA at 0.8 kV/3 μF) (kindly provided by Jeremy Stark; JS251; Bennardo et al., 2008). This targeting vector was generated by cloning the *EJ2SceGFP* gene into the pim-DR-GFP vector (Moynahan et al., 2001; Bennardo et al., 2008). Following electroporation, ES cells grown on feeders were selected with hygromycin and genomic DNA was prepared from the surviving colonies. Southern analysis was performed by digesting the DNA with *Hinc*II and hybridizing with the "*P22*" probe (see Figure 3 of Moynahan et al., 2001a). This probe detects a 3.6 kb *Hinc*II fragment on the wildtype *Pim1* allele and a 2.4 kb fragment on targeted alleles generated by proper homologous integration of the EJ2-GFP-hyg reporter into the mouse *Pim1* locus. The ability to repair I-*Sce*I-induced DSBs by alt-NHEJ was then examined using several correctly targeted *Ctip*$^{+/-}$ *EJ2-GFP* and *Ctip*$^{S326A/-}$ *EJ2-GFP* ES clones identified by Southern analysis.

N. Clonogenic survival assays

For each ES cell line, a 90% confluent well of a 6-well plate was trypsinized and the live cells were enumerated by counting trypan-blue negative cells. 1000 cells/well (for untreated controls) or 5000 cells/well (for drug-treated cultures) were then seeded onto 6-

well feeder plates pre-coated with gelatin. Per condition, each ES cell line was plated in triplicate. At 24 hours post-seeding, ES cells were exposed for 24 hours to varying doses of camptothecin (CPT dissolved in DMSO, Sigma) (CPT: 0 ng/mL, 20 ng/mL, 40 ng/mL, 80 ng/mL, and 100 ng/mL) or etoposide (ETO dissolved in DMSO, Sigma) (ETO: 0 ng/mL, 30 ng/mL, 60 ng/mL, 90 ng/mL, 120 ng/mL, and 150 ng/mL). At 48 hours post-seeding, ES cells were exposed for 4 hours to varying doses of mitomycin C (MMC dissolved in PBS, Sigma) (MMC: 0 ng/mL, 50 ng/mL, 100 ng/mL, 150 ng/mL, and 200 ng/mL). Following drug treatment, all cells were washed twice with 1X PBS, provided fresh media, and allowed to grow at 37°C undisturbed for 7-9 days. Colonies of surviving cells were then fixed in 10% buffered formalin for 30 minutes, stained with 0.5% Crystal violet (Sigma) for 15 minutes, washed in water three times, and then counted.

O. Cytogenetic analysis

Metaphase spreads were prepared from subconfluent ES cells, primary MEFs, and mammary tumor cells treated with or without mitomycin C (MMC 40 ng/mL; Sigma) for 16 hours. For ES cells, 0.05 ug/mL of KaryoMAX Colcemid solution (Gibco/Invitrogen) was added directly to the culture 4 hours prior to the end of MMC treatment (–/+ MMC). In contrast, for primary MEFs and mammary tumor cells, 0.05 ug/mL KaryoMAX Colcemid solution (Gibco/Invitrogen) was added 2 hours prior to the end of MMC treatment (–/+ MMC). Since many mitotic cells are among the floating and poorly attached cells, at the end of MMC treatment, the media on all cells was collected, as was

the 1X PBS wash. The remaining attached cells were then trypsinized and added to the collected media/wash. The combined cell solution was then centrifuged at 1500 rpm for 5 minutes. The ES and primary MEF cell pellets were resuspended by vigorously flicking in ~1 mL of 0.56% KCL (w/v) hypotonic solution prepared fresh and pre-warmed at 37ºC. The mammary tumor cell pellets on the other hand were dislodged by vigorously flicking in pre-warmed 0.38% KCL (w/v) hypotonic solution. Once the pellets were resuspended, the volume in the tube was brought up to 12 mL with the appropriate KCL solution (depends on cell type, see above). The tubes were quickly inverted two times and submerged to the level of the KCL solution in a 37ºC water bath for 20 minutes (mammary tumor cells) or 30 minutes (ES cells and primary MEFs). Following KCL treatment, ~0.5 mL of freshly made pre-chilled (at -20ºC) fixative (3:1 Methanol/Glacial Acetic Acid) was added dropwise directly to the KCL solution in each tube and mixed by gently inverting the tube twice. An additional 0.5 mL of cold fixative was added and mixed before the tubes were centrifuged at 1200 rpm for 5 minutes and the supernatant was removed. The swollen cell pellets were resuspended by adding ~0.5 mL cold fixative drop by drop to the tube and softly tapping the sides. The tube was then held over a constant gentle vortex while 5 mL of cold fixative was added dropwise. The samples were then spun down at 1500 rpm for 5 minutes. Two additional rounds of the cold fixative wash took place before the cells were resuspended in 5 mL of fixative and stored at -20ºC overnight. The next day, the cells were spun down at 1500 rpm for 5 minutes and washed an additional two times in cold fixative as done the previous day. The fixed cell suspensions were then resuspended in ~1 mL of cold fixative and dropped onto glass slides. Gentle blowing across the slide helped to spread the chromosomes.

Once dried, the slides were stained with the KaryoMAX Giemsa stain stock solution (Gibco/Invitrogen) for 3 minutes. Excess stain solution was washed away with water and an air-stream was used to dry the slides. At least 15 metaphases were scored per sample.

P. Proliferation assays

The MTT assay was used to evaluate the proliferation rate of early passage primary MEFs. Four 96-well flat bottom gelatinized plates were needed, one for each day of measurement (Day 0 – Day 3). 8 wells of each cell line were seeded onto the four 96-well plates; therefore, each cell line was seeded into 32 wells. 4000 cells/well were seeded for each triple ABC mutant cell line, while 2000 cells/well were seeded for the control cell lines. The cells were cultured with MTT/solubilization solution either 24 hours (Day 0 plate), 48 hours (Day 1 plate), 72 hours (Day 2 plate), or 96 hours (Day 3 plate) after seeding. On the appropriate day, the media was discarded from the 96-well plate and MTT stock (3-[4,5-dimethylthiazol-2-yl]-2,5-diphenyltetrazolium bromide; Sigma) (5 mg/mL in sterile PBS) diluted in MEF media was added to each well to produce a final MTT concentration of 500 ug/mL. The cells were cultured with MTT for 4 hours at 37°C to allow the formation of purple formazan crystals from MTT cleavage. 100 ul of solubilization solution (10% SDS in 0.01 M HCL) was then added directly to each well and the cells were cultured at 37°C overnight. The next day, the intensity of the precipitated formazan product was detected by measuring the UV absorbance with the Bio-Tek μQuant microplate spectrophotometer and the KC Junior Software (BioTek Instruments).

Q. Centrosome staining

Primary MEFs were seeded onto Poly-L lysine (Sigma) coated coverslips in a 12-well plate (~70,000 cells/well) and allowed to attach for 2-3 days until 50% confluent. The cells were rinsed twice in 1X PBS before being fixed on ice in cold 100% methanol for 10 minutes. The cells were then incubated in 1X PBS for 5 minutes with gentle shaking followed by incubation in serum-free DMEM for 5 minutes again with gentle shaking. Net gel (150 mM NaCL, 5 mM EDTA, 50 mM Tris-Cl, 0.05% NP40, 0.25% Gelatin IV bloom 75, Type B (Sigma), 0.02% Na-azide, pH 7.4) was used to rinse the cells twice prior to permeabilization with 0.5% Triton-X/net gel at room temperature for 10 minutes. The cells were then gently shaken in 5% BSA/PBS blocking solution for 30 minutes. Double immunostaining was then performed using a rabbit polyclonal anti-pericentrin (1:250 dilution) (Abcam) and a mouse monoclonal anti-α-tubulin (1:1000 dilution) (Calbiochem) antibody diluted in 1% BSA/PBS for 1 hour at room temperature on the bench. The cells were then washed three times for 5 minutes in 1% BSA/PBS before being incubated in Alexa Fluor 568 goat anti-rabbit IgG (1:400 dilution) and Alexa Fluor 488 goat anti-mouse IgG (1:400 dilution) (Invitrogen) secondary antibodies diluted in 1% BSA/PBS for 30 minutes. Following four 5 minute washes in 1% BSA/PBS, the coverslips were stained with 4', 6-diamidino-2-phenylindole (DAPI) (1:20,000 dilution, Sigma) for 5 minutes and mounted with Aqua-Poly/Mount mounting media (Polysciences, Inc.) onto a glass slide and sealed with nail polish.

R. Immunofluorescence staining

Cells were seeded onto Poly-L lysine (Sigma) coated coverslips in a 6-well plate and allowed to attach for 2 days until 50% confluent, at which point, the cells were either treated with or without 10 Gys of ionizing radiation (IR) (Gammacell 40). One hour post-IR, the cells were rinsed twice in cold 1X PBS and fixed in freshly made cold 3.7% paraformaldehyde/PBS pH 7.4 for 15 minutes at room temperature on the bench. The cells were then washed and incubated for 5 minutes in cold serum-free DMEM. Following this incubation, the cells were washed twice with cold 1X PBS, permeabilized in cold 0.5% Triton-X/net gel for 10 minutes at room temperature, and washed twice in net gel (150 mM NaCL, 5 mM EDTA, 50 mM Tris-Cl, 0.05% NP40, 0.25% Gelatin IV bloom 75, Type B (Sigma), 0.02% Na-azide, pH 7.4). The cells were then blocked in 1% BSA/PBS at 4°C for at least 15 minutes. Once the cells were blocked, they were incubated with primary antibody (diluted in 1% BSA/PBS) for 45 minutes at room temperature on the bench followed by two rinses and three washes with gentle shaking in 1% BSA/PBS (5 minutes for the first two washes, 10 minutes for the last). Next, the cells were incubated with the secondary antibody diluted in 1% BSA/PBS for 45 minutes. Again, the cells were rinsed and washed in 1% BSA/PBS (four 5-minute washes with gentle shaking). Cold 1X PBS was used to rinse the cells twice before they were stained with 4', 6-diamidino-2-phenylindole (DAPI) (1:20,000 dilution, Sigma) for 5 minutes and mounted onto a glass slide with a drop of Aqua-Poly/Mount mounting media (Polysciences, Inc.).

R1. Antibodies

Immunofluorescence was performed with a rabbit polyclonal antibody raised against amino acids 1484-1812 of mouse Brca1 (mB-57J, 1:500 dilution) (Section I1), a monoclonal mouse anti-CtIP antibody (14-1; 1:10 dilution) (Yu and Baer, 2000), a rabbit polyclonal anti-Rad51 antibody (1:50 dilution) (Santa Cruz), and an anti-RPA (Ab-3, total RPA) mouse monoclonal antibody (1:100 dilution) (Calbiochem). For staining with the anti-RPA mouse monoclonal antibody (Calbiochem), the cells were incubated in cold Extraction Buffer (10 mM Pipes pH 6.8, 100 mM Nalco, 300 mM sucrose, 3 mM $MgCL_2$, 1 mM EGTA, 0.5% Triton X-100) for 5 minutes at 4°C prior to the two washes in 1X PBS and fixation in 3.7% paraformaldehyde/PBS. Additionally, as a marker of DNA damage sites, either a rabbit polyclonal anti-γH2AX antibody (1:50 dilution) (Cell Signaling) or a mouse monoclonal anti-γH2AX antibody (JBW301, 1:200 dilution) (Millipore) was used. The secondary antibodies used included Alexa Fluor 488 and 568 goat anti-mouse IgG (Invitrogen) as well as Alexa Fluor 488 and 568 goat anti-rabbit IgG (Invitrogen).

CHAPTER III

THE ROLE OF THE BRCA1-CTIP INTERACTION IN GENOME STABILITY AND TUMOR SUPPRESSION

A. INTRODUCTION

Germline mutations of the *BRCA1* tumor suppressor gene are a common cause of familial breast and ovarian cancer. Its protein product has been implicated in a remarkably broad spectrum of cellular processes that includes ubiquitination, cell cycle checkpoint control, DNA repair, centrosome duplication, and transcriptional regulation (reviewed in Deng, C.-X., 2006; Nagaraju and Scully, 2007; Greenberg, R. A., 2008; Huen et al., 2010; Moynahan and Jasin, 2010; Roy et al., 2011). While it remains unclear which of these cellular functions are relevant for tumor suppression, the BRCA1 protein harbors an N-terminal RING domain which possesses E3 ubiquitin ligase activity and two tandem C-terminal BRCT repeats that form a phosphopeptide binding domain (Miki et al., 1994; Joazeiro and Weissman, 2000; Hashizume et al., 2001; Manke et al., 2003; Yu et al., 2003). Although most cancer-predisposing mutations involve gross truncations of the BRCA1 protein, single amino acid substitutions in the RING or BRCT domains of BRCA1 have been found in some familial patients (Miyake et al., 2000). Therefore, these domains are critical for the tumor suppression activity of BRCA1.

BRCA1 exerts its pleiotropic functions by interacting with a diverse set of proteins. *In vivo*, most BRCA1 polypeptides interact with the related protein BARD1 to form a heterodimer that exhibits ubiquitin E3 ligase activity (Wu et al., 1996; Yu and Baer, 2000; Hashizume et al., 2001; reviewed in Baer and Ludwig, 2002; Irminger-Finger and Jefford, 2006; Huen et al., 2010). Formation of the BRCA1/BARD1 heterodimer is mediated by sequences encompassing their respective RING domains (Wu et al., 1996). In addition, the BRCT domains of BRCA1 interact *in vivo* with phosphorylated isoforms of the repair proteins Abraxas/CCDC98, BACH1/BRIP1/FancJ, and CtIP (Wong et al.,

1998; Yu et al., 1998; Cantor et al., 2001; Magnard et al., 2002; Manke et al., 2003; Rodriguez et al., 2003; Yu et al., 2003; Yu et al., 2004; Kim et al., 2007; Liu, Z. et al., 2007; Wang et al., 2007). Thus, the BRCA1/BARD1 heterodimer forms a distinct complex with each of these BRCT-interacting phosphoproteins, in a mutually exclusive manner, to mediate unique aspects of BRCA1 function in response to DNA damage (Yu and Chen, 2004; Greenberg et al., 2006; Kim et al., 2007; Liu, Z. et al., 2007; Wang et al., 2007; reviewed in Huen et al., 2010; Moynahan and Jasin, 2010).

Of the three major BRCT phospho-ligands, CtIP is the only one known to be an enzymatic substrate of BRCA1/BARD1's E3 ligase activity (Yu et al., 2006). However, we recently found that the phosphopeptide binding property of the BRCT repeats, but not the E3 ligase activity of the RING domain, is required for BRCA1-mediated tumor suppression (Shakya et al., 2011). Since tumor suppression is dependent on BRCA1 association with its BRCT phospho-ligands, the CtIP interaction may contribute to BRCA1-mediated tumor suppression by promoting genome stability. Indeed, CtIP plays a diverse role in maintaining genome integrity by activating the transient G_2/M checkpoint (Yu and Chen, 2004) and promoting DNA resection and homology-directed repair of DSBs (Sartori et al., 2007). Moreover, site-specific mutations designed to ablate phosphorylation of human CtIP (S327A) are known to disrupt its interaction with BRCA1 (Yu and Chen, 2004). Indeed, a peptide competition assay performed by Yu and Chen (2004) showed that only the phosphorylated CtIP-S327 peptide, but not the unphosphorylated control peptide, competed with endogenous CtIP for binding to the BRCA1 BRCT domains.

Therefore, to elucidate the role of the BRCA1-CtIP interaction in genome stability and tumor suppression, we examined murine cells that express Ctip polypeptides (Ctip-S326A) that fail to interact with Brca1. Using embryonic stem (ES) cell technology we generated the $Ctip^{S326A}$ knock-in allele and introduced it into the mouse germline. Isogenic subclones of ES cells and mouse embryonic fibroblasts (MEFs) that express either the wildtype $Ctip^{+}$ or mutant $Ctip^{S326A}$ allele were then used to examine the genome stability functions of the Brca1-Ctip interaction. In addition, we have assessed tumor formation in mice expressing the Ctip-S326A mutant polypeptide.

B. RESULTS

B1. The Ctip-S326A knock-in targeting constructs

To knock the S326A missense mutation into the *Ctip* gene of murine ES cells, we produced two targeting constructs: $Ctip^{S326A\text{-}neo}$ and $Ctip^{S326A\text{-}hyg}$. For the $Ctip^{S326A\text{-}neo}$ construct, we introduced the S326A mutation into the coding sequence of exon 11 and a *loxP*-flanked PGK promoter-driven neomycin gene cassette into the adjacent upstream intron (Figure 7B). Additionally, a gene cassette encoding HSV thymidine kinase (HSV-TK) was included in the targeting construct as a negative selection marker. To target cells already carrying neomycin resistance, we also prepared an analogous $Ctip^{S326A\text{-}hyg}$ targeting construct by replacing the *loxP*-flanked neomycin resistance cassette in intron 10 with a *loxP*-flanked hygromycin selection marker (data not shown).

B2. Generation of $Ctip^{S326A}$ mutant ES cells

To assess whether the Brca1-Ctip interaction is required for ES cell viability, we electroporated the $Ctip^{S326A\text{-}hyg}$ targeting construct into neomycin-resistant $Ctip^{+/-}$ ES cells, which are heterozygous for a *Ctip* null allele ($Ctip^{-}$) (unpublished data; Ludwig, Baer, and Efstratiadis) (Section A1 of Chapter II). If the $Ctip^{S326A\text{-}hyg}$ targeting construct recombines with the endogenous $Ctip^{+}$ allele of the heterozygous ES cells, then the resulting cells should solely express Ctip-S326A polypeptides that fail to interact with Brca1. Indeed, Southern analysis of the hygromycin-resistant colonies identified several independent subclones that had undergone homologous recombination at the $Ctip^{+}$ allele to yield $Ctip^{S326A\text{-}hyg/-}$ ES subclones (Figure 8). To excise the hygromycin gene cassette

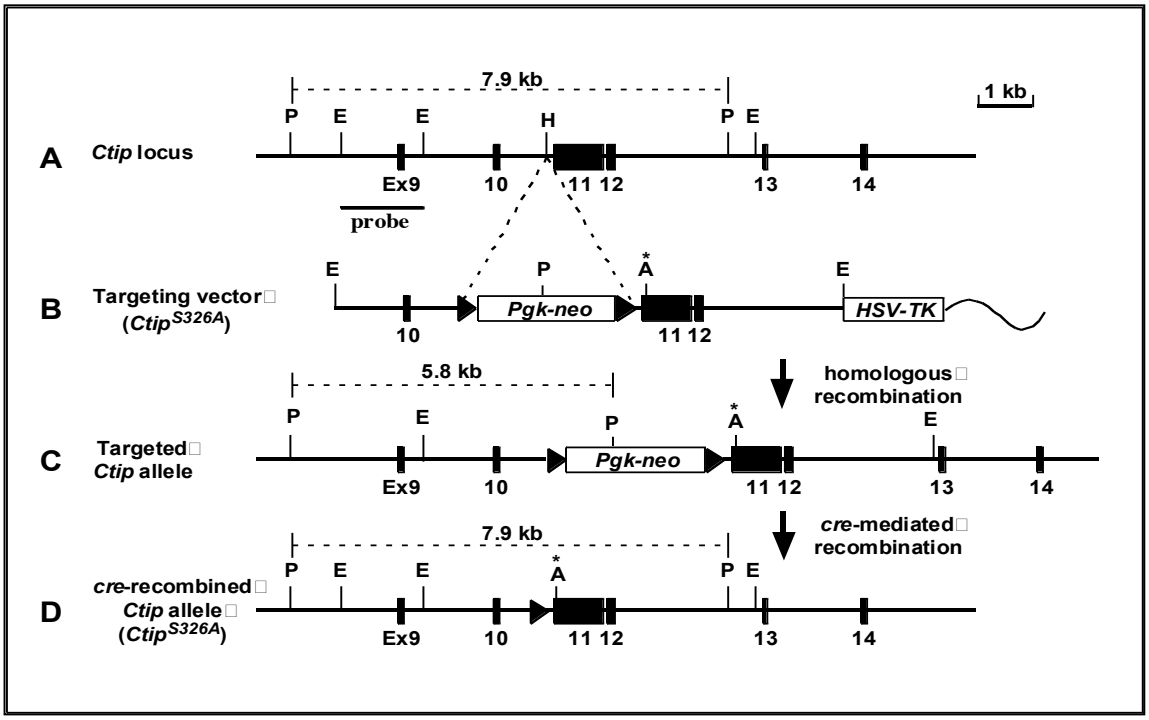

Figure 7. Design of the mutant *Ctip*^{S326A} allele. A map of the wildtype *Ctip* locus encompassing exons 9-14 is shown (A), along with a diagram of the targeting vector (B), and maps of the *Ctip* locus after homologous recombination (*Ctip*$^{S326A\text{-}neo}$) (C) and cre-mediated recombination (*Ctip*^{S326A}) (D). To prepare the targeting vector, a neomycin expression cassette flanked by *loxP* signals (closed triangles) was inserted into the *Hpa*I site of intron 10 and both an *Age*I restriction site and the *Ctip*^{S326A} mutation (asterisk) were introduced into exon 11 by site-directed mutagenesis. The *Pgk* promoter of the expression cassette controls transcription of the *neo* gene. A gene cassette encoding HSV thymidine kinase (HSV-TK) was included as a negative selection marker. The wavy line represents plasmid sequences of the targeting vector. Relevant restriction enzyme sites are: *Pvu*II (P), *Eco*RI (E), *Hpa*I (H), and *Age*I (A). The position of a *Ctip* probe ("*Ctip #6*") for Southern analysis is shown, together with the *Pvu*II fragments recognized by this probe. An analogous *Ctip*$^{S326A\text{-}hyg}$ targeting construct was prepared by replacing the *loxP*-flanked neomycin resistance cassette in intron 10 with a *loxP*-flanked hygromycin selection marker. (Note that the hygromycin gene cassette lacks a *Pvu*II restriction enzyme site).

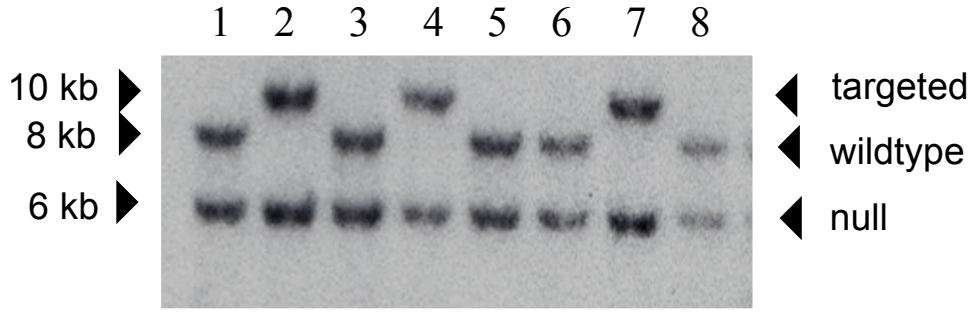

Figure 8. Identification of properly targeted *Ctip*$^{S326A\text{-}hyg/-}$ ES cells. The *Ctip*$^{S326A\text{-}hyg}$ targeting construct was electroporated into neomycin-resistant *Ctip*$^{+/-}$ ES cells, and *Pvu*II-digested genomic DNAs from hygromycin-resistant clones were evaluated by Southern hybridization using a 5' flanking *Ctip* probe ("*Ctip #6*"; Figure 7A). The 10.4 kb *Pvu*II fragment represents the targeted *Ctip* allele, while the 7.9 kb and 6 kb fragments represent the wildtype (*Ctip*$^{+}$) and null (*Ctip*$^{-}$) alleles, respectively. Properly targeted ES clones are seen in lanes 2, 4 and 7.

from the knock-in allele, the targeted ES cells were transiently transfected with the Adeno-cre virus and properly recombined *Ctip*$^{S326A/-}$ ES clones (Figure 7D) were identified by Southern analysis and confirmed by sequence analysis (data not shown). The fact that *Ctip*$^{S326A/-}$ subclones were readily generated indicates that the Brca1-Ctip interaction is not required for the viability of ES cells, despite the fact that Brca1 (McCarthy et al., 2003; Reid et al., 2008) and Ctip (data not shown) are individually required. Thus, the interaction with Brca1 is not essential for all cellular functions of Ctip. The *Ctip*$^{+/-}$ and *Ctip*$^{S326A/-}$ clones, which represent isogenic ES cell lines expressing either wildtype or S326A-mutant Ctip, were then used in our studies of cellular Ctip function (see below).

B3. Generation of Ctip^{S326A} mutant MEFs

To produce isogenic MEF lines that express either wildtype or S326A-mutant Ctip, 129/Sv ES cells were electroporated with the *Ctip*$^{S326A\text{-}neo}$ targeting construct and selected for neomycin-resistance. Genomic DNAs prepared from the surviving drug-resistant ES cell subclones were digested with the *Pvu*II restriction endonuclease and analyzed by Southern blotting with a 5' flanking genomic *Ctip* probe spanning exon 9 ("*Ctip #6*") (Figure 7A). Several independent neomycin-resistant *Ctip*$^{S326A\text{-}neo/+}$ ES cells were identified (Figure 9), and the presence of the S326A mutation was confirmed by sequence analysis (data not shown).

Two independently derived *Ctip*$^{S326A\text{-}neo/+}$ 129/Sv ES clones were then injected into C57BL/6J blastocysts to establish the mutant allele in the mouse germline. Chimeric

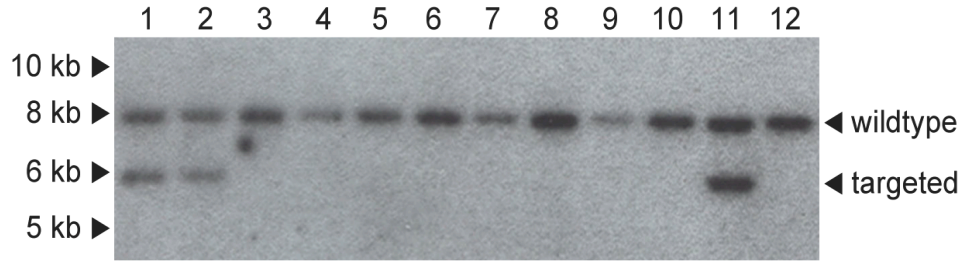

Figure 9. Identification of properly targeted *Ctip*$^{S326A\text{-}neo/+}$ ES cells. 129/Sv ES cells were electroporated with the *Ctip*$^{S326A\text{-}neo}$ targeting construct (Figure 7B), and *Pvu*II-digested genomic DNAs from the neomycin-resistant ES clones were evaluated by Southern hybridization using a 5' flanking *Ctip* probe ("*Ctip #6*"; Figure 7A). The 7.9 kb *Pvu*II fragment represents the wildtype *Ctip* locus (Figure 7A) while the 5.8 kb fragment represents the targeted *Ctip* allele (Figure 7C). Properly targeted ES clones are seen in lanes 1, 2, and 11.

male *Ctip*$^{S326A\text{-}neo/+}$ mice were mated with females carrying a ubiquitously expressed *Cre* transgene driven by the mouse *Rosa26* gene promoter (*Rosa*^{Cre}) (provided by Dr. Thomas Ludwig, Columbia University) to excise the *loxP*-flanked neomycin expression cassette from the targeted allele (Figure 7C) and produce offspring expressing the *Ctip*^{S326A} allele (Figure 7D). Significantly, when heterozygous *Ctip*$^{S326A/+}$ mice were intercrossed, *Ctip*$^{S326A/S326A}$ pups were born at the expected (25%) Mendelian ratio, indicating that the S326A mutation does not appreciably affect embryonic development. For confirmation, pregnant females from this intercross were sacrificed on E13.5 to isolate homozygous *Ctip*$^{S326A/S326A}$ embryos. Unlike animals homozygous for either the *Brca1*- or *Ctip*-null allele, which undergo embryonic lethality prior to gastrulation (precluding the generation of MEFs) (Hakem et al., 1996; Liu et al., 1996; Ludwig et al., 1997; Chen, P.-L. et al., 2005), homozygous *Ctip*$^{S326A/S326A}$ embryos were viable and observed at the expected Mendelian frequency at E13.5 (data not shown). For studies of cellular Ctip functions in MEFs, primary *Ctip*$^{+/+}$, *Ctip*$^{S326A/+}$, and *Ctip*$^{S326A/S326A}$ MEFs were prepared from day E13.5 embryos, and isogenic MEF lines were established by immortalization with Simian virus 40 large-T antigen (Schuermann M., 1990).

B4. The Ctip^{S326A} mutation is sufficient to ablate the Brca1-Ctip interaction

Importantly, the mutant Ctip protein of *Ctip*$^{S326A/S326A}$ MEFs is expressed at normal levels (Figure 10), indicating that the amino acid substitution did not affect the stability of the Ctip protein. Previous studies have shown the corresponding S327A mutation of human CtIP abolishes its association with BRCA1 in human cells (Yu and Chen, 2004). Therefore, we conducted co-immunoprecipitation studies to ascertain whether the mutant

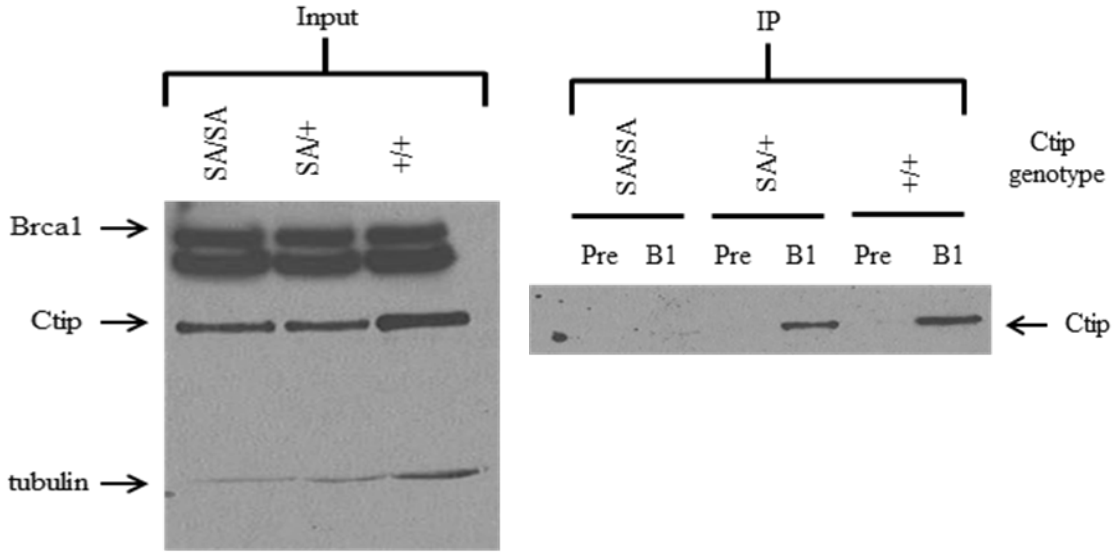

Figure 10. Co-immunoprecipitation of Ctip with a Brca1-specific antibody. Ctip-S326A (SA) polypeptides do not interact with Brca1 *in vivo*. Brca1 and Ctip levels were examined by immunoblotting nuclear extracts of $Ctip^{+/+}$, $Ctip^{SA/+}$ and $Ctip^{SA/SA}$ MEFs (left). Nuclear extracts were also immunoblotted with antibodies specific for α-tubulin as a loading control. Note that a non-specific band runs just below Brca1 in extracts of each genotype. To evaluate the Brca1-Ctip interaction, the extracts were immunoprecipitated with mouse Brca1-specific antiserum (B1) or the corresponding pre-immune serum (Pre) and immunoblotted with CtIP-specific monoclonal antibodies (right). The input (left) represents 6.25% of the protein amount used for immunoprecipitation (right).

Ctip polypeptides of *Ctip*$^{S326A/S326A}$ MEFs interact with murine Brca1. Nuclear extracts of *Ctip*$^{+/+}$, *Ctip*$^{S326A/+}$, and *Ctip*$^{S326A/S326A}$ immortalized MEFs were immunoprecipitated with a mouse Brca1-specific antiserum (B1) or the corresponding pre-immune serum (Pre) and immunoblotted with CtIP-specific monoclonal antibody 14-1 (Yu and Baer, 2000). As shown in Figure 10, Ctip was efficiently co-immunoprecipitated from both wildtype *Ctip*$^{+/+}$ and heterozygous *Ctip*$^{S326A/+}$ MEFs with the Brca1 antiserum. In contrast, Ctip failed to co-immunoprecipitate with Brca1 from homozygous *Ctip*$^{S326A/S326A}$ MEFs (Figure 10), indicating that Ctip-S326A polypeptides do not interact with Brca1 *in vivo*.

B5. The effect of the Brca1-Ctip interaction on gene-targeting efficiency

B5a. *Ctip*^{S326A} *mutant cells are more efficient in gene targeting than control cells*

Given the known requirements for BRCA1 and CtIP individually in homology-directed repair (HDR) (Moynahan et al., 1999; Moynahan et al., 2001; Sartori et al., 2007; Bennardo et al., 2008), we sought to determine whether the BRCA1-CtIP interaction is also required for this process. To do this, we first used gene-targeting assays to measure the ability of isogenic *Ctip*$^{+/-}$ and *Ctip*$^{S326A/-}$ ES cells to homologously integrate exogenous DNA. Although the relationship between homologous integration and HDR is unclear, deficiencies in gene targeting are often attributed to cellular defects in homologous recombination (Moynahan et al., 1999; Snouwaert et al., 1999; Moynahan et al., 2001). To measure homologous integration at the *Pim1* locus, *Ctip*$^{+/-}$ and *Ctip*$^{S326A/-}$ ES cells were electroporated with p59xDR-GFP6, a DNA construct that contains the DR-GFP recombination substrate (described below) and a promoterless

hygromycin-resistance marker flanked by targeting arms comprised of mouse *Pim1* genomic DNA (Moynahan et al., 2001a). After hygromycin selection, the drug-resistant subclones were examined for homologous integration at the *Pim1* locus by Southern analysis (Moynahan et al., 2001a). Surprisingly, *Pim1* targeting was observed in 96% of the hygromycin-resistant $Ctip^{S326A/-}$ clones and 46% of the drug-resistant $Ctip^{+/-}$ clones (Figure 11A; Table 2). A similar two-fold increase in gene-targeting efficiency was also observed in $Ctip^{S326A/-}$ cells electroporated with the Rb-G targeting vector designed for homologous integration at the *Rb* chromosomal locus (Figure 11B; Table 2) (te Riele et al., 1992). Thus, in the absence of the Brca1-Ctip interaction, cells reproducibly display a greater capacity to support homologous integration.

B6. Recombination reporter assays to measure HDR, SSA, and alt-NHEJ

B6a. *The Brca1-Ctip interaction is not required for DSB repair by homology-directed repair (HDR)*

The HDR of DSBs at a defined chromosomal locus was also examined by using an integrated DR-GFP recombination substrate (Pierce et al., 2001). The DR-GFP substrate consists of two defective GFP genes: *Sce*GFP, which contains the cleavage site for the rare-cutting I-*Sce*I endonuclease; and *i*GFP, which lacks the N- and C-terminal coding sequences of GFP. I-*Sce*I endonuclease expression triggers cleavage of *Sce*GFP, resulting in a chromosomal DSB at the I-*Sce*I site. Proficient repair of this DSB by HDR using *i*GFP as a template will generate a functional GFP gene, an event which can be quantified by flow cytometry (Pierce et al., 2001). Since the p59xDR-GFP6 targeting construct contains the DR-GFP substrate, the hygromycin-resistant $Ctip^{+/-}$ and $Ctip^{S326A/-}$

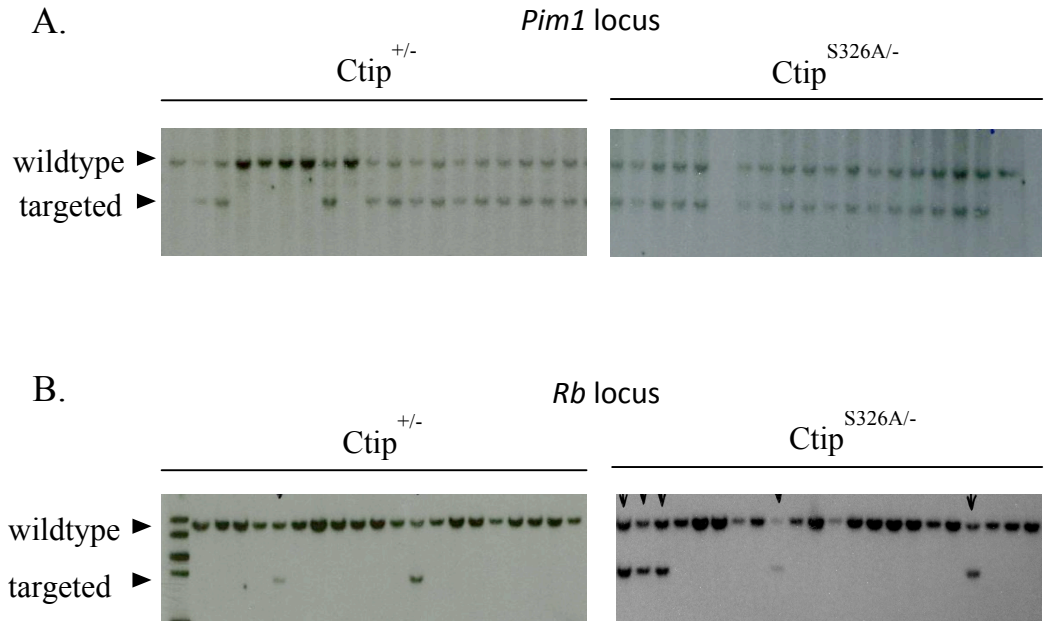

Figure 11. Gene-targeting efficiency of *Ctip*$^{+/-}$ and *Ctip*$^{S326A/-}$ ES cells at the *Pim1* and *Rb* loci. (A) Gene-targeting was measured at the *Pim1* locus by electroporating *Ctip*$^{+/-}$ and *Ctip*$^{S326A/-}$ ES cells with linearized p59xDR-GFP6 targeting vector DNA, selecting for hygromycin resistance, and evaluating the drug-resistant clones for gene targeting by Southern analysis. A 3.6 kb fragment represents the wildtype *Pim1* allele while a 2.4 kb fragment represents the targeted *Pim1* allele. (B) *Ctip*$^{+/-}$ and *Ctip*$^{S326A/-}$ ES cells were also electroporated with linearized Rb-G (Rb-pgkhyg) targeting vector DNA. ES cells were selected with hygromycin and genomic DNA was prepared from the surviving clones for Southern analysis. The wildtype and targeted *Rb* alleles are 9.7 kb and 4.9 kb, respectively.

Table 2. Gene-targeting efficiency of *Ctip*$^{+/-}$ and *Ctip*$^{S326A/-}$ ES cells at the *Pim1* and *Rb* loci.

	Targeting construct	
ES cells	Pim1, p59xDR-GFP6	Rb , G
Ctip$^{+/-}$	46%, 44/96	7.9%, 15/189
Ctip$^{S326A/-}$	96%, 90/94	15.3%, 29/189

Gene-targeting efficiencies were determined by Southern analysis for the *Pim1* and *Rb* loci. Number of targeted clones/total analyzed.

subclones that arose upon homologous integration of this construct (Figure 11A; Table 2) possess the DR-GFP substrate at identical positions in the *Pim1* locus.

To measure HDR of an induced chromosomal DSB, $Ctip^{+/-}$ *DR-GFP* and $Ctip^{S326A/-}$ *DR-GFP* subclones were evaluated for the appearance of GFP-positive cells after transient transfection with an expression vector encoding the I-*Sce*I endonuclease (pCβASce). In the absence of I-*Sce*I expression, GFP-positive cells were seldom detected (<0.02%) in cell lines of either Ctip genotype (Figure 12), indicating that spontaneous intrachromosomal gene conversion is rare. As expected, I-*Sce*I expression induced the HDR of chromosomal DSBs within the integrated DR-GFP substrate in control $Ctip^{+/-}$ ES cells, as reflected by the increased percentage of GFP-positive cells (2.4%-2.74%) (Figure 12, A and B). Surprisingly, I-*Sce*I expression induced similar proportions of $Ctip^{S326A/-}$ GFP-positive cells (2.13%-2.26%) (Figure 12, C and D), suggesting that the Brca1-Ctip interaction is not required for proficient HDR. Consistent with previous reports (Moynahan et al., 1999; Snouwaert et al., 1999; Moynahan et al., 2001), a subclone of the Brca1-null ES cell line 236.44 ($Brca1^{\Delta 223\text{-}763/\Delta 223\text{-}763}$) with the DR-GFP substrate integrated at the same position in the *Pim1* locus, displayed significantly reduced HDR efficiency (0.64%) (Figure 12E). Thus, as with gene targeting, HDR of an induced chromosomal break is not diminished in $Ctip^{S326A/-}$ ES cells. Although Brca1 and, more specifically, its BRCT phospho-recognition binding property are required for HDR of chromosomal DNA breaks (Moynahan et al., 1999; Moynahan et al., 2001; Shakya et al., 2011), the Brca1-Ctip interaction appears to be dispensable. Furthermore, since HDR of a DSB is dependent on DNA resection, these results suggest that the Brca1-Ctip interaction is not essential for resection of DSB ends.

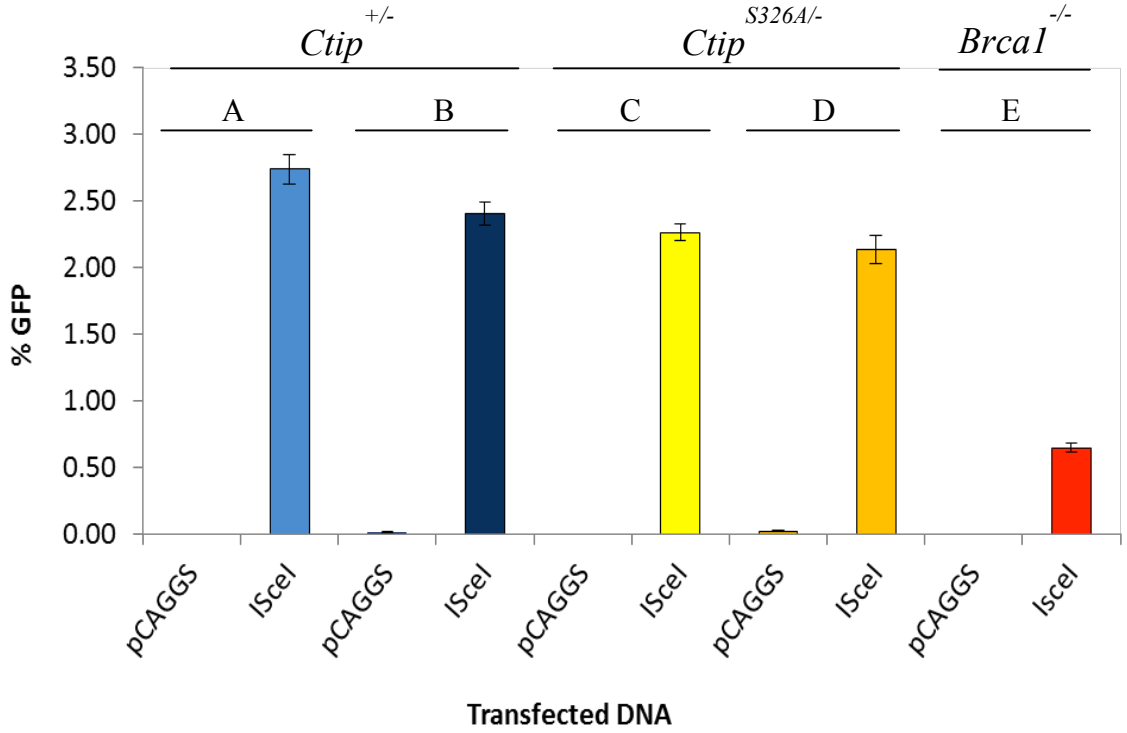

Figure 12. Cells lacking the Brca1-Ctip interaction are proficient for HDR of DSBs. Several control *Ctip*$^{+/-}$ (clones A and B) and mutant *Ctip*$^{S326A/-}$ (clones C and D) ES subclones containing the direct repeat-green fluorescent protein (DR-GFP) substrate integrated into the *Pim1* locus were transfected with either an I-*Sce*I expression vector or empty vector (pCAGGS). GFP-positive cells were rarely generated on transfection with the empty vector. In contrast, I-*Sce*I expression strongly induced the proportion of GFP-positive *Ctip*$^{+/-}$ cells (clones A and B) and *Ctip*$^{S326A/-}$ cells (clones C and D), indicating efficient homology-directed repair (HDR). Additionally, a subclone of the Brca1-mutant ES cell line 236.44 (*Brca1*$^{\Delta 223\text{-}763/\Delta 223\text{-}763}$) with the DR-GFP substrate integrated at the same position in the *Pim1* locus, denoted here as *Brca1*$^{-/-}$ (clone E), was used as a control since it is known to be deficient in HDR (Moynahan et al., 1999). Each ES subclone was assayed in triplicate with three independent transfections, and the error bars represent SE of the mean. Similar results were also observed in separate experiments using additional independently-derived *Ctip*$^{+/-}$ and *Ctip*$^{S326A/-}$ ES subclones.

B6b. *The Brca1-Ctip interaction is not required for DSB repair by single-strand annealing (SSA)*

Single-strand annealing (SSA) is another DSB repair pathway initiated by DNA resection. In the SSA pathway, complementary sequences (>30 bp) within the ssDNA overhangs of both DSB ends anneal with one another, allowing ligation of the ends and deletion of the intervening sequences (Stark et al., 2004; Bennardo et al., 2008; McVey and Lee, 2008; Huertas, P., 2010). Although both BRCA1 and CtIP promote SSA of DSBs (Stark et al., 2004; Bennardo et al., 2008), it is unclear whether the BRCA1-CtIP interaction is required for this repair pathway. To explore this possibility, isogenic $Ctip^{+/-}$ and $Ctip^{S326A/-}$ ES cells were electroporated with the hprtSAGFP targeting construct (Stark et al., 2004), and subclones that carry an SA-GFP recombination substrate integrated into the *Hprt* locus were derived.

Like the DR-GFP recombination substrate, the SA-GFP substrate consists of two non-functional GFP fragments (5'GFP and *Sce*GFP3') (Stark et al., 2004). A DSB triggered by I-*Sce*I cleavage of *Sce*GFP3' can be repaired by SSA when a DNA strand from *Sce*GFP3' anneals to the complementary strand of 5'GFP, resulting in formation of a functional GFP gene and deletion of the intervening sequence (Stark et al., 2004). Importantly, HDR of the SA-GFP reporter does not restore a functional GFP gene (Stark et al., 2004); therefore, GFP positive products are specifically produced by SSA. In addition to the SA-GFP reporter, the hprtSAGFP targeting construct also has homology to the *Hprt* locus and contains a puromycin resistance marker (Stark et al., 2004). Upon proper integration of the hprtSAGFP targeting construct into $Ctip^{+/-}$ and $Ctip^{S326A/-}$ ES cells, the *Hprt* gene is inactivated, rendering the cells resistant to the nucleotide analog 6-

thioguanine (6-TG) (Stark et al., 2004; Pierce et al., 2001). Therefore, only correctly targeted clones should be resistant to both puromycin and 6-TG. We prepared genomic DNA from the doubly-resistant ES clones for Southern analysis and identified multiple *Ctip*$^{+/-}$ *SA-GFP* and *Ctip*$^{S326A/-}$ *SA-GFP* reporter ES subclones (data not shown).

To analyze the SSA efficiency of *Ctip*$^{+/-}$ and *Ctip*$^{S326A/-}$ ES subclones bearing the integrated SA-GFP substrate, we transiently transfected these cells with an I-*Sce*I expression vector (pCβASce) or the empty vector (pCAGGS) alone. The experiments were performed in triplicate with three independent transfections and all cells were examined 72 hours post-transfection by flow cytometry. Very few GFP-positive cells were detected (< 0.01%) in any of the cell lines in the absence of I-*Sce*I expression (Figure 13). After transfection with the I-*Sce*I expression vector, however, GFP-positive cells were readily detected in both *Ctip*$^{+/-}$ (0.76%-1.13%) and *Ctip*$^{S326A/-}$ (1.07%-1.40%) cells (Figure 13, A-E). Thus, although Brca1 and Ctip are both essential for SSA at chromosomal DSBs (Stark et al., 2004; Bennardo et al., 2008), the Brca1-Ctip interaction appears to be dispensable for this mode of DSB repair.

B6c. *The Brca1-Ctip interaction is not required for DSB repair by alternative non-homologous end joining (alt-NHEJ)*

Unlike HDR and SSA, non-homologous end joining (NHEJ) ligates DSB ends without a requirement for extensive sequence homology (reviewed in Haber, J. E., 2000; Karran, P., 2000). NHEJ appears to be comprised of two subpathways: classical-NHEJ and alternative-NHEJ (alt-NHEJ) (Bennardo et al., 2008; McVey and Lee, 2008). Classical-NHEJ results in little or no processing of the DSB ends for repair and requires several

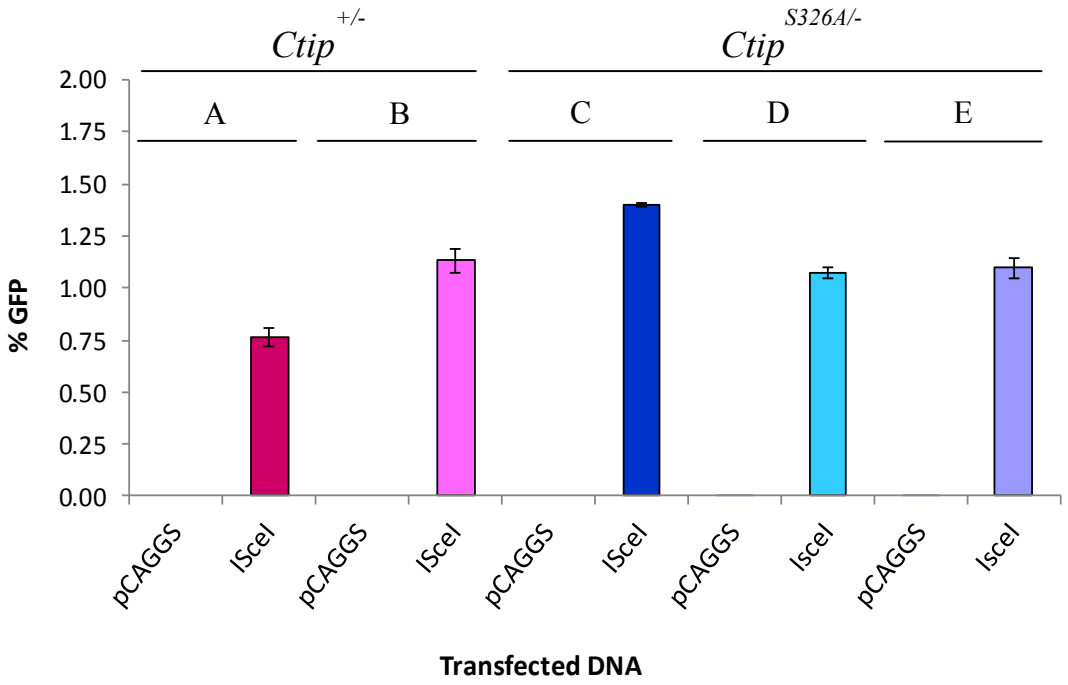

Figure 13. Cells lacking the Brca1-Ctip interaction are proficient for SSA of DSBs. Several control *Ctip*$^{+/-}$ (clones A and B) and mutant *Ctip*$^{S326A/-}$ (clones C to E) ES subclones containing the SA-GFP reporter substrate integrated into the *Hprt* locus were transfected with either an I-*Sce*I expression vector or empty vector (pCAGGS). GFP-positive cells were rarely generated on transfection with the empty vector. I-*Sce*I expression induced a similar number of GFP-positive *Ctip*$^{+/-}$ cells (clones A and B) and *Ctip*$^{S326A/-}$ cells (clones C to E). Thus, the Brca1-Ctip interaction is not required for DSB repair by single-strand annealing (SSA). Each ES subclone was assayed in triplicate with three independent transfections, and the error bars represent SE of the mean.

key NHEJ factors, including the Ku70/80 (Ku) heterodimer, XRCC4, DNA Ligase IV and DNA-PKcs (reviewed in Haber, J. E., 2000; Karran, P., 2000). In contrast, alt-NHEJ is independent of these factors. Instead, alt-NHEJ appears to be mediated by the annealing of short homology stretches or microhomologies (usually 2-3 bp) which are exposed at the DSB ends by DNA resection (Bennardo et al., 2008; McVey and Lee, 2008, Huertas, P., 2010). Thus, like HDR and SSA, alt-NHEJ is suppressed by Ku binding and promoted by CtIP-mediated DSB end resection (Bennardo et al., 2008).

To examine whether the BRCA1-CtIP interaction is required for alt-NHEJ, we electroporated isogenic $Ctip^{+/-}$ and $Ctip^{S326A/-}$ ES cells with the pim-EJ2-GFP-hyg targeting vector, which contains the EJ2-GFP recombination substrate and genomic sequences for targeting the *Pim1* locus. The EJ2-GFP reporter consists of an N-terminal tag fused to GFP which is disrupted by an 8 nucleotide microhomology repeat that flanks an I-*Sce*I site and an in-frame stop codon (Bennardo et al., 2008). If alt-NHEJ occurs by annealing of the microhomology repeats, the intervening 35 nucleotide sequence is deleted, the coding frame between the N-terminal tag and GFP is restored, and a functional *GFP*-positive gene is reconstructed (Bennardo et al., 2008). Following electroporation with the pim-EJ2-GFP-hyg targeting vector, $Ctip^{+/-}$ and $Ctip^{S326A/-}$ ES cells were selected with hygromycin and DNA was prepared from the surviving colonies. Southern analysis revealed proper homologous integration of the EJ2-GFP reporter into the mouse *Pim1* locus of several $Ctip^{+/-}$ and $Ctip^{S326A/-}$ ES subclones (data not shown).

To measure alt-NHEJ of an induced chromosomal DSB, $Ctip^{+/-}$ *EJ2-GFP* and $Ctip^{S326A/-}$ *EJ2-GFP* subclones were transiently transfected with an expression vector

encoding I-*Sce*I and evaluated for the appearance of GFP-positive cells by flow cytometry. GFP expression as a result of spontaneous intrachromosomal gene conversion events was rare, as very few GFP-positive cells were detected (< 0.05%) in $Ctip^{+/-}$ and $Ctip^{S326A/-}$ ES clones transfected with the empty vector (Figure 14). Following transfection with the I-*Sce*I expression vector, $Ctip^{+/-}$ and $Ctip^{S326A/-}$ ES clones exhibited a comparable percentage of GFP-positive cells, 0.64%-0.71% and 0.62%-0.64%, respectively (Figure 14, A-D). Thus, as with the other resection-dependent repair pathways (HDR and SSA), the Brca1-Ctip interaction appears to be dispensable for alt-NHEJ repair of chromosomal DSBs.

B7. Immunofluorescent analyses of nuclear recombination foci

B7a. *The Brca1-Ctip interaction is not required for Ctip, Brca1, RPA or Rad51 focus formation in S-phase and IR-treated cells*

In cells subjected to ionizing radiation (IR), protein accumulation at sites of DNA damage can take the form of cytologically discernible foci, as observed for the repair proteins CtIP, BRCA1, RPA, and Rad51 (Haaf et al., 1995; Scully et al., 1997b; Choudhary and Li, 2002; Yu et al., 2006; Sartori et al., 2007). The formation of IR-induced foci (IRIFs) of CtIP, which can be visualized by immunofluorescent microscopy, may reflect the role of CtIP in resection of DSB ends (Yu et al., 2006; Sartori et al., 2007; You et al., 2009). In human cells, CtIP localization to IRIFs appears to require the BRCA1-CtIP interaction, as CtIP IRIFs fail to form in HCC1937 cells, which express a C-terminally truncated BRCA1 polypeptide that lacks the BRCT repeat, or in 293T cells transfected with an exogenous S327A-mutant CtIP that cannot bind BRCA1 (Yu et al.,

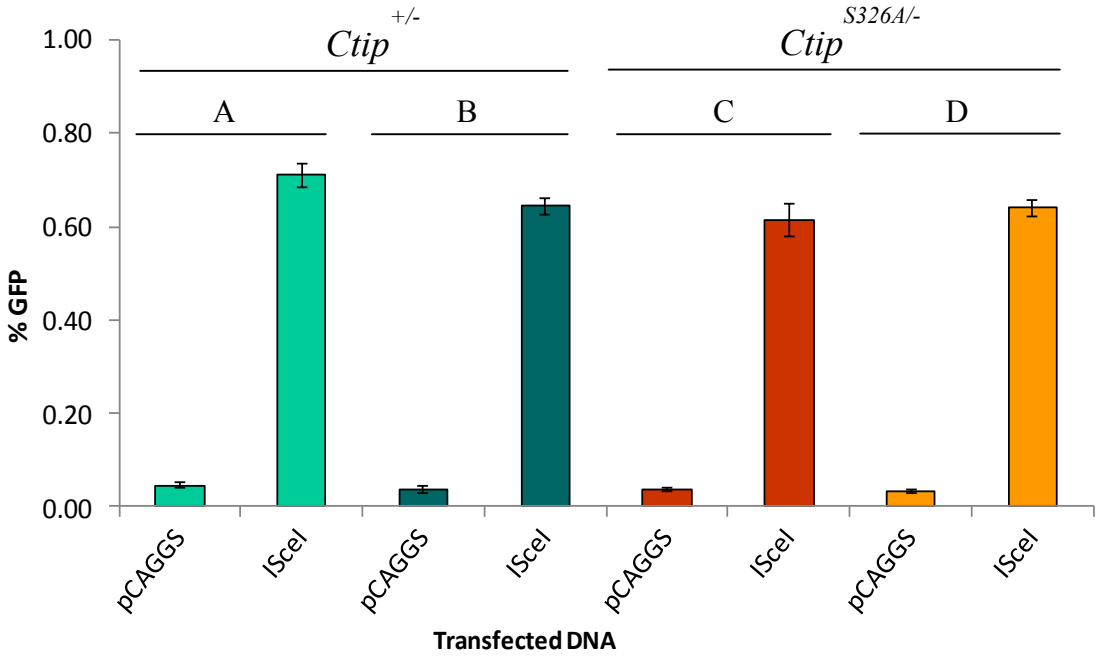

Figure 14. Cells lacking the Brca1-Ctip interaction are proficient for alt-NHEJ of DSBs. Several control *Ctip*$^{+/-}$ (clones A and B) and mutant *Ctip*$^{S326A/-}$ (clones C and D) ES subclones containing the EJ2-GFP reporter substrate integrated into the *Pim1* locus were transfected with either an I-*Sce*I expression vector or empty vector (pCAGGS). Very few GFP-positive cells were detected in *Ctip*$^{+/-}$ and *Ctip*$^{S326A/-}$ ES clones following transfection with the empty vector. I-*Sce*I expression induced a similar number of GFP-positive cells in both *Ctip*$^{+/-}$ cells (clones A and B) and *Ctip*$^{S326A/-}$ cells (clones C and D) indicating efficient alternative non-homologous end joining (alt-NHEJ). Each ES subclone was assayed in triplicate with three independent transfections, and the error bars represent SE of the mean. Similar results were also observed in separate experiments using additional independently-derived *Ctip*$^{+/-}$ and *Ctip*$^{S326A/-}$ ES subclones.

2006). In contrast, however, we observed comparable recruitment of Ctip to IRIFs in *Ctip*$^{S326A/S326A}$ and *Ctip*$^{+/+}$ immortalized MEFs (Figure 15). This result is consistent with our data showing that resection-dependent repair (i.e., HDR, SSA, and alt-NHEJ) is proficient in *Ctip*$^{S326A/-}$ ES cells (Figures 12-14). Thus, the Brca1-Ctip interaction is not required for recruitment of Ctip to sites of DNA damage in murine cells. Moreover, Ctip recruitment to the S-phase nuclear foci of unstressed cells also appears to be unaffected by the S326A mutation (Figure 15). This result is consistent with published data that amino acid residues 505-546 of CtIP are necessary and sufficient for targeting CtIP to S-phase replication foci in human cells (Gu and Chen, 2009).

Similarly, we observed comparable recruitment of Brca1 polypeptides to both S-phase nuclear foci and IRIFs in *Ctip*$^{+/+}$ and *Ctip*$^{S326A/S326A}$ MEFs (Figure 16). This result is consistent with the normal BRCA1 focus formation reported for human cells expressing S327A-mutant Flag-tagged CtIP (Yu et al., 2006). Therefore, although the BRCT phosphopeptide binding property of Brca1 is required for proper formation of Brca1 foci after DNA damage (Shakya et al., 2011), Brca1's interaction with the BRCT phospho-ligand Ctip is not essential for Brca1 localization. Instead, BRCA1 recruitment is reported to require its BRCT phospho-dependent interaction with the Abraxas/RAP80 complex, as cells bearing the Abraxas-S406A mutation, which ablates the BRCA1-Abraxas interaction, fail to target BRCA1 to sites of DNA damage (Kim et al., 2007; Kim et al., 2007a; Liu, Z. et al., 2007; Sobhian et al., 2007; Wang et al., 2007; Wang and Elledge, 2007).

A.

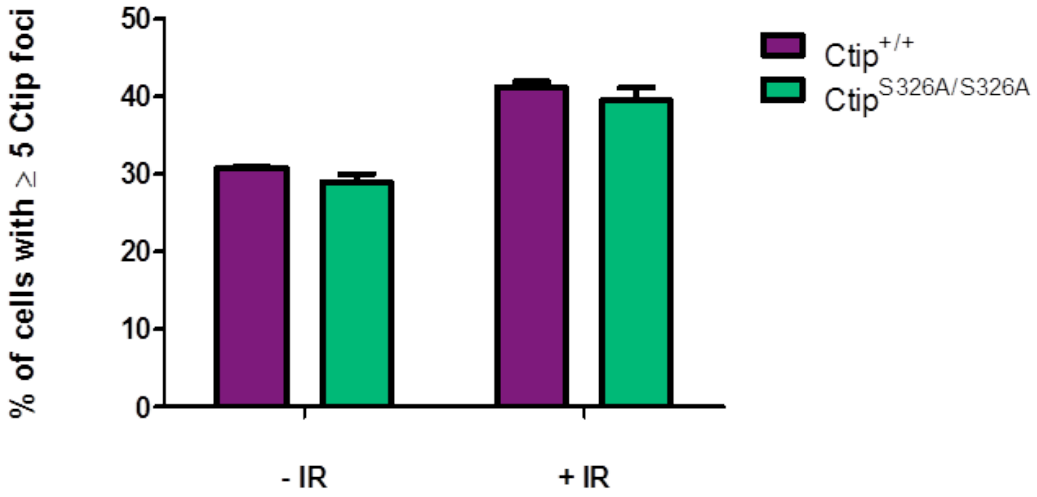

B.

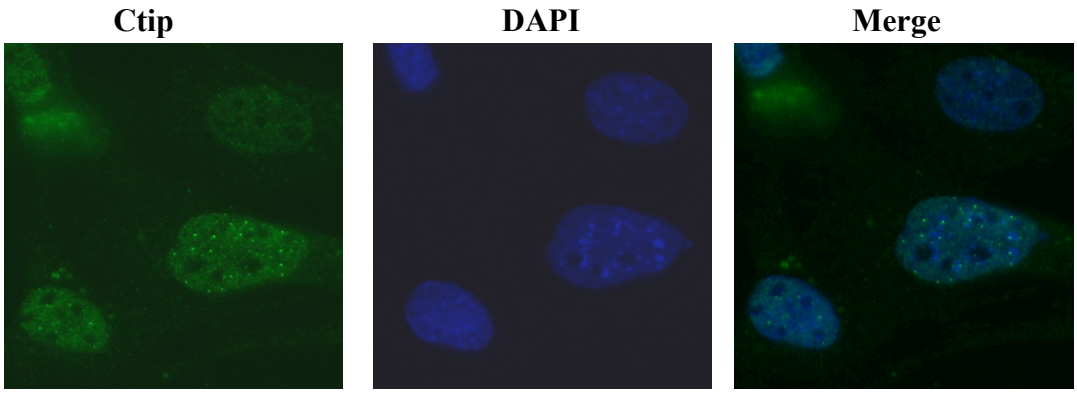

Figure 15. Proper Ctip focus formation in the absence of the Brca1-Ctip interaction. (A) *Ctip*$^{+/+}$ and *Ctip*$^{S326A/S326A}$ immortalized MEFs were either untreated to assess S-phase focus formation or exposed to IR (10 Gy) to assess IRIF formation. Immunostaining with CtIP-specific antibodies occurred 1 hour post-irradiation. Ctip-containing S-phase foci and IRIFs were counted in 300 cells of two independent MEF lines for each genotype, and the error bars represent SE of the mean. Ctip S-phase foci and IRIF formation was comparable in *Ctip*$^{+/+}$ and *Ctip*$^{S326A/S326A}$ MEFs. (B) Representative image of Ctip mobilization to IRIFs in *Ctip*$^{S326A/S326A}$ MEFs. 4', 6-diamidino-2-phenylindole (DAPI) was used for nuclear staining.

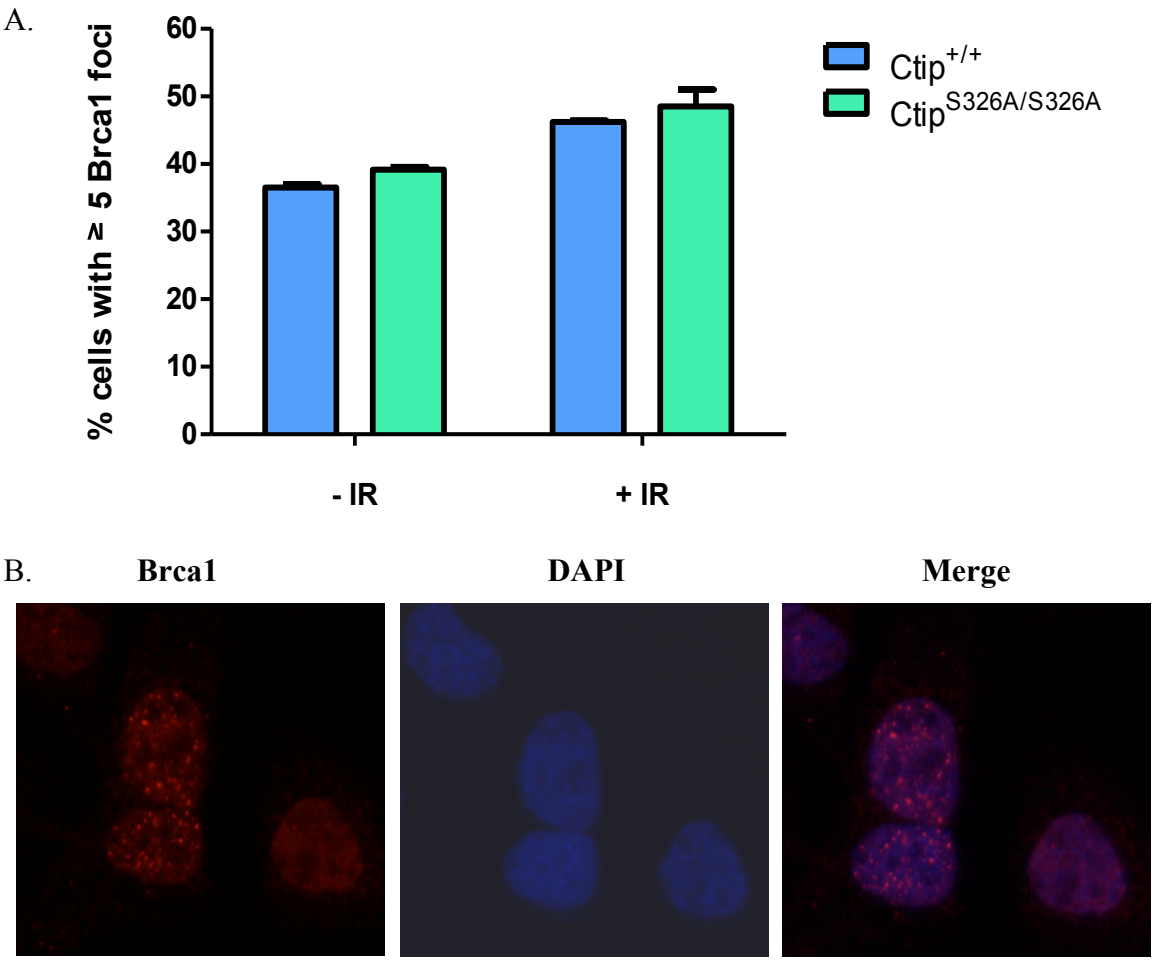

Figure 16. Proper Brca1 focus formation in the absence of the Brca1-Ctip interaction. *Ctip*$^{+/+}$ and *Ctip*$^{S326A/S326A}$ immortalized MEFs were either untreated to assess S-phase focus formation or exposed to IR (10 Gy) to assess IRIF formation. The cells were immunostained at 1 hour post-irradiation with a mouse-specific Brca1 antibody. Brca1-containing S-phase foci and IRIFs were counted in 300 cells of two independent MEF lines for each genotype, and the error bars represent SE of the mean. Brca1 was efficiently recruited to the S-phase foci and IRIFs in *Ctip*$^{S326A/S326A}$ MEFs, indicating that the Brca1-Ctip interaction is dispensable for Brca1 focus formation. (B) Representative image of Brca1 mobilization to IRIFs in *Ctip*$^{S326A/S326A}$ MEFs. 4', 6-diamidino-2-phenylindole (DAPI) was used for nuclear staining.

The role of BRCA1, once at sites of DNA damage, remains unclear. One attractive notion, given that BRCA1, CtIP, and MRN form a discrete protein complex *in vivo* (BRCA1 complex C), is that BRCA1 is required for the DNA resection activities ascribed to CtIP and MRN (Greenberg et al., 2006; Chen et al., 2008). Of note, efficient association of BRCA1 with MRN appears to require the BRCA1-CtIP interaction (Chen et al., 2008). To determine whether the BRCA1-CtIP interaction is essential for DNA resection, we examined RPA focus formation in isogenic $Ctip^{+/+}$ and $Ctip^{S326A/S326A}$ immortalized MEFs. Upon DNA resection, RPA is rapidly loaded onto the nascent single-stranded DNA (ssDNA), an event which can be observed cytologically by the formation of nuclear foci that stain with RPA-specific antibodies. By immunofluorescent microscopy, we observed indistinguishable levels of RPA-staining of S-phase foci and IRIFs in both $Ctip^{S326A/S326A}$ and $Ctip^{+/+}$ MEFs (Figure 17). This result suggests that the Brca1-Ctip interaction is dispensable for DNA resection, and that CtIP and MRN likely mediate DNA resection independently of BRCA1. This observation is also consistent with the fact that resection-dependent repair (i.e., HDR, SSA, and alt-NHEJ) is proficient in $Ctip^{S326A/-}$ ES cells (Figures 12-14).

We also examined the effect of the Ctip-S326A mutation on localization of the recombination protein Rad51. At chromosomal breaks, Rad51 can displace RPA from resected ssDNA tails to form a nucleoprotein filament that mediates the search for a homologous DNA template. A requirement for the BRCT phosphopeptide binding property of BRCA1 in this process was established by the fact that Rad51 accumulation into IRIFs is dramatically reduced in $Brca1^{S1598F/S1598F}$ MEFs relative to isogenic

A.

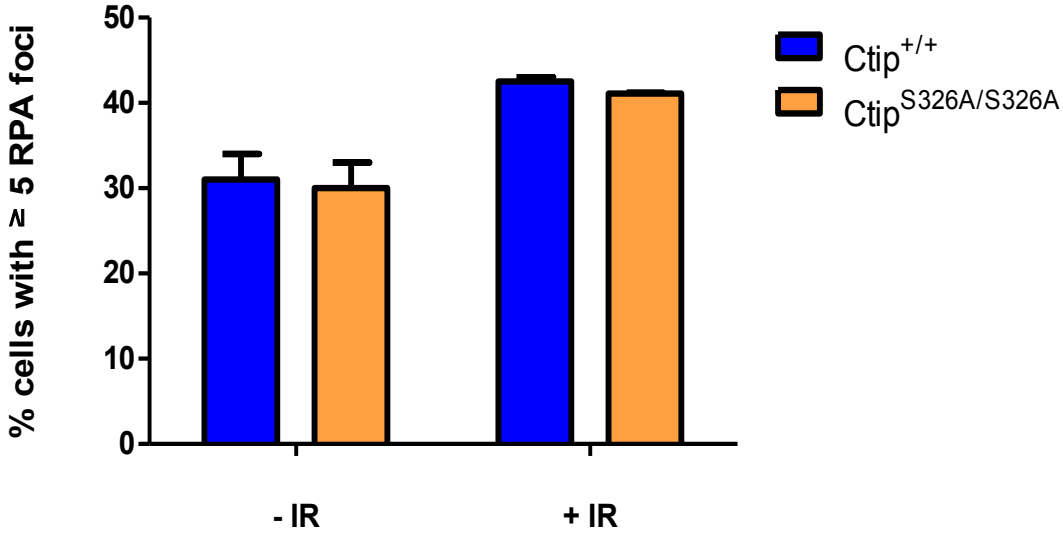

B.

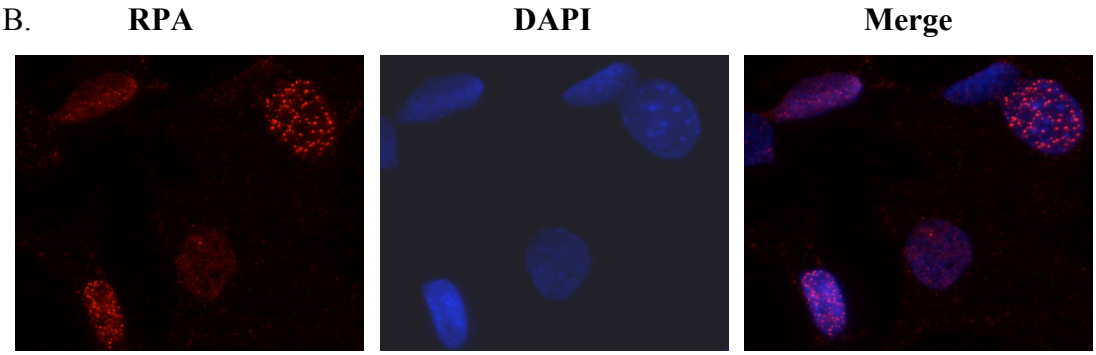

Figure 17. Proper RPA focus formation in the absence of the Brca1-Ctip interaction. *Ctip*$^{+/+}$ and *Ctip*$^{S326A/S326A}$ immortalized MEFs were either untreated to assess S-phase focus formation or exposed to IR (10 Gy) to assess IRIF formation. Foci formation was assessed 1 hour post-irradiation by immunostaining with RPA-specific antibodies. RPA-containing S-phase foci and IRIFs were counted in 300 nuclei of two independent MEF lines for each genotype, and the error bars represent SE of the mean. RPA S-phase foci and IRIF formation was comparable in *Ctip*$^{+/+}$ and *Ctip*$^{S326A/S326A}$ MEFs; thus, the Brca1-Ctip interaction is not required for RPA recruitment to sites of DNA damage. (B) Representative image of RPA mobilization to IRIFs in *Ctip*$^{S326A/S326A}$ MEFs. 4', 6-diamidino-2-phenylindole (DAPI) was used for nuclear staining.

Brca1$^{+/+}$ MEFs (Shakya et al., 2011). To determine whether the Brca1-Ctip interaction is required for proper Rad51 recruitment, we compared the assembly of Rad51 in the S-phase foci and IRIFs of *Ctip*$^{+/+}$ and *Ctip*$^{S326A/S326A}$ immortalized MEFs. As shown in Figure 18, the levels of Rad51-staining S-phase foci and IRIFs were comparable in MEFs expressing either the wildtype or S326A-mutant Ctip polypeptide. Thus, Rad51 recruitment to sites of DNA damage, a key step in DSB repair by homologous recombination, depends on the BRCT phospho-recognition property of Brca1, but not its interaction with the phospho-ligand Ctip.

B8. Clonogenic survival

B8a. *Ctip*^{S326A} *mutant cells are resistant to MMC-induced genotoxic stress*

In clonogenic survival assays, cells lacking the BRCT phosphopeptide binding property of Brca1 (*Brca1*$^{S1598F/S1598F}$) are hypersensitive to mitomycin C (MMC), a DNA cross-linking agent that can potentiate DSB formation (Shakya et al., 2011). To ascertain whether Brca1's interaction with the BRCT phospho-ligand Ctip mediates its cellular resistance to MMC, we used a clonogenicity assay to evaluate the response of isogenic *Ctip*$^{+/-}$ and *Ctip*$^{S326A/-}$ ES cells to this genotoxic agent. As shown in Figure 19, the MMC survival curves of two *Ctip*$^{S326A/-}$ ES clones completely overlap with those of the *Ctip*$^{+/-}$ and *Brca1*$^{+/-}$ control cells. In parallel, we also analyzed homozygous *Brca1*-null ES cells (*Brca1*$^{\Delta 223\text{-}763/\Delta 223\text{-}763}$). In accord with published data (Moynahan et al., 2001; Reid et al., 2008), we found that these cells, unlike *Ctip*$^{S326A/-}$ cells, display a pronounced hypersensitivity to MMC (Figure 19). Thus, the Brca1-Ctip interaction is not required for Brca1-mediated MMC resistance.

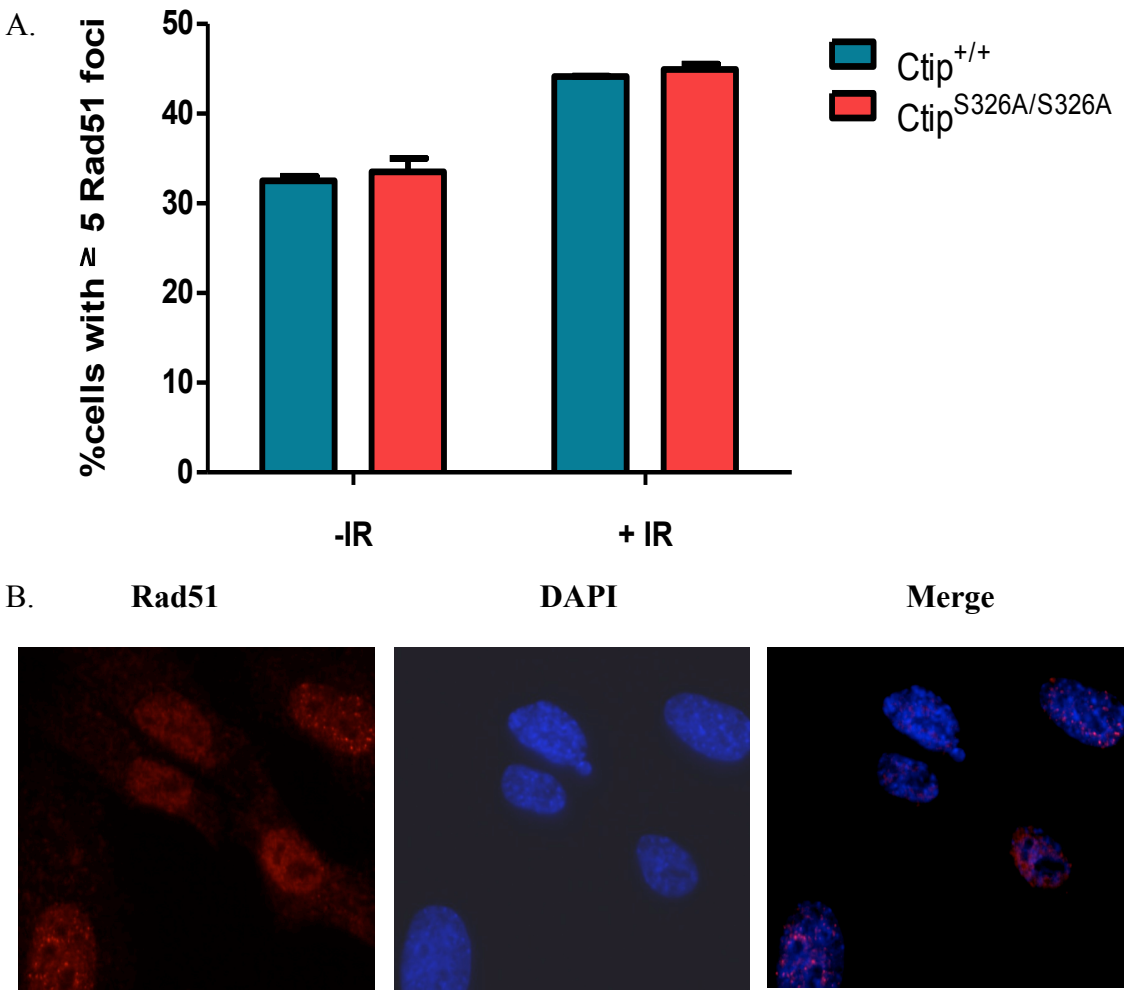

Figure 18. Proper Rad51 focus formation in the absence of the Brca1-Ctip interaction. *Ctip*$^{+/+}$ and *Ctip*$^{S326A/S326A}$ immortalized MEFs were either untreated to assess S-phase focus formation or exposed to IR (10 Gy) to assess IRIF formation. Foci formation was assessed 1 hour later by immunostaining with Rad51-specific antibodies. Rad51-containing S-phase foci and IRIFs were counted in 300 nuclei of two independent MEF lines for each genotype, and the error bars represent SE of the mean. The levels of Rad51-staining S-phase foci and IRIFs were comparable in MEFs expressing either the wildtype or Ctip-S326A mutant polypeptides. (B) Representative image of Rad51 mobilization to IRIFs in *Ctip*$^{S326A/S326A}$ MEFs. 4', 6-diamidino-2-phenylindole (DAPI) was used for nuclear staining.

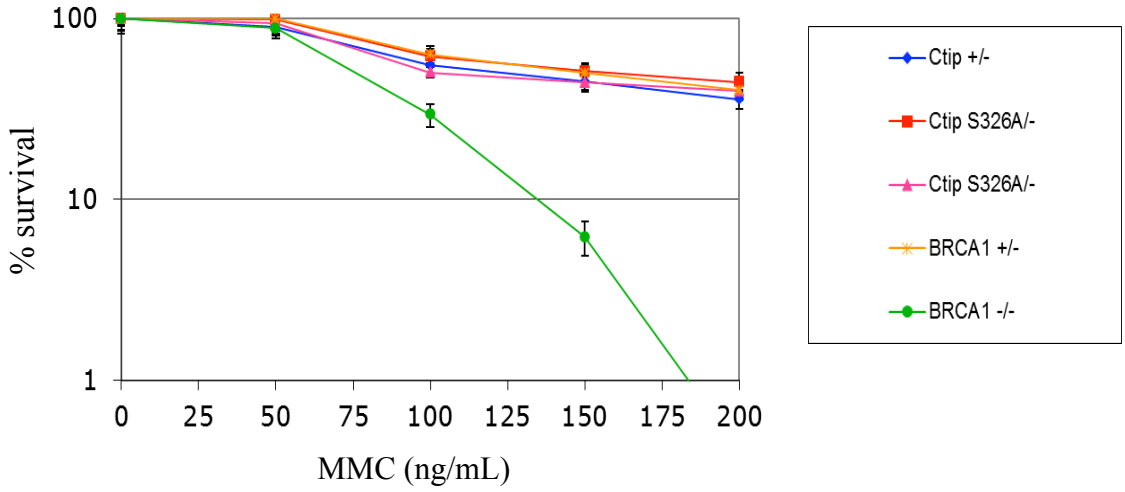

Figure 19. *Ctip*$^{S326A/-}$ ES cells are resistant to MMC-induced genotoxic stress. Isogenic *Ctip*$^{+/-}$ and *Ctip*$^{S326A/-}$ ES cells were examined for mitomycin C (MMC) sensitivity in clonogenic survival assays, together with ES cells homozygous for the hypomorphic *Brca1*$^{\Delta 223\text{-}763}$ mutation (denoted here as *Brca1*$^{-/-}$), and control ES cells (*Brca1*$^{+/-}$). Cells were plated and treated with various concentrations of MMC for 4 hours. After 7-9 days, the surviving colonies were stained with Crystal violet and counted. Survival is calculated as a percentage of colonies in the mock-treated plates. Each subclone was tested in triplicate, and the error bars represent the SE of the mean of survival for each subclone. Similar results were also observed in separate experiments using additional independently-derived *Ctip*$^{+/-}$ and *Ctip*$^{S326A/-}$ ES subclones.

B8b. *Ctip^{S326A} mutant cells are slightly sensitive to camptothecin and etoposide*

Additionally, we investigated the role of the Brca1-Ctip interaction in the cellular response to the topoisomerase I inhibitor camptothecin (CPT) and the topoisomerase II inhibitor etoposide (ETO). CPT and ETO stabilize their respective Topo-cleavage complexes by preventing DNA religation, thereby inducing DSBs predominantly in S-phase (for CPT) or throughout the cell cycle (for ETO) (Pommier, Y., 2006; Sartori et al., 2007; Nitiss, J. L., 2009; Nakamura et al., 2010). Importantly, repair of CPT- and ETO-induced DSBs requires removal of the covalently-bound polypeptides from the DNA ends (Nakamura et al., 2010). Since cellular resistance to CPT and ETO depends on some aspect of CtIP function (Sartori et al., 2007), we assessed whether the Brca1-Ctip interaction is required for resistance to these topoisomerase inhibitors.

To this end, *Ctip$^{+/-}$* and *Ctip$^{S326A/-}$* ES clones were exposed for 24 hours to varying doses of CPT and ETO and allowed to recover for 7-9 days. As shown in Figure 20A, two independent *Ctip$^{S326A/-}$* ES clones exhibit slight sensitivity to the topoisomerase I inhibitor CPT relative to control *Ctip$^{+/-}$* cells. For both mutant clones, the apparent difference in sensitivity is only observed at the two highest CPT doses (Figure 20A). Similarly, although we observe clonal variation, in response to the topoisomerase II inhibitor ETO, *Ctip$^{S326A/-}$* cells display a slight decrease in survival compared to control *Ctip$^{+/-}$* cells (Figure 20B). In contrast, ES cells homozygous for the *Brca1$^{\Delta 223-763}$* hypomorphic allele show significant hypersensitivity to CPT (Figure 20A) and a modest sensitivity to ETO (Figure 20B). These results suggest that the Brca1-Ctip interaction is

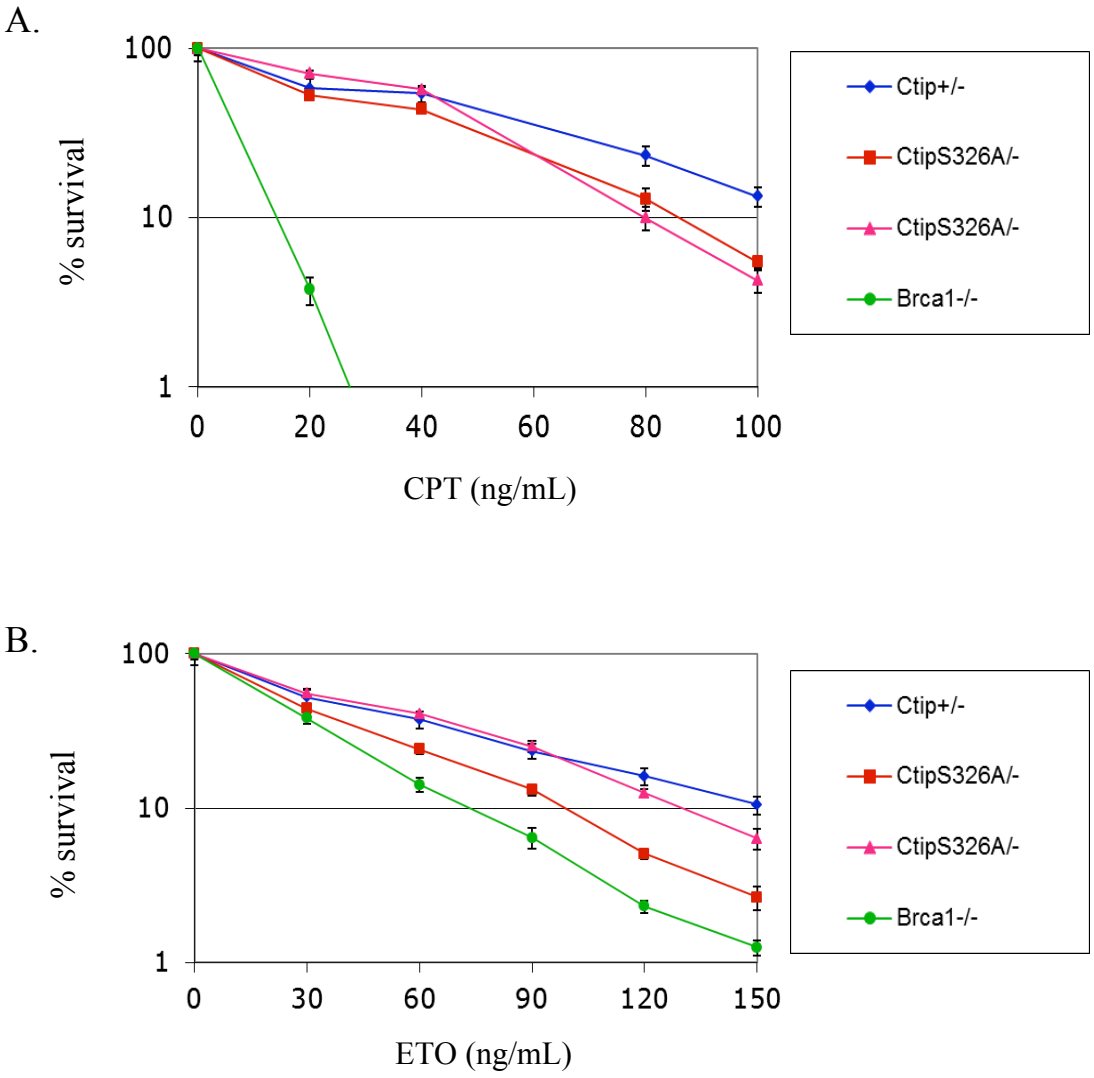

Figure 20. ***Ctip*$^{S326A/-}$ ES cells are slightly sensitive to CPT- and ETO-induced genotoxic stress.** *Ctip*$^{+/-}$ and *Ctip*$^{S326A/-}$ ES cells were examined for (A) camptothecin (CPT) and (B) etoposide (ETO) sensitivity in clonogenic survival assays, together with ES cells homozygous for the hypomorphic *Brca1*$^{\Delta 223\text{-}763}$ mutation (denoted here as *Brca1*$^{-/-}$). Cells were plated and exposed for 24 hours to varying doses of CPT and ETO and allowed to recover for 7-9 days. The surviving colonies were stained with Crystal violet and counted. Survival is calculated as a percentage of colonies in the mock-treated plates. Each subclone was tested in triplicate, and the error bars represent the SE of the mean of survival for each subclone.

required for some, but not all, of the cellular resistance mediated by Brca1 in response to the topoisomerase inhibitors CPT and ETO.

B9. Cytogenetic analysis

B9a. *$Ctip^{S326A}$ mutant cells can suppress both spontaneous and MMC-induced chromosomal rearrangements*

Deficiencies in DSB repair can give rise to chromosomal instability, which may in turn promote tumorigenesis. Consistent with this, *$Brca1^{S1598F/S1598F}$* cells, which express Brca1 polypeptides that lack BRCT phospho-recognition, display HDR defects and marked chromosomal instability (Shakya et al., 2011). To determine whether the Brca1-Ctip interaction is required for Brca1-mediated chromosome maintenance, we examined the metaphase spreads of several early passage *$Ctip^{+/+}$* and *$Ctip^{S326A/S326A}$* primary MEF subclones. As shown in Figure 21A and Table 3, *$Ctip^{S326A/S326A}$* MEFs display low levels of spontaneous chromosomal rearrangements, comparable with those of wildtype *$Ctip^{+/+}$* MEFs. Thus, in the absence of exogenous DNA damage, the Brca1-Ctip interaction is dispensable for Brca1-mediated suppression of spontaneous chromosomal instability.

In addition, *$Ctip^{S326A/S326A}$* MEFs also display normal resistance to MMC-induced chromosomal rearrangements, as these cells accumulate cytogenetic defects to the same extent as *$Ctip^{+/+}$* MEFs when subjected to DNA damage by MMC exposure (Figure 21B; Table 3). As shown in Table 3, the types of spontaneous and MMC-induced chromosomal rearrangements observed in cells of either Ctip genotype are predominantly chromatid/chromosome breaks and gaps, as opposed to complex rearrangements or

A.

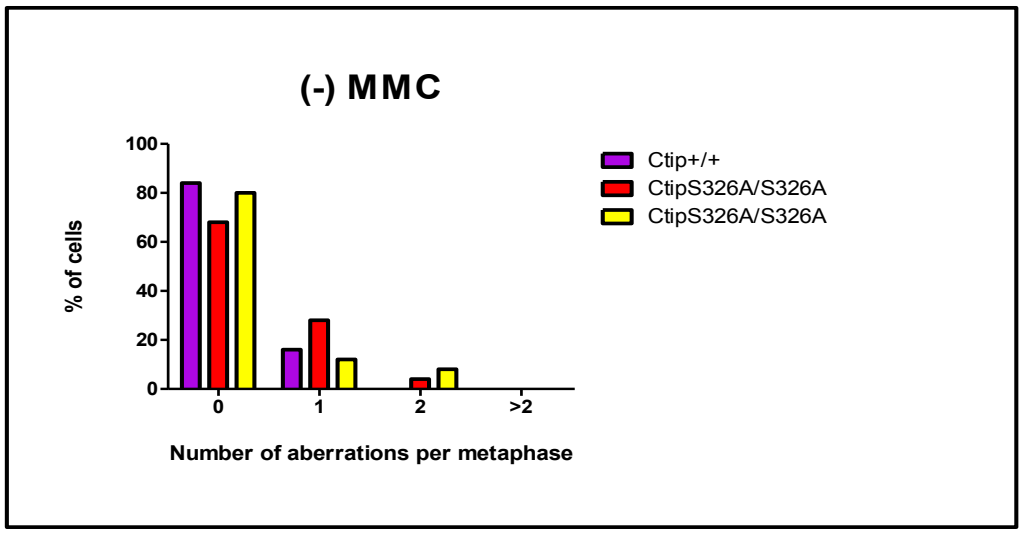

B.

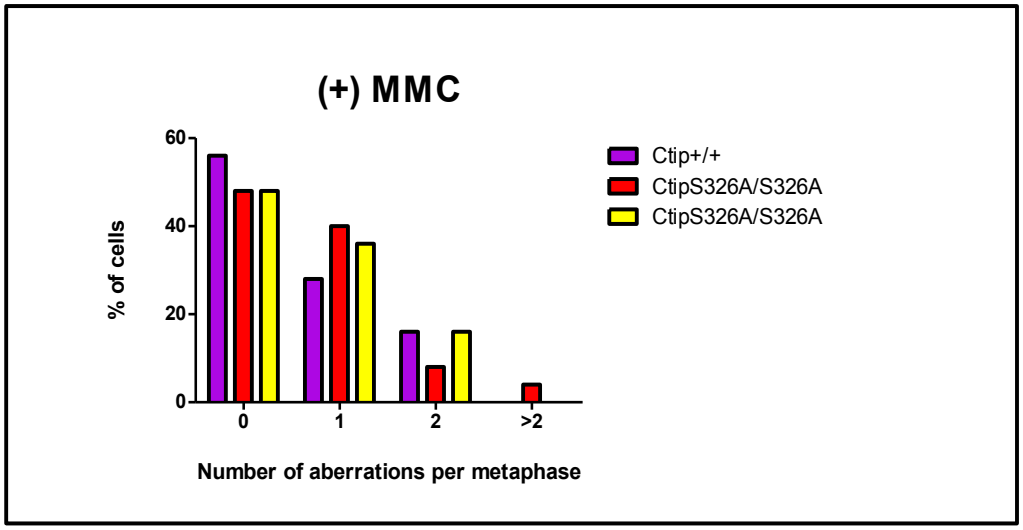

Figure 21. Low levels of spontaneous and MMC-induced chromosomal aberrations in *Ctip*$^{S326A/S326A}$ primary MEFs. Primary *Ctip*$^{+/+}$ and *Ctip*$^{S326A/S326A}$ MEFs were cultured in the (A) absence or (B) presence of MMC (40 ng/mL, 16 h) and subjected to karyotype analysis. Following colcemid treatment, exposure to a hypotonic solution, and methanol/acetic acid fixation, the cell suspensions were dropped onto glass slides and stained with Giemsa. Twenty-five metaphase spreads per cell line were examined for each treatment condition for numerical and structural chromosomal aberrations.

Table 3. Spontaneous and induced chromosomal aberrations in primary MEFs with different Ctip genotypes.

				Aberrations	
Ctip genotype	Metaphases analyzed	MMC treatment	Metaphase aberrations, %	Chr/Cht breaks and gaps	Exchange/Other
Ctip+/+ (#12)	25	-	16	4	0
	25	+	44	14	1
CtipS326A/S326A (#10)	25	-	32	9	0
	25	+	52	15	2
CtipS326A/S326A (#11)	25	-	20	7	0
	25	+	52	14	3

MMC, mitomycin C / Chr, chromosome / Cht, chromatid

The percentage of metaphases containing one or more aberrations and a breakdown of aberration-type is shown for each primary MEF cell line in both the absence (–) and presence (+) of MMC.

exchanges. Moreover, aneuploidy was not observed in the spreads of *Ctip*$^{S326A/S326A}$ cells, which contained on average the expected 40 mouse chromosomes (data not shown). Therefore, although Brca1 suppresses both spontaneous and MMC-induced chromosomal instability (Moynahan et al., 2001; Reid et al., 2008), its interaction with Ctip is not required for these functions.

Since undifferentiated ES cells and MEFs sometimes manifest different DNA damage responses (Moynahan et al., 2001), we also examined the karyotypes of several *Ctip*$^{+/-}$ and *Ctip*$^{S326A/-}$ ES subclones. Like the *Ctip*$^{S326A/S326A}$ MEFs, *Ctip*$^{S326A/-}$ ES cells also accumulate spontaneous and MMC-induced chromosomal aberrations at the same rate as control (*Ctip*$^{+/-}$ ES) cells (Figure 22, A and B). Thus, regardless of the cell type, and consistent with our observation of proficient DSB repair in *Ctip*$^{S326A/-}$ ES cells (Figures 12-14), chromosomal stability is maintained in the absence of the Brca1-Ctip interaction. Overall, these results indicate that significant aspects of BRCA1 and CtIP function in genome maintenance are independent of the BRCA1-CtIP interaction.

B10. Viability and IR sensitivity of Ctip^{S326A} mice

B10a. *Ctip*^{S326A} *mutant mice are viable, healthy, fertile, and resistant to IR*

To evaluate whether the Brca1-Ctip interaction is required for animal development and tumor suppression, we examined mice that solely express mutant Ctip-S326A polypeptides which fail to interact with Brca1 (i.e., *Ctip*$^{S326A/S326A}$ and *Ctip*$^{S326A/-}$ mice). In contrast to the early embryonic lethality of *Ctip*- and *Brca1*-null animals (Hakem et al., 1996; Liu et al., 1996; Ludwig et al., 1997; Chen, P.-L. et al., 2005), *Ctip*$^{S326A/S326A}$ and

A.

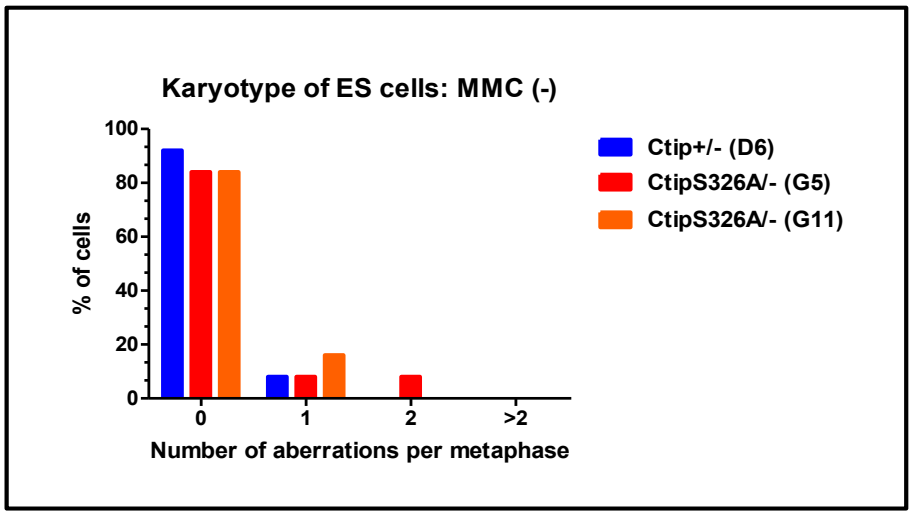

B.

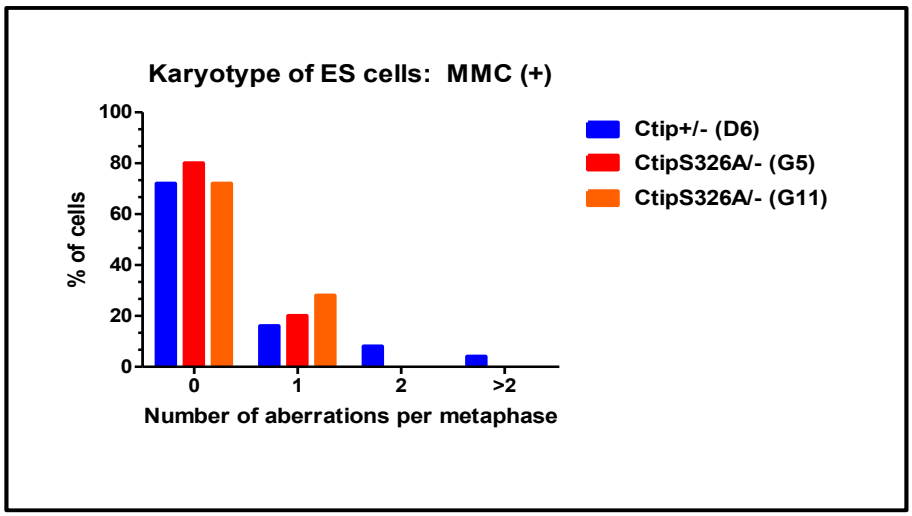

Figure 22. Low levels of spontaneous and MMC-induced chromosomal aberrations in *Ctip*$^{S326A/-}$ ES cells. Metaphase spreads were prepared from (A) untreated or (B) MMC-treated (40 ng/mL, 16 h) isogenic *Ctip*$^{+/-}$ and *Ctip*$^{S326A/-}$ ES subclones. Following colcemid treatment, exposure to a hypotonic solution, and methanol/acetic acid fixation, the cell suspensions were dropped onto glass slides and stained with Giemsa. For each treatment condition, at least twenty-five metaphase spreads per ES subclone were examined for numerical and structural chromosomal aberrations.

Ctip$^{S326A/-}$ mice were born at the expected Mendelian ratios, survived to adulthood, were fertile, and otherwise appeared to be indistinguishable from their littermate controls (data not shown). The viability of *Ctip*$^{S326A/S326A}$ and *Ctip*$^{S326A/-}$ mice again indicates that the Brca1-Ctip interaction is not essential for all Brca1 and all Ctip functions.

To assess whether the Brca1-Ctip interaction is required for *in vivo* resistance to genotoxic stress, we tested the sensitivity of *Ctip*$^{S326A/S326A}$ mice to whole-body ionizing radiation (IR). Homozygous (*Ctip*$^{S326A/S326A}$) mutant mice and control mice (*Ctip*$^{S326A/+}$ and *Ctip*$^{+/+}$*)* at two months of age were exposed to a sublethal dose of 8 Gys of gamma irradiation. While 10 out of 11 control mice survived at least 6 weeks post-irradiation, 11 out of 12 *Ctip*$^{S326A/S326A}$ mutant mice also survived (data not shown). Thus, *Ctip*$^{S326A/S326A}$ mutant mice are resistant to whole-body IR, suggesting that the Brca1-Ctip interaction is not essential for *in vivo* resistance to genotoxic stress.

B11. Whole-body tumor formation

B11a. *Ablation of the Brca1-Ctip interaction does not enhance spontaneous tumor formation*

Although Ctip is reported to serve as a tumor suppressor (Chen, P.-L. et al., 2005), it is not known whether this function reflects its activity in the BRCA1 pathway and, as such, would be relevant to human breast and ovarian cancer. Therefore, to ascertain whether the BRCA1-CtIP interaction is required for BRCA1-mediated tumor suppression, we monitored *Ctip*$^{S326A/S326A}$ and *Ctip*$^{S326A/-}$ mice for whole-body tumor development over a 24-month observation period. As shown in Figure 23, *Ctip*$^{S326A/S326A}$

and *Ctip*$^{S326A/-}$ mutant mice (n=40) developed tumors at a very advanced age. The frequency and kinetics of spontaneous tumor formation in these mutant mice were comparable with those of control mice (n=47; *Ctip*$^{+/+}$, *Ctip*$^{+/-}$, and *Ctip*$^{S326A/+}$) (Figure 23). Thus, consistent with the observed genomic stability of mutant Ctip-S326A ES cells and MEFs, ablation of the Brca1-Ctip interaction does not enhance spontaneous tumor formation in mice. Moreover, although the ability of the BRCT domain to bind its phospho-ligands is critical for BRCA1 tumor suppression (Shakya et al., 2011), the tumor suppression function of BRCA1 is not dependent on its interaction with the phospho-ligand CtIP.

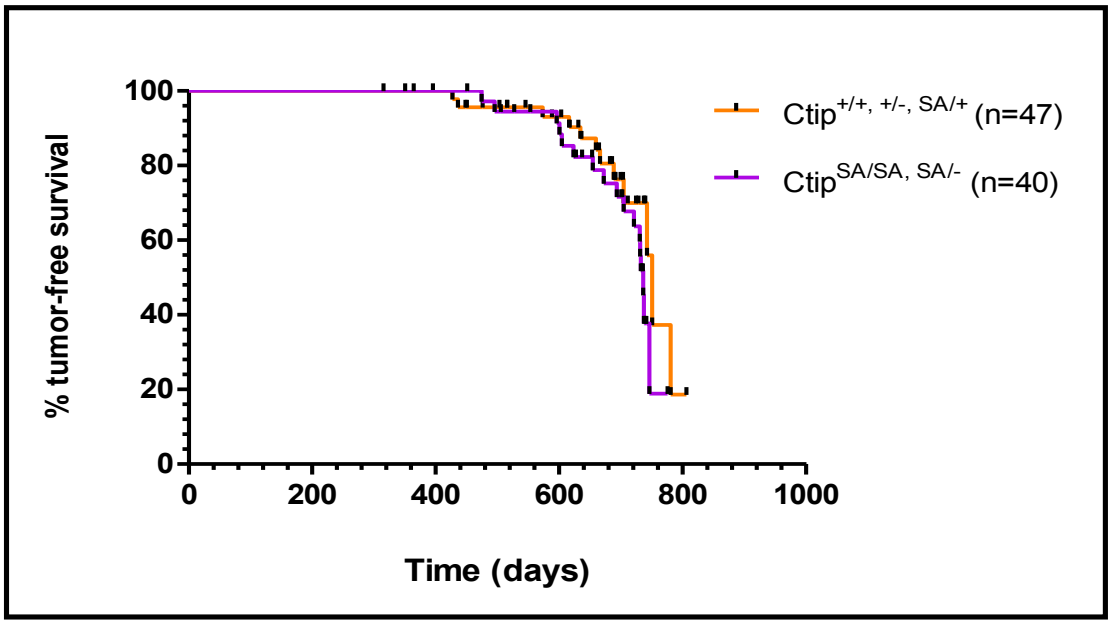

Figure 23. The Brca1-Ctip interaction is dispensable for tumor suppression. Kaplan-Meier tumor-free survival curves of control *Ctip*$^{+/+,\ +/-,\ SA/+}$ (orange curve; n = 47) mice compared with *Ctip*$^{SA/SA,\ SA/-}$ (purple curve; n = 40; P = 0.2249) mice. Significance was estimated with the log-rank test using Graph-Pad Prism (version 4) software. Values were considered statistically significant at $P < 0.05$.

C. DISCUSSION

Although the mechanisms of BRCA1 tumor suppression are not understood, the tumor suppressor activity of BRCA1 is thought to derive, at least in part, from its ability to promote genomic integrity (reviewed in Scully and Livingston, 2000; Jasin, M., 2002; Deng, C.-X., 2006; Nagaraju and Scully, 2007). Consistent with this, a BRCT phospho-recognition mutant of Brca1 (Brca1-S1598F) fails to suppress both chromosomal instability in cells and tumor formation in animals (Shakya et al., 2011). Notably, the BRCT sequences of BRCA1 preferentially bind the phosphorylated isoforms of repair proteins Abraxas/CCDC98, BACH1/BRIP1/FancJ, and CtIP to mediate BRCA1 function in response to DNA damage (Greenberg et al., 2006; reviewed in Huen et al., 2010; Moynahan and Jasin, 2010). Given that CtIP has prominent functions in genome stability and is the only known BRCT phospho-ligand that is also an enzymatic substrate of BRCA1/BARD1's E3 ligase activity, we sought to determine whether CtIP's interaction with BRCA1 mediates its genome maintenance and tumor suppression functions.

To this end, we introduced the S326A mutation into the mouse *Ctip* gene of ES cells by homologous recombination. Previous studies have established that the *in vivo* association of human CtIP and BRCA1 requires phosphorylation of CtIP at residue S327, which corresponds to Ctip residue S326 in mice (Yu and Chen, 2004). Thus, the Ctip-S326A missense mutation prevents phosphorylation of Ctip residue S326 and, as anticipated, it ablates the Brca1-Ctip interaction (Figure 10). Surprisingly, we found that the BRCA1-CtIP interaction is dispensable for mammalian cell viability, critical aspects of BRCA1 function in genome stability, and BRCA1-mediated tumor suppression.

Individually, BRCA1 and CtIP are each essential for the viability of mammalian cells (Elledge and Amon, 2002; Chen, P.-L. et al., 2005; Reid et al., 2008). This is consistent with the early embryonic lethality of mice bearing homozygous-null mutations of either *Brca1* (Hakem et al., 1996; Ludwig et al., 1997) or *Ctip* (Chen, P.-L. et al., 2005), the inability to culture MEFs from *Brca1*-null (Hakem et al., 1996; Ludwig et al., 1997) or *Ctip*-null (Chen, P.-L. et al., 2005) embryos, and the failure to generate viable ES cells by targeted inactivation of both alleles of either Brca1 (McCarthy et al., 2003) or Ctip (unpublished data). In contrast, with relative ease we were able to generate mice, MEFs, and ES cells that solely express mutant Ctip-S326A polypeptides. Thus, our data indicate that the Brca1-Ctip interaction is dispensable for mammalian cell viability and that the interaction is not required for all Brca1 or all Ctip functions. In accord with these findings, *Ctip*-null mice die at an earlier stage of embryogenesis than *Brca1*-null mice, suggesting that Ctip likely executes at least some functions independent of Brca1 (Chen, P.-L. et al., 2005).

CtIP initiates HDR of DSBs through its role in DNA resection, a process in which the 5' strand of a DSB end is degraded to yield 3' single-stranded DNA (ssDNA) overhangs (Sartori et al., 2007; Bennardo et al., 2008; Yun and Hiom, 2009; reviewed in Symington and Gautier 2011). Although a specific biochemical function for BRCA1 in HDR has yet to be elucidated, the discovery of the BRCA1-CtIP interaction raised the possibility that BRCA1 collaborates with CtIP to resect DSB ends. Consistent with this hypothesis, biochemical studies show that the BRCA1, CtIP, and MRN polypeptides form a discrete protein complex *in vivo* (Greenberg et al., 2006; Chen et al., 2008), and BRCA1 appears to function at an upstream stage of the HDR pathway (Stark et al., 2004). To address

whether BRCA1 modulates DNA resection through its interaction with CtIP, we examined the ability of Ctip-S326A mutant cells to repair DSBs through several resection-dependent pathways and recruit the ssDNA-binding protein RPA to sites of DNA damage.

Cells bearing mutations in certain DSB repair genes often display defects in both gene targeting and HDR, although the relationship between the two processes is not fully understood (Moynahan et al., 1999; Snouwaert et al., 1999; Moynahan et al., 2001). Gene targeting with an exogenous DNA fragment involves two distal recombination reactions in which the one-ended DSB intermediates of the linearized targeting construct invade a chromosome with homologous sequences (Pierce et al., 2001). HDR, on the other hand, occurs through a single recombination reaction that involves two proximal DSB ends preferentially invading an intact sister chromatid (Pierce et al., 2001). Since BRCA1 and CtIP are individually required for HDR (Moynahan et al., 1999; Moynahan et al., 2001; Sartori et al., 2007; Bennardo et al., 2008) we used two distinct assays to ascertain whether the BRCA1-CtIP interaction is required for this process.

First, gene-targeting assays were used to measure the efficiency by which transfected DNA fragments are integrated homologously at two independent chromosomal loci in isogenic $Ctip^{+/-}$ and $Ctip^{S326A/-}$ ES cells. Surprisingly, at both the *Pim1* and *Rb* loci, we observed a 2-fold increase in the gene-targeting efficiency of $Ctip^{S326A/-}$ cells relative to control $Ctip^{+/-}$ cells. Additionally, when HDR was measured using an integrated DR-GFP recombination substrate, we observed equivalent levels of HDR in ES cells that do or do not allow the Brca1-Ctip interaction. Thus, these results suggest that the BRCA1-CtIP interaction is not required for HDR of chromosomal DNA breaks. Because HDR

requires DNA resection, these results further suggest that the BRCA1-CtIP interaction is dispensable for DSB end processing.

Recently, two independent groups using chicken DT40 cells and an I-*Sce*I-induced reporter assay published conflicting results on the role of the BRCA1-CtIP interaction in HDR. Yun and Hiom (2009) reported that *CtIP*-null chicken DT40 cells reconstituted with an exogenous cDNA expression vector encoding human S327A mutant CtIP ($CtIP^{-/-/-}$ + hCtIP-S327A) were defective for HDR. On this basis, they concluded that the BRCA1-CtIP interaction is required for DNA resection and, in turn, HDR. In contrast, a second group observed normal levels of HDR in CtIP-S332A mutant ($CtIP^{S332A/-/-}$) DT40 clones (note: the chicken CtIP-S332A mutation is equivalent to the murine Ctip-S326A and human CtIP-S327A mutations) (Nakamura et al., 2010). Although the cause of these discrepant results remains unclear, Nakamura et al. (2010) argue that their approach, in which the S332A mutation was knocked into the endogenous chicken *CtIP* gene, is more physiological as it should preserve normal regulation of *CtIP* gene expression. Like Nakamura et al. (2010), we used a knock-in approach to introduce the S326A mutation into the mouse *Ctip* gene and found proficient HDR in the absence of the Brca1-Ctip interaction. Using this approach, expression of the Ctip-S326A mutant is controlled by the endogenous *Ctip* promoter, allowing for proper cell-cycle dependent regulation (Yu and Baer, 2000).

In addition to HDR, CtIP promotes DSB repair by SSA and alt-NHEJ, two distinct pathways that also require DNA resection (Bennardo et al., 2008). To determine the role of the BRCA1-CtIP interaction in these pathways, we generated isogenic $Ctip^{+/-}$ and $Ctip^{S326A/-}$ ES cell subclones containing the SSA or alt-NHEJ recombination substrate

integrated into the *Hprt* or *Pim1* locus, respectively. Following I-*Sce*I endonuclease expression, we observed proficient repair of an induced DSB through either SSA or alt-NHEJ in the absence of the Brca1-Ctip interaction. Thus, although CtIP promotes resection-dependent repair by HDR, SSA, and alt-NHEJ (Bennardo et al., 2008), the BRCA1-CtIP interaction appears to be dispensable for these repair pathways.

Consistent with proficient DSB repair in the absence of the Brca1-Ctip interaction, we observed proper recruitment of several DNA repair proteins to sites of DNA damage in $Ctip^{S326A/S326A}$ MEFs. For example, both Brca1 and Ctip readily accumulate into IR-induced foci (IRIFs) in these cells. Moreover, RPA recruitment to IRIFs was normal in $Ctip^{S326A/S326A}$ MEFs, suggesting that resection-dependent formation of ssDNA occurs in the absence of the Brca1-Ctip interaction. The Rad51 protein was also efficiently loaded onto resected DNA in $Ctip^{S326A/S326A}$ cells. Taken together, these data indicate that the BRCA1-CtIP interaction is not required for CtIP-mediated DNA resection.

Prior to these studies, the data regarding the role of BRCA1 in DNA resection was limited and in some respects contradictory. On one hand, Chen et al. (2008) reported that RPA recruitment to IRIFs is impaired in HCC1937, a breast tumor cell line that expresses C-terminally truncated BRCA1 polypeptide lacking the BRCT repeats. On the other hand, Zhao et al. (2007) found normal IR-induced RPA focus formation in HeLa cells after siRNA-mediated BRCA1 depletion. Moreover, proper laser-induced RPA accumulation and IR-induced Rad51 focus formation was observed in the absence of the BRCA1-CtIP interaction in $CtIP^{S332A/-/-}$ DT40 cells (Nakamura et al., 2010). The discrepant results obtained from different laboratories may reflect differences in the approach to gene modulation (e.g., gene targeting vs. siRNA knockdown) and/or the

limitations inherent in using RPA accumulation as a downstream measure of DNA resection. Importantly, when our group and Nakamura et al. (2010) used a gene knock-in approach to ablate the BRCA1-CtIP interaction, we both found proficient recruitment of RPA and Rad51 to sites of DNA damage.

Given that resection-dependent DSB repair appears to be proficient in the absence of the Brca1-Ctip interaction, it is not surprising that we observed normal suppression of spontaneous and MMC-induced chromosomal rearrangements in Ctip-S326A mutant cells, as well as normal cellular tolerance to MMC treatment. Interestingly, however, $Ctip^{S326A/-}$ ES cells show a slight sensitivity to the topoisomerase inhibitors CPT and ETO, both of which stabilize the Topo-DNA cleavage complex. This suggests that the Brca1-Ctip interaction facilitates cellular tolerance to topoisomerase inhibitors, perhaps by mediating the removal of covalently-bound polypeptides from DSB ends. In fact, a requirement for the BRCA1-CtIP interaction in CPT and ETO resistance was demonstrated in $CtIP^{S332A/-/-}$ chicken DT40 cells (Nakamura et al., 2010). However, unlike the modest effects observed in mammalian cells, $CtIP^{S332A/-/-}$ DT40 cells displayed marked hypersensitivity to both CPT and ETO (Nakamura et al., 2010). Thus, the extent to which the BRCA1-CtIP interaction is involved in the removal of topoisomerases from DNA may differ between species.

In summary, we have demonstrated that the BRCA1-CtIP interaction is not required for all functions of either BRCA1 or CtIP in cell viability and genome maintenance. In mammalian cells, the BRCA1-CtIP interaction is dispensable for resection-dependent DSB repair, RPA focus formation, suppression of spontaneous and MMC-induced chromosomal rearrangements, and cellular resistance to MMC. However, the Ctip-

S326A mutation does have a slight effect on the clonogenic survival of cells to topoisomerase inhibitors CPT and ETO. Therefore, we examined the role of the BRCA1-CtIP interaction in BRCA1-mediated tumor suppression by monitoring spontaneous tumor formation in mice that express the Ctip-S326A mutant. Interestingly, these mice were not tumor prone. Thus, although BRCA1 tumor suppression depends on BRCT phosphoprotein binding (Shakya et al., 2011), it does not depend specifically on its interaction with the phospho-ligand CtIP. Given that BRCA1 also forms distinct protein complexes based on BRCT-mediated interactions with the repair proteins Abraxas/CCDC98 and BACH1/BRIP1/FancJ, it will be important to determine if one of these interactions (and/or others yet to be discovered) mediates the tumor suppression function of BRCA1. It is also conceivable that a combination of BRCT-mediated interactions may be required for BRCA1 tumor suppression. Although CtIP is not required for BRCA1-mediated tumor suppression, future studies should resolve whether CtIP has functions relevant to tumor suppression independent of its interaction with BRCA1 and identify which of its diverse functions influence human carcinogenesis.

CHAPTER IV

THE ROLE OF CTIP IN TUMORIGENESIS

A. INTRODUCTION

Given its pivotal role in the DNA damage response and its *in vivo* association with several established tumor suppressors, CtIP was itself proposed to function as a tumor suppressor (Chen, P.-L., et al., 2005; Chinnadurai, G., 2006). Although mutational screening of cDNA sequences from 89 human tumor cell lines did not detect homozygous deletions within the *CtIP* gene, five missense mutations in the coding region were observed in cell lines derived from breast, ovarian, pancreas, and colon carcinomas (Wong et al., 1998). Interestingly, the wildtype *CtIP* allele was absent in a pancreatic carcinoma cell line with a non-conservative K337E missense mutation, suggesting possible loss of heterozygosity (Wong et al., 1998). Although the K337E variant did not ablate the BRCA1-CtIP interaction, it could conceivably affect other aspects of CtIP function (Wong et al., 1998).

CtIP was also identified as a target gene for microsatellite instability in colorectal cancer (Vilkki et al., 2002). Microsatellite instability (MSI) occurs when microsatellites or simple tandem repeat sequences are mutated at high frequency due to defects in mismatch DNA repair (Chinnadurai, G., 2006). A screen of 109 colorectal cancers revealed that an A9 mononucleotide repeat was mutated on one allele of the *CtIP* gene (one base-pair deletion) at a high rate (22.9%) compared to control intronic mononucleotide repeats (Vilkki et al., 2002). This lesion alters the reading frame such that *CtIP* would encode a grossly truncated polypeptide lacking the C-terminal 540 amino acids (Vilkki et al., 2002). Nevertheless, biallelic lesions of the *CtIP* gene were not observed in these tumors (Vilkki et al., 2002).

The possibility that CtIP acts as a tumor suppressor was further suggested by an analysis of mutant mice carrying a null *Ctip* allele (Chen, P.-L. et al., 2005). The null allele ($Ctip^{-}$) was generated by inserting a pgkneopA cassette into exon 5 of *Ctip*. While homozygous ($Ctip^{-/-}$) animals died in early embryogenesis, heterozygous ($Ctip^{+/-}$) mice were healthy, but developed tumors, primarily lymphomas, at an increased rate (average tumor latency T_{50} = 625 days) relative to $Ctip^{+/+}$ mice (T_{50} = 780 days) (Chen, P.-L. et al., 2005). Importantly, tumor cells retained the wildtype *Ctip* allele and tumor tissue stained positively for Ctip. On this basis, Chen, P.-L. et al. (2005) proposed that monoallelic *Ctip* lesions can promote tumor formation by haploid insufficiency.

Although a potential role for CtIP in tumor suppression is suggested, these studies do not address whether CtIP serves as a tumor suppressor in mammary epithelial cells, an intriguing possibility given its interaction with BRCA1. To determine whether CtIP is required for tumor suppression in mammary epithelial cells, and if so, whether this activity is epistatic with BRCA1-mediated tumor suppression, we used a Cre-loxP gene targeting system to generate mice that inactivate *Ctip* in a mammary-specific fashion. To bypass the early embryonic lethality of *Ctip*-nullizygous ($Ctip^{-/-}$) mice (Chen, P.-L. et al., 2005), we bred mice to carry a Ctip conditional-null allele ($Ctip^{Co}$) and the mammary-specific Wap^{Cre} transgene. Since this is the same *Cre* transgene used to induce mammary tumors in conditional *Brca1*-null mice (Shakya et al., 2008), the tumorigenic consequences of *Ctip* and *Brca1* inactivation could be compared in a common biological setting.

B. RESULTS

B1. Generation of the Ctip conditional-null (*Ctip*^{Co}) knock-in targeting construct

To generate the Ctip conditional-null allele (*Ctip*^{Co}), we constructed a targeting vector in which exon 2 of *Ctip* is flanked by two *loxP* recombination sites (Figure 24B). Consequently, this exon, which encodes the N-terminal 36 amino acids of Ctip, including the initiator methionine, can be deleted upon Cre-mediated recombination. In addition, a PGK promoter-driven neomycin expression cassette flanked by *FRT* (Flpe recombinase target) sites was positioned adjacent to the downstream *loxP* signal in intron 2. An HSV thymidine kinase (HSV-TK) gene cassette was also included in the targeting vector for negative selection.

B2. Identification of properly targeted ES clones

129/Sv ES cells were electroporated with the Ctip conditional-null (*Ctip*$^{Co\text{-}neo}$) targeting construct and selected for neomycin resistance. Genomic DNA prepared from the surviving drug-resistant ES cell clones was digested with *Spe*I and analyzed by Southern blotting with a 5' flanking *Ctip* probe ("*Ctip-2*") located upstream of exon 1 (Figure 24). In this manner, several independent neomycin-resistant ES clones harboring the *Ctip*$^{Co\text{-}neo}$ knock-in allele were identified (Figure 25).

B3. The Cre-recombined product of the conditional *Ctip*^{Co} allele is functionally null

Two independent *Ctip*$^{Co\text{-}neo/+}$ 129/Sv ES clones were injected into C57BL/6J blastocysts to obtain germline-transformed mice bearing the *Ctip*$^{Co\text{-}neo}$ allele. To excise

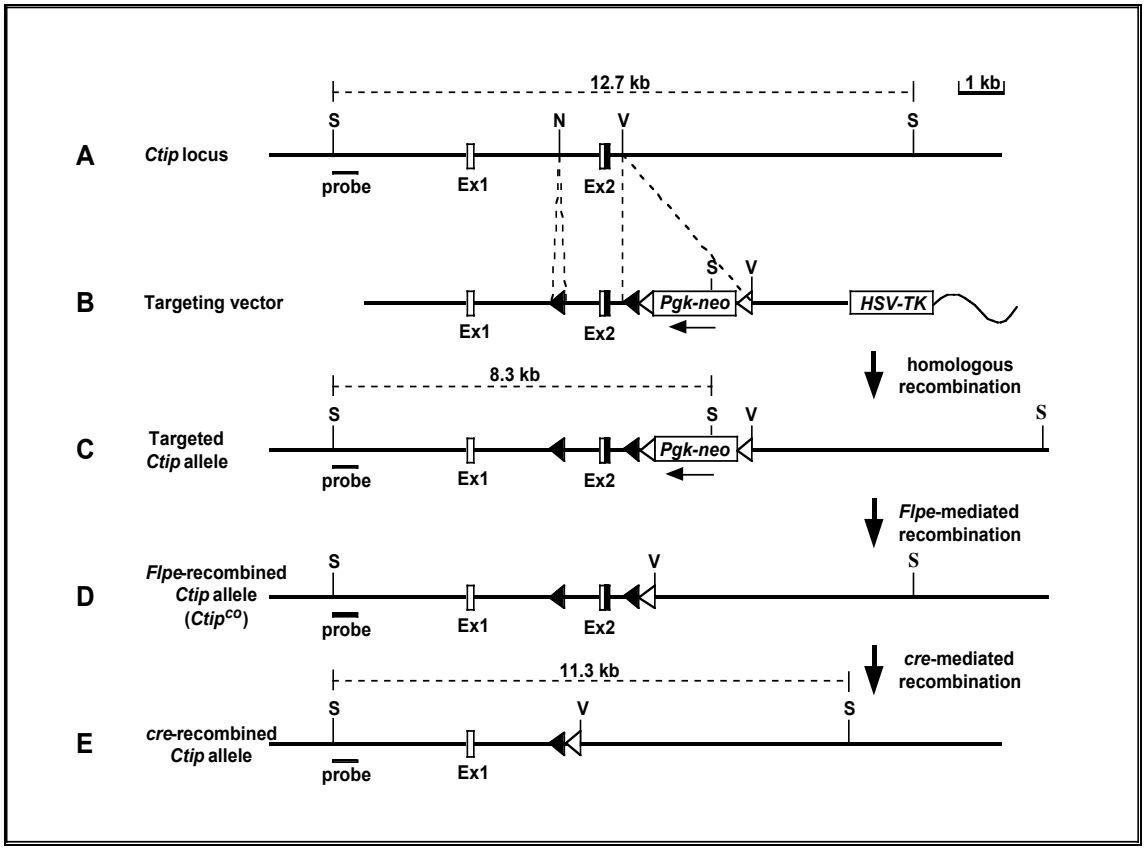

Figure 24. Design of the conditional-null *Ctip*^{Co} allele. A map of the wildtype *Ctip* locus encompassing exons 1 and 2 is shown (A), followed by a diagram of the targeting vector (B), and maps of the *Ctip* locus after homologous recombination (*Ctip*$^{Co\text{-}neo}$) (C), Flpe-mediated recombination (*Ctip*^{Co}) (D), and cre-mediated recombination (*Ctip*$^{Co\text{-}rec}$) (E). The coding sequence of *Ctip* exons are represented by closed rectangles while non-coding sequences are depicted by open rectangles. (Note that the initiator methionine is located in exon 2). To prepare the targeting vector, a single *loxP* recombination signal (closed triangle) was inserted into the *Nhe*I restriction site of intron 1, while a second *loxP* signal, together with a neomycin expression cassette flanked by *FRT* signals (open triangles), were inserted into the *Eco*RV site of intron 2. The *Pgk* promoter of the expression cassette controls transcription of the *neo* gene. An HSV thymidine kinase (HSV-TK) gene cassette was also included in the targeting vector for negative selection. The wavy line represents plasmid sequences of the targeting vector. Relevant restriction enzyme sites are: *Nhe*I (N), *Eco*RV (V), and *Spe*I (S). The position of the 5' flanking *Ctip* probe ("*Ctip-2*") used for Southern analysis and the sizes of the *Spe*I fragments recognized by the probe are also shown.

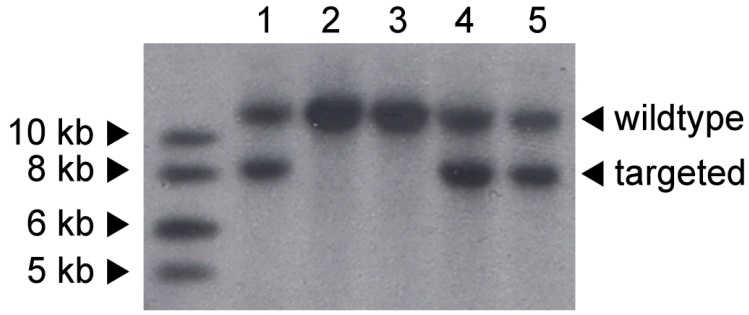

Figure 25. Identification of properly targeted *Ctip*$^{Co\text{-}neo/+}$ ES cells. 129/Sv ES cells were electroporated with the conditional *Ctip*$^{Co\text{-}neo}$ targeting construct (Figure 24B), and *Spe*I-digested genomic DNAs from the neomycin-resistant ES clones were evaluated by Southern hybridization using a 5' flanking *Ctip* probe ("*Ctip-2*"; Figure 24). The 12.7 kb *Spe*I fragment represents the wildtype *Ctip* locus (Figure 24A) while the 8.3 kb fragment represents the targeted *Ctip* allele (Figure 24C). Properly targeted ES clones are seen in lanes 1, 4, and 5.

the neomycin expression cassette from the targeted allele (Figure 24C), *Ctip*$^{Co\text{-}neo/+}$ heterozygous mice were mated with Flpe-expressing mice to produce offspring in which the *FRT*-flanked neomycin cassette has been removed, converting the *Ctip*$^{Co\text{-}neo}$ allele into the desired *Ctip*^{Co} allele (Figure 24D). These animals were then intercrossed to obtain homozygous *Ctip*$^{Co/Co}$ mice (Figure 26). In contrast to the early lethality of *Ctip*-nullizygous embryos (Chen, P.-L. et al., 2005), homozygous *Ctip*$^{Co/Co}$ mice were viable, healthy, fertile, and had a normal lifespan, indicating that the two *loxP* sites and single *FRT* site of the conditional *Ctip*^{Co} allele (Figure 24D) did not interfere with normal gene function.

Ctip$^{Co/Co}$ mice were mated with animals that carry a ubiquitously expressed *Cre* transgene (*Rosa*^{Cre}) driven by the mouse *Rosa26* gene promoter (provided by Dr. Thomas Ludwig, Columbia University) to obtain heterozygous *Ctip*$^{Co\text{-}rec/+}$/*Rosa*$^{Cre/+}$ animals (Figure 24E). To assess the function of the Cre-recombined product (*Ctip*$^{Co\text{-}rec}$) of the *Ctip*^{Co} allele, these mice were intercrossed and their progeny identified by genotyping. Although wildtype and heterozygous pups appeared at the expected 1:2 ratio, homozygous *Ctip*$^{Co\text{-}rec/Co\text{-}rec}$ offspring (0 out of 113 viable pups) were not obtained from this intercross, suggesting an early embryonic death (data not shown). Furthermore, to analyze the stage of lethality, embryos from heterozygous *Ctip*$^{Co\text{-}rec/+}$/*Rosa*$^{Cre/+}$ intercrosses were genotyped and the gross morphologies of the embryos and histological sections of dissected deciduas were examined at embryonic day 7.5. As expected, we observed 5 homozygous *Ctip*$^{Co\text{-}rec/Co\text{-}rec}$ embryos out of 16 total embryos examined (~25%) (data not shown). As shown in Figure 27 (A and C), all normal (wildtype *Ctip*$^{+/+}$

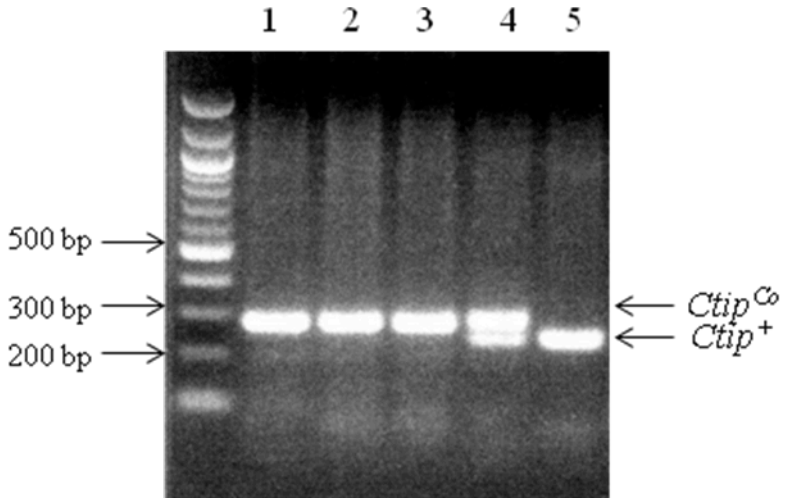

Figure 26. Identification of homozygous *Ctip*$^{Co/Co}$ mice. PCR genotyping of homozygous *Ctip*$^{Co/Co}$ mice was performed on genomic DNA prepared from mouse tails. Using primers 3 and 4 listed in Table 1, the *Ctip*^{Co} allele is amplified as a 290 bp band while the *Ctip*$^{+}$ allele is amplified as a 250 bp band. Homozygous *Ctip*$^{Co/Co}$ mice are shown in lanes 1, 2 and 3, along with a heterozygous *Ctip*$^{Co/+}$ mouse (lane 4) and a wildtype *Ctip*$^{+/+}$ mouse (lane 5).

and heterozygous *Ctip*$^{Co\text{-}rec/+}$) embryos examined at E7.5 had gastrulated to form a third (mesodermal) germ layer. In contrast, none of the *Ctip*$^{Co\text{-}rec/Co\text{-}rec}$ embryos developed past the egg cylinder stage (Figure 27, B and D). Therefore, *Ctip*$^{Co\text{-}rec/Co\text{-}rec}$ mutant embryos display severe growth and morphogenic defects by the onset of gastrulation and die prior to E7.5. This phenotype is remarkably similar to that reported for *Ctip*$^{-/-}$ nullizygous embryos (Chen, P.-L. et al., 2005), confirming that the Cre-recombined product of the conditional *Ctip*^{Co} allele is functionally null.

B4. The embryonic lethal phenotype of *Ctip*-null embryos is not ameliorated by concomitant loss of Ku70

Although DSB repair by non-homologous end joining (NHEJ) can proceed with little or no nucleolytic processing, other modes of DSB repair, such as homology-directed repair (HDR), are highly dependent on DNA resection of the DSB ends. NHEJ is initiated by the recognition and binding of broken DNA ends by the Ku70/Ku80 heterodimer. Once bound, Ku protects the ends from degradation and mediates the recruitment of downstream NHEJ factors (Daley et al., 2005). HDR, on the other hand, is initiated by the 5' to 3' resection of DSBs to generate single stranded DNA (ssDNA) overhangs. Recent studies have shown that CtIP and its orthologs regulate the initial stage of DNA resection, where it functions together with the MRN complex to process DSB ends into the 3'-ssDNA tails required for ATR checkpoint signaling and homology-directed repair (Limbo et al., 2007; Penkner et al., 2007; Sartori et al., 2007; Gravel et al., 2008; Mimitou and Symington, 2008; Zhu et al., 2008).

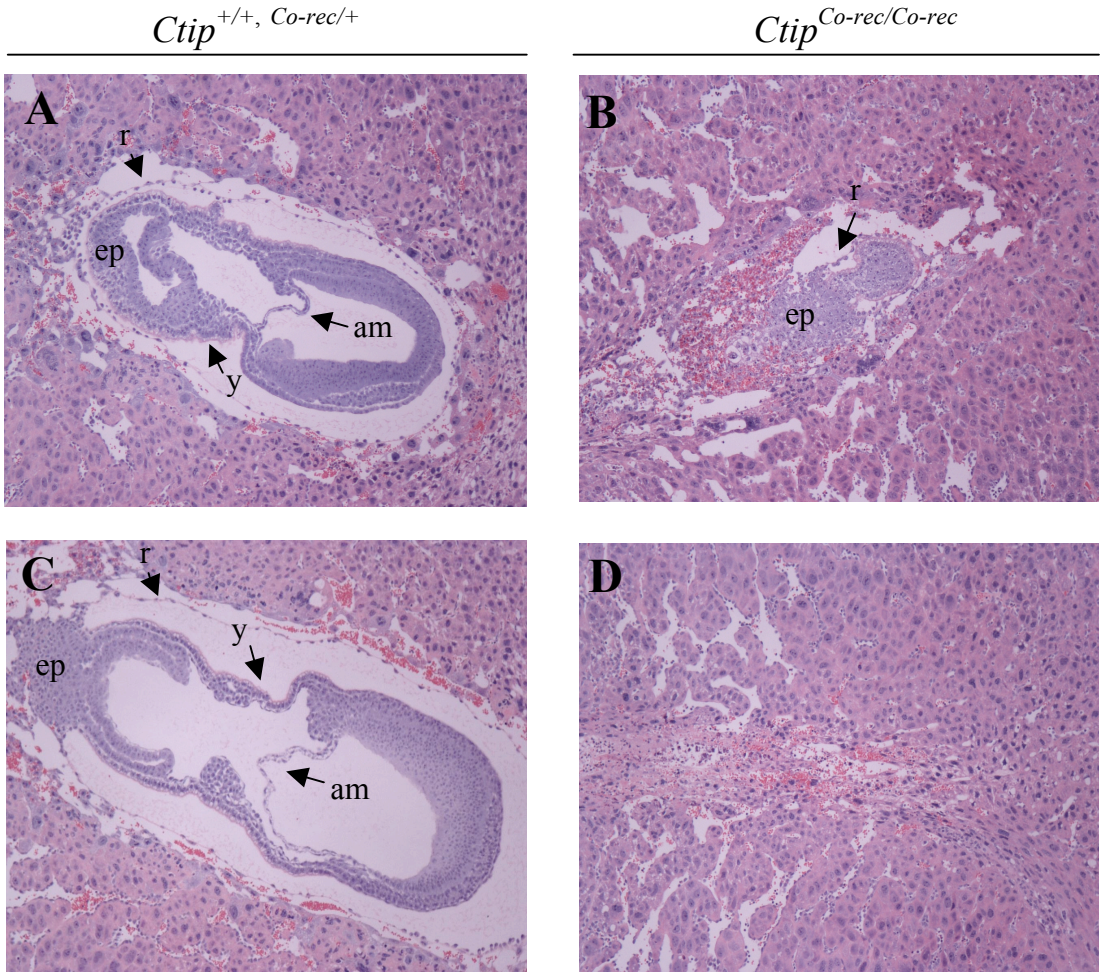

Figure 27. Embryonic lethality of *Ctip*$^{Co\text{-}rec/Co\text{-}rec}$ embryos. Hematoxylin- and eosin-stained sagittal sections of wildtype (A and C) and *Ctip*$^{Co\text{-}rec/Co\text{-}rec}$ (B and D) embryos at E7.5 are shown. (A and C) Normal (*Ctip*$^{+/+,Co\text{-}rec/+}$) post-gastrulation embryos with three distinct germ layers. (B and D) Developmentally retarded homozygous *Ctip*$^{Co\text{-}rec/Co\text{-}rec}$ mutant embryos. am, amnion; ep, ectoplacental cone; r, Reichardt's membrane; y, yolk sac.

In *S. cerevisiae*, the initial step of DNA resection mediated by MRX-Sae2 creates a less appealing substrate for Ku binding, committing cells to extensive resection and HDR (Mimitou and Symington, 2010). Mutants lacking Sae2 or any component of the MRX complex are highly sensitive to IR (Ivanov et al., 1992; Tsubouchi and Ogawa, 1998; Bressan et al., 1999; Moreau et al., 2001; Mimitou and Symington, 2010). Notably, the IR sensitivity of the *mre11*Δ (Bressan et al., 1999) and *sae2*Δ (Mimitou and Symington, 2010) mutants is highly suppressed by deletion of yeast Ku70. The increased IR resistance of *mre11*Δ*/yku70*Δ and *sae2*Δ*/yku70*Δ double mutants is thought to be the result of DNA resection occurring in the absence of Mre11 or Sae2 due to the loss of DNA end protection by Ku (Mimitou and Symington, 2010).

Given these results, we sought to determine whether loss of Ku70 can mitigate the early embryonic lethality phenotype of $Ctip^{Co\text{-}rec/Co\text{-}rec}$ mutant embryos. To this end, $Ctip^{Co\text{-}rec/+}$ mice were crossed with $Ku70^{-/-}$ mice (provided by Dr. Shan Zha, Columbia University) to generate $Ctip^{Co\text{-}rec/+}/Ku70^{+/-}$ animals. These mice were subsequently intercrossed to obtain the desired $Ctip^{Co\text{-}rec/Co\text{-}rec}/Ku70^{-/-}$ genotype at an expected Mendelian ratio of 1:16. Embryos from this intercross were isolated and analyzed at E9.5 of gestation. 76 total embryos were genotyped by PCR and all 9 genotypes were identified. Among the 76 embryos, 54 were live and 22 were in resorption. As expected, no viable $Ctip^{Co\text{-}rec/Co\text{-}rec}$ mutant embryos were identified at E9.5 in a *Ku70* wildtype or *Ku70* heterozygous background. Additionally, no $Ctip^{Co\text{-}rec/Co\text{-}rec}/Ku70^{-/-}$ mutant embryos survived until E9.5, indicating that the *Ku70* mutation does not rescue, or even partially rescue, the early embryonic lethality of *Ctip*-null mice (Table 4).

Table 4. The *Ku70* mutation does not rescue *Ctip*-null lethality.

Genotype	Number of E9.5 embryos	
	Observed	Expected
$Ctip^{+/+}$ $Ku70^{+/+}$	3	4.75
$Ctip^{+/+}$ $Ku70^{+/-}$	7	9.5
$Ctip^{+/+}$ $Ku70^{-/-}$	4	4.75
$Ctip^{Co\text{-}rec/+}$ $Ku70^{+/+}$	9	9.5
$Ctip^{Co\text{-}rec/+}$ $Ku70^{+/-}$	19	19
$Ctip^{Co\text{-}rec/+}$ $Ku70^{-/-}$	12	9.5
$Ctip^{Co\text{-}rec/Co\text{-}rec}$ $Ku70^{+/+}$	0 [a]	4.75
$Ctip^{Co\text{-}rec/Co\text{-}rec}$ $Ku70^{+/-}$	0 [a]	9.5
$Ctip^{Co\text{-}rec/Co\text{-}rec}$ $Ku70^{-/-}$	0 [a, b]	4.75
Total number of embryos	76	

[a] Among the 76 embryos, 22 were in resorption at E9.5. Homozygous $Ctip^{Co\text{-}rec/Co\text{-}rec}$ mutants die before E7.5 (Figure 27, B and D) much like *Ctip*-null mice (Chen, P.-L. et al., 2005).

[b] *Ku70*-nullizygosity does not rescue, or even partially rescue, the *Ctip*-null early embryonic lethality, as viable $Ctip^{Co\text{-}rec/Co\text{-}rec}/Ku70^{-/-}$ embryos were not observed at E9.5.

B5. Mammary epithelial cell-specific inactivation of Ctip

B5a. *Generating a cohort of $Ctip^{Co/–,Co/Co}/Wap^{Cre/+}$ females for tumor monitoring*

To evaluate whether Ctip affects tumor suppression, we applied a mouse model of familial breast cancer in which the Wap^{Cre} transgene elicits mammary-specific inactivation of the conditional-null $Ctip^{Co}$ allele (Ludwig et al., 2001a; Shakya et al., 2008). Therefore, homozygous $Ctip^{Co/Co}$ mice were crossed with $Ctip^{+/–}$ mice that harbor a *Cre* transgene knocked into the whey acidic protein (*Wap*) locus, expression of which is restricted to mammary epithelial cells during late pregnancy and lactation (Ludwig et al., 2001a). This cross generated control ($Ctip^{Co/+}/Wap^{Cre/+}$) and experimental ($Ctip^{Co/–}/Wap^{Cre/+}$) females for tumor analysis. Also, additional experimental $Ctip^{Co/Co}/Wap^{Cre/+}$ females were derived by intercrossing $Ctip^{Co/+}/Wap^{Cre/+}$ mice. All female mice appeared normal in that they were fertile, had normal litter sizes, and were able to nurse their pups.

B5b. *Cre-dependent recombination of $Ctip^{Co}$ in mammary epithelial cells*

To demonstrate the activity of the Wap^{Cre} allele, we examined recombination of the conditional $Ctip^{Co}$ allele in the mammary glands of experimental $Ctip^{Co/Co}/Wap^{Cre/+}$ females at various time points throughout pregnancy. Importantly, the endogenous *Wap* gene is expressed specifically in mammary epithelial cells at high levels only for a time period that includes late pregnancy and lactation (Robinson et al., 1995). Although limited *Wap* expression also occurs in some fraction of the putative stem cell population, Cre-mediated deletion persists despite massive apoptotic loss of epithelial cells during gland involution (Ludwig et al., 2001a). Notably, one round of pregnancy is necessary

and sufficient for Cre-mediated recombination (Ludwig et al., 2001a). Therefore, we prepared genomic DNA from pregnant (E13.5 and E18.5), lactating (10 days postpartum), and involuted (10 days post-wean) mammary glands of experimental $Ctip^{Co/Co}/Wap^{Cre/+}$ female mice. As a control, genomic DNA was also prepared from each female's tail. Additionally, tail and mammary gland DNA was prepared from $Ctip^{Co/Co}/Wap^{+/+}$ females that lack the Wap^{Cre} transgene. As expected, PCR analysis identified the Cre-recombined Ctip product only in the E18.5 and lactating mammary glands of experimental ($Ctip^{Co/Co}/Wap^{Cre/+}$) females (Figure 28). Thus, *Cre* expression following pregnancy and lactation renders the mammary epithelial cells of $Ctip^{Co/Co}/Wap^{Cre/+}$ females genotypically *Ctip*-null ($Ctip^{Co\text{-}rec/Co\text{-}rec}$).

B5c. *Mammary-specific inactivation of Ctip does not induce breast carcinogenesis in mice*

If CtIP is required for tumor suppression in mammary epithelial cells, then mammary-specific inactivation of the murine *Ctip* gene should elicit breast tumors. Moreover, if the tumor suppression activities of Ctip and Brca1 are epistatic, then these tumors should closely resemble the basal-like mammary carcinomas that arise upon mammary-specific ablation of Brca1 (Shakya et al., 2008). To test this hypothesis, the experimental cohort of conditional *Ctip* (n=21; 14 $Ctip^{Co/Co}/Wap^{Cre/+}$ and 7 $Ctip^{Co/-}/Wap^{Cre/+}$) females was mated to induce at least one round of pregnancy and lactation, and then monitored for tumor formation. Unlike conditional $Brca1^{Co/Co}/Wap^{Cre/+}$ females (n=33), which develop basal-like breast tumors with an average latency (T_{50}) of 512 days

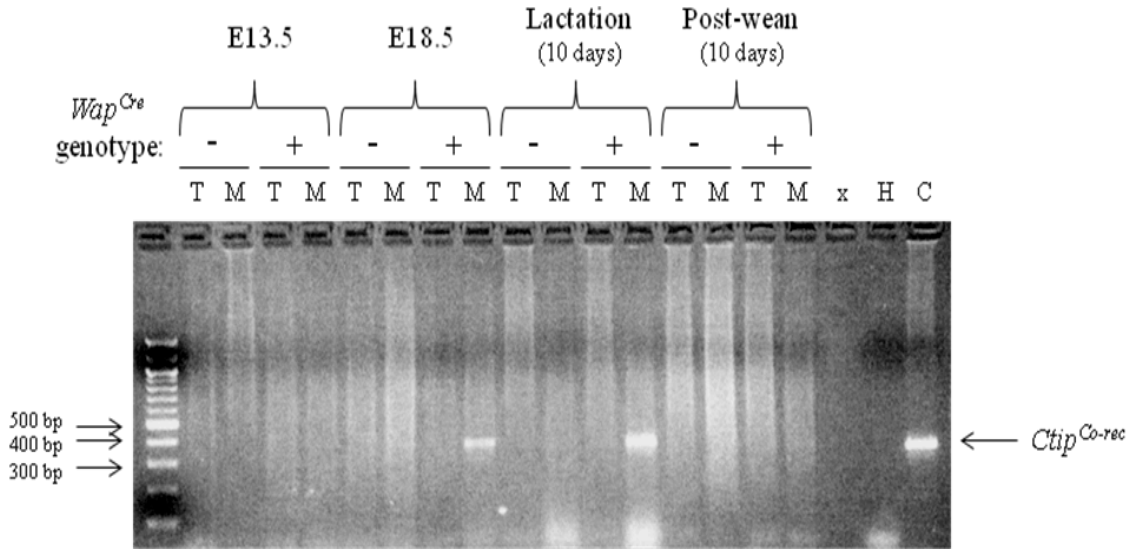

Figure 28. Cre-mediated *Ctip*^{Co} recombination in E18.5 and lactating mammary glands. Genomic DNA was prepared from pregnant (E13.5 and E18.5), lactating (10 days postpartum), and involuted (10 days post-wean) mammary glands of control *Ctip*$^{Co/Co}$/*Wap*$^{+/+}$ females that lack the *Wap*^{Cre} transgene (–), and experimental *Ctip*$^{Co/Co}$/*Wap*$^{Cre/+}$ females that carry the *Wap*^{Cre} transgene (+). As a control, genomic DNA was also prepared from the tail of each female. PCR analysis was performed on tail (T) and mammary gland (M) DNA using primers 3 and 5 listed in Table 1. The *Ctip*$^{Co\text{-}rec}$ allele is amplified as a 350 bp band. The PCR product of the recombined *Ctip*$^{Co\text{-}rec}$ allele is only observed in the mammary glands of E18.5 and lactating *Ctip*$^{Co/Co}$/*Wap*$^{Cre/+}$ experimental females. x, empty lane; H, water lane; C, positive control lane.

(Shakya et al., 2008), all conditional *Ctip* experimental animals remained tumor-free over an entire 24-month observation period (Figure 29), as did the control animals (n=10; $Ctip^{Co/+}/Wap^{Cre/+}$) (data not shown). Thus, Ctip appears to be dispensable for tumor suppression in this breast cancer model.

B5d. *Assessing the tumor suppression function of Ctip in tumor-prone settings*

B5di. Ctip inactivation increases the latency of breast tumor formation induced by mammary-specific inactivation of the *p53* gene

The experiment shown in Figure 29 indicates that conditional inactivation of Ctip does not elicit breast tumors in mice. However, it is possible that Ctip has only a weak tumor suppression activity (relative to Brca1) such that its inactivation does not appreciably affect the kinetics of breast cancer formation in our mouse model. Therefore, before concluding that Ctip is unnecessary for tumor suppression in mammary epithelial cells, we also examined its activity in a tumor-prone setting using a *p53* conditional-null mutation ($p53^{flex7}$, which will be designated herein as "$p53^{Co}$" for clarity; Chen, Z. et al., 2005). The rationale for this strategy is based on the well-established observation that p53 deficiency accelerates tumor formation in animals bearing Brca1 mutations, including various conditional *Brca1*-null mouse models (Brodie and Deng, 2001; Ludwig et al., 2001; Moynahan, M. E., 2002; Evers and Jonkers, 2006; Shakya et al., 2011). Therefore, if Ctip suppresses tumor formation, we would expect tumors to develop with a shorter latency in *Ctip/p53* double-deficient mice compared to *p53*-deficient alone mice. On the other hand, if Ctip is dispensable for mammary tumor suppression, then *Ctip/p53*

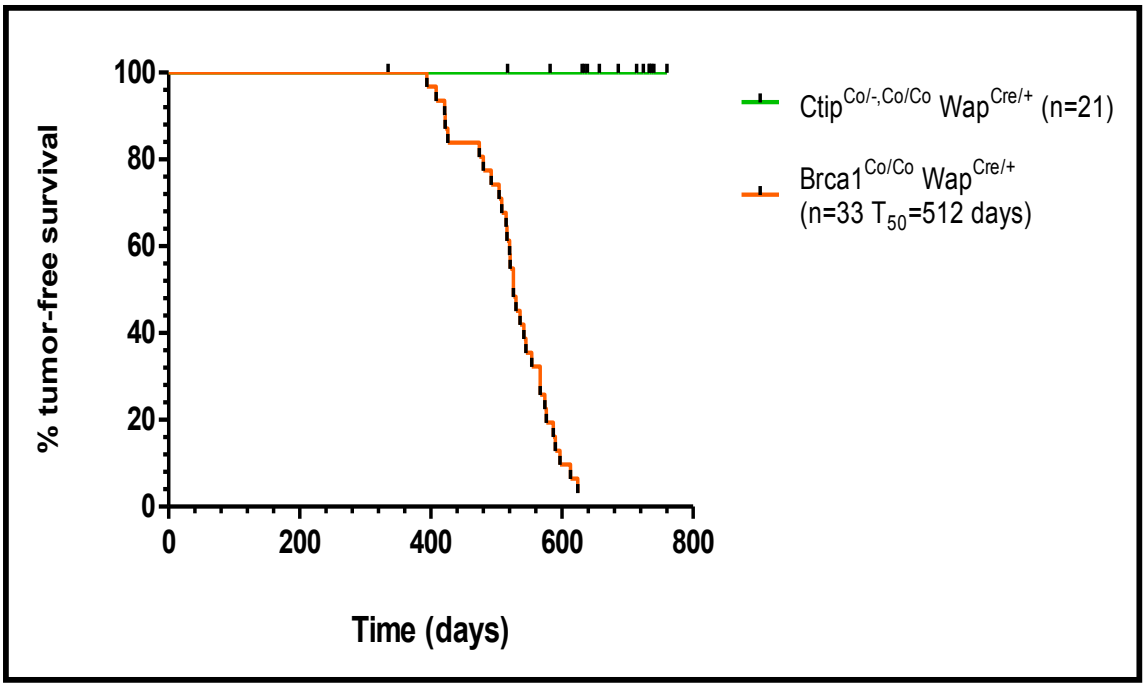

Figure 29. Normal suppression of mammary tumorigenesis in the absence of Ctip. Kaplan-Meier survival curves of *Brca1*$^{Co/Co}$/*Wap*$^{Cre/+}$ (orange curve; n=33; T_{50} = 512 days) females (Shakya et al., 2008) compared with *Ctip*$^{Co/–,Co/Co}$/*Wap*$^{Cre/+}$ (green curve; n=21; P < 0.0001) females. Significance was estimated with the log-rank test using Graph-Pad Prism (version 4) software. Values were considered statistically significant at P < 0.05.

double-deficient mice should develop tumors with the same latency and penetrance as *p53*-deficient alone animals.

To assess tumor development in this sensitized background, we generated Wap^{Cre} females carrying either one or two alleles of the *p53* conditional-null mutation ($p53^{Co}$) (Chen, Z. et al., 2005) together with the conditional-null *Ctip* ($Ctip^{Co}$) allele. Specifically, we produced two experimental cohorts ($Ctip^{Co/-,Co/Co}/p53^{Co/Co}/Wap^{Cre/+}$ and $Ctip^{Co/-,Co/Co}/p53^{Co/+}/Wap^{Cre/+}$) and two corresponding control cohorts ($Ctip^{Co/+,+/+}/p53^{Co/Co}/Wap^{Cre/+}$ and $Ctip^{Co/+,+/+}/p53^{Co/+}/Wap^{Cre/+}$). These female mice were all healthy, fertile, and able to properly lactate and nurse normal-size litters. As shown in Figure 30 (A and B), mammary tumors occurred in the two control cohorts with average latencies of 309 days ($Ctip^{Co/+,+/+}/p53^{Co/Co}/Wap^{Cre/+}$ mice; n=38) and 330.5 days ($Ctip^{Co/+,+/+}/p53^{Co/+}/Wap^{Cre/+}$ mice; n=10), respectively. These results are consistent with previous studies of mammary-specific p53 inactivation (Wijnhoven et al., 2005). Surprisingly, however, tumor formation was dramatically delayed by mammary-specific Ctip inactivation in both experimental cohorts: $Ctip^{Co/-,Co/Co}/p53^{Co/Co}/Wap^{Cre/+}$ (T_{50} = 605 days; n=11) (Figure 30A) and $Ctip^{Co/-,Co/Co}/p53^{Co/+}/Wap^{Cre/+}$ (T_{50} = not applicable; n=24) (Figure 30B). Thus, in contrast to our expectation that Ctip inactivation would potentiate tumorigenesis, we observed that loss of Ctip function markedly inhibits breast cancer formation in p53-deficient mice.

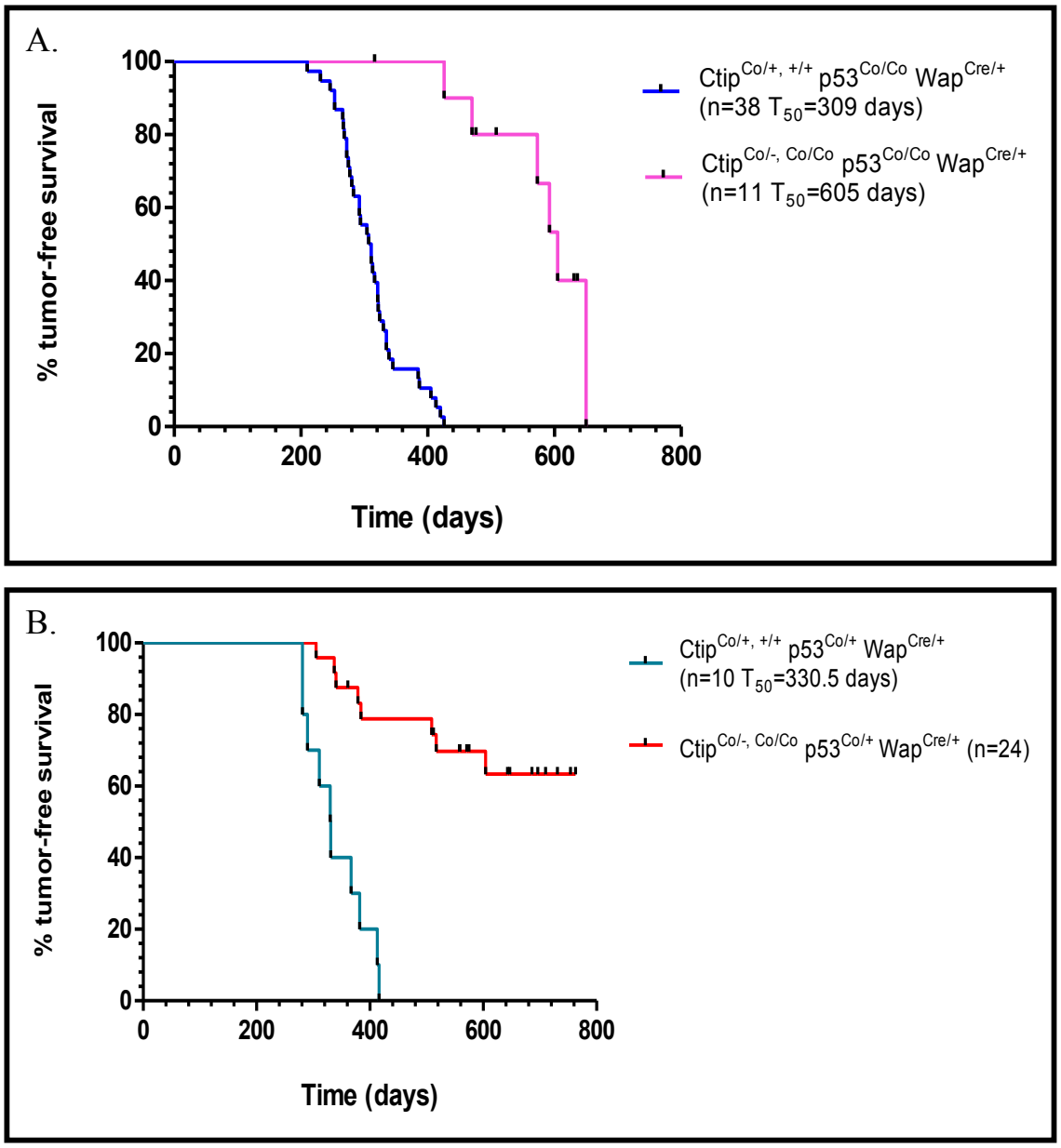

Figure 30. Loss of Ctip function markedly inhibits breast cancer formation in p53-deficient mice. (A) Kaplan-Meier survival curves of $Ctip^{Co/+,+/+}/p53^{Co/Co}/Wap^{Cre/+}$ (blue curve; n=38; T_{50} = 309 days) females compared with $Ctip^{Co/-,Co/Co}/p53^{Co/Co}/Wap^{Cre/+}$ (pink curve; n=11; T_{50} = 605 days; P < 0.0001) females. (B) Kaplan-Meier survival curves of $Ctip^{Co/+,+/+}/p53^{Co/+}/Wap^{Cre/+}$ (light blue curve; n=10; T_{50} = 330.5 days) females compared with $Ctip^{Co/-,Co/Co}/p53^{Co/+}/Wap^{Cre/+}$ (red curve; n=24; P < 0.0001) females. Significance was estimated with the log-rank test using Graph-Pad Prism (version 4) software. Values were considered statistically significant at P < 0.05.

B5dii. Ctip inactivation also increases the latency of breast tumor formation induced by mammary-specific expression of mutant p53

Since missense mutations in p53 are among the most common genetic lesions associated with human cancer, we also examined the effect of Ctip inactivation on tumorigenicity in mice bearing the conditional $p53^{LSL\text{-}R270H}$ point mutation (Olive et al., 2004). This gain-of-function mutation in murine *p53* corresponds to the human R273H hotspot mutation often associated with breast cancer (Olive et al., 2004; Wijnhoven et al., 2005). Importantly, the mutant *p53* allele was designed such that expression of the $p53^{R270H}$ polypeptide is blocked until removal of a Lox-STOP-Lox (LSL) cassette by Cre recombinase (Olive et al., 2004; Tuveson et al., 2004). Thus, the unrecombined $p53^{LSL\text{-}R270H}$ allele is functionally null.

To examine the tumor suppression function of Ctip in this tumor-prone setting, we generated Wap^{Cre} females that carry both the conditional $p53^{LSL\text{-}R270H}$ point mutation (Olive et al., 2004) and the conditional-null *Ctip* ($Ctip^{Co}$) allele. Thus, homozygous $Ctip^{Co/Co}$ mice were crossed with $p53^{LSL\text{-}R270H/+}/Wap^{Cre/+}$ mice to produce control $Ctip^{Co/+}/p53^{LSL\text{-}R270H/+}/Wap^{Cre/+}$ females. These animals were subsequently mated with $Ctip^{Co/+}$ mice to yield the experimental cohort of $Ctip^{Co/Co}/p53^{LSL\text{-}R270H/+}/Wap^{Cre/+}$ females, as well as additional control $Ctip^{+/+}/p53^{LSL\text{-}R270H/+}/Wap^{Cre/+}$ females. Following at least one complete round of pregnancy to induce Cre-dependent mammary-specific inactivation of Ctip and expression of the $p53^{R270H}$ point mutant, the control and experimental mice were monitored for tumor formation. Consistent with previous studies (Wijnhoven et al., 2005; Shakya et al., 2011), mammary tumors developed in control $Ctip^{Co/+,+/+}/p53^{LSL\text{-}R270H/+}/Wap^{Cre/+}$ females (n=38) with an average latency of 400 days

(Figure 31). Notably, the kinetics of tumor development was significantly slower upon conditional Ctip inactivation in the $Ctip^{Co/Co}/p53^{LSL\text{-}R270H/+}/Wap^{Cre/+}$ experimental females (n=26; T_{50} = not applicable) (Figure 31). Furthermore, inactivation of Ctip and expression of the dominant-negative $p53^{R270H}$ allele resulted in an extremely low incidence (8.3%; 2/24) of invasive breast tumors. Of note, the final two experimental $Ctip^{Co/Co}/p53^{LSL\text{-}R270H/+}$ $Wap^{Cre/+}$ females of the cohort are still alive at 510 days old.

Interestingly, while control $Ctip^{Co/+,+/+}/p53^{LSL\text{-}R270H/+}/Wap^{Cre/+}$ females developed breast tumors before an osteosarcoma could develop, 13 out of 24 $Ctip^{Co/Co}/p53^{LSL\text{-}R270H/+}/Wap^{Cre/+}$ experimental females succumbed to osteosarcomas. This predominant tumor type was rarely observed in the females of the p53 conditional-null cohort ($p53^{Co}$) due to a difference in the design of the unrecombined $p53^{LSL\text{-}R270H}$ and $p53^{Co}$ alleles. The control and experimental females in the p53 conditional-null cohort are in essence $p53^{+/+}$ throughout their entire body (Chen, Z. et al., 2005), while the $p53^{LSL\text{-}R270H}$ allele is functionally null, rendering the p53 point mutant control and experimental females $p53^{+/-}$ throughout their entire body (Olive et al., 2004; Tuveson et al., 2004). With this in mind, our results are consistent with the well-established reports indicating that osteosarcomas are the predominant spontaneous tumor type of $p53^{+/-}$ mice (Harvey et al., 1993). Nonetheless, as observed with the p53 conditional-null mutation (Figures 30, A and B), Ctip loss also inhibited mammary tumor induction by a dominant-negative p53 missense mutation commonly observed in human breast cancer (Figure 31).

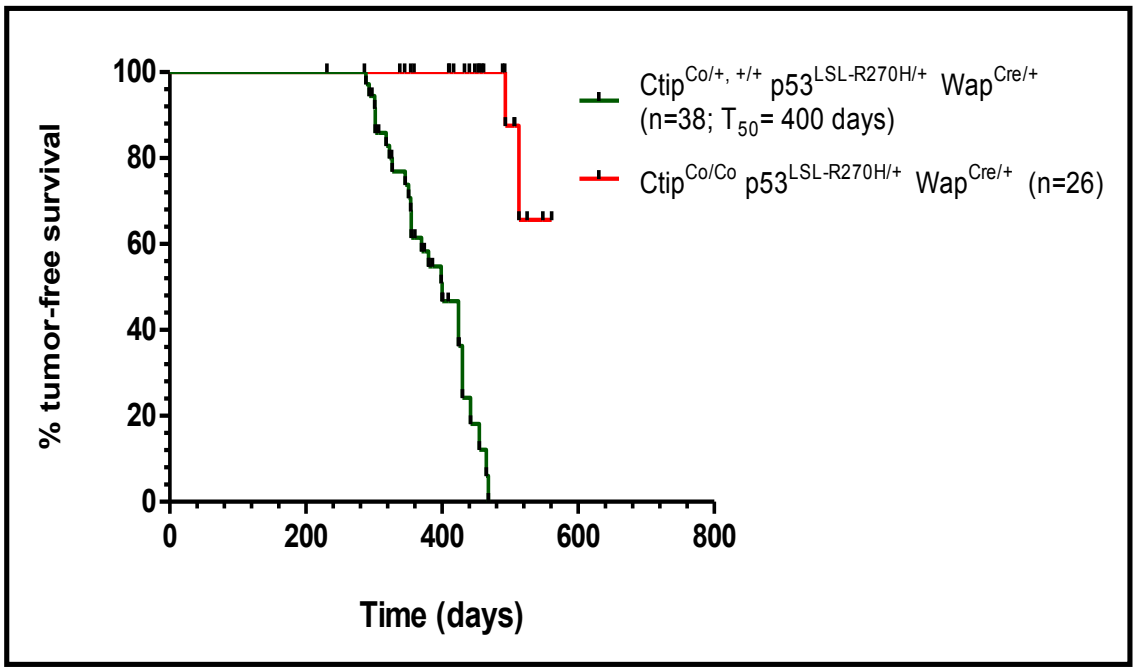

Figure 31. Ctip loss inhibits mammary tumor induction by a dominant-negative p53 missense mutation. Kaplan-Meier tumor-free survival curves of *Ctip*$^{Co/+,+/+}$/*p53*$^{LSL-R270H}$/*Wap*$^{Cre/+}$ (green curve; n=38; T_{50} = 400 days) females compared with *Ctip*$^{Co/Co}$/*p53*$^{LSL-R270H}$/*Wap*$^{Cre/+}$ (red curve; n=26; $P < 0.0001$) females. Significance was estimated with the log-rank test using Graph-Pad Prism (version 4) software. Values were considered statistically significant at $P < 0.05$.

B6. Analysis of the mammary tumor phenotype

The mammary tumors that arose in the conditional Ctip/p53-mutant females were invasive adenocarcinomas with a predominantly solid-glandular or solid-nodular primary pattern. Widespread or multifocal ductal carcinoma *in situ* (DCIS) was detected both adjacent and distal to many of the invasive carcinomas examined, and within separate mammary glands, suggesting that one or more of these pre-invasive foci likely progressed to form the invasive carcinoma. DCIS was rarely observed, however, in the mammary glands of the Ctip/p53-deficient animals that remained mammary tumor free.

The solid-glandular or solid-nodular patterns observed in the Ctip/p53-deficient mammary tumors were quite uniform and resembled the histological patterns of breast tumors that develop following mammary-specific co-inactivation of Brca1 and p53 (personal communication with Dr. Thomas Ludwig, Columbia University). This pattern was in stark contrast to the sarcomatous or spindle-like pattern observed in the breast tumors of p53-deficient alone mice.

Furthermore, by immunohistochemistry, most Ctip/p53-deficient invasive neoplasms stained for the cytoskeletal markers of basal-like breast cancer, including CK5 (6 of 10 tumors), CK14 (10 of 10), and vimentin (5 of 10) (Figure 32, A, B, and C; respectively). These tumors retained the E-cadherin staining (9 of 10) typical of normal epithelial cells (Figure 32D), and most were estrogen receptor (ER) (7 of 10) and progesterone receptor (PR) (9 of 10) negative (Figure 32, E and F; respectively). Therefore, on this basis, a majority of the Ctip/p53-deficient mammary tumors were characterized as basal-like breast carcinomas, a characteristic shared with Brca1/p53-deficient mammary tumors.

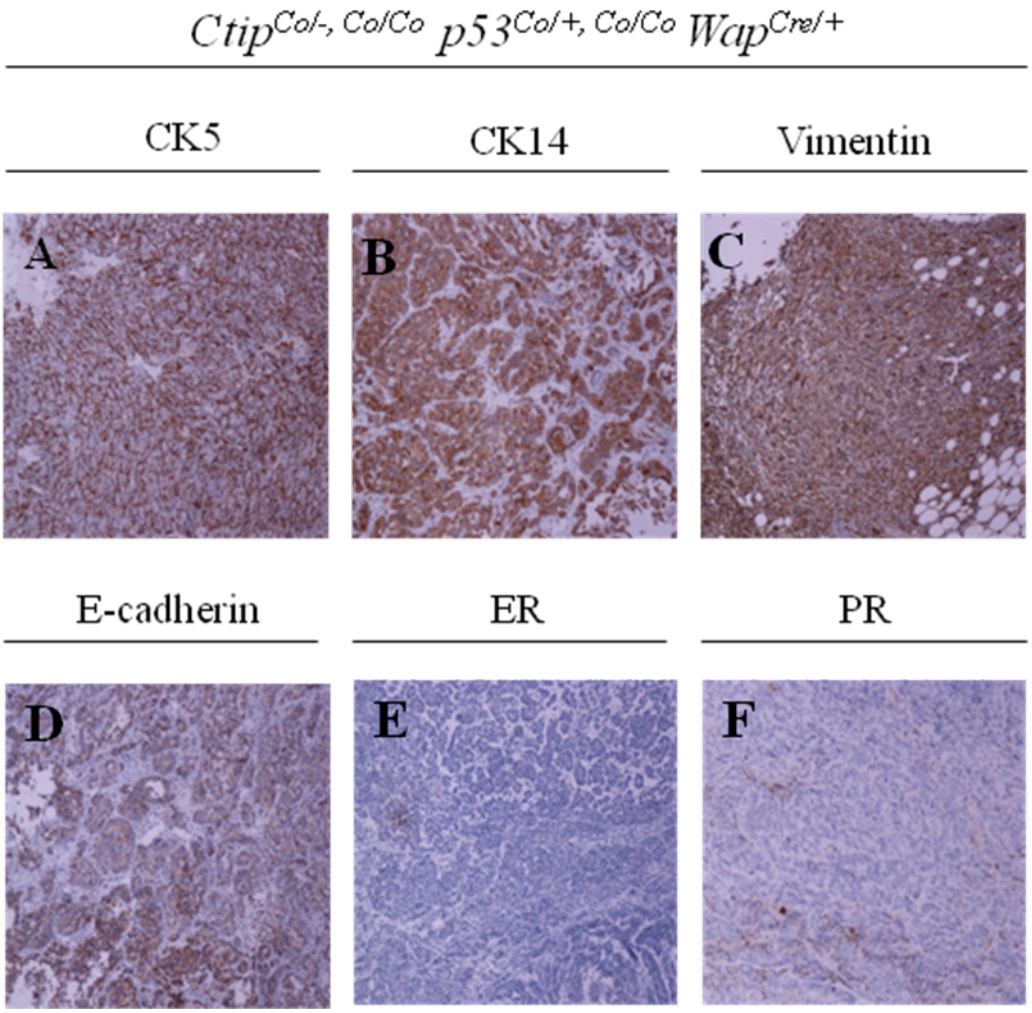

Figure 32. The immunohistochemical phenotype of Ctip/p53-deficient mammary carcinomas. Ctip/p53-deficient mammary carcinomas (*Ctip*$^{Co/–,Co/Co}$*/p53*$^{Co/+,Co/Co}$*/Wap*$^{Cre/+}$) exhibit a basal-like phenotype, a characteristic shared with Brca1/p53-deficient mammary tumors that includes strong immunolabeling for CK5 (A), CK14 (B), and vimentin (C), retention of E-cadherin (D) expression, and negative staining for the estrogen (ERα) (E) and progesterone receptors (PR) (F).

Although the Brca1/p53-deficient and Ctip/p53-deficient mammary tumors exhibited a similar basal-like phenotype, their incidence and latency differed dramatically (Shakya et al., 2011), as co-inactivation of Ctip and p53 resulted in a low incidence (33%; 8/24 in the $p53^{Co/+}$state and 55%; 6/11 in the $p53^{Co/Co}$ state) of breast tumors that developed after a long latency, longer in fact than p53 inactivation alone (recall Figure 30). Moreover, unlike the Brca1/p53-deficient tumors (data not shown), both p53- and Ctip/p53-deficient mammary tumors exhibited amplification of the proto-oncogene c-*Met* (Figure 33). Therefore, to summarize, the Ctip/p53-deficient mammary tumors shared characteristics of both Brca1/p53-deficient tumors (basal-like features) and p53-deficient alone tumors (c-*Met* amplification), while having their own unique tumor incidence and latency.

B7. Assessing the role of Ctip in genome stability with mammary tumor cells

B7a. *Analysis of the mammary tumor cells*

Mammary carcinoma cell lines were derived from several independent breast tumors of both the control ($Ctip^{Co/+}/p53^{Co/+}/Wap^{Cre/+}$) and experimental ($Ctip^{Co/-}/p53^{Co/+}/Wap^{Cre/+}$) cohorts, and genomic DNA from each line was examined by Southern analysis to assess Cre-mediated conversion of the conditional $Ctip^{Co}$ allele to the recombined $Ctip^{Co\text{-}rec}$ null allele. As shown in Figure 34, we observed full recombination of the conditional $Ctip^{Co}$ allele, with retention of the wildtype $Ctip^{+}$ and null $Ctip^{-}$ alleles, respectively, in both control and experimental mammary tumor lines.

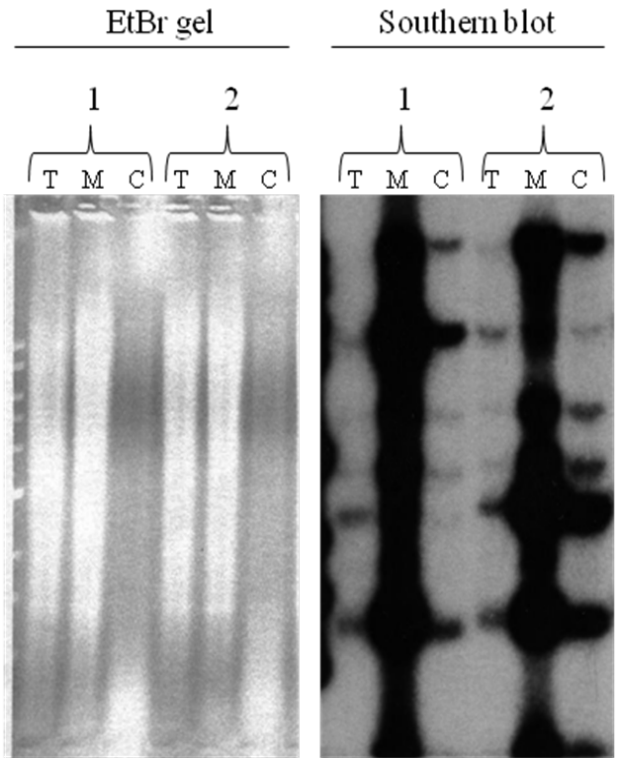

Figure 33. c-*Met* amplification in p53- and Ctip/p53-deficient mammary tumors. Control $Ctip^{Co/+}/p53^{Co/+}/Wap^{Cre/+}$ (1) and experimental $Ctip^{Co/-}/p53^{Co/+}/Wap^{Cre/+}$ (2) tail (T), mammary tumor tissue (M), and mammary tumor cell line (C) genomic DNA was prepared for Southern analysis. The DNA (left) was hybridized with a "*c-Met*" probe (right). The intensity of the bands relative to the amount of DNA loaded on the gel was compared across samples using the corresponding tail DNA, which lacks c-*Met* amplification, as a control. c-*Met* amplification is observed in both control p53-deficient (1) and experimental Ctip/p53-deficient (2) mammary tumor tissue (M) and mammary tumor cells (C). Similar results were observed in the Ctip/p53-deficient mammary tumors of $Ctip^{Co/Co}/p53^{Co/Co}/Wap^{Cre/+}$ experimental females.

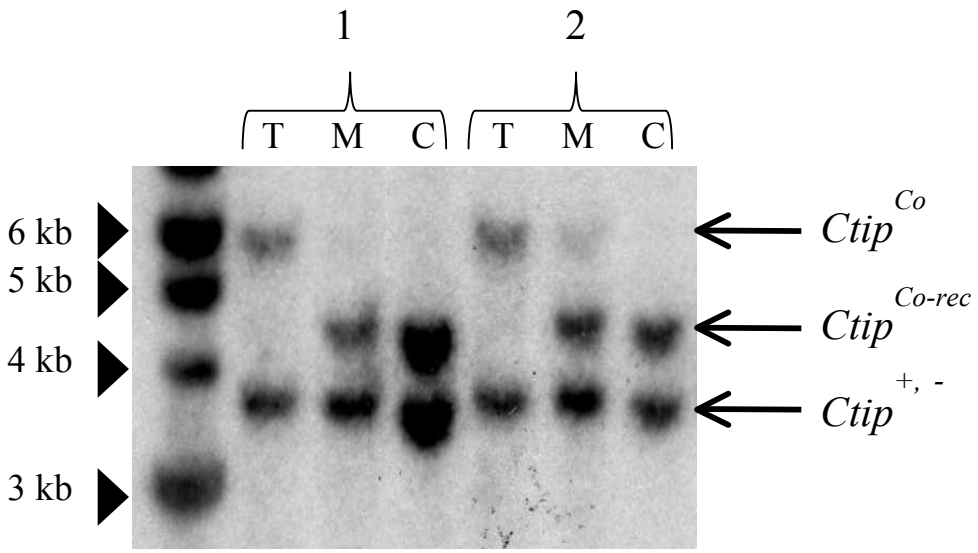

Figure 34. Southern blot analysis of *Ctip*^{Co} recombination in mammary tumor cells. Control *Ctip*$^{Co/+}$/*p53*$^{Co/+}$/*Wap*$^{Cre/+}$ (1) and experimental *Ctip*$^{Co/-}$/*p53*$^{Co/+}$/*Wap*$^{Cre/+}$ (2) tail (T), mammary tumor tissue (M), and mammary tumor cell line (C) genomic DNA was prepared for Southern analysis. *Bgl*II/*Nhe*I-digested DNA was hybridized with the "*Ctip*^{Co}*-SmaI*" probe spanning exon 1. The 5.6 kb *Bgl*II/*Nhe*I fragment represents the unrecombined (*Ctip*^{Co}) allele while the 4.2 kb fragment represents the recombined (*Ctip*$^{Co\text{-}rec}$) allele. The wildtype (*Ctip*$^{+}$) and null (*Ctip*$^{-}$) alleles cannot be discriminated and are recognized as a 3.3 kb band. In both control (*Ctip*$^{Co\text{-}rec/+}$) (1) and experimental (*Ctip*$^{Co\text{-}rec/-}$) (2) mammary tumor cells (C) there is complete recombination of the *Ctip*^{Co} allele, with retention of the *Ctip* wildtype and null alleles, respectively.

Moreover, lysates were prepared from several mammary tumor cell lines to examine Ctip protein expression. By immunoblotting with a CtIP-specific antibody, we observed endogenous Ctip protein in the control, but not in the experimental, mammary tumor cell lines (Figure 35). Surprisingly, therefore, the experimental mammary tumor cells ($Ctip^{Co\text{-}rec/-}$), unlike normal ES cells and MEFs (Chen, P.-L. et al., 2005), are viable despite the complete absence of Ctip expression. Southern analysis also showed complete recombination of the conditional $p53^{Co}$ allele, as well as loss of the wildtype $p53^{+}$ allele, in both the control and experimental mammary tumor lines (Figure 36). Thus, we successfully generated mammary tumor lines that are either double Ctip/p53-null (from the experimental cohort or p53-null alone (from the control cohort). Hereafter, for simplicity, these cells will be referred to as $Ctip^{Co\text{-}rec/-}$ and $Ctip^{Co\text{-}rec/+}$, respectively.

B7b. *Analysis of $Ctip^{Co\text{-}rec/-}$ mammary tumor cells by immunofluorescence*

B7bi. S-phase and IR-treated $Ctip^{Co\text{-}rec/-}$ mammary tumor cells lack Ctip nuclear foci

To confirm the absence of Ctip expression in $Ctip^{Co\text{-}rec/-}$ mammary tumor cells, we used immunofluorescent microscopy to visualize S-phase and IR-induced nuclear foci (IRIFs). In unstressed cells, CtIP localizes to DNA replication foci during S-phase (Gu and Chen, 2009). However, in response to DNA damage, CtIP disperses from S-phase foci and re-emerges to form IRIFs with several other repair proteins (Yu et al., 2006; Sartori et al., 2007). As expected, proficient formation of Ctip-staining S-phase foci and IRIFs were observed in $Ctip^{Co\text{-}rec/+}$ mammary tumor cells, but Ctip recruitment to nuclear foci was absent in both S-phase and IR-treated $Ctip^{Co\text{-}rec/-}$ cells (Figure 37). Therefore, in

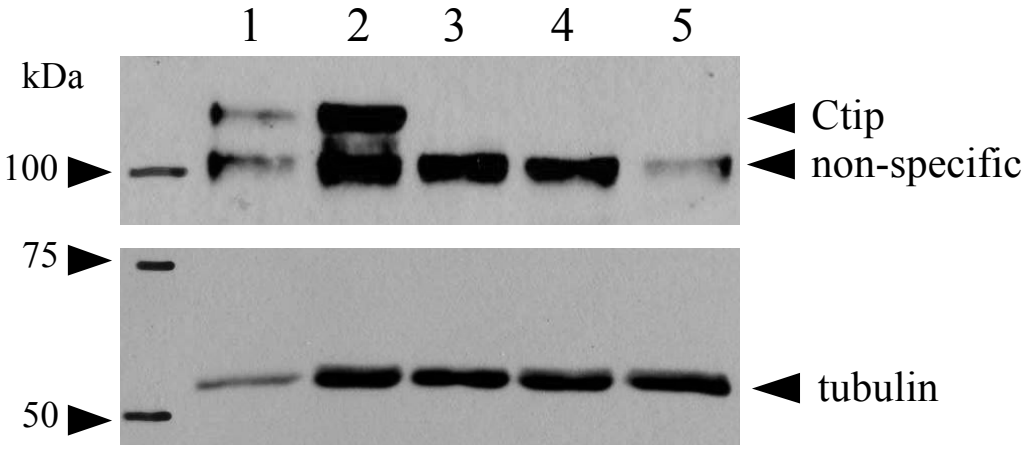

Figure 35. Ctip protein expression in mammary tumor cells. Whole cell lysates were prepared from several independent control *Ctip*$^{Co\text{-}rec/+}$ (lanes 1 and 2) and experimental *Ctip*$^{Co\text{-}rec/–}$ (lanes 3-5) mammary tumor cell lines. The cell lysates were then fractionated by PAGE and immunoblotted with antibodies specific for CtIP or α-tubulin. The experimental *Ctip*$^{Co\text{-}rec/–}$ mammary tumor cells (lanes 3-5) lack endogenous Ctip protein expression. Similar results were also observed in separate experiments using independently derived *Ctip*$^{Co\text{-}rec/Co\text{-}rec}$ mammary tumor cell lines.

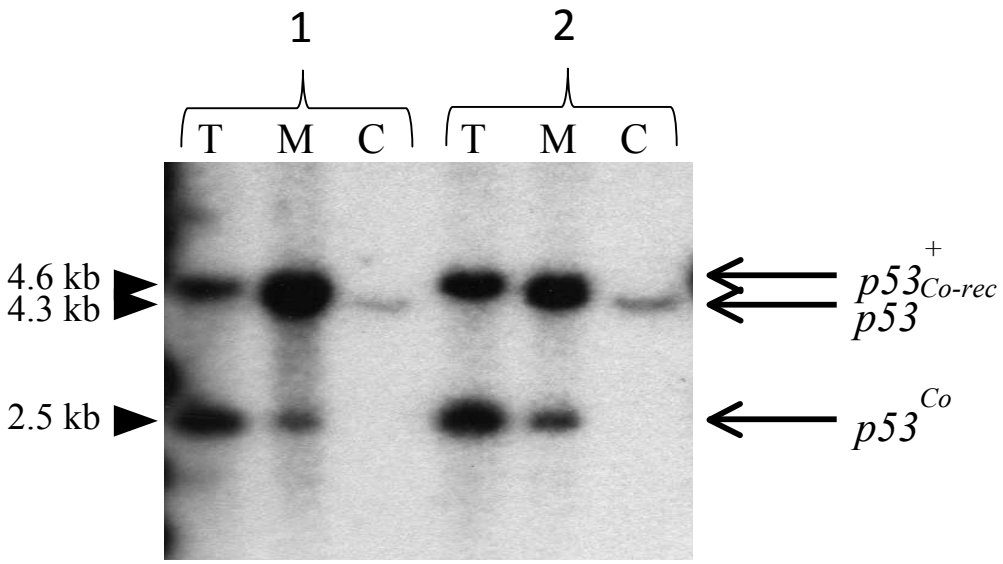

Figure 36. Southern blot analysis of $p53^{Co}$ recombination and loss of wildtype $p53^{+}$ in mammary tumor cells. Control $Ctip^{Co/+}/p53^{Co/+}/Wap^{Cre/+}$ (1) and experimental $Ctip^{Co/-}/p53^{Co/+}/Wap^{Cre/+}$ (2) tail (T), mammary tumor tissue (M), and mammary tumor cell line (C) genomic DNA was prepared for Southern analysis. *Eco*RV-digested DNA was hybridized with the "$p53^{Co}$" probe, which recognizes the wildtype $p53^{+}$ (4.6 kb), recombined $p53^{Co\text{-}rec}$ (4.3 kb) and unrecombined $p53^{Co}$ (2.5 kb) alleles. In both control (1) and experimental (2) mammary tumor cells (C) there is complete recombination of the $p53^{Co}$ allele as well as loss of the wildtype $p53^{+}$ allele; therefore, these cells are p53-null.

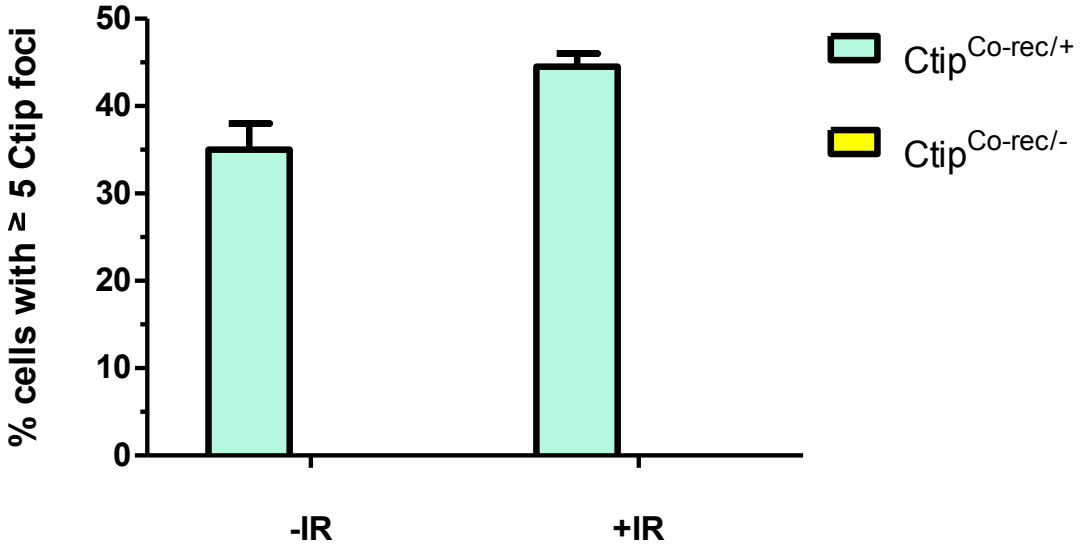

Figure 37. Ctip focus formation is absent in *Ctip*$^{Co\text{-}rec/–}$ mammary tumor cells. *Ctip*$^{Co\text{-}rec/+}$ and *Ctip*$^{Co\text{-}rec/–}$ mammary tumor cells were subjected to 10 Gy of IR or left untreated; 1 hour later, cells were fixed and stained with CtIP-specific antibodies. Ctip-containing S-phase foci and IRIFs were counted in 300 cells of two independent mammary carcinoma cell lines for each genotype, and the error bars represent SE of the mean. Ctip S-phase foci and IRIF formation was absent in *Ctip*$^{Co\text{-}rec/–}$ mammary carcinoma cells, consistent with the lack of endogenous Ctip protein expression in these cells (Figure 35, lanes 3-5).

accord with the immunoblotting data (Figure 35), immunofluorescent staining of Ctip is not observed in *Ctip*$^{Co\text{-}rec/-}$ mammary tumor cells.

B7bii. Brca1, RPA, and Rad51 polypeptides are recruited normally to S-phase foci and IRIFs in *Ctip*$^{Co\text{-}rec/-}$ mammary tumor cells

Given the viability of *Ctip*$^{Co\text{-}rec/-}$ mammary tumor cells, we were able to evaluate whether Ctip is required for the localization of other repair proteins (e.g., Brca1, RPA, and Rad51) to both S-phase foci and IRIFs. Although we and others have observed proper Brca1 focus formation in the absence of the Brca1-Ctip interaction (Yu et al., 2006; Section B7a of Chapter III), these data do not rule out the possibility that Ctip indirectly recruits Brca1 to sites of DNA damage. Nevertheless, as shown in Figure 38, Brca1 was properly recruited to S-phase foci and IRIFs in both control *Ctip*$^{Co\text{-}rec/+}$ and Ctip-deficient *Ctip*$^{Co\text{-}rec/-}$ mammary tumor cells.

To ascertain whether loss of Ctip affects DNA resection, we examined IR-induced focus formation by the RPA complex. Since RPA readily coats the ssDNA tracts generated by 5' to 3' resection to form RPA/ssDNA nucleoprotein filaments, RPA recruitment to sites of DNA damage is commonly used as an indirect readout of DNA resection. Although CtIP is reported to promote ssDNA formation (Sartori et al., 2007; Chen et al., 2008; Nakamura et al., 2010), we observed normal RPA localization to IRIFs in both control *Ctip*$^{Co\text{-}rec/+}$ and Ctip-deficient *Ctip*$^{Co\text{-}rec/-}$ mammary tumor cells (Figure 39). The levels of RPA assembly at S-phase nuclear foci were also comparable in *Ctip*$^{Co\text{-}rec/+}$ and *Ctip*$^{Co\text{-}rec/-}$ cells (Figure 39). Surprisingly, these results suggest that ssDNA

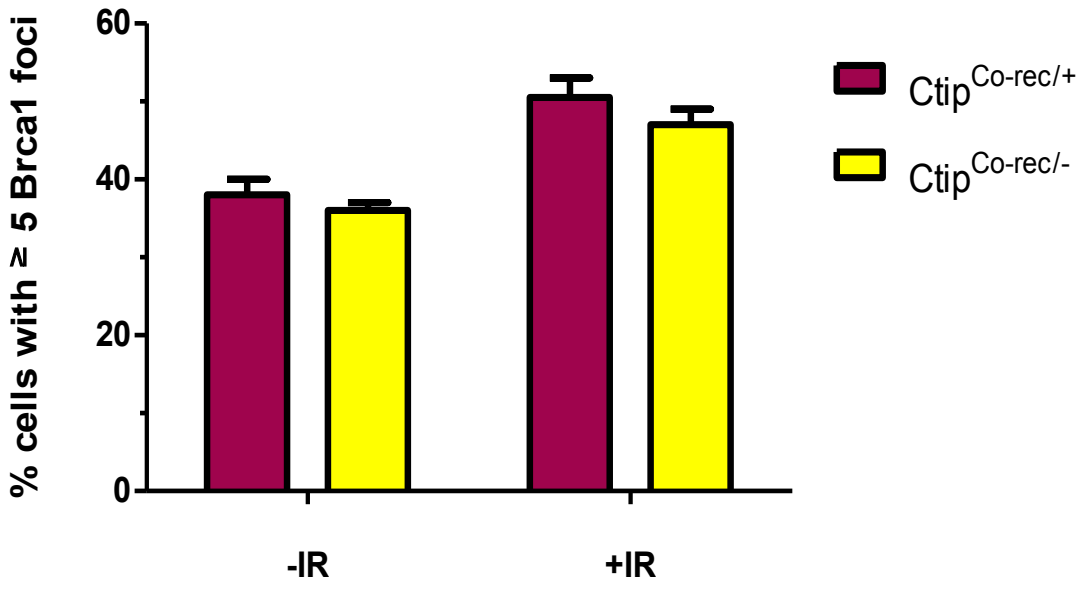

Figure 38. Proficient formation of Brca1 foci in *Ctip*$^{Co\text{-}rec/–}$ mammary tumor cells. Primary *Ctip*$^{Co\text{-}rec/+}$ and *Ctip*$^{Co\text{-}rec/–}$ mammary carcinoma cells were either untreated to assess S-phase foci formation or exposed to IR (10 Gy) to assess IRIF formation. 1 hour post-irradiation the cells were immunostained with a mouse-specific Brca1 antibody. Brca1-containing S-phase foci and IRIFs were counted in 300 cells of two independent mammary tumor cell lines for each genotype, and the error bars represent SE of the mean. Brca1 was efficiently recruited to both S-phase foci and IRIFs in Ctip-deficient *Ctip*$^{Co\text{-}rec/–}$ mammary tumor cells.

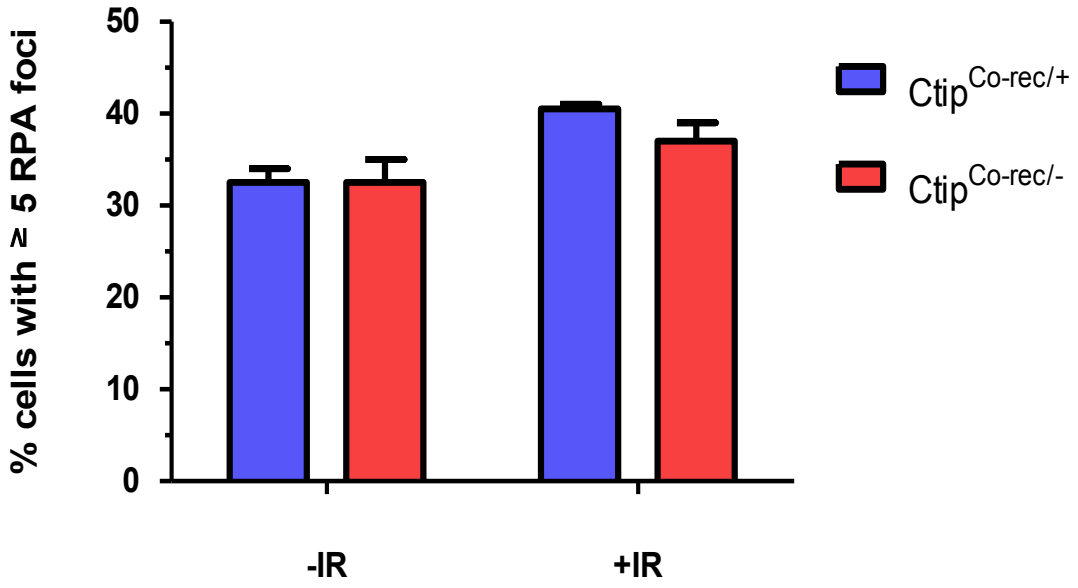

Figure 39. Proficient formation of RPA foci in *Ctip*$^{Co\text{-}rec/–}$ mammary tumor cells. *Ctip*$^{Co\text{-}rec/+}$ and *Ctip*$^{Co\text{-}rec/–}$ mammary carcinoma cells were either untreated to assess S-phase foci formation or exposed to IR (10 Gy) to assess IRIF formation. Foci formation was assessed 1 hour post-irradiation by immunostaining with RPA-specific antibodies. RPA-containing S-phase foci and IRIFs were counted in 300 nuclei of two independent mammary tumor cell lines for each genotype. The error bars represent SE of the mean. RPA localization to S-phase foci and IRIFs was comparable in *Ctip*$^{Co\text{-}rec/+}$ and *Ctip*$^{Co\text{-}rec/–}$ mammary carcinoma cells.

formation by end resection may be independent of Ctip in *Ctip*$^{Co\text{-}rec/–}$ mammary tumor cells.

During the DNA damage response, the Rad51 recombination protein can displace RPA from RPA/ssDNA filaments to form a Rad51/ssDNA nucleoprotein filament that initiates strand invasion and homologous recombination. To determine if Rad51 recruitment to sites of DNA damage is dependent on Ctip, we assessed Rad51 focus formation in *Ctip*$^{Co\text{-}rec/–}$ mammary tumor cells. As shown in Figure 40, we observed proficient formation of Rad51-staining S-phase foci and IRIFs in *Ctip*$^{Co\text{-}rec/–}$ cells. Rad51 was recruited to these nuclear structures with the same efficiency as observed in the control *Ctip*$^{Co\text{-}rec/+}$ cells (Figure 40). Thus, Ctip is not required for the localization of Rad51 to sites of DNA damage. Since these nuclear structures likely reflect the assembly of Rad51/ssDNA nucleofilaments, this result indirectly suggests that DNA resection can take place in the absence of Ctip. Overall, Ctip may be dispensable for DNA resection and HDR given the proper recruitment of Brca1, RPA, and Rad51 to DSB sites in Ctip-deficient cells.

B7c. *Cytogenetic analysis of chromosomal stability*

B7ci. *Ctip*$^{Co\text{-}rec/–}$ mammary tumor cells suppress both spontaneous and MMC-induced chromosomal rearrangements

Next we used cytogenetic analysis to assess the ability of Ctip-deficient cells to suppress spontaneous and MMC-induced chromosomal rearrangements. Interestingly, low levels of spontaneous chromosomal rearrangements were observed in metaphase spreads of both *Ctip*$^{Co\text{-}rec/–}$ and *Ctip*$^{Co\text{-}rec/+}$ mammary tumor cells (Figure 41A). This

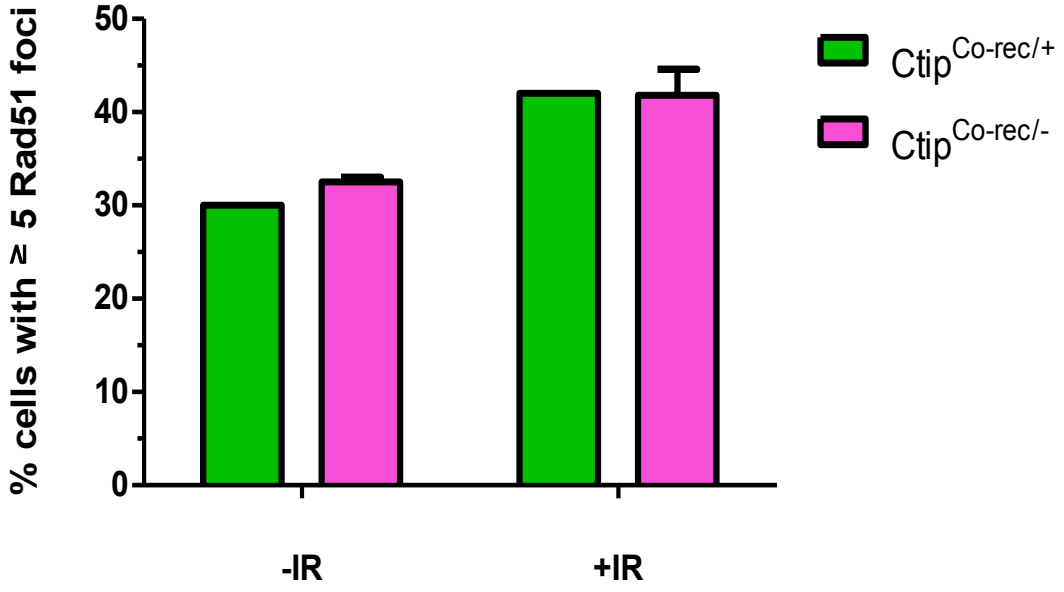

Figure 40. Proficient formation of Rad51 foci in *Ctip*$^{Co\text{-}rec/–}$ mammary tumor cells. *Ctip*$^{Co\text{-}rec/+}$ and *Ctip*$^{Co\text{-}rec/–}$ mammary tumor cells were subjected to 10 Gy of IR or left untreated; 1 hour later, the cells were fixed and stained with Rad51-specific antibodies. Rad51-containing S-phase foci and IRIFs were counted in 300 nuclei of two independent mammary tumor cell lines for each genotype. The error bars represent SE of the mean. Rad51 localization to S-phase foci and IRIFs was comparable in mammary tumor cells of either *Ctip* genotype.

result indicates that Ctip-deficient cells display normal resistance to spontaneous chromosomal instability. We also compared metaphase spreads from $Ctip^{Co\text{-}rec/-}$ and $Ctip^{Co\text{-}rec/+}$ cells treated for 16 hours with 40 ng/mL of the DNA interstrand crosslinking agent mitomycin C (MMC). In response to MMC, the $Ctip^{Co\text{-}rec/-}$ mammary tumor cells again accumulated cytogenetic defects at a similar rate to control $Ctip^{Co\text{-}rec/+}$ cells (Figure 41B) suggesting that Ctip is not required for the suppression of MMC-induced chromosomal aberrations. The types of spontaneous and MMC-induced chromosomal rearrangements observed in the $Ctip^{Co\text{-}rec/-}$ and $Ctip^{Co\text{-}rec/+}$ cells were predominantly chromatid/chromosome breaks and gaps, as opposed to complex rearrangements or exchanges (Table 5). Furthermore, pronounced aneuploidy was not observed in the $Ctip^{Co\text{-}rec/-}$ mammary tumor cells relative to $Ctip^{Co\text{-}rec/+}$ cells (data not shown). Thus, in these tumor lines, Ctip appears to be dispensable for recruitment of key repair proteins (Brca1, RPA, and Rad51) to sites of DNA damage and for suppression of spontaneous and MMC-induced chromosomal abnormalities.

A.

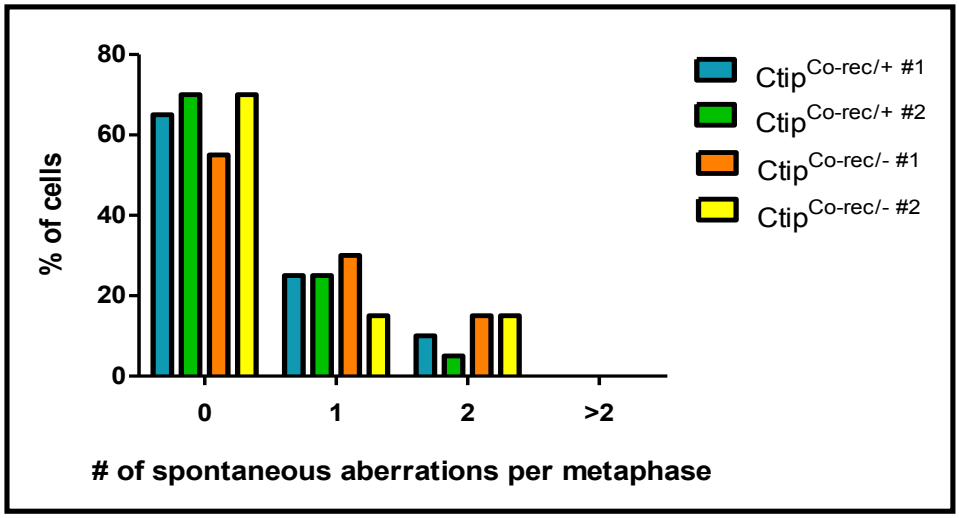

B.

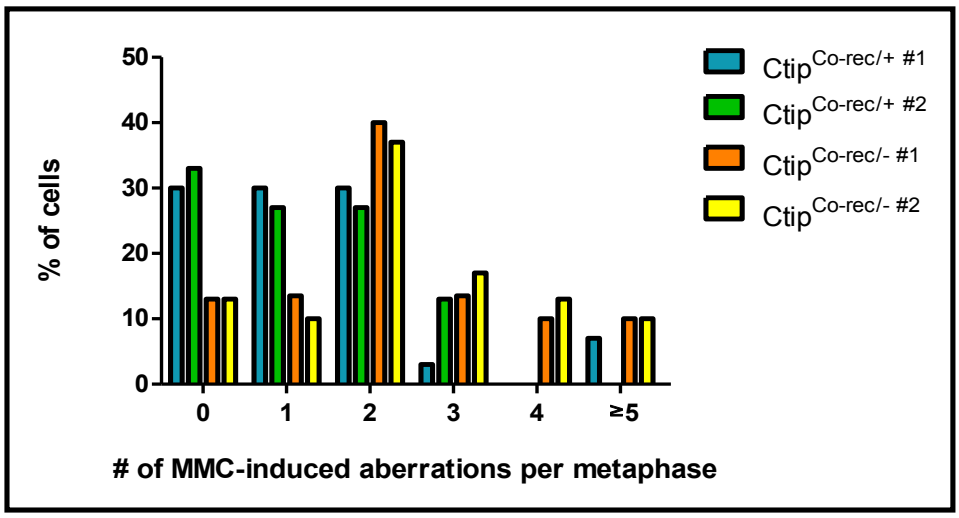

Figure 41. Low levels of spontaneous and MMC-induced chromosomal aberrations in *Ctip*$^{Co\text{-}rec/-}$ mammary tumor cells. Primary *Ctip*$^{Co\text{-}rec/+}$ and *Ctip*$^{Co\text{-}rec/-}$ mammary carcinoma cells were cultured in the (A) absence or (B) presence of MMC (40 ng/mL, 16 hours) and subjected to karyotype analysis. Following colcemid treatment, exposure to a hypotonic solution, and methanol/acetic acid fixation, the cell suspensions were dropped onto glass slides and stained with Giemsa. For each treatment condition, at least twenty metaphase spreads per cell line were examined for numerical and structural chromosomal aberrations.

Table 5. Spontaneous and induced chromosomal aberrations in mouse mammary tumor cells with different Ctip genotypes.

				Aberrations	
Ctip genotype	Metaphases analyzed	MMC treatment	Metaphase aberrations, %	Chr/Cht breaks and gaps	Exchange/Other
CtipCo-rec/+ (#1)	20	-	35	6	0
	30	+	70	32	0
CtipCo-rec/+ (#2)	20	-	30	5	0
	30	+	67	29	2
CtipCo-rec/- (#1)	20	-	45	9	0
	30	+	87	51	2
CtipCo-rec/- (#2)	20	-	30	8	0
	30	+	87	57	3

MMC, mitomycin C / Chr, chromosome / Cht, chromatid

The percentage of metaphases containing one or more aberrations, as well as a breakdown of aberration-type, is shown for each mammary carcinoma cell line in both the absence (–) and presence (+) of MMC.

C. DISCUSSION

Apart from an amino-terminal coiled-coil domain that is now known to mediate protein homodimerization (Dubin et al., 2004), the amino acid sequence of CtIP does not harbor obvious structural features. Thus, the first clues to the biological function of CtIP were provided by the identification of CtIP-interacting partners. CtIP contains several short sequence motifs required for its interaction with the transcriptional co-repressor CtBP (Schaeper et al., 1998), the tumor suppressor Rb (Fusco et al., 1998), and the tumor suppressor BRCA1 (Wong et al., 1998; Yu et al., 1998). These interactions are thought to mediate CtIP function in transcriptional regulation, the DNA damage response, and cell cycle checkpoint control (Meloni et al., 1999; Li et al., 2000; Yu and Chen, 2004; Chen, P.-L. et al., 2005; Liu and Lee, 2006).

Further studies also raised the possibility that CtIP may itself serve as a tumor suppressor. Monoallelic genetic alterations of the *CtIP* gene have been identified in some human tumor cells, including mismatch repair-deficient colorectal carcinomas (Wong et al., 1998; Vilkki et al., 2002). Furthermore, heterozygous $Ctip^{+/-}$ mice develop tumors at an increased rate relative to wildtype $Ctip^{+/+}$ mice, suggesting that haploid insufficiency of *Ctip* can lead to tumorigenesis (Chen, P.-L. et al., 2005). However, none of these studies addressed whether CtIP exerts tumor suppression activity in mammary epithelial cells, an intriguing possibility given that CtIP interacts with the BRCA1 tumor suppressor.

To test this hypothesis, we generated a conditional-null Ctip ($Ctip^{Co}$) allele in ES cells and introduced it into the mouse germline. Importantly, we showed that the $Ctip^{Co\text{-}rec}$ allele that arises upon Cre-mediated recombination of $Ctip^{Co}$ is non-functional.

Therefore, by restricting Cre expression to mammary epithelial cells, we were able to inactivate the $Ctip^{Co}$ allele in a mammary-specific fashion. This strategy mimics the approach used to demonstrate the tumor suppressor activity of Brca1 (Shakya et al., 2008), and thus the tumorigenic consequences of *Ctip* and *Brca1* inactivation could be directly compared.

Conditional inactivation of Brca1 elicits mammary carcinomas that phenotypically resemble the basal-like breast tumors of human BRCA1 mutation carriers (Shakya et al., 2008). In contrast, we report here that mammary-specific Ctip inactivation does not generate breast tumors in mice. Although BRCA1 and CtIP are both essential for the viability of non-malignant mammalian cells, such as ES cells and MEFs (Elledge and Amon, 2002; Chen, P.-L. et al., 2005; Reid et al., 2008), the embryonic lethality phenotype of *Ctip*-null embryos is reported to be more severe than that of *Brca1* nullizygotes (Chen, P.-L. et al., 2005). By PCR analysis, we were able to detect the recombined $Ctip^{Co\text{-}rec}$ allele in the mammary glands of experimental pregnant (E18.5) and lactating females (Figure 28), suggesting that *Ctip*-nullizygous mammary epithelial cells are not eliminated immediately by cell death upon Cre-mediated recombination of the $Ctip^{Co}$ allele. Nevertheless, unlike the *Brca1*-null cells produced by mammary-specific inactivation of $Brca1^{Co}$ (Shakya et al., 2008), *Ctip*-null cells did not give rise to mammary tumors.

Since p53 mutations are prevalent in BRCA1-associated tumors (Crook et al., 1997; Xu et al., 1999a), we examined the effect of Ctip conditional inactivation in a tumor-prone setting using a p53 conditional-null mutation. Strikingly, we observed an increased latency and a reduced incidence of mammary tumor development upon conditional co-

inactivation of Ctip and p53, relative to conditional p53 inactivation alone. This result indicates not only that Ctip inactivation fails to potentiate p53-induced mammary tumor formation, but that Ctip loss actually provides a protective effect against tumorigenesis in this setting. This phenomenon was observed whether p53 deficiency was achieved by monoallelic or biallelic *p53* gene inactivation or by expression of a dominant-negative p53 mutant polypeptide. Thus, our results challenge the assumption that Ctip acts as a tumor suppressor and question whether the monoallelic mutations of human CtIP observed in mismatch repair-deficient colorectal carcinomas are truly oncogenic.

Several possible explanations can be invoked to account for the prolonged tumor latency observed following conditional inactivation of Ctip. First, loss of Ctip may inhibit tumor development by reducing the viability of precancerous cells. It should be noted, however, that mammary tumors are readily generated by a similar protocol of Brca1 inactivation, despite the fact that *Brca1*-null ES cells and MEFs are also inviable (Elledge and Amon, 2002; Reid et al., 2008). Second, Ctip loss may delay tumorigenesis by preventing the formation of oncogenic chromosome translocations (Zhang and Jasin, 2011). This intriguing possibility emerged from a recent study which implicated CtIP-mediated alt-NHEJ, a resection-dependent repair process, in the formation of tumor-associated chromosomal translocations (Zhang and Jasin, 2011). Third, CtIP is reported to relieve an Rb-mediated G_1 restraint, since Ctip depletion arrests $Rb^{+/+}$, but not $Rb^{-/-}$, MEFs in the G_1 phase of the cell cycle (Chen, P.-L. et al., 2005; Chinnadurai, G., 2006). As such, loss of CtIP may inhibit tumor formation by allowing Rb-dependent cell cycle arrest. This notion is attractive because the CtIP protein (also called RBBP8) harbors an LxCxE motif that is reported to bind the interaction pocket of the Rb tumor suppressor

(Fusco et al., 1998). However, inspection of the GenBank database reveals that the motif is poorly conserved; thus, while LxCxE is present in the mouse and rat orthologs of CtIP, it has diverged in many other mammals, including orangutans, dogs, cows, horses, and platypuses.

Interestingly, the mammary tumors that arise upon co-inactivation of Ctip and p53 are phenotypically distinct from those obtained by either Brca1/p53 co-inactivation or by p53 inactivation alone. Specifically, like Brca1/p53-deficient mammary tumors, the Ctip/p53-deficient neoplasms display a solid-glandular and solid-nodular histopathology, stain for the basal cytokeratins CK5 and CK14, and lack expression of the estrogen and progesterone receptors. However, in contrast to Brca1/p53-deficient tumors, the Ctip/p53-deficient tumors show amplification of the c-*Met* proto-oncogene, a common feature of p53-deficient alone tumors (Rong et al., 1995). Thus, the Ctip/p53-deficient tumors appear to incorporate different phenotypic features of the Brca1/p53-deficient and p53-deficient tumors.

Although *Ctip*-nullizygous mouse ES cells and MEFs are not viable (Chen, P.-L. et al., 2005), we were able to generate permanent cell lines from the mammary tumors of experimental $Ctip^{Co/-}/p53^{Co/+}/Wap^{Cre/+}$ mice. As such, these represent the first mammalian *Ctip*-null cells to be cultured *in vitro*. Southern analysis established that these cells are genetically null for Ctip ($Ctip^{Co\text{-}rec/-}$), and Western analysis confirmed the absence of Ctip protein expression. Although we do not know the mechanism by which these cells retain viability in the absence of Ctip expression, as malignant cells, they may harbor additional genetic lesions that compensate for the absence of Ctip.

There is substantial evidence that CtIP is required for maintenance of genomic stability, at least in part through its role in resection and repair of DSBs (Sartori et al., 2007; Bennardo et al., 2008). Nevertheless, we found that the levels of spontaneous and genotoxin-induced chromosomal rearrangements were indistinguishable in mammary carcinoma cell lines that did ($Ctip^{Co\text{-}rec/+}$) or did not ($Ctip^{Co\text{-}rec/-}$) express Ctip. In addition, immunofluorescent microscopy revealed that essential components of the HDR machinery, including Brca1 and Rad51, were proficiently recruited to sites of DNA damage in the absence of Ctip. We also observed normal assembly of IR-induced RPA foci, suggesting that Ctip is not essential for the formation of ssDNA ends by resection in $Ctip^{Co\text{-}rec/-}$ cells. These results are in stark contrast to previous studies, in which siRNA-mediated knockdown of CtIP disrupted both RPA focus formation and an anti-BrdU staining of ssDNA foci in genotoxic-treated human tumor lines (Sartori et al., 2007; Chen et al., 2008).

Although we do not know the mechanisms by which $Ctip^{Co\text{-}rec/-}$ mammary tumor cells retain chromosomal stability in the absence of Ctip, one can envision scenarios in which an additional genetic lesion might compensate for loss of Ctip. For example, one untested, but plausible, possibility would be a defect in the function of the Ku70/Ku80 heterodimer, a critical upstream factor in the NHEJ pathway of DSB repair. A two-stage DSB resection process has been identified in yeast and mammalian cells (Gravel et al., 2008; Mimitou and Symington, 2008; Raynard et al., 2008; Zhu et al., 2008), whereby MRN(MRX) and CtIP(Sae2) generate minimally resected DSB intermediates to recruit nucleases/helicases that catalyze extensive and processive resection. In *S. cerevisiae*, the initial processing of a DSB end by MRX-Sae2 creates a less appealing substrate for

binding of the Ku70/Ku80 complex (Mimitou and Symington, 2010). Interestingly, yeast *sae2*Δ mutants are highly sensitive to IR, presumably because DNA-bound Ku70/Ku80 blocks end resection (Mimitou and Symington, 2010), but deletion of Ku70 rescues the IR sensitivity phenotype of *sae2*Δ mutants. This observation suggests that loss of end protection by Ku70/Ku80 allows extensive resection by the processive nucleases/helicases to occur in the absence of Sae2 (Mimitou and Symington, 2010). Perhaps, therefore, an analogous loss of Ku70/Ku80 function would allow $Ctip^{Co\text{-}rec/-}$ tumor cells to execute DNA resection and other aspects of the DNA damage response without Ctip function. Clearly, further studies will be required to ascertain the mechanisms of DSB repair in $Ctip^{Co\text{-}rec/-}$ tumor cells.

In summary, $Ctip^{Co\text{-}rec/-}$ mammary tumor cells appear to resect DSB ends and respond to DNA damage properly. This is further supported by the ability of these cells to suppress both spontaneous and MMC-induced chromosomal aberrations. Thus, key aspects of genomic stability are maintained in the $Ctip^{Co\text{-}rec/-}$ mammary tumor cells. Remarkably, the *in vivo* inactivation of Ctip provided a protective effect against the development of mammary tumors due to p53 deficiency. Understanding how loss of Ctip exerts this protective effect may offer novel opportunities for therapeutic intervention.

CHAPTER V

THE ROLE OF THE BRCT PHOSPHO-LIGANDS OF BRCA1 IN GENOME STABILITY AND TUMOR SUPPRESSION

A. INTRODUCTION

The two BRCA1 carboxy-terminal (BRCT) motifs of BRCA1 form a phosphoprotein recognition domain (Koonin et al., 1996; Manke et al., 2003; Yu et al., 2003) that preferentially binds the pSer-x-x-Phe motif (Manke et al., 2003; Rodriguez et al., 2003) of three known repair proteins, Abraxas/CCDC98, BACH1/BRIP1/FancJ, and CtIP (reviewed in Huen et al., 2010; Moynahan and Jasin, 2010). Importantly, the phospho-recognition surface of tandem BRCT motifs can only accommodate one phospho-ligand at a time; therefore, a single BRCA1 polypeptide will bind Abraxas, BACH1, or CtIP in a mutually exclusive manner (Yu and Chen, 2004; Greenberg et al., 2006; Kim et al., 2007; Liu, Z. et al., 2007; Wang et al., 2007). Thus, BRCA1 forms a distinct complex with each of these BRCT-interacting phosphoproteins to mediate unique aspects of its function in response to DNA damage (Greenberg et al., 2006; reviewed in Huen et al., 2010).

Since the phosphopeptide binding property of the BRCT repeats is critical for BRCA1 tumor suppression (Shakya et al., 2011), we, in collaboration with Dr. Thomas Ludwig (Columbia University), sought to determine which phosphoprotein interaction mediates this function. To do this, single amino acid (serine-to-alanine) substitutions were made in Abraxas, BACH1, and CtIP to ablate the phosphoprotein interaction with the BRCT domain of BRCA1. As described earlier in this thesis, mice bearing the Ctip-S326A mutation are not tumorigenic and thus, BRCA1 tumor suppression is not mediated exclusively by its interaction with CtIP (Section B11a of Chapter III). Similarly, tumor formation was not observed in mice harboring either the Abraxas-S404A or the Bach1-S994A point mutation (data not shown). Therefore, BRCA1 tumor suppression is not dependent on its individual interaction with the phospho-ligands Abraxas, BACH1, or

CtIP. Instead tumor suppression may require the interaction of BRCA1 with two or more of these phosphoproteins (and/or other as yet undiscovered phosphoproteins).

To determine if BRCA1 tumor suppression is mediated by the interaction of BRCA1 with two of its known BRCT phospho-ligands, we generated each of the three combinations of double homozygous mutant mice (*Abx*$^{S404A/S404A}$/*Bach1*$^{FH\text{-}S994A/FH\text{-}S994A}$, *Abx*$^{S404A/S404A}$/*Ctip*$^{S326A/S326A}$, and *Bach1*$^{FH\text{-}S994A/FH\text{-}S994A}$/*Ctip*$^{S326A/S326A}$) and monitored them for tumor development. For convenience, these animals will be referred to as "AB", "AC", and "BC" mice, respectively. Additionally, we bred triple homozygous mutant mice (*Abx*$^{S404A/S404A}$/*Bach1*$^{FH\text{-}S994A/FH\text{-}S994A}$/*Ctip*$^{S326A/S326A}$; "ABC" mice) to determine if BRCA1 tumor suppression requires BRCA1's association with all three BRCT-interacting phosphoproteins. Since the genome maintenance functions of BRCA1 are thought to be critical for its tumor suppression activity, we also examined chromosomal stability and the DNA damage response in cells bearing each of these genotypes.

B. RESULTS

B1. Genome stability and tumor suppression in double mutant (AB, AC, and BC) cells and animals

B1a. *Generation of AB, AC, and BC double mutant MEFs*

Mouse embryonic fibroblasts (MEFs) derived from tumor-prone *Brca1*$^{S1598F/S1598F}$ mice display a genomic instability phenotype that includes chromosomal abnormalities and defective DNA damage responses (Shakya et al., 2011). Since the Brca1-S1598F mutation ablates the phospho-recognition property of the BRCT domain, these results indicate that the genome stability functions of BRCA1 are mediated by its interaction with one or more of its BRCT phospho-ligands. Since *Ctip*$^{S326A/S326A}$ MEFs do not display a comparable genomic instability phenotype, this aspect of BRCA1 function is not solely dependent on the Brca1-Ctip interaction (Chapter III of this thesis). Likewise, this genomic instability phenotype is also not observed in either *Abx*$^{S404A/S404A}$ or *Bach1*$^{FH\text{-}S994A/FH\text{-}S994A}$ MEFs (data not shown). Therefore, we sought to determine whether genome stability is maintained when the interactions of BRCA1 with two of its known BRCT phospho-ligands are simultaneously ablated.

To this end, we crossed homozygous *Ctip*$^{S326A/S326A}$ mice with homozygous *Abx*$^{S404A/S404A}$ or *Bach1*$^{FH\text{-}S994A/FH\text{-}S994A}$ mice (kindly provided by Dr. Thomas Ludwig, Columbia University) to produce double heterozygous mutant animals which, when intercrossed, would yield the desired double homozygous mutant AC (*Abx*$^{S404A/S404A}$/*Ctip*$^{S326A/S326A}$) and BC (*Bach1*$^{FH\text{-}S994A/FH\text{-}S994A}$/*Ctip*$^{S326A/S326A}$) mice. In a similar fashion, we also generated double homozygous mutant AB (*Abx*$^{S404A/S404A}$/*Bach1*$^{FH\text{-}S994A/FH\text{-}S994A}$) mice. Notably, the double homozygous mutant

mice of each genotype (AB, AC, and BC) were viable, healthy, fertile, and indistinguishable from their littermate controls.

Due to the viability of the double homozygous mutant mice, cultured MEFs of each genotype were readily established. Matings were set up and E13.5 day embryos were aseptically dissected from the pregnant mother mouse and minced under sterile conditions to generate primary MEFs. The phenotypes of the double homozygous AB, AC, and BC mutant MEFs were then examined.

B1b. *AB, AC, and BC double mutant MEFs proliferate normally*

Brca1$^{S1598F/S1598F}$ cells, which express a Brca1 polypeptide that fails to interact with its BRCT phospho-ligands, display a marked proliferation defect which may be triggered by their inability to mount normal cellular responses to DNA damage (Shakya et al., 2011). Therefore, we examined the proliferation rate of early passage primary AB, AC, and BC double mutant MEFs using the MTT assay. As shown in Figure 42, the proliferation rates of AB and BC double mutant MEFs were comparable to those of heterozygous control MEFs (*Abx*$^{S404A/+}$/*Bach1*$^{FH\text{-}S994A/+}$/*Ctip*$^{S326A/+}$). Additionally, we observed normal proliferation rates for the AC double mutant MEFs (data not shown).

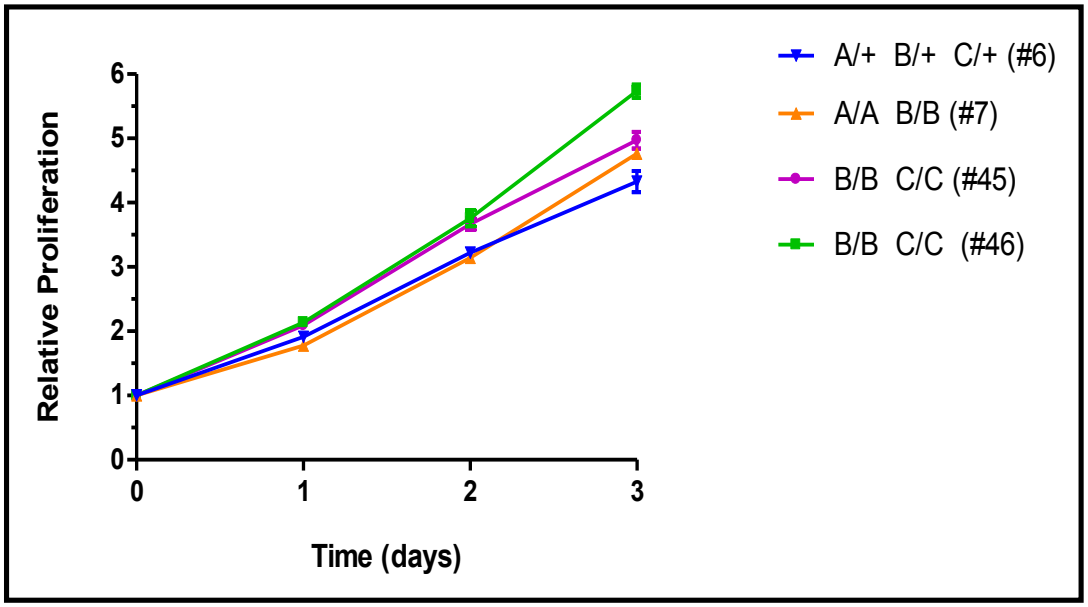

Figure 42. Double mutant BRCT phospho-ligand MEFs proliferate normally. The cellular proliferation of double homozygous AB (A/A B/B) and BC (B/B C/C) early passage primary MEFs was measured and compared to the proliferation rate of control (A/+ B/+ C/+) MEFs. Cells were seeded on 96-well plates at a density of 2000 cells per well. At the indicated time points, cell numbers were determined using an MTT assay. Values on the Y-axis represent folds of increase in cell numbers. The error bars represent the mean ± SD of triplicate samples. A = *Abraxas*^{S404A}; B = *Bach1*$^{FH\text{-}S994A}$; C = *Ctip*^{S326A}

B1c. *The IR sensitivity of AB, AC, and BC double mutant mice*

One of the hallmarks of a defective DNA damage response is increased radiation sensitivity. As described in Section B10a of Chapter III, loss of the Brca1-Ctip interaction did not render $Ctip^{S326A/S326A}$ mice hypersensitive to ionizing radiation (IR). Furthermore, normal IR resistance was also observed in homozygous $Abx^{S404A/S404A}$ and $Bach1^{FH\text{-}S994A/FH\text{-}S994A}$ mice (data not shown). Thus, the interaction of BRCA1 with each of these three BRCT phospho-ligands is not individually required for IR resistance. To determine whether the interaction with a combination of these phospho-ligands is required for resistance to IR, we irradiated AB, AC, and BC double mutant mice at two months of age with a sublethal dose of 8 Gys. Strikingly, all mice (n=10 for each genotype) survived at least 6 weeks post-irradiation (data not shown). In contrast, 100% of *Bach1*-null mice (n=22) died by 20 days post-irradiation (unpublished data). This result suggests that the AB, AC, and BC double mutant mice retain a sufficient DNA damage response to allow resistance to whole-body IR.

B1d. *The tumor susceptibility of AB, AC, and BC double mutant mice*

Since BRCA1 tumor suppression requires the phosphopeptide binding property of the BRCT repeats (Shakya et al., 2011), but not its individual interaction with the phospho-ligands Abraxas, BACH1, or CtIP (Figure 23, Section B11a of Chapter III; and data not shown), we asked whether simultaneous disruption of two or more of these interactions affects BRCA1-mediated tumor suppression. First, we assessed whole-body tumor development in AB, AC, and BC double mutant mice. Although whole-body tumor

monitoring of homozygous *Brca1*$^{S1598F/S1598F}$ mice revealed highly penetrant tumor development with an average latency (T_{50}) of 575 days (Shakya et al., 2011), the kinetics of tumor development in BC (n=9) double mutant mice was significantly slower (P = 0.0032) and indistinguishable from that of control *Bach1*$^{+/+}$/*Ctip*$^{+/+}$ mice (P = 0.8786) (Figure 43). Thus, disrupting the interaction of Brca1 with Bach1 and Ctip simultaneously does not render mice susceptible to tumor formation. At present, whole-body tumor monitoring of AB (n=20) and AC (n=23) double mutant mice is ongoing. Mice of each genotype have remained tumor-free for over a year (data not shown).

B2. The phenotype of triple mutant (ABC) cells

B2a. *Generation of ABC triple mutant MEFs*

Given that AB, AC, and BC double mutant cells appeared to be normal for all parameters tested, we next examined the phenotype of ABC triple mutant MEFs. To obtain these cells, we first mated homozygous AB and BC mice to produce animals bearing a total of four mutant alleles (e.g., *Abx*$^{S404A/+}$/*Bach1*$^{FH\text{-}S994A/FH\text{-}S994A}$/*Ctip*$^{S326A/+}$). These mice were then intercrossed to generate progeny bearing five mutant alleles. Assuming complete viability, crosses of the latter mice should yield pups with the desired ABC genotype (*Abx*$^{S404A/S404A}$/*Bach1*$^{FH\text{-}S994A/FH\text{-}S994A}$/*Ctip*$^{S326A/S326A}$) at a frequency of 25%. Therefore, we sacrificed pregnant females from these crosses on day E13.5. Importantly, viable ABC triple mutant E13.5 embryos were obtained at the expected Mendelian frequency (Figure 44; Table 6). However, these embryos were usually smaller in size,

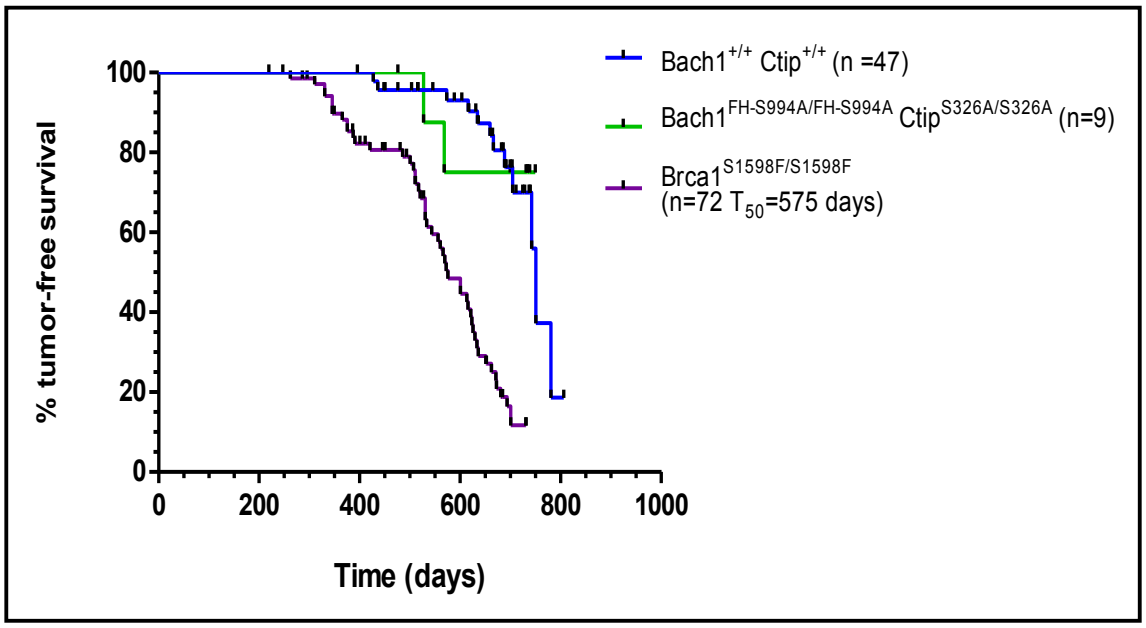

Figure 43. BC double mutant mice are not tumorigenic. Kaplan-Meier tumor-free survival curves of *Bach1*$^{+/+}$/*Ctip*$^{+/+}$ (blue curve; n=47) mice compared with *Bach1*$^{FH\text{-}S994A/FH\text{-}S994A}$/*Ctip*$^{S326A/S326A}$ (green curve; n=9; P = 0.8786) and *Brca1*$^{S1598F/S1598F}$ (purple curve; n=72; T_{50}=575 days; P < 0.0001) mice. Statistical significance was estimated with the log-rank test using Graph-Pad Prism (version 4) software. Values were considered statistically significant at P < 0.05.

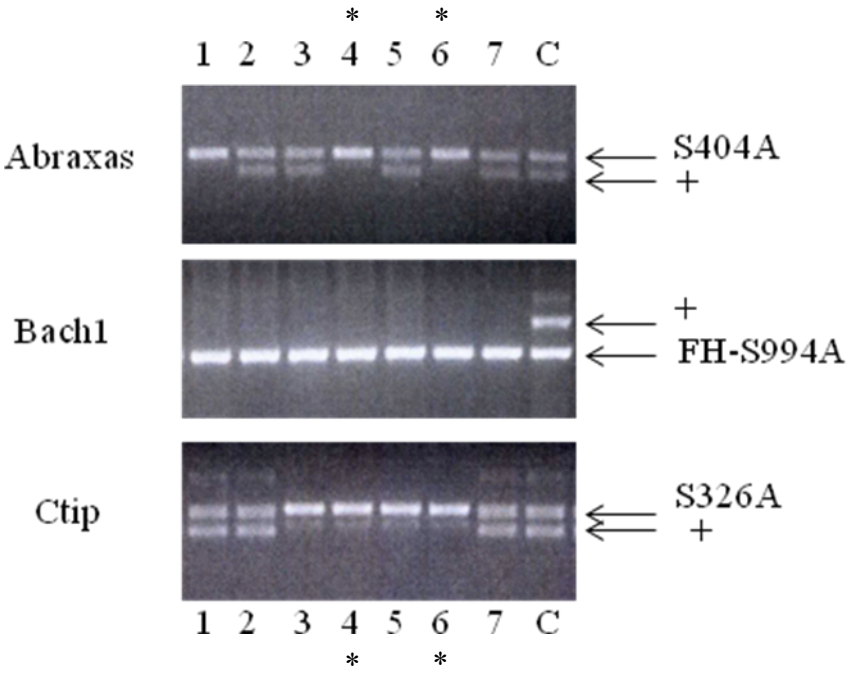

Figure 44. ABC triple mutant embryos are viable at E13.5. PCR analysis of E13.5 embryos from a five mutant allele cross (e.g., A/+ B/B C/C and A/A B/B C/+). The Abraxas (top), Bach1 (middle), and Ctip (bottom) mutant-specific PCRs were used to genotype the DNA isolated from yolk sacs at E13.5. All four expected offspring genotypes were observed, including A/A B/B C/C (triple ABC mutant (*); lanes 4 and 6), A/+ B/B C/+ (lanes 2 and 7), A/+ B/B C/C (lanes 3 and 5), and A/A B/B C/+ (lane 1). Additionally, control A/+ B/+ C/+ DNA was loaded in lane C. A = *Abraxas*^{S404A}; B = *Bach1*$^{FH\text{-}S994A}$; C = *Ctip*^{S326A}

Table 6. The observed frequency of ABC triple mutant embryos at E13.5.

Genotype [a]	Number of E13.5 embryos	
	Observed	Expected
A/+ B/B C/+	4	3.75
A/+ B/B C/C	3	3.75
A/A B/B C/+	4	3.75
A/A B/B C/C	4 [b]	3.75
Total number of embryos	15	

[a] Matings were set up between A/+ B/B C/C females and A/A B/B C/+ males. A = *Abraxas*^{S404A}; B = *Bach1*$^{FH\text{-}S994A}$; C = *Ctip*^{S326A}

[b] Among the 15 embryos examined, 4 were triple ABC mutant (A/A B/B C/C). Thus, at E13.5 ABC triple mutant embryos are viable and obtained at the expected Mendelian frequency.

and some exhibited exencephaly, a neural tube defect in which the brain is located outside the skull (Figure 45). The modest phenotypic variation observed between different ABC embryos may reflect the mixed genetic background (C57Bl6 x 129Sv) of the offspring. In any case, we were able to successfully generate primary and SV40-immortalized MEFs from ABC triple mutant embryos, and compare their phenotype with those of control MEFs, as well as *Brca1*$^{S1598F/S1598F}$ MEFs that express a Brca1 polypeptide that fails to interact with its BRCT phospho-ligands.

B2b. *ABC triple mutant MEFs have a proliferation defect*

To assess the proliferative potential of ABC triple mutant cells, we examined primary MEFs at passage 1 using the MTT assay. As shown in Figure 46A, by the second day in culture the proliferation rate of ABC primary MEFs was significantly reduced compared to that of primary MEFs derived from either littermate controls, or from AB, AC, and BC double mutant mice (Figure 42, Section B1b of Chapter V). Similar results were obtained using additional independently-derived primary MEF subclones at passage 2 (Figure 46B). Notably, the proliferation rate of ABC cells was reduced to the same extent as that of *Brca1*$^{S1598F/S1598F}$ cells (data not shown), which express a Brca1 polypeptide that lacks BRCT phospho-recognition. These results indicate that in the absence of one or two of the three known BRCT phospho-ligand interactions, the other known phospho-ligand interactions can compensate to allow normal cell proliferation. Thus, proliferation is not appreciably diminished unless all three known BRCT phospho-ligand interactions are disrupted (as in ABC MEFs) or the BRCT phosphopeptide binding

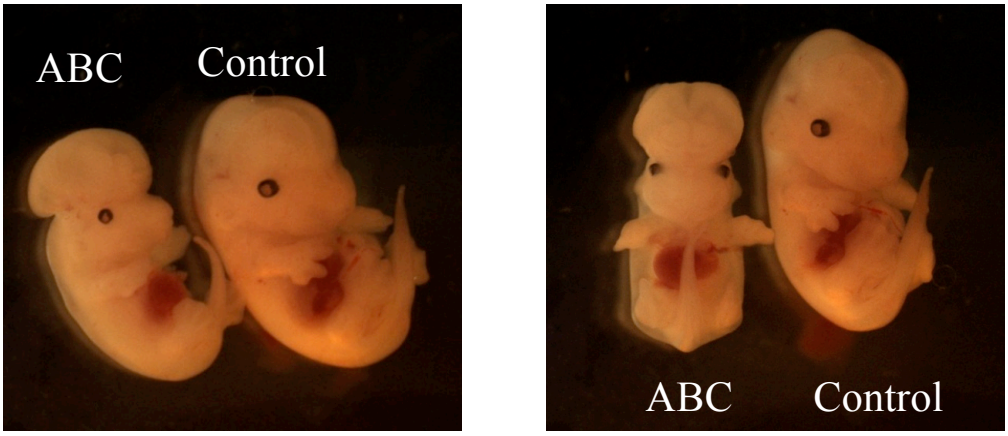

Figure 45. Exencephaly of some ABC triple mutant embryos at E13.5. The neural tube has failed to close in this E13.5 ABC triple mutant embryo (left). This is in contrast to its littermate control embryo (right) exhibiting normal morphology.

A.

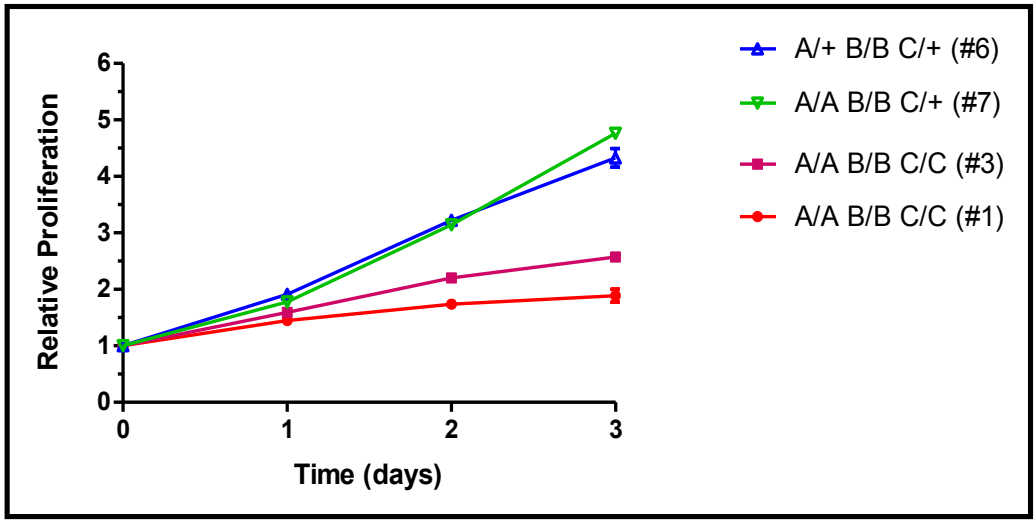

B.

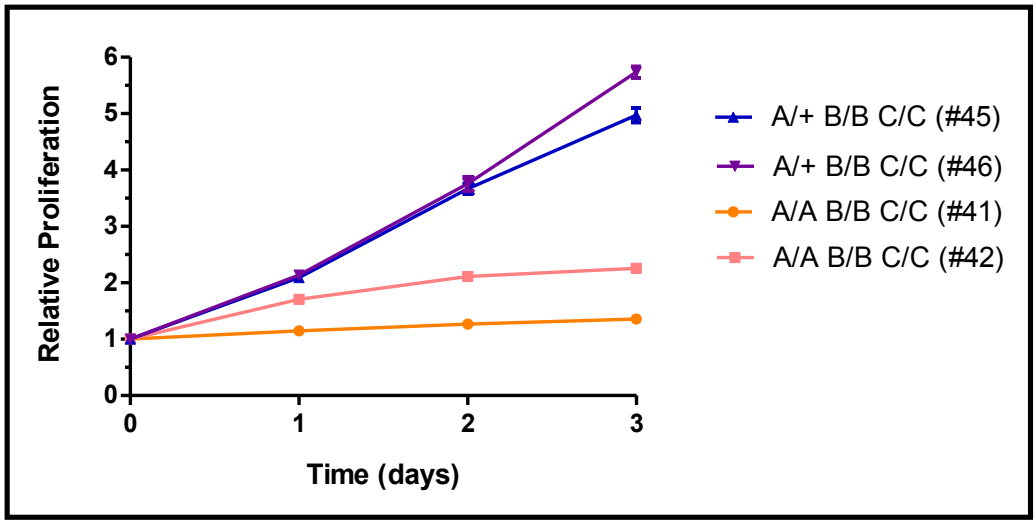

Figure 46. Reduced proliferation in ABC triple mutant MEFs. To evaluate the proliferation rate of (A) passage 1 and (B) passage 2 control (A/+ B/B C/+, A/A B/B C/+, and A/+ B/B C/C) and ABC triple mutant (A/A B/B C/C) MEFs, cells were trypsinized, counted, and seeded on 96-well plates. 4000 cells per well were seeded for each ABC triple mutant line while 2000 cells per well were seeded for the control lines. At the indicated time points, cell numbers were quantified using an MTT assay. Values on the Y-axis represent folds of increase in cell numbers. The error bars represent the mean ± SD of triplicate samples. A = *Abraxas*^{S404A}; B = *Bach1*$^{FH\text{-}S994A}$; C = *Ctip*^{S326A}

potential of Brca1 is ablated entirely (as in *Brca1*$^{S1598F/S1598F}$ MEFs).

B2c. *ABC triple mutant MEFs exhibit centrosome amplification*

Supernumerary centrosomes (>2 centrosomes/cell) are frequently observed in cells that display genetic instability due to defects in the DNA damage response. Indeed, centrosome amplification can lead to the formation of multiple spindle poles during mitosis, which may in turn promote chromosomal aneuploidy, genomic instability, and ultimately tumorigenesis (Deng, C.-X., 2002). Since centrosome amplification is observed in *Brca1*$^{S1598F/S1598F}$ MEFs, the BRCT phospho-recognition property of Brca1 is required to maintain normal centrosome duplication (Shakya et al., 2011). To examine whether the interaction of BRCA1 with its three known BRCT phospho-ligands is required for control of centrosome duplication, immunofluorescent staining with a pericentrin-specific antibody was used to compare centrosome numbers in passage 3 ABC triple mutant MEFs and control MEFs. While one or two centrosomes were commonly detected in control cells at interphase and at various stages of M phase, ~35% of ABC MEFs contained more than two centrosomes (Figure 47A). A similar result was observed when pericentrin staining was performed on passage 4 ABC and control MEFs (Figure 47B). In the most extreme case, one ABC cell was found to contain 10 centrosomes (data not shown). Therefore, ABC cells undergo centrosome amplification in a manner reminiscent of *Brca1*$^{S1598F/S1598F}$ MEFs (Shakya et al., 2011).

A.

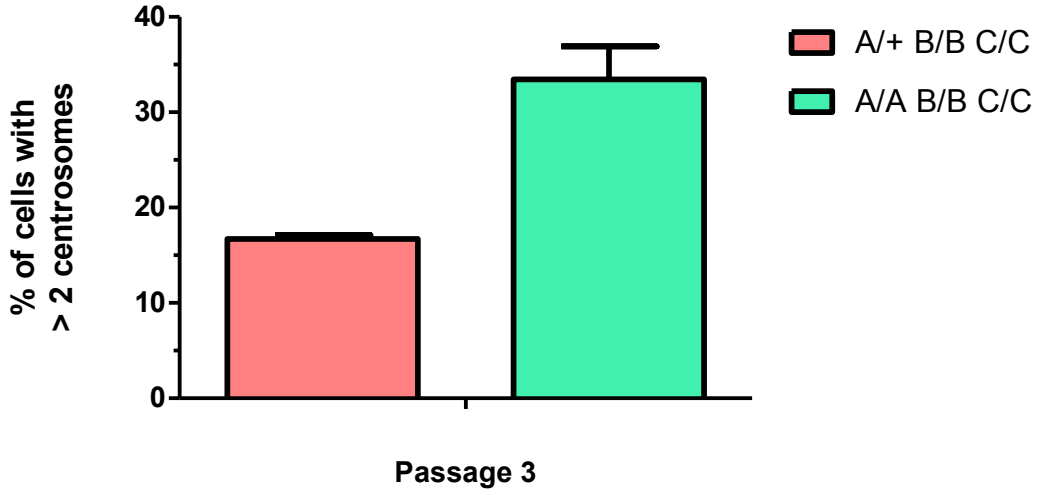
40
30
20
10
0
% of cells with
> 2 centrosomes
A/+ B/B C/C
A/A B/B C/C
Passage 3

B.

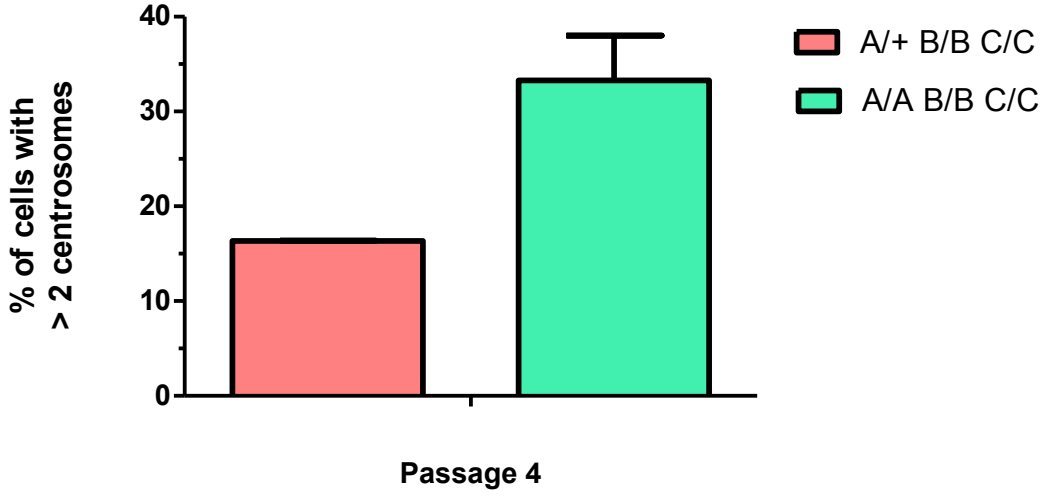
40
30
20
10
0
% of cells with
> 2 centrosomes
A/+ B/B C/C
A/A B/B C/C
Passage 4

C.

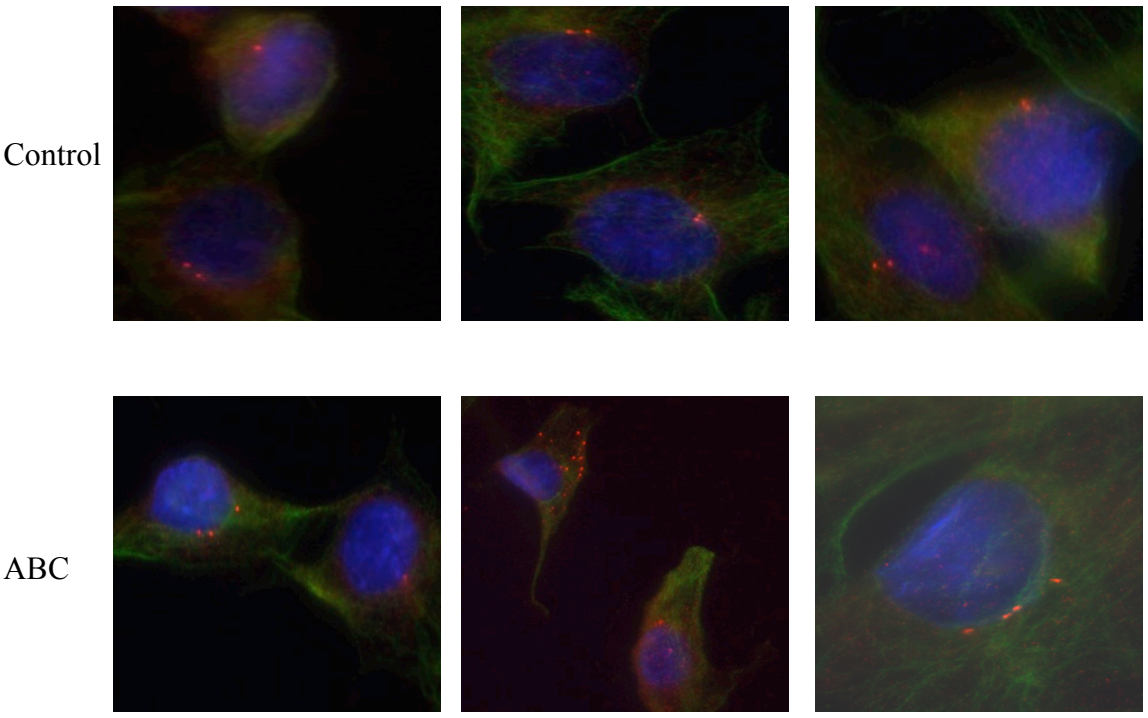

Figure 47. Centrosome amplification in ABC triple mutant MEFs. Primary control (A/+ B/B C/C) and ABC triple mutant (A/A B/B C/C) MEFs at (A) passage 3 and (B) passage 4 were immunostained with anti-pericentrin and anti-α-tubulin and stained with 4', 6-diamidino-2-phenylindole (DAPI). The number of centrosomes per cell was determined by immunofluorescent microscopy of 300 cells of each genotype. The mean value from two cell lines of each genotype is presented; error bars indicate the standard error of mean (S.E.M). (C) Representative images of control (top row) and ABC mutant (bottom row) MEFs immunostained with anti-pericentrin (red) and anti-α-tubulin (green) and then stained with DAPI (blue) for visualization of nuclei. A = *Abraxas*^{S404A}; B = *Bach1*$^{FH\text{-}S994A}$; C = *Ctip*^{S326A}

B2d. *Impaired recruitment of repair proteins to the S-phase foci and IRIFs of ABC triple mutant MEFs*

The localization of BRCA1 to damaged DNA is reportedly mediated, at least in part, by its interaction with the BRCT phospho-ligand Abraxas (Kim et al., 2007a; Liu, Z. et al., 2007; Sobhian et al., 2007; Wang et al., 2007). Abraxas bridges the association between BRCA1 and RAP80, a nuclear protein that harbors a ubiquitin-interacting motif (UIM). In turn, the UIM of RAP80 recognizes and binds the ubiquitinated histones at DNA damage sites, thereby bringing Abraxas-bound BRCA1 polypeptides to damaged DNA (Kim et al., 2007a; Liu, Z. et al., 2007; Sobhian et al., 2007; Wang et al., 2007). By immunofluorescent microscopy, we observed a reduction in Brca1 recruitment to S-phase foci and IR-induced foci (IRIFs) of immortalized *Abraxas*$^{S404A/S404A}$ MEFs relative to control cells (data not shown). Since BRCA1 foci still form, albeit at reduced levels, in the absence of the Brca1-Abraxas interaction, these results suggest that BRCA1 recruitment to S-phase foci and IRIFs is not solely dependent on its association with Abraxas. Importantly, Brca1 focus formation was normal in *Bach1*$^{FH-S994A/FH-S994A}$ (data not shown) and *Ctip*$^{S326A/S326A}$ (Section B7a of Chapter III) MEFs.

Surprisingly, when we examined ABC MEFs, we observed a marked reduction in Brca1 recruitment to the S-phase foci relative to *Abx*$^{S404A/S404A}$ MEFs (Figure 48). This result suggests that Bach1 and/or Ctip, through their interactions with Brca1, provide a compensatory mechanism to recruit Brca1 in the absence of the Brca1-Abraxas interaction. Notably, Brca1 focus formation was not completely absent in ABC triple mutant MEFs, suggesting the existence of yet another mechanism(s) for Brca1 recruitment. This alternative mechanism(s) is probably independent of BRCT

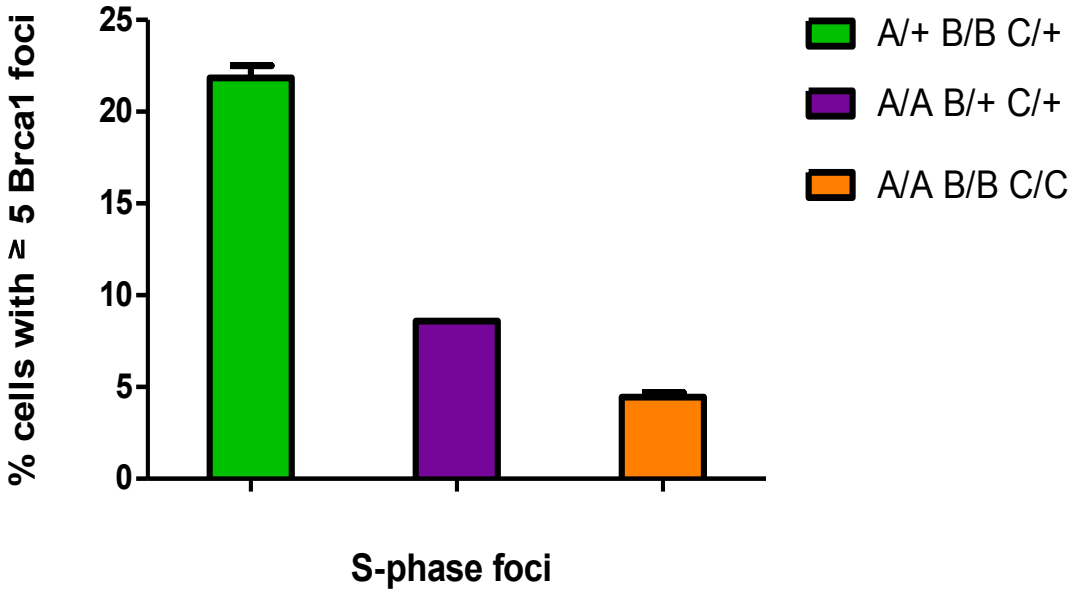

Figure 48. ABC triple mutant MEFs display a reduction in Brca1 recruitment to S-phase foci relative to *Abx*$^{S404A/S404A}$ MEFs. *Bach1*$^{FH\text{-}S994A/FH\text{-}S994A}$ (A/+ B/B C/+), *Abraxas*$^{S404A/S404A}$ (A/A B/+ C/+), and triple ABC (A/A B/B C/C) primary MEFs were immunostained with a mouse-specific Brca1 antibody. Brca1-containing S-phase foci were counted in 400 nuclei of two independent *Bach1*$^{FH\text{-}S994A/FH\text{-}S994A}$ and ABC MEF lines and a single *Abraxas*$^{S404A/S404A}$ MEF line. The error bars represent SE of the mean. Relative to control *Bach1*$^{FH\text{-}S994A/FH\text{-}S994A}$ MEFs, the number of Brca1-staining S-phase foci was reduced in *Abraxas*$^{S404A/S404A}$ MEFs, and even further reduced in ABC MEFs. A = *Abraxas*^{S404A}; B = *Bach1*$^{FH\text{-}S994A}$; C = *Ctip*^{S326A}

phosphopeptide binding since Brca1 focus formation was also reduced, but detectable, in *Brca1*$^{S1598F/S1598F}$ MEFs (Shakya et al., 2011).

Next, we assessed the effects of ionizing radiation (IR) on BRCA1 localization in ABC triple mutant MEFs. Control *Bach1*$^{FH\text{-}S994A/FH\text{-}S994A}$ single mutant and ABC triple mutant cells were either untreated or treated with 10 Gys of IR and allowed to recover for one hour. As shown in Figure 49A, Brca1 recruitment to both S phase foci and IRIFs was dramatically reduced in ABC MEFs relative to *Bach1*$^{FH\text{-}S994A/FH\text{-}S994A}$ control MEFs. Thus, ABC cells display a defect in Brca1 focus formation similar to that reported for *Brca1*$^{S1598F/S1598F}$ MEFs (Shakya et al., 2011). We also examined the localization of Rad51, a key homologous recombination protein, to S-phase foci and IRIFs in ABC triple mutant MEFs. Importantly, normal Rad51 focus formation was observed in cells homozygous for each of the individual BRCT phospho-ligand mutants (i.e., *Abx*$^{S404A/S404A}$; *Bach1*$^{FH\text{-}S994A/FH\text{-}S994A}$; and *Ctip*$^{S326A/S326A}$ MEFs) (Section B7a of Chapter III, and data not shown). Significantly, however, Rad51 accumulation at both S-phase foci and IRIFs was dramatically diminished in ABC triple mutant MEFs (Figure 49B), in a manner reminiscent of *Brca1*$^{S1598F/S1598F}$ MEFs (Shakya et al., 2011).

B2e. *Levels of spontaneous and damage-induced chromosomal abnormalities are elevated in ABC triple mutant MEFs*

Given the impaired recruitment of Brca1 and Rad51 to sites of DNA damage in ABC triple mutant MEFs, we examined whether chromosomal aberrations accumulate in these cells. To assay for chromosome defects, we examined the karyotypes of ABC passage 3 primary MEFs. Giemsa-stained metaphase spreads were prepared and scored from two

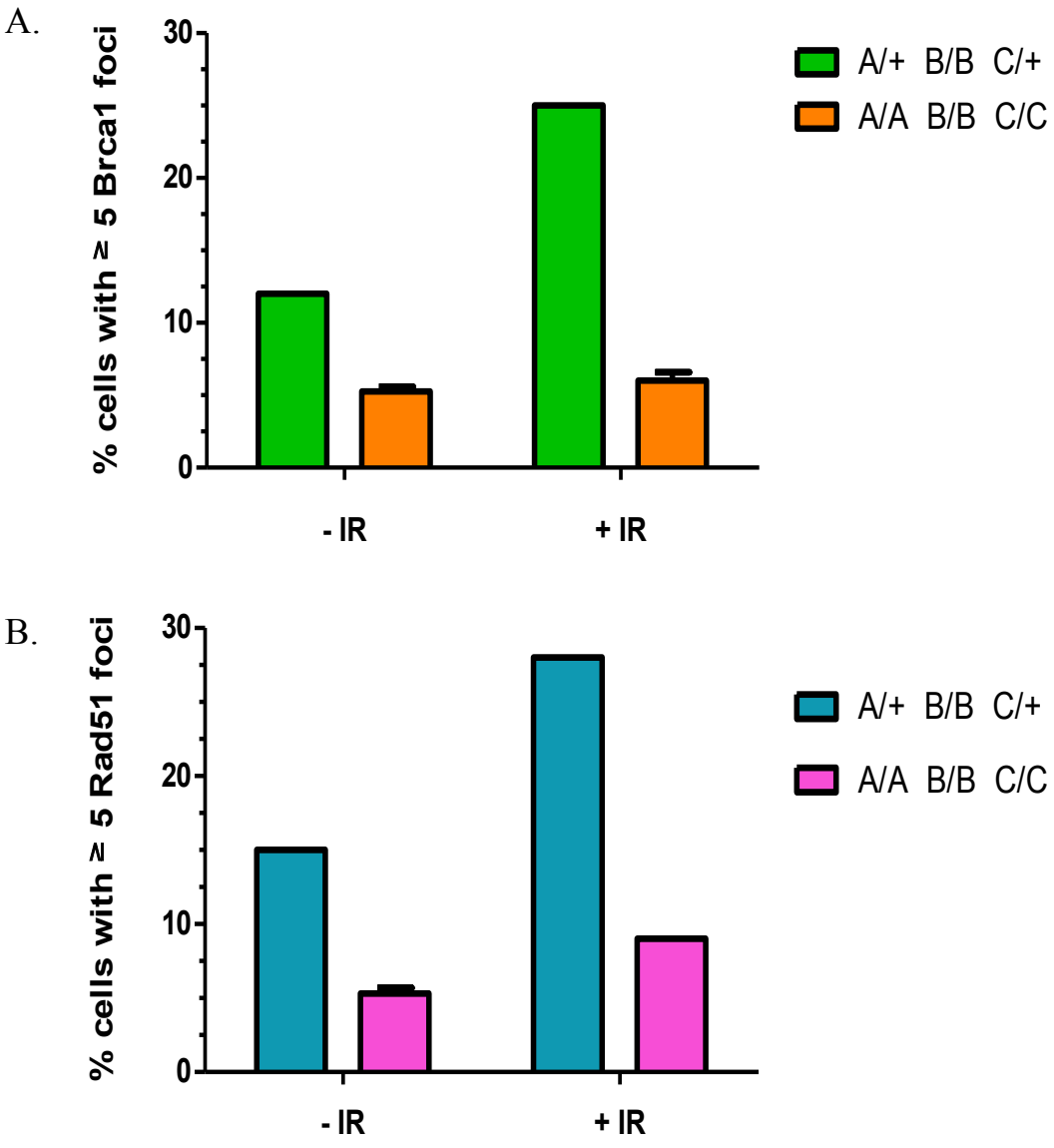

Figure 49. ABC MEFs are deficient for assembly of Brca1 and Rad51 S-phase foci and IRIFs. Control *Bach1*$^{FH\text{-}S994A/FH\text{-}S994A}$ (A/+ B/B C/+) and ABC triple mutant (A/A B/B C/C) primary MEFs were exposed to 10 Gy of IR or left untreated; 1 hour later, the cells were fixed and stained with (A) Brca1- and (B) Rad51-specific antibodies. Brca1- and Rad51- containing S-phase foci and IRIFs were counted in 200 nuclei of two independent ABC MEF lines and a single *Bach1*$^{FH\text{-}S994A/FH\text{-}S994A}$ MEF line. The error bars represent SE of the mean. A = *Abraxas*^{S404A}; B = *Bach1*$^{FH\text{-}S994A}$; C = *Ctip*^{S326A}

independent MEF cultures derived from different ABC embryos, as well as a culture of isogenic control (*Abx*$^{S404A/+}$/*Bach1*$^{FH\text{-}S994A/FH\text{-}S994A}$/*Ctip*$^{S326A/+}$) MEFs. As shown in Figure 50A, significantly increased levels of spontaneous chromosomal rearrangements were observed in the ABC MEFs relative to control MEFs. Thus, ABC cells display heightened chromosomal instability in the absence of exogenous DNA damage.

As shown in Figure 50B, ABC cells also accumulate cytogenetic defects at high rates relative to control cells in response to the DNA interstrand cross-linking agent mitomycin C (MMC). Indeed, in both the presence and absence of MMC, the percentage of ABC cells with aberrant metaphases was double that of control MEFs (Table 7). The abnormalities of ABC cells include chromatid and chromosome breaks and gaps, as well as a high frequency of exchanges, including triradial and quadriradial chromosomes (Table 7). Aneuploidy, however, was not increased in the triple ABC mutant cells (data not shown). Therefore, normal suppression of spontaneous and MMC-induced chromosomal instability is abrogated when the phospho-dependent BRCT interactions of BRCA1 with Abraxas, BACH1, and CtIP are simultaneously disrupted.

B2f. *Brca1 is efficiently hyperphosphorylated in response to HU in ABC cells*

BRCA1 is phosphorylated by the ATR kinase in response to the DNA replication inhibitor hydroxyurea (HU) (Tibbetts et al., 2000). To examine whether HU-induced Brca1 hyperphosphorylation requires the interaction of Brca1 with its three known BRCT phospho-ligands, wildtype and ABC immortalized MEFs were exposed to 1 mM HU,

A.

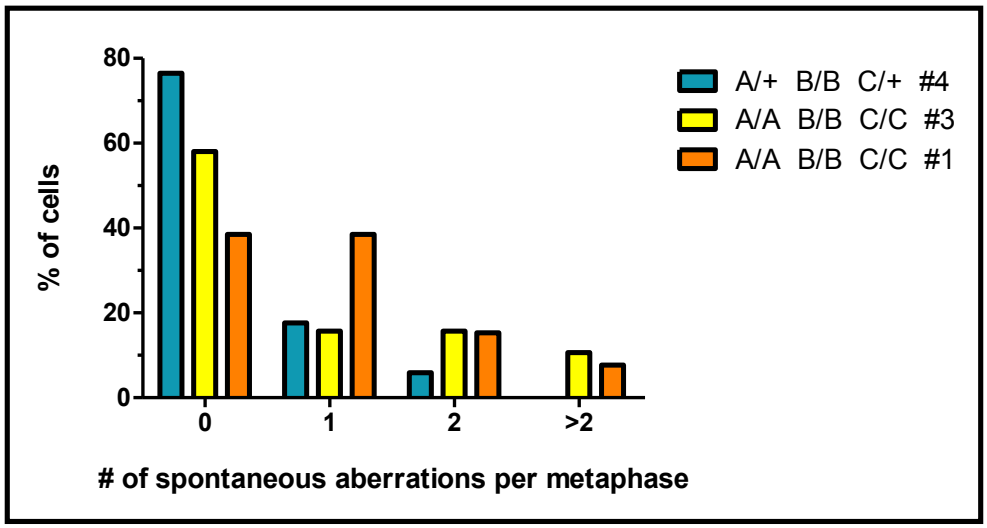

B.

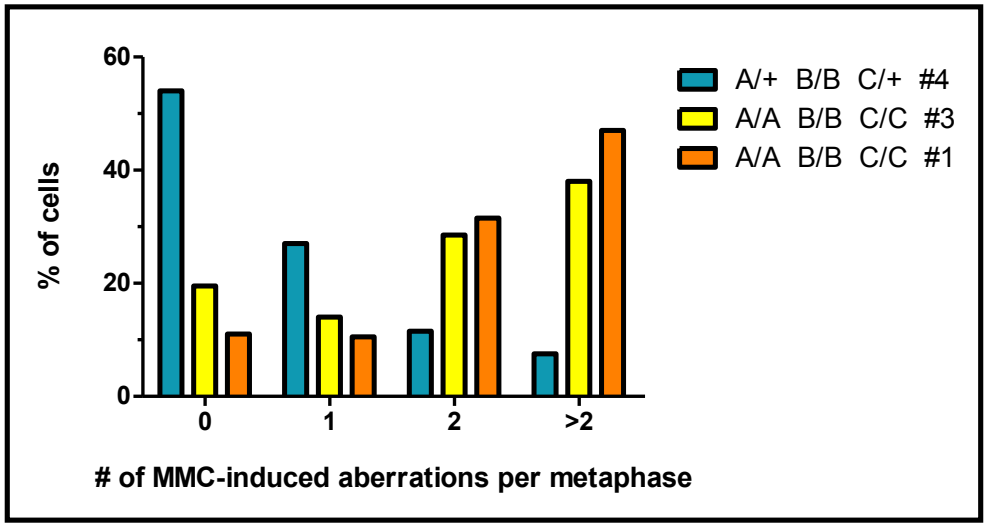

Figure 50. Elevated levels of spontaneous and MMC-induced chromosomal aberrations in ABC MEFs. Metaphase spreads were prepared from (A) untreated or (B) MMC-treated (40 ng/mL, 16 h) control (A/+ B/B C/+) and ABC triple mutant (A/A B/B C/C) passage 3 primary MEFs. Following colcemid treatment, exposure to a hypotonic solution, and methanol/acetic acid fixation, the cell suspensions were dropped onto glass slides and stained with Giemsa. At least fifteen metaphase spreads per cell line were examined for each treatment condition for numerical and structural chromosomal aberrations. A = *Abraxas*^{S404A}; B = *Bach1*$^{FH\text{-}S994A}$; C = *Ctip*^{S326A}

Table 7. Spontaneous and induced chromosomal aberrations in ABC triple mutant primary MEFs.

Genotype	Metaphases analyzed	MMC treatment	Metaphase aberrations, %	Aberrations	
				Chr/Cht breaks and gaps	Exchange/Other
A/+ B/B C/+ (#4)	17	-	23.5	5	0
	26	+	46	16	3
A/A B/B C/C (#3)	19	-	42	12	3
	21	+	80.5	31	11
A/A B/B C/C (#1)	15	-	61.5	11	1
	19	+	89	31	26

MMC, mitomycin C / Chr, chromosome / Cht, chromatid

The percentage of metaphases containing one or more aberrations and a breakdown of aberration-type is shown for each primary MEF cell line in both the absence (–) and presence (+) of MMC. A = *Abraxas*^{S404A}; B = *Bach1*$^{FH\text{-}S994A}$; C = *Ctip*^{S326A}

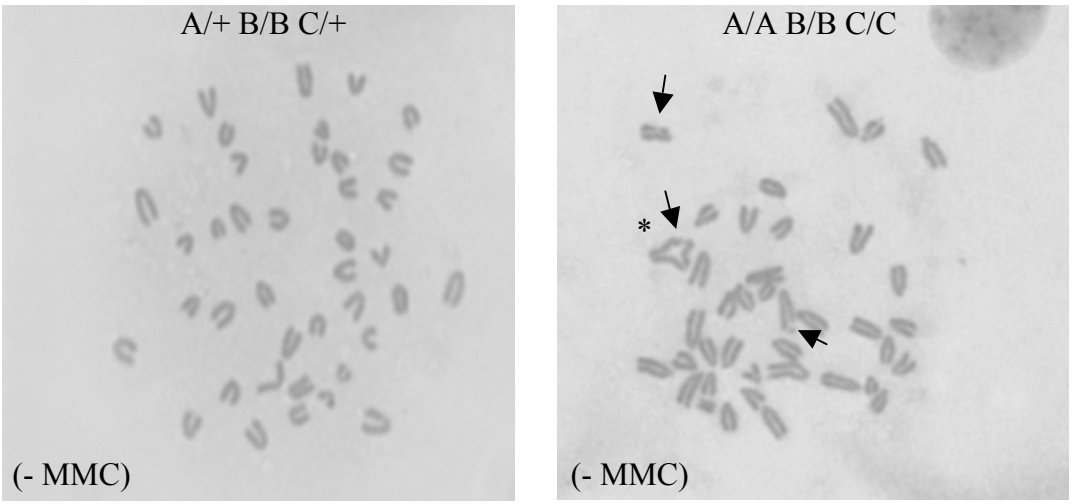

Representative examples of Giemsa-stained metaphase spreads of control (A/+ B/B C/+) and ABC (A/A B/B C/C) MEFs in the absence of MMC treatment. Arrows point to a number of spontaneous chromosomal aberrations, including an exchange (*) observed in ABC cells. A = *Abraxas*^{S404A}; B = *Bach1*$^{FH\text{-}S994A}$; C = *Ctip*^{S326A}

and cell lysates were immunoblotted with an antiserum raised against mouse Brca1. Additionally, we also examined HU-induced Brca1 hyperphosphorylation in MEFs homozygous for two different BRCT phospho-recognition mutations (*Brca1*$^{S1598F/S1598F}$ and *Brca1*$^{M1717R/M1717R}$). As shown in Figure 51, the Brca1 polypeptides of both wildtype and ABC MEFs displayed electrophoretic mobility shifts indicative of hyperphosphorylation. In contrast, HU-induced Brca1 hyperphosphorylation was impaired in two different BRCT phospho-recognition mutants (*Brca1*$^{S1598F/S1598F}$ and *Brca1*$^{M1717R/M1717R}$) (Figure 51). These results suggest that HU-induced phosphorylation of BRCA1 is dependent on its BRCT phosphopeptide binding activity, but not its BRCT phospho-dependent interactions with Abraxas, BACH1, and CtIP.

B3. The phenotype of triple mutant (ABC) mice

B3a. *ABC mice are viable, but are born at a lower than expected frequency*

To assess the phenotype of ABC triple mutant mice, we intercrossed animals bearing five mutant alleles (i.e., *Abx*$^{S404A/+}$/*Bach1*$^{FH\text{-}S994A/FH\text{-}S994A}$/*Ctip*$^{S326A/S326A}$ or *Abx*$^{S404A/S404A}$/*Bach1*$^{FH\text{-}S994A/FH\text{-}S994A}$/*Ctip*$^{S326A/+}$) on a mixed genetic background (C57Bl6 x 129Sv) to generate ABC (*Abx*$^{S404A/S404A}$/*Bach1*$^{FH\text{-}S994A/FH\text{-}S994A}$/*Ctip*$^{S326A/S326A}$) triple mutant mice. Although the expected Mendelian yield of ABC mice from this intercross is 25%, viable ABC mice were obtained at a significantly lower frequency (3.8%) (data not shown).

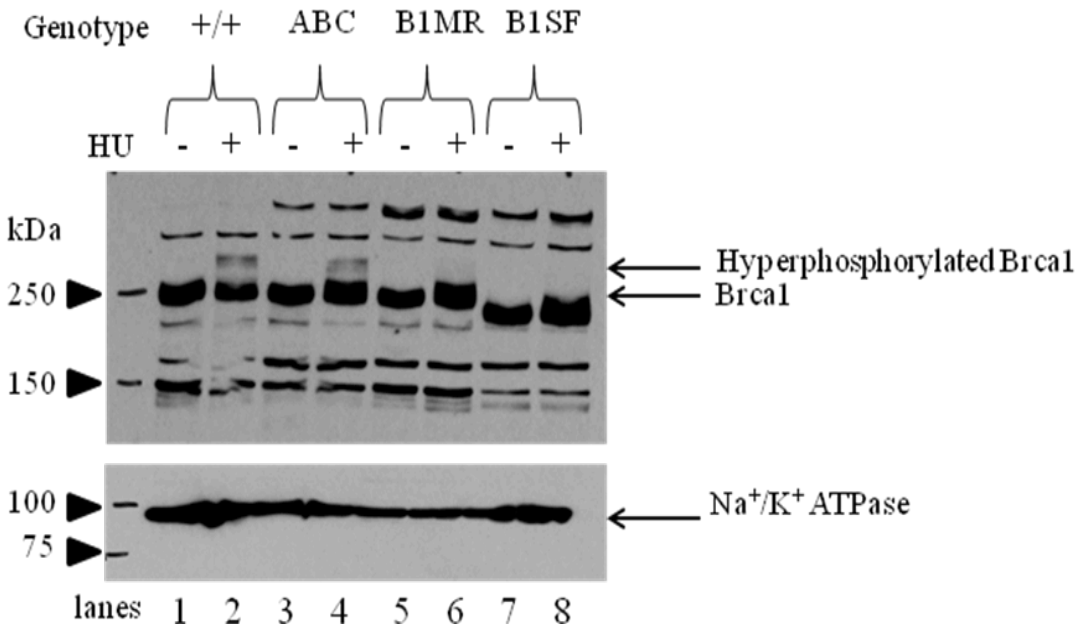

Figure 51. HU-induced Brca1 hyperphosphorylation in ABC triple mutant MEF lysate. Immortalized MEFs were treated with 1 mM hydroxyurea (HU) for 1 hour or left untreated; 1 hour post-drug removal, lysates were prepared from wildtype (+/+; lanes 1 and 2), ABC (lanes 3 and 4), *Brca1*$^{M1717R/M1717R}$ (B1MR; lanes 5 and 6) and *Brca1*$^{S1598F/S1598F}$ (B1SF; lanes 7 and 8) cells. The cell lysates were then fractionated by SDS-PAGE and immunoblotted with antibodies specific for mouse Brca1 or, as a loading control, sodium/potassium-ATPase (Na^+/K^+ ATPase).

Since ABC embryos were present at the expected Mendelian frequency on day E13.5 (Figure 44 and Table 6; Section B2a of Chapter V), most ABC mutants likely die immediately before (perinatally) or just after (postnatally) birth. Consistent with this, we observed some ABC embryos at E13.5 with the embryonic lethal condition exencephaly (Figure 45) as well as some ABC mutants that were dead within hours after delivery (data not shown). Perhaps the variation in viability among different ABC mice is due in part to the mixed genetic background (C57Bl6 x 129Sv) of these animals. In any case, the viability of ABC mice is significantly reduced relative to each of the double mutant (i.e., AB, AC, and BC) mice. We do not understand how simultaneous disruption of these three BRCT phospho-ligand interactions affects animal viability. Surprisingly, mice that are homozygous (*Brca1*$^{S1598F/S1598F}$) for a mutation that presumably ablates the interaction of BRCA1 with all of its (known and unknown) BRCT phospho-ligands are born at the expected Mendelian ratio (Shakya et al., 2011).

B3b. *ABC mice have a developmental defect*

An equal number of male and female ABC mice survive to adulthood (data not shown). Compared to their littermate controls, these mice exhibit numerous developmental defects of variable severity. In particular, ABC mice are ~30% smaller than same-sex littermate controls for the first four postnatal weeks (Figure 52, A and B) and throughout adulthood (data not shown). Furthermore, ABC mice have characteristic white hind feet (Figure 52B) and an occasional white belly spot (Figure 52C). These white markings likely result from faulty migration of melanocytes from the neural crest,

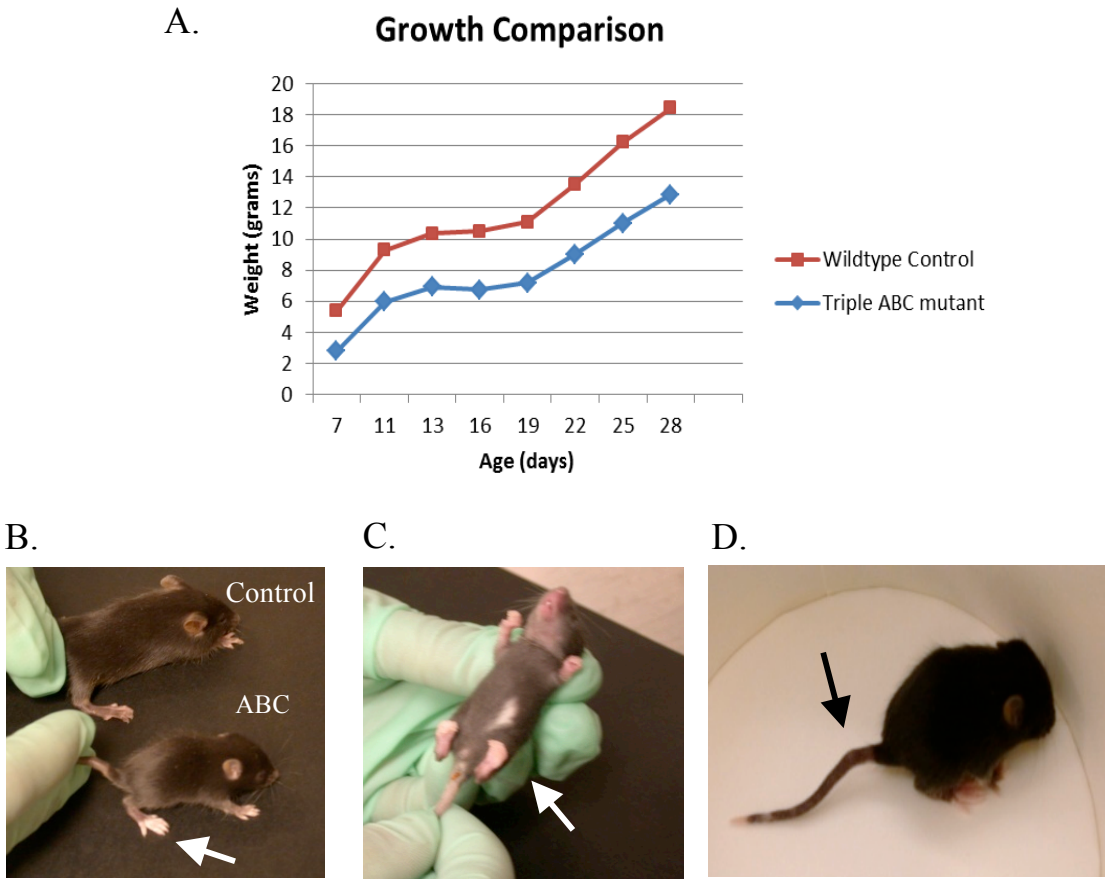

Figure 52. The developmental defects of ABC triple mutant mice. (A) ABC triple mutant mice are growth retarded. The weight of an ABC triple mutant male mouse and a male littermate control was measured at different time points during postnatal growth. (B) Representative image of an ABC mutant and same-sex littermate control animal showing growth retardation and white hind feet (arrow) of the ABC mutant. (C) An ABC triple mutant mouse with a white belly spot (arrow) and (D) kinked tail (arrow) is also shown.

which renders the extremities and midline devoid of pigment cells (Gilbert, S. F., 2003; Oliver et al., 2004). ABC mice also display skeletal abnormalities in the form of kinked tails (Figure 52D). Notably, *Brca1*$^{S1598F/S1598F}$ mice exhibit these same developmental defects (data not shown).

B3c. *ABC mice show reduced fertility*

Homozygous *Brca1*$^{S1598F/S1598F}$ mice display male, but not female, sterility (Shakya et al., 2011). To assess the fertility of ABC animals, a 10-week-old ABC male mouse was mated with three wildtype C57BL6 females of the same age, and the females were monitored daily for the presence of a vaginal plug. The time when the vaginal plug was detected was denoted as 0.5 dpc (days post copulation). On E9.5, the uterus was removed from the mated females and the number of implantation sites was determined. Notably, we observed a reduced number (average of 2.7 per mouse) of implantation sites (data not shown). In contrast, an average of 6.6 implantation sites per mouse were obtained when wildtype females were mated with a wildtype male (data not shown). Furthermore, two additional ABC males were setup with multiple wildtype females and allowed to mate for 6 months. During this time, not a single female produced a litter, suggesting a more severe fertility phenotype in these ABC mutant males. Despite the observed variability, ABC triple mutant males appear to be sub-fertile.

We also assessed the fertility of several ABC females by mating them with wildtype males. The ABC females are fertile in the sense that they can carry their pups to term and produce viable offspring. However, their litter sizes were small, perhaps as a

consequence of their low body weight or a reduced fertility (further investigation needed). Overall, the observed phenotype of the triple ABC mutant animals indicates that the interaction of BRCA1 with its three known BRCT phospho-ligands is necessary for optimal fertility.

B3d. *Whole-body tumor formation in ABC mice*

To ascertain whether the phenotypic defects associated with ABC cells and mice are relevant for BRCA1-mediated tumor suppression, it will be important to compare tumor development in ABC animals with control animals, including double mutant (AB, AC, or BC) animals (Section B1d of Chapter V) and $Brca1^{S1598F/S1598F}$ mice, which develop tumors with an average latency (T_{50}) of 575 days (Shakya et al., 2011). Therefore, we plan to monitor a cohort of ABC animals for whole-body tumor formation over a 24-month observation period. At present, our oldest ABC mouse is 450 days old (~15 months), but as yet shows no signs of distress or tumor development.

If ABC triple mutant mice develop tumors with increased kinetics (penetrance and latency) relative to control animals, we will conclude that tumor susceptibility arises when the interactions of BRCA1 with each of its three known BRCT phospho-ligands (Abraxas, Bach1, and Ctip) are ablated simultaneously. On one hand, if these mice develop tumors with the same kinetics as $Brca1^{S1598F/S1598F}$ mice, we will further conclude that the tumor suppression activity of Brca1 is mediated primarily through these three BRCT interactions. On the other hand, if other as yet unidentified BRCT phospho-ligands also contribute to the tumor suppression activity of Brca1, then tumor formation

in the triple ABC mutant mice may be increased with respect to control mice, but reduced (longer latency and/or lower frequency) with respect to *Brca1*$^{S1598F/S1598F}$ mice. Given the long latency for tumor development in the *Brca1*$^{S1598F/S1598F}$ mice, a large cohort of triple ABC mutant animals may be necessary to attain statistical significance. Finally, it is possible that tumor formation will not occur in the triple ABC mutant animals. In this case, we will conclude that the tumor suppression function of Brca1 is mediated primarily by its interaction(s) with unknown BRCT phospho-ligands. In any event, analysis of the tumor susceptibility of ABC mice should provide invaluable insights into the mechanisms by which BRCT phospho-recognition mediates BRCA1 tumor suppression.

C. DISCUSSION

Since the germline *BRCA1* lesions implicated in familial breast cancer are usually frameshift or nonsense mutations, most tumor-associated *BRCA1* alleles encode truncated polypeptides that have lost one or both BRCT motifs (Williams et al., 2003; Wooster and Weber, 2003). Moreover, in some breast cancer families, tumor susceptibility can be ascribed to missense mutations that cause a single amino acid substitution in either the first (e.g., the S1655F mutation) or the second (e.g., the M1775R mutation) BRCT domain (Williams et al., 2001), underscoring the importance of the BRCT domain in modulating tumor susceptibility. Although the exact mechanism of tumor suppression by BRCA1 remains elusive, it is likely that BRCA1 suppresses tumor formation in part by promoting genome stability.

The BRCT sequences of BRCA1 engage in interactions with different phospho-ligands to mediate unique aspects of BRCA1 function in the DNA damage response (Greenberg et al., 2006). For example, the interaction of BRCA1 with the phosphorylated isoform of BACH1 is required for activation of the G_2 accumulation checkpoint (Yu et al., 2003), while its interaction with phosphorylated CtIP mediates the transient G_2/M checkpoint (Yu and Chen, 2004). More recently, the BRCT sequences of BRCA1 were also found to bind the Abraxas protein in a phospho-dependent manner to facilitate BRCA1 localization to sites of DNA damage (Kim et al., 2007; Kim et al., 2007a; Liu, Z. et al., 2007; Sobhian et al., 2007; Wang et al., 2007; Yan et al., 2007). Not surprisingly, cells with a mutation that prevents BRCT phosphopeptide binding by BRCA1 (e.g., *Brca1*$^{S1598F/\text{S1598F}}$) have a highly unstable genome (Shakya et al., 2011). *Brca1*$^{S1598F/\text{S1598F}}$ MEFs display proliferation defects, chromosomal instability,

centrosome amplification, as well as impaired recruitment of Brca1 and Rad51 to sites of DNA damage (Shakya et al., 2011). Furthermore, mice homozygous for the Brca1-S1598F mutation are tumor-prone (Shakya et al., 2011), indicating that the BRCT phosphopeptide binding property of BRCA1 is necessary for tumor suppression. Thus, the genome maintenance functions of BRCA1 appear to be a major determinant of its tumor suppression activity.

To determine which phosphoprotein interaction mediates the tumor suppression function of Brca1, a single amino acid substitution was made to eliminate the cognate phosphorylation site of Abraxas (S404A), Bach1 (S994A), or Ctip (S326A). Unexpectedly, the genome maintenance and tumor suppression activities of BRCA1 appeared to be normal in cells expressing any of the three BRCT phospho-ligand mutants (data not shown (Abraxas and Bach1); Chapter III (Ctip)). Therefore, we examined whether these aspects of BRCA1 function are affected by simultaneous disruption of its interaction with two or more of these phosphoproteins.

To test this hypothesis, we generated each of the three combinations of homozygous double mutant animals: AB ($Abx^{S404A/S404A}/Bach1^{FH\text{-}S994A/FH\text{-}S994A}$), AC ($Abx^{S404A/S404A}/Ctip^{S326A/S326A}$), and BC ($Bach1^{FH\text{-}S994A/FH\text{-}S994A}/Ctip^{S326A/S326A}$). These double mutant mice were born at the expected Mendelian ratio and were indistinguishable from littermate controls. MEFs derived from each of the double mutant mice proliferate normally. Moreover, the AB, AC, and BC double mutant mice showed normal resistance to ionizing radiation and the BC mice displayed no signs of tumor susceptibility (AB and AC mice are still being monitored). Thus, although cells

expressing a Brca1 polypeptide that lacks BRCT phospho-recognition entirely (i.e., *Brca1*$^{S1598F/S1598F}$) are markedly compromised with respect to genome maintenance and tumor suppression (Shakya et al., 2011), the interaction of Brca1 with any one of its three known BRCT phospho-ligands appears to be sufficient to overcome these defects.

Remarkably, many of the phenotypic abnormalities associated with the *Brca1*$^{S1598F/S1598F}$ genotype are recapitulated when, as in ABC triple mutant cells, the interaction of Brca1 with its three known BRCT phospho-ligands are ablated simultaneously. In particular, ABC MEFs display proliferation defects, centrosome amplification, chromosomal instability, and impaired recruitment of Brca1 and Rad51 to sites of DNA damage. Yet some phenotypic differences were observed. For example, HU-induced Brca1 hyperphosphorylation occurs in ABC MEFs, but not *Brca1*$^{S1598F/S1598F}$ MEFs. This result suggests that HU-induced phosphorylation of Brca1 may be dependent on its interaction with a distinct, as yet undiscovered, BRCT phospho-ligand. Nonetheless, at the cellular level, the phenotype of ABC MEFs closely resembles that of *Brca1*$^{S1598F/S1598F}$ MEFs. Thus, although the three major BRCA1 supercomplexes (complexes A, B, and C) are thought to have distinct functions in BRCA1-mediated genome stability (Yu et al., 2003; Yu and Chen, 2004; Greenberg et al., 2006; Sobhian et al., 2007; Wang et al., 2007; Huen et al., 2010), our results suggest that these complexes also have the potential to act in a compensatory fashion with respect to one another, at least within the biological settings examined here.

Previous studies have shown that the BRCA1-Abraxas interaction facilitates the recruitment of BRCA1 polypeptides to the remodeled chromatin that forms adjacent to

chromosomal DSBs (Kim et al., 2007; Kim et al., 2007a; Liu, Z. et al., 2007; Sobhian et al., 2007; Wang et al., 2007; Yan et al., 2007). In accord with this notion, we observed impaired recruitment of Brca1 to the S-phase foci of *Abraxas*$^{S404A/S404A}$ single mutant MEFs (Figure 48). Surprisingly, however, the localization of Brca1 to these structures was further impaired in ABC triple mutant MEFs (Figure 48), suggesting that the Brca1-Bach1 and/or Brca1-Ctip interactions promote Brca1 localization in the absence of the Brca1-Abraxas interaction. To assess which of these interaction(s) are compensatory, one could compare Brca1 focus formation in *Abx*$^{S404A/S404A}$ single mutant, AB double mutant, and AC double mutant MEFs. Given that AB and AC double mutant MEFs display relatively normal genome stability phenotypes, it is likely that both the Brca1-Bach1 and the Brca1-Ctip interactions can act in a compensatory manner when the Brca1-Abraxas interaction is ablated. Interestingly, CtIP was recently detected in immunoprecipitates of RAP80 (Wang et al., 2007), a protein that harbors the ubiquitin-interacting motif (UIM) and targets BRCA1 to sites of DNA damage through its association with Abraxas (Kim et al., 2007a; Liu, Z. et al., 2007; Sobhian et al., 2007; Wang et al., 2007). Thus, in the absence of Abraxas, CtIP may bridge the association between RAP80 and BRCA1, thereby mediating BRCA1 localization to sites of DNA damage.

A scenario can be envisioned in which the proportion of the BRCA1 polypeptide pool that binds a yet to be discovered BRCT phospho-ligand, if it exists, increases following simultaneous ablation of BRCA1's interaction with its three known BRCT phospho-ligands. This fourth BRCA1 supercomplex may inhibit BRCA1 function in response to DNA damage eliciting the phenotypic abnormalities observed with the ABC mutations.

Therefore, future studies should be aimed at identifying any unknown BRCA1 BRCT-interacting phospho-ligands and determining their *in vivo* functions.

To determine whether BRCA1's interaction with all three known BRCT phosphoproteins is involved in animal development and tumor suppression, we generated ABC triple mutant mice. In contrast to $Brca1^{S1598F/S1598F}$ mice, which are born at the expected Mendelian ratio (Shakya et al., 2011), ABC mice were observed at a much lower frequency than expected. Since mothers of either genotype ($Abx^{S404A/+}/Bach1^{FH\text{-}S994A/FH\text{-}S994A}/Ctip^{S326A/S326A}$ or $Abx^{S404A/S404A}/Bach1^{FH\text{-}S994A/FH\text{-}S994A}/Ctip^{S326A/+}$) produced a comparable number of viable ABC pups, a sub-optimal uterine environment is unlikely to account for the reduced viability of ABC progeny (data not shown). Instead, ABC mice may have a developmental defect that renders them less fit than their littermates, and consequently more susceptible to late gestation/postnatal arrest.

Consistent with this reduced viability, we observed phenotypic variation among the ABC embryos examined at E13.5. While some exhibited the embryonic lethal condition exencephaly, others appeared normal despite being smaller in size. Additionally, we noticed that a number of ABC animals died just after birth on P0. The appearance of ABC embryos at the expected Mendelian frequency on E13.5 defines the time of death for some ABC mutants between E13.5 and P10, when the viable pups were genotyped. The phenotypic variation observed among ABC embryos and mice may be due to differences in their mixed genetic background (C57BL6 x 129Sv).

Despite variability in the severity of the ABC phenotype, we successfully generated viable ABC mice that survive to adulthood. Similar to the BRCT phospho-recognition

mutant *Brca1*$^{S1598F/S1598F}$ mice (data not shown), the viable ABC mice showed a number of developmental defects to varying degrees, including growth retardation, white hind feet/belly spot, and kinked tails. Thus, not only do ABC triple mutants share a phenotypic resemblance to the *Brca1*$^{S1598F/S1598F}$ mutants at the cellular level, but also at the organismal level. However, unlike the male sterility of *Brca1*$^{S1598F/S1598F}$ mice (Shakya et al., 2011), ABC males are sub-fertile, suggesting that other unknown BRCT phospho-ligands may also contribute to BRCA1 function in spermatogenesis.

Our results show that BRCA1 functions in animal development, cell proliferation, centrosome regulation, assembly of DNA repair foci, and chromosomal stability, are grossly perturbed when the interaction of BRCA1 with its three known BRCT phospho-ligands are simultaneously ablated. Notably, these effects are only observed in the absence of all three phosphoprotein interactions, suggesting that the major BRCA1 supercomplexes assembled from these interactions (complexes A, B, and C) have the potential to act in a compensatory manner with respect to one another. Ultimately it will be important to determine whether tumor suppression requires the interaction of BRCA1 with these three BRCT phosphoproteins. Thus, future analysis of tumor susceptibility in ABC mice may provide novel insights into the molecular mechanisms underlying BRCA1-mediated tumor suppression.

CHAPTER VI

CONCLUSIONS AND FUTURE DIRECTIONS

Germline mutations in the *BRCA1* gene confer an increased risk of breast and ovarian cancer, but the mechanisms by which its protein product suppresses tumor formation remain elusive. The BRCA1 protein is involved in a broad spectrum of biological processes and interacts with many diverse proteins. One of these, CtIP, associates with the BRCT sequences of BRCA1 in a phosphorylation-dependent manner to mediate BRCA1 function in response to DNA damage (Wong et al., 1998; Yu et al., 1998; Yu and Chen, 2004; Greenberg et al., 2006). A missense mutation in the BRCT repeats of Brca1 (Brca1-S1598F) that ablates the Brca1-Ctip interaction has been shown to promote genomic instability in cells and tumorigenesis in mice (Shakya et al., 2011). Importantly, this single amino acid substitution not only prevents CtIP binding to BRCA1, but the binding of all known BRCA1 BRCT phospho-ligands, including Abraxas/CCDC98 and BACH1/ BRIP1/FancJ (reviewed in Huen et al., 2010; Moynahan and Jasin, 2010; Shakya et al., 2011).

As a candidate tumor suppressor itself, CtIP may modulate the tumor suppressor function of its interacting partner BRCA1 by promoting genome stability. CtIP has been implicated in at least two critical aspects of the DNA damage response: cell cycle checkpoint control (Yu and Chen, 2004) and DNA resection and homology-directed repair (HDR) of double-strand breaks (DSBs) (Sartori et al., 2007). In this study, we examined the role of CtIP in BRCA1-mediated genome stability and tumor suppression using murine cells expressing Ctip polypeptides (Ctip-S326A) that fail to interact with Brca1. Moreover, to assess whether CtIP is itself required for tumor suppression, we evaluated tumor development in mice following mammary-specific inactivation of a conditional *Ctip* gene. Finally, given our recent finding that BRCA1 tumor suppression

does not depend on its individual interaction with the BRCT phospho-ligands Abraxas, BACH1, or CtIP (a collaboration with Dr. Thomas Ludwig; Columbia University), we are currently analyzing how the phospho-dependent interaction of BRCA1 with two or more of its BRCT-binding partners affects its tumor suppressor activity.

The role of the BRCA1-CtIP interaction in genome stability

To analyze the role of the BRCA1-CtIP interaction in genome stability, we used a knock-in approach to introduce the S326A mutation into the mouse *Ctip* gene by homologous recombination. By doing this, we produced isogenic panels of ES cells and MEFs that express either wildtype Ctip or the Ctip-S326A mutant. We also demonstrated that this single amino acid substitution in Ctip was sufficient to ablate the Brca1-Ctip interaction (Figure 10).

Assembly of repair proteins at sites of DNA damage in mutant Ctip-S326A cells

In cells subjected to ionizing radiation (IR), several repair proteins, including BRCA1, CtIP, RPA, and Rad51, accumulate at sites of DNA damage to form IR-induced foci (IRIFs) which can be visualized by immunofluorescent microscopy. We examined how loss of the BRCA1-CtIP interaction affected recruitment of these proteins to IRIFs in Ctip-S326A mutant murine cells. To our surprise, we found that the BRCA1-CtIP interaction is dispensable for proper recruitment of BRCA1, CtIP, RPA, and Rad51 to sites of DNA damage (Figures 15-18).

In response to DNA damage, BRCA1 ubiquitinates CtIP in manner that depends on CtIP's association with the BRCT repeats of BRCA1 (Yu et al., 2006). It has been reported that BRCA1-dependent ubiquitination of CtIP is required for CtIP focus formation and activation of the transient G_2/M checkpoint in human cells (Yu et al., 2006). Thus, the BRCA1 RING and BRCT domains appear to act together to regulate the genomic stability functions of BRCA1, and in doing so, may modulate its tumor suppressor function.

In contrast to human cells (Yu et al., 2006), we observed normal Ctip focus formation in Ctip-S326A mutant MEFs. Although this result indicates that the Brca1-Ctip interaction is dispensable for Ctip accumulation at sites of DNA damage, it does not specifically address whether the E3 ligase activity of Brca1 is required for Ctip recruitment. Given that resection-dependent events, such as Rad51 foci formation and HDR of DSBs, occur normally in E3 ligase-deficient Brca1-I26A mutant murine cells (Reid et al., 2008), it seems likely that Ctip can accumulate at sites of DNA damage in the absence of Brca1's E3 ligase activity. In any case, it should be feasible to address this issue by testing whether Ctip can localize to IRIFs in Brca1-I26A mutant MEFs (Reid et al., 2008).

CtIP functions together with the MRN complex to promote DNA resection, a process in which DSB ends are converted into 3' single-stranded DNA (ssDNA) tails (Sartori et al., 2007; Gravel et al., 2008; Raynard et al., 2008). Since BRCA1 can form an *in vivo* protein complex (BRCA1 complex C) involving CtIP and MRN (Greenberg et al., 2006; Chen et al., 2008), both of which have been implicated in DNA resection, BRCA1 may

collaborate with these proteins to resect DSB ends. In the absence of the BRCA1-CtIP interaction, however, we observed normal assembly of RPA at sites of DNA damage. Although the BRCA1-CtIP interaction is essential for *in vivo* assembly of BRCA1 complex C (Chen et al., 2008), our result suggests that BRCA1 is not required for CtIP-mediated DNA resection.

Recently, BRCA1 and CtIP have each been individually implicated in ssDNA formation at ultraviolet (UV)-stalled forks (Pathania et al., 2011). Moreover, CtIP recruitment to UV-damaged DNA was impaired in BRCA1-depleted U2OS cells (Pathania et al., 2011). Therefore, in contrast to our work, which focused on IR-induced DNA damage, future studies should also explore the role of the BRCA1-CtIP interaction in response to UV-induced DNA damage.

DNA resection and DSB repair in mutant Ctip-S326A cells

BRCA1 and CtIP are individually required for several DSB repair pathways, including homology-directed repair (HDR), single-strand annealing (SSA), and alternative non-homologous end joining (alt-NHEJ) (Moynahan et al., 1999; Moynahan et al., 2001; Zhong et al., 2002; Stark et al., 2004; Sartori et al., 2007; Bennardo et al., 2008). Importantly, each of these repair pathways requires CtIP-mediated DNA resection (Bennardo et al., 2008). To elucidate the role of the BRCA1-CtIP interaction in DSB repair and to further assess whether BRCA1 mediates the DNA resection function of CtIP, we generated wildtype and Ctip-S326A mutant ES cells that contain a recombination substrate specific for each of the above repair pathways integrated into a defined chromosomal locus. In this study, we report that the BRCA1-CtIP interaction is

dispensable for proficient repair by each of these resection-dependent repair pathways (Figures 12-14). Thus, in contrast to previous reports (Chen et al., 2008; Yun and Hiom, 2010), but consistent with recent studies of resection in *Xenopus* cell-free extracts (Peterson et al., 2011), our data collectively demonstrates that BRCA1 is not required for CtIP-mediated DNA resection.

Future studies should examine which properties of CtIP are required for its DNA resection function. The conserved C-terminal sequence of mammalian CtIP, referred to here as the "Sae2 motif", was implicated in DNA resection because an siRNA-resistant CtIP C-terminal truncation mutant failed to promote RPA focus formation upon camptothecin treatment (Sartori et al., 2007). In yeast, two specific elements of the Sae2 motif, a CxxC sequence and a potential CDK phosphorylation site (T847 in humans), have been implicated in DNA resection (Limbo et al., 2007; Huertas et al., 2008). Thus, it should be possible to use a similar gene knock-in approach in murine cells to determine whether the resection function of these residues is conserved in mammals.

Chromosomal stability and cellular resistance to genotoxic stress in mutant Ctip-S326A cells

The inability to properly repair DSBs gives rise to chromosomal instability and cellular sensitivity to DNA damaging agents. Consistent with this, cells bearing the Brca1-S1598F phospho-recognition mutation display impaired HDR, marked chromosomal instability, and hypersensitivity to the DNA cross-linking agent mitomycin C (MMC) (Shakya et al., 2011). Since resection-dependent DSB repair pathways are proficient in the absence of the BRCA1-CtIP interaction (Figures 12-14), it was not

surprising to find normal suppression of spontaneous and MMC-induced chromosomal rearrangements (Figures 21-22; Table 3), as well as normal cellular resistance to MMC-induced genotoxic stress (Figure 19), in Ctip-S326A mutant cells. Thus, although BRCA1-mediated suppression of both chromosomal instability and MMC sensitivity requires the BRCT phospho-recognition property of BRCA1 (Shakya et al., 2011), the BRCA1-CTIP interaction itself does not appear to be essential for these aspects of BRCA1 function.

Of note, ablation of the BRCA1-CtIP interaction caused a weak hypersensitivity to the topoisomerase inhibitors camptothecin (CPT) and etoposide (ETO) (Figure 20). Importantly, the survival of Ctip-S326A mutant cells was not impaired to the same extent as that of ES cells homozygous for the hypomorphic *Brca1*$^{\Delta 223\text{-}763}$ mutation (Figure 20). Thus, the BRCA1-CtIP interaction is required for some, but not all, of the cellular resistance mediated by BRCA1 in response to the topoisomerase inhibitors CPT and ETO. Given that Ctip-S326A mutant cells are modestly sensitive to CPT and ETO, despite being proficient in HDR (Figure 12) and NHEJ (as assessed by a total-NHEJ reporter assay; data not shown), we conclude that the BRCA1-CtIP interaction promotes cellular tolerance to CPT and ETO independently of HDR or NHEJ, possibly by eliminating covalently-bound polypeptides from DSB ends.

A role for the BRCA1-CtIP complex in eliminating covalently-bound topoisomerases from DSBs was recently shown in avian cells; in contrast to the modest effects observed in mammalian Ctip-S326A cells (Figure 20), chicken DT40 cells bearing the corresponding mutation (S332A) displayed marked hypersensitivity to CPT and ETO (Nakamura et al., 2010). Moreover, Nakamura et al. (2010) observed that CtIP-S332A

chicken DT40 cells are also hypersensitive to the DNA alkylating agent methyl methanesulfonate (MMS). Therefore, it would be interesting to see if the BRCA1-CtIP interaction is required for cellular resistance to MMS in mammalian cells, especially since HCC1937 human breast cancer cells, which encode a C-terminally-truncated BRCA1 polypeptide that lacks one of the tandem BRCT motifs, displayed hypersensitivity to this genotoxic agent (Zhong et al., 1999). Additionally, given that BRCA1 suppresses hypersensitivity to UV (Pathania et al., 2011) and CtIP appears to be involved in BRCA1-dependent ssDNA gap formation at UV-stalled forks (Pathania et al., 2011), the sensitivity of Ctip-S326A mutant cells to UV-induced DNA damage should also be examined.

Cell cycle checkpoint control and damage-induced phosphorylation of CtIP in mutant Ctip-S326A cells

Since cell cycle checkpoints induced by genotoxic stress are common targets for oncogenic lesions in human cancer (Zhou and Elledge, 2000; Abraham, R. T. 2001; Shiloh and Kastan, 2001), the checkpoint functions of BRCA1 may represent an important aspect of its tumor suppression activity. Both BRCA1 and CtIP have been implicated in the IR-induced transient G_2/M checkpoint (Xu, B. et al., 2001; Xu, B. et al., 2002; Yu and Chen, 2004). Moreover, activation of this checkpoint in human cells appears to require the BRCA1-CtIP interaction, as well as the E3 ligase activity of the BRCA1/BARD1 heterodimer (Yu and Chen, 2004; Yu et al., 2006). In light of our results, which demonstrate proficient DSB repair and normal suppression of

chromosomal rearrangements in Ctip-S326A murine cells, it would be interesting to ascertain whether checkpoint functions are also intact in these cells.

In response to IR, CtIP is phosphorylated in an ATM-dependent manner on residues S664 and S745 (Li et al., 2000). It has been suggested that the BRCA1-CtIP interaction may facilitate the subsequent hyperphosphorylation of CtIP by ATM since BRCA1 is required for damage-induced phosphorylation of CtIP (Foray et al., 2003). Therefore, to address this issue, hyperphosphorylation of CtIP in response to DNA damage should also be examined in the Ctip-S326A mutant cells.

Conclusions

Overall, the results presented in this study indicate that significant aspects of BRCA1 and CtIP function in genome maintenance are independent of the BRCA1-CtIP interaction. In mammalian cells, the BRCA1-CtIP interaction is dispensable for the assembly of repair proteins at sites of DNA damage, resection-dependent DSB repair, suppression of spontaneous and MMC-induced chromosomal rearrangements, and cellular resistance to MMC-induced genotoxic stress. However, the BRCA1-CtIP interaction does appear to modestly affect clonogenic survival to the topoisomerase inhibitors CPT and ETO.

The role of the BRCA1-CtIP interaction in development and tumor suppression

To determine whether the BRCA1-CtIP interaction is required for normal animal development and tumor suppression, we injected *Ctip*$^{S326A\text{-}neo/+}$ 129Sv ES clones (Figure 9) into C57Bl6 blastocysts to obtain germline-transformed mice bearing the Ctip-S326A mutant allele. A breeding regimen was then employed to generate mice that solely express Ctip-S326A mutant polypeptides which fail to interact with the BRCT domains of Brca1 (i.e., *Ctip*$^{S326A/-}$ and *Ctip*$^{S326A/S326A}$ mice).

Animal development in mutant Ctip-S326A mice

BRCA1 and CtIP are individually thought to be essential for the viability of mammalian cells (Elledge and Amon, 2002; Chen, P.-L. et al., 2005). This is consistent with the early embryonic lethality of mice bearing homozygous-null mutations of either *Brca1* (Hakem et al., 1996; Ludwig et al., 1997) or *Ctip* (Chen, P.-L. et al., 2005). Importantly, *Ctip*-null mice die at an earlier stage of embryogenesis than *Brca1*-null mice, suggesting that Ctip likely executes at least some functions independent of Brca1 (Chen, P.-L. et al., 2005).

We report that the BRCA1-CtIP interaction is dispensable for mammalian cell viability. Consistent with our ability to generate Ctip-S326A mutant ES cells and MEFs with relative ease, viable *Ctip*$^{S326A/-}$ and *Ctip*$^{S326A/S326A}$ mice were born at the expected Mendelian ratios, survived to adulthood, were fertile, and otherwise appeared indistinguishable from their littermate controls (data not shown). Thus, the BRCA1-CtIP interaction is not required for all functions of either BRCA1 or CtIP. Additionally, we

examined the sensitivity of Ctip-S326A mutant mice to whole-body ionizing radiation (IR). In accord with the proficient DSB repair observed in Ctip-S326A cells (see above), Ctip-S326A mutant mice were resistant to a sublethal dose of IR (data not shown).

Tumor suppression in mutant Ctip-S326A mice

Given that CtIP is a BRCT phospho-ligand and enzymatic substrate of BRCA1 with prominent functions in genome stability, we investigated the role of the BRCA1-CtIP interaction in tumor suppression. In contrast to the marked tumor susceptibility of mice expressing a Brca1 polypeptide that lacks BRCT phospho-recognition activity (*Brca1*$^{S1598F/S1598F}$) (Shakya et al., 2011), Ctip-S326A animals developed tumors with kinetics indistinguishable from control mice (Figure 23). Thus, suppression of spontaneous tumor development occurs normally in the absence of the Brca1-Ctip interaction. This result indicates that the tumor suppression function of BRCA1 is not mediated specifically by its interaction with the BRCT phospho-ligand CtIP.

The BRCT repeats of BRCA1 form distinct protein complexes with at least two other DNA damage response proteins, Abraxas and BACH1 (reviewed in Huen et al., 2010; Moynahan and Jasin, 2010). Surprisingly, mice bearing mutations that specifically ablate either the Brca1-Abraxas or the Brca1-Bach1 interaction, like Ctip-S326A animals, do not display a heightened susceptibility to tumor formation (unpublished data). This result suggests that the tumor suppression function of BRCA1 is not dependent on its individual association with any of its three known BRCT phospho-ligands.

Conclusions

We have demonstrated that most functions of BRCA1 and CtIP in normal animal development are independent of the BRCA1-CtIP interaction. Thus, unlike *Brca1*- and *Ctip*-null animals, which undergo early embryonic lethality (Hakem et al., 1996; Liu et al., 1996; Ludwig et al., 1997; Chen, P.-L. et al., 2005), Ctip-S326A mice are viable, healthy, fertile, and resistant to IR. Moreover, these mice do not display a heightened susceptibility to tumor formation. Thus, the BRCA1-CtIP interaction appears to be dispensable for BRCA1-mediated tumor suppression.

The role of CtIP in tumor suppression

Previous studies have raised the possibility that CtIP functions as a tumor suppressor (Wong et al., 1998; Vilkki et al., 2002; Chen, P.-L. et al., 2005). For example, monoallelic genetic alterations of the *CtIP* gene have been identified in several human tumor cell lines derived from breast, ovarian, pancreas, and colon carcinomas (Wong et al., 1998). Furthermore, since heterozygous $Ctip^{+/-}$ mice developed tumors at an increased rate (T_{50} = 625 days) relative to wildtype $Ctip^{+/+}$ mice (T_{50} = 780 days), Chen, P.-L. et al. (2005) proposed that haploid insufficiency of *Ctip* leads to tumorigenesis. Thus, although a potential role for CtIP in tumor suppression has been suggested, these studies do not address whether CtIP serves as a tumor suppressor in mammary epithelial cells. As an interacting partner with the breast cancer-associated protein BRCA1, we proposed that CtIP may be involved in mammary tumorigenesis.

The effects of Ctip inactivation on tumor suppression

To determine whether CtIP is required for tumor suppression, we used a Cre-loxP gene targeting system to generate mice that inactivate the *Ctip* gene in a mammary-specific fashion. Since *Ctip*-null ($Ctip^{-/-}$) mice are embryonic lethal (Chen, P.-L. et al., 2005), we bred mice to carry a Ctip conditional-null allele ($Ctip^{Co}$) (Figure 24). We then showed that the Cre-recombined product of the $Ctip^{Co}$ allele is functionally null (Figure 27) and that $Ctip^{Co}$ recombination is specifically induced in mammary cells during late pregnancy and lactation in mice bearing the Wap^{Cre} transgene (Figure 28). Given these findings, $Ctip^{Co/+}/Wap^{Cre/+}$ control and $Ctip^{Co/–,Co/\ Co}/Wap^{Cre/+}$ experimental females were mated to induce pregnancy, lactation, Cre recombinase expression, and mammary-specific $Ctip^{Co}$ inactivation. Surprisingly, these mice remained tumor-free over the entire 24-month observation period (Figure 29) suggesting that Ctip is dispensable for suppression of mammary tumorigenesis.

The effects of Ctip inactivation on tumor suppression in a p53-deficient background

Given the well-established observation that p53 deficiency accelerates tumor formation in animals bearing Brca1 mutations (Brodie and Deng, 2001; Ludwig et al., 2001; Moynahan, M. E., 2002; Evers and Jonkers, 2006; Shakya et al., 2011), we examined the effects of mammary-specific Ctip inactivation in tumor-prone settings incurred by either a p53 conditional-null mutation ($p53^{Co}$) (Chen, Z. et al., 2005) or a p53 dominant-negative point mutation ($p53^{LSL\text{-}R270H}$) (Olive et al., 2004). Quite unexpectedly, tumor formation in $Ctip^{Co/–,Co/Co}/p53^{Co/+,Co/Co}/Wap^{Cre/+}$ experimental mice was

significantly reduced (longer latency and lower frequency) relative to control mice ($Ctip^{+/+,Co/+}/p53^{Co/+,\ Co/Co}/Wap^{Cre/+}$) (Figure 30). This result indicates not only that Ctip inactivation does not potentiate mammary tumorigenesis, but also that Ctip loss instead provides a protective effect against mammary tumorigenesis in a p53-deficient background. Similarly, Ctip also inhibited mammary tumor formation induced by expression of the dominant-negative $p53^{R270H}$ allele (Figure 31). Thus, in two independent tumor-prone settings, we observed prolonged tumor latency as a result of Ctip loss. This study raises new questions regarding whether Ctip is a *bona fide* tumor suppressor and whether the monoallelic mutations observed in human CtIP are truly oncogenic.

The Ctip/p53 double-deficient mammary tumors that arise with delayed kinetics relative to Brca1/p53 double-deficient and p53 single-deficient tumors display an interesting phenotype. Like the Brca1/p53 tumors, but unlike the p53-only tumors, the Ctip/p53 tumors are basal-like, in that they stain positive for the basal cytoskeletal markers, CK5 and CK14, and negative for the estrogen and progesterone receptors (Figure 32). However, like the p53 tumors and unlike the Brca1/p53 tumors, the Ctip/p53 tumors exhibit amplification of the proto-oncogene c-*Met* (Figure 33). Thus, the mammary carcinomas arising on conditional co-inactivation of the *Ctip/p53* genes display a unique phenotype that appears to be intermediate to that of the Brca1/p53 and p53-only tumors.

Conclusions

In this study, we have established that CtIP is not required for tumor suppression in mammary epithelial cells. Moreover, loss of CtIP appears to provide a protective effect against mammary tumorigenesis in tumor-prone settings resulting from p53-deficiency. The mechanisms by which CtIP loss inhibits tumorigenesis are unclear, but their elucidation may alter our current understanding of the role of CtIP in cancer development.

The role of CtIP in genome stability

Although *Ctip*-null ES cells and MEFs are not viable (Chen, P.-L. et al., 2005), *Ctip*-null mammary cell lines from the breast tumors of conditional Ctip/p53-mutant female mice were readily cultured *in vitro*. In addition to the programmed p53 lesions, these cells presumably harbor additional genetic defects that arose during oncogenic development and may allow for viability in the absence of Ctip (Figures 34-35, 37). In any case, through analysis of these cells, we were able to evaluate several parameters of genomic stability in the absence of Ctip expression.

The DNA damage response in Ctip-null tumor cells

There is substantial evidence that CtIP is required for maintenance of genome stability, particularly through its role in DNA resection and DSB repair (Sartori et al., 2007; Chen et al., 2008). For example, previous studies have shown that siRNA-mediated depletion of CtIP dramatically impairs ssDNA generation and RPA focus

formation (Sartori et al 2007; Chen et al., 2008). In contrast, however, we observe proper recruitment of RPA to IRIFs in *Ctip*-null ($Ctip^{Co\text{-}rec/-}$) mammary tumor cells (Figure 39), suggesting that Ctip is not essential for DNA resection. To explore this provocative finding more rigorously, independent methods to monitor ssDNA formation in $Ctip^{Co\text{-}rec/-}$ tumor cells should be applied, such as anti-BrdU staining to detect replication-dependent incorporation of BrdU (Sartori et al., 2007). In any case, this observation, as well as the normal recruitment of Brca1 and Rad51 to sites of DNA damage in $Ctip^{Co\text{-}rec/-}$ cells (Figures 38 and 40, respectively), suggests that at least some aspects of the DNA damage response can be elicited in the absence of Ctip. It would be intriguing to determine via recombination reporter assays whether the resection-dependent DSB repair pathways (HDR, SSA, and alt-NHEJ) are also functional in $Ctip^{Co\text{-}rec/-}$ tumor cells. Furthermore, cytogenetic analyses of the cell lines derived from Ctip/p53 and p53-alone mammary tumors suggest that Ctip loss does not enhance either spontaneous or damage-induced chromosomal instability (Figure 41; Table 5). Although we do not understand how these *Ctip*-null tumor cells mediate aspects of the DNA damage response that are thought to be Ctip-dependent, perhaps genetic lesions acquired during the oncogenic process facilitate not only the viability of these cells in the absence of Ctip, but also their capacity to mount a DNA damage response.

Chromosomal stability in Ctip-null tumor cells

Recent evidence suggests that chromosomal translocations arise when DSBs on different chromosomes are misjoined by alternative non-homologous end joining (alt-

NHEJ), a resection-dependent repair process (Zhang and Jasin, 2011). Consistent with this notion, the rate of chromosomal rearrangements was dramatically reduced in ES cells by shRNA-mediated Ctip depletion (Zhang and Jasin, 2011). In light of these results, it would be interesting to compare the translocation frequency in Ctip/p53 and p53-alone mammary tumors by spectral karyotyping (SKY). Based on the findings published by Zhang and Jasin (2011), we would expect to see fewer chromosomal translocations in the Ctip/p53-deficient mammary tumor cells relative to p53-deficient cells. However, since chromosomal translocations are relatively infrequent in p53-alone mammary tumors (Shakya et al., 2008), it may be difficult to accurately measure a reduction in translocation frequency due to Ctip loss. Therefore, it may be beneficial to integrate the pCr15 translocation reporter (Zhang and Jasin, 2011) into Ctip/p53-deficient and p53-deficient mammary tumor cells. Repair of two I-*Sce*I-induced DSBs on independent chromosomes by alt-NHEJ results in a chromosomal translocation and neo^{+} gene expression; thus, the translocation frequency can be quantified by counting the surviving neomycin-resistant colonies (Zhang and Jasin, 2011). The results from this experiment may provide an explanation as to how Ctip loss inhibits mammary tumor induction in p53-deficient mice.

A second source of Ctip-null cells (MEFs)

To assess the genomic stability functions of CtIP in non-malignant cells, we recently generated control ($Ctip^{Co/+}/Rosa^{CreERT2/+}$) and experimental ($Ctip^{Co/-}/Rosa^{CreERT2/+}$) immortalized MEFs (data not shown). In these cells, Cre recombinase is expressed as a

fusion protein with the estrogen receptor T2 (ERT2) moiety. Although the Cre-ERT2 fusion is normally retained in the cytosol, upon 4-OH-Tamoxifen treatment, it is transported to the nucleus, where it catalyzes recombination and inactivation of the $Ctip^{Co}$ allele. In preliminary studies, we observed cellular senescence of the experimental $Ctip^{Co/-}$ $Rosa^{CreERT2/+}$ cells within 72 hours after 4-OH-Tamoxifen treatment (data not shown). These results are consistent with the fact that Ctip is essential for the viability of ES cells, MEFs, and murine embryos (Chen, P.-L. et al., 2005). In any case, this inducible system of Ctip inactivation may allow Ctip functions to be evaluated in the period prior to cell senescence. Indeed, a similar approach has been used successfully to study the genome maintenance functions of loss-of-viability mutants of the Mre11 repair protein (Buis et al., 2008). It would be particularly interesting to compare results obtained in this MEF-based system, in which Ctip loss occurs in the absence of secondary oncogenic lesions, to the findings reported in this study using *Ctip*-null mammary tumor cells.

Conclusions

These results show that viable *Ctip*-null cells can be derived from mouse mammary tumors. Although these cells lack Ctip, they appear to be proficient for several aspects of the DNA damage response, including recruitment of repair proteins (Brca1, RPA, and Rad51) to sites of DNA damage and suppression of both spontaneous and MMC-induced chromosomal aberrations. Perhaps genetic lesions acquired during the oncogenic process can facilitate cell viability and genomic maintenance in the absence of Ctip.

The role of the BRCT phospho-ligands of BRCA1 in genome stability and tumor suppression

Analysis of AB, AC, and BC double mutant mice

Although BRCT phospho-recognition is critical for the genome stability and tumor suppression functions of BRCA1 (Shakya et al., 2011), these processes are not abrogated when the interactions of BRCA1 with its known phospho-ligands (Abraxas, BACH1, or CtIP) are individually disrupted. To assess whether these functions are dependent on the interaction of BRCA1 with two of its known BRCT phospho-ligands, we generated each of the three possible combinations of double homozygous mutant mice (*Abx*$^{S404A/S404A}$/*Bach1*$^{FH\text{-}S994A/FH\text{-}S994A}$, *Abx*$^{S404A/S404A}$/*Ctip*$^{S326A/S326A}$, and *Bach1*$^{FH\text{-}S994A/FH\text{-}S994A}$/*Ctip*$^{S326A/S326A}$), denoted herein as AB, AC, and BC mice, respectively. Of note, these mice were fully viable and appeared to be indistinguishable from their littermate controls. The AB, AC, and BC mice also displayed normal resistance to a sub-lethal dose of whole-body ionizing radiation (data not shown). Moreover, double homozygous mutant MEFs derived from these mice proliferate normally *in vitro* (Figure 42). Thus, disrupting the interaction of BRCA1 with any combination of two of its three known BRCT phospho-ligands does not appear to affect its functions in cell viability and genome maintenance. Importantly, BC mice do not display a heightened susceptibility to tumor development (Figure 43). Although further monitoring of the AB and AC double mutant animals is necessary, they have remained tumor-free for over a year.

Analysis of ABC triple mutant mice

In parallel, we have begun to examine whether the genome maintenance and tumor suppression functions of BRCA1 are affected when the interaction of BRCA1 with its three known BRCT phospho-ligands are ablated simultaneously. To this end, we generated ABC (*Abx*$^{S404A/S404A}$/*Bach1*$^{FH\text{-}S994A/FH\text{-}S994A}$/*Ctip*$^{S326A/S326A}$) triple mutant mice. It is important to note, that in these cells, unlike the BRCT phospho-recognition mutant cells (*Brca1*$^{S1598F/S1598F}$), the BRCT domains of Brca1 should retain the ability to interact with other undiscovered phospho-ligands, if they exist. As described in Chapter V, viable ABC triple mutant mice were obtained, but at a significantly lower frequency then expected based on the Mendelian ratios (data not shown). The ABC animals that survive to adulthood display a plethora of developmental defects, including growth retardation, white hind feet/belly spot, and kinked tails (Figure 52). In addition, male ABC mice are sub-fertile (data not shown). Nonetheless, we were able to generate both primary and SV40-immortalized MEFs from ABC mice.

Although ABC MEFs undergo damage-induced Brca1 hyperphosphorylation (Figure 51), they display proliferation defects (Figure 46), centrosome amplification (Figure 47), chromosomal instability (Figure 50; Table 7), and diminished recruitment of Brca1 and Rad51 to sites of DNA damage (Figure 49). Thus, ABC cells exhibit defects in genome maintenance similar to those observed in *Brca1*$^{S1598F/S1598F}$ MEFs (Shakya et al., 2011). Since the genomic stability functions of BRCA1 are only impaired upon simultaneous disruption of all three known BRCT phospho-ligand interactions, and not after ablation of any individual interaction or combination of two interactions, it appears that the major

BRCA1 supercomplexes assembled from these interactions (complexes A, B, and C) have the potential to act in a compensatory manner with respect to one another.

To confirm that the defects we observe are due to ablation of these BRCT phospho-ligand interactions and not a result of reduced protein expression, the steady-state levels of mutant Abraxas, Bach1, and Ctip polypeptides should be examined in ABC triple mutant MEFs. As yet, there are no reliable antibodies to recognize mouse Abraxas. We have already established that mutant Bach1 and Ctip polypeptides are expressed at wildtype levels in the corresponding single mutant (*Bach1*$^{FH\text{-}S994A/FH\text{-}S994A}$ and *Ctip*$^{S326A/S326A}$) MEFs, but it will also be necessary to ascertain whether these levels of expression are maintained in double mutant (AB, AC, and BC) and triple mutant (ABC) MEFs. Given the normal phenotype of AB, AC, and BC cells, we anticipate that the steady-state levels of these mutant polypeptides will be normal in each of the double mutant settings. Nonetheless, it is conceivable that the combined loss of all three BRCT phospho-ligand interactions may inadvertently affect the stability of one or more of these proteins in a manner that elicits the phenotypic abnormalities observed in ABC cells. Therefore, it is essential to confirm normal steady-state expression of mutant Abraxas, Bach1, and Ctip polypeptides in ABC triple mutant MEFs.

Since the impaired recruitment of HDR factors Brca1 and Rad51 to sites of DNA damage in ABC cells suggests a potential HDR defect (Figure 49), it would be intriguing to examine HDR directly in these cells by using an integrated DR-GFP recombination reporter. In addition, clonogenicity assays could be used to evaluate the cellular resistance of ABC MEFs to genotoxic stresses, such as the DNA cross-linking agent

MMC. In this regard, *Brca1*$^{S1598F/S1598F}$ cells are hypersensitive to MMC, indicating that BRCT phospho-recognition is necessary for BRCA1-mediated MMC resistance (Shakya et al., 2011). Additionally, cellular tolerance to the topoisomerase inhibitors CPT and ETO should be examined, especially since the Brca1-Ctip interaction is required for some, but not all, of the cellular resistance mediated by Brca1 in response to the topoisomerase inhibitors CPT and ETO (Figure 20). Furthermore, since one of the hallmarks of a defective DNA damage response is increased sensitivity to ionizing radiation, it would be interesting to assess the IR sensitivity of ABC mice.

The tumor suppression activity of ABC triple mutant mice

Overall, this study indicates that the animal development and genome maintenance functions of BRCA1 are disrupted only when its interactions with the three known BRCT phospho-ligands are ablated simultaneously. However, the most relevant function of BRCA1 from a medical standpoint is its ability to suppress breast and ovarian cancer. To assess the effects of these lesions on BRCA1-mediated tumor suppression it will be critical to monitor whole-body tumor formation in ABC triple mutant mice. If these interactions are required, then triple ABC mutant mice will likely develop tumors in various tissues, including the mammary glands. The timing and manner of tumor development should be compared to the BRCT phospho-recognition mutant mice (*Brca1*$^{S1598F/S1598F}$), which develop tumors with an average latency (T_{50}) of 575 days (Shakya et al., 2011).

It would also be intriguing to determine the effect of the triple mutant (ABC) genotype on suppression of basal-like breast cancer. To this end, a cohort of conditional ABC ($Abx^{S404A/S404A}/Bach1^{FH\text{-}S994A/FH\text{-}S994A}/Ctip^{S326A/Co}/Wap^{Cre/+}$) females could be prepared. Females of this genotype should appear at the expected Mendelian ratios, and therefore, it may be easier to generate a sizable cohort. Following pregnancy, lactation, Cre recombinase expression, and mammary-specific recombination of the conditional-null $Ctip^{Co}$ allele, these females will express the triple ABC mutations specifically in their mammary epithelial cells. If breast tumors do not develop in these females or occur at a low penetrance and/or long latency, tumorigenicity could also be examined in a p53-deficient background.

Conclusions

Given the importance of genomic instability in tumor development, the genome maintenance functions of BRCA1 may be a key aspect of its tumor suppression activity. In this study, we have provided substantial evidence that the interaction of all three BRCT phospho-ligands with BRCA1 serves to maintain the genomic stability functions of BRCA1. The relevance of these findings to BRCA1-mediated tumor suppression is an important avenue of future research, as these interactions may provide valuable targets for therapeutic intervention.

CHAPTER VII

REFERENCES

Abbott, D. W., Thompson, M. E., Robinson-Benion, C., Tomlinson, G., Jensen, R. A., and Holt, J. T. (1999). BRCA1 expression restores radiation resistance in BRCA1-defective cancer cells through enhancement of transcription-coupled DNA repair. J. Biol. Chem., 274(26): 18809-18812.

Abraham, R. T. (2001). Cell cycle checkpoint signaling through the ATM and ATR kinases. Genes & Dev. 15: 2177-2196.

Aylon, Y., Liefshitz, B., and Kupiec, M. (2004). The CDK regulates repair of double-strand breaks by homologous recombination during the cell cycle. EMBO, 23: 4868-4875.

Baer, R. and Ludwig, T. (2002). The BRCA1/BARD1 heterodimer, a tumor suppressor complex with ubiquitin E3 ligase activity. Curr. Opin. Genet. Dev., 12(1): 86-91.

Barber, L. J. and Boulton, S. J. (2006). BRCA1 ubiquitylation of CtIP: Just the tIP of the iceberg? DNA Repair, 5: 1499-1504.

Bennardo, N., Cheng, A., Huang, N., and Stark, J. M. (2008). Alternative-NHEJ is a mechanistically distinct pathway of mammalian chromosome break repair. PLoS Genet., 4(6): e1000110.

Bennett, L. M., Haugen-Strano, A., Cochran, C., Brownlee, H. A., Fiedorek, F. T., Jr., and Wiseman, R. W. (1995). Isolation of the mouse homologue of BRCA1 and genetic mapping to mouse chromosome 11. Genomics, 29: 576-581.

Bork, P., Hofmann, K., Bucher, P., Neuwald, A. F., Altschul, S. F., and Koonin, E. V. (1997). A superfamily of conserved domains in DNA damage-responsive cell cycle checkpoint proteins. FASEB J., 11: 68-76.

Bressan, D. A., Baxter, B. K., and Petrini, J. H. (1999). The Mre11-Rad50-Xrs2 protein complex facilitates homologous recombination-based double-strand break repair in Saccharomyces cerevisiae. Mol. Cell Biol., 19: 7681-7687.

Brodie, S. G. and Deng, C. X. (2001). BRCA1-associated tumorigenesis: what have we learned from knockout mice? Trends Biochem. Sci., 17: S18-S22.

Brzovic, P. S., Rajagopal, P., Hoyt, D. W., King, M.-C., and Klevit, R. E. (2001). Structure of a BRCA1-BARD1 heterodimeric RING-RING complex. Nat. Struct. Biol., 8(10): 833-837.

Buis, J., Wu, Y., Deng, Y., Leddon, J., Westfield, G., Eckersdorff, M., Sekiguchi, J. M., Chang, S., and Ferguson, D. O. (2008). Mre11 nuclease activity has essential roles in DNA repair and genomic stability distinct from ATM activation. Cell, 135: 85-96.

Callebaut, I. and Mornon, J.-P. (1997). From BRCA1 to RAP1: a widespread BRCT module closely associated with DNA repair. FEBS Lett., 400(1): 25-30.

Cantor, S. B., Bell, D. W., Ganesan, S., Kass, E. M., Drapkin, R., Grossman, S., Wahrer, D. C., Sgroi, D. C., Lane, W. S., Haber, D. A., and Livingston, D. M. (2001). BACH1, a novel helicase-like protein, interacts directly with BRCA1 and contributes to its DNA repair function. Cell, 105: 149-160.

Chen, L, Nievera, C. J., Lee, A. Y., and Wu, X. (2008). Cell cycle-dependent complex formation of BRCA1-CtIP-MRN is important for DNA double-strand break repair. J. Biol. Chem., 283(12): 7713-7720.

Chen, P.-L., Liu, F., Cai, S., Lin, X., Li, A., Chen, Y., Gu, B., Lee, E. Y., and Lee, W.-H. (2005). Inactivation of CtIP leads to early embryonic lethality mediated by G1 restraint and to tumorigenesis by haploid insufficiency. Mol. Cell Biol., 25(9): 3535-3542.

Chen, Y., Farmer, A. A., Chen, C.-F., Jones, D. C., Chen, P.-L., and Lee, W.-H. (1996). BRCA1 is a 220-kDa nuclear phosphoprotein that is expressed and phosphorylated in a cell cycle-dependent manner. Cancer Res, 56: 3168-3172.

Chen, Z., Trotman, L. C., Shaffer, D., Lin, H.-K., Dotan, Z. A., Niki, M., Koutcher, J. A., Scher, H. I., Ludwig, T., Gerald, W., Cordon-Cardo, C., and Pandolfi, P. P. (2005). Crucial role of p53-dependent cellular senescence in suppression of Pten-deficient tumorigenesis. Nature, 436: 725-730.

Chinnadurai, G. (2006). CtIP, a candidate tumor susceptibility gene is a team player with luminaries. Biochim. Biophys. Acta., 1765: 67-73.

Choudhary, S. K. and Li, R. (2002). BRCA1 modulates ionizing radiation-induced nuclear focus formation by the replication protein A p34 subunit. J. Cell Biochem., 84: 666-674.

Clapperton, J. A., Manke, I. A., Lowery, D. M., Ho, T., Haire, L. F., Yaffe, M. B., and Smerdon, S. J. (2004). Structure and mechanism of BRCA1 BRCT domain recognition of phosphorylated BACH1 with implications for cancer. Nat Struct Biol, 11(6): 512-518.

Costanzo, V., Robertson, K., Bibikova, M., Kim, E., Grieco, D., Gottesman, M., Carroll, D., and Gautier, J. (2001). Mre11 protein complex prevents double-strand break accumulation during chromosomal DNA replication. Mol. Cell, 8: 137-147.

Critchlow, S. E. and Jackson, S. P. (1998). DNA end-joining: from yeast to man. TIBS, 23: 394-398.

Crook, T., Crossland, S., Crompton, M. R., Osin, P., and Gusterson, B. A. (1997). p53 mutations in BRCA1-associated familial breast cancer. Lancet, 350: 638-639.

D'Amours, D., and Jackson, S. P. (2002). The Mre11 complex: at the crossroads of DNA repair and checkpoint signaling, Nat. Rev. Mol Cell Biol., 3: 317-327.

Daley, J. M., Palmbos, P. L., Wu, D., Wilson, T. E. (2005). Non-homologous end joining in yeast. Annu. Rev. Genet., 39: 431-451.

De Brakeleer, S., De Greve, J., Loris, R., Janin, N., Lissens, W., Sermijn, E., and Teugels, E. (2010). Cancer predisposing missense and protein truncating BARD1 mutations in non-BRCA1 or BRCA2 breast cancer families. Human Mutation, 31(3): e1175-e1185.

Deng, C.-X. and Brodie, S. G. (2000). Roles of BRCA1 and its interacting proteins. BioEssays, 22: 728-737.

Deng, C.-X. and Scott, F. (2000). Role of the tumor suppressor gene Brca1 in genetic stability and mammary gland tumor formation. Oncogene, 19: 1059-1064.

Deng, C.-X. (2001). Tumorigenesis as a consequence of genetic instability in Brca1 mutant mice. Mutation Res, 477: 183-189.

Deng, C.-X. (2002). Roles of BRCA1 in centrosome duplication. Oncogene, 21(40): 6222-6227.

Deng, C.-X. (2006). BRCA1: cell cycle checkpoint, genetic instability, DNA damage response and cancer evolution. Nucleic Acids Res., 34(5): 1416-1426.

Donehower, L. A., Harvey, M., Slagle, B. L., McArthur, M. J., Montgomery, C. A. Jr., Butel, J. S., and Bradley, A. (1992). Mice deficient for p53 are developmentally normal but susceptible to spontaneous tumours. Nature, 356(6366): 215-221.

Dubin, M. J., Stokes, P. H., Sum, E. Y., Williams, R. S., Valova, V. A., Robinson, P. J., Lindeman, G. J., Glover, J. N., Visvader, J. E., and Matthews, J. M. (2004). Dimerization of CtIP, a BRCA1- and CtBP-interacting protein, is mediated by an N-terminal coiled-coil motif. J. Biol. Chem., 279(26): 26932-26938.

Elledge, S. J. and Amon, A. (2002). The BRCA1 suppressor hypothesis: An explanation for the tissue-specific tumor development in BRCA1 patients. Cancer Cell, 1(2): 129-132.

Evers, B. and Jonkers, J. (2006). Mouse models of BRCA1 and BRCA2 deficiency: past lesions, current understanding and future prospects. Oncogene, 25: 5885-5897.

Foray, N., Marot, D., Gabriel, A., Randrianarison, V., Carr, A. M., Perricaudet, M., Ashworth, A., and Jeggo, P. (2003). A subset of ATM- and ATR-dependent phosphorylation events requires the BRCA1 protein. EMBO J., 22(11): 2860-2871.

Freemont, P. S. (1993). The RING finger: A novel protein sequence motif related to the zinc finger. Ann. NY Acad. Sci., 684: 174-192.

Fusco, C., Reymond, A., and Zervos, A. S. (1998). Molecular cloning and characterization of a novel retinoblastoma-binding protein. Genomics, 51(3): 351-358.

Gilbert, S. F. (2003). Developmental biology, 7th ed. Sinauer Associates, Inc., Sunderland, MA

Glover, J. N., Williams, R. S., and Lee, M. S. (2004). Interactions between BRCT repeats and phosphoproteins: tangled up in two. Trends Biochem. Sci., 29:579-585.

Gorringe, K. L, Choong, D. Y., Lindeman, G. J., Visvader, J. E., and Campbell, I. G. (2008). Breast cancer risk and the BRCA1 interacting protein CTIP. Breast Cancer Res. Treat., 112: 351-352.

Gravel, S., Chapman, J. R., Magill, C., and Jackson, S. P. (2008). DNA helicases Sgs1 and BLM promote DNA double-strand break resection. Genes & Dev., 22: 2767-2772.

Greenberg, R. A., Sobhian, B., Pathania, S., Cantor, S. B., Nakatani, Y., and Livingston, D. M. (2006). Multifactorial contributions to an acute DNA damage response by BRCA1/BARD1-containing complexes. Genes & Dev., 20: 34-46.

Greenberg, R. A. (2008). Recognition of DNA double strand breaks by the BRCA1 tumor suppressor network. Chromosoma, 117(4): 305-317.

Gu, B. and Chen, P.-L. (2009). Expression of PCNA-binding domain of CtIP, a motif required for CtIP localization at DNA replication foci, causes DNA damage and activation of DNA damage checkpoint. Cell Cycle, 8(9): 1409-1420.

Haaf, T., Golub, E. I., Reddy, G., Radding, C. M., and Ward, D. C. (1995). Nuclear foci of mammalian Rad51 recombination protein in somatic cells after DNA damage and its localization in synaptonemal complexes. Proc. Natl. Acad. Sci. USA, 92: 2298-2302.

Haber, J. E. (2000). Partners and pathways repairing a double-strand break. Trends Genet., 16(6): 259-264.

Hakem, R., de la Pompa, J. L., Sirard, C., Mo, R., Woo, M., Hakem, A., Wakeham, A., Potter, J., Reitmair, A., Billia, F., Firpo, E., Hui, C. C., Roberts, J., Rossant, J., and Mak, T. W. (1996). The tumor suppressor gene Brca1 is required for embryonic cellular proliferation in the mouse. Cell, 85: 1009-1023.

Hakem, R., de la Pompa, J. L., Elia, A., Potter, J., and Mak, T. W. (1997). Partial rescue of Brca1$^{5-6}$ early embryonic lethality by p53 or p21 null mutation. Nat Genet, 16: 298-302.

Harvey, M., McArthur, M. J., Montgomery, C. A. Jr., Butel, J. S., Bradley, A., and Donehower, L. A. (1993). Spontaneous and carcinogen-induced tumorigenesis in p53-deficient mice. Nat. Genet., 5: 225-229.

Hashizume, R., Fukuda, M., Maeda, I., Nishikawa, H., Oyake, D., Yabuki, Y., Ogata, H., and Ohta, T. (2001). The RING heterodimer BRCA1-BARD1 is a ubiquitin ligase inactivated by a breast cancer-derived mutation. J. Biol. Chem., 276(18): 14537-14540.

Helleday, T., Lo, J., van Gent, D. C., and Engelward, B. P. (2007). DNA double-strand break repair: From mechanistic understanding to cancer treatment. DNA Repair, 6: 923-935.

Huen, M. S., Sy, S. M., and Chen, J. (2010). BRCA1 and its toolbox for the maintenance of genome integrity. Nat. Rev. Mol. Cell Biol., 11: 138-148.

Huertas, P., Cortes-Ledesma, F., Sartori, A. A., Aguilera, A., and Jackson, S. P. (2008). CDK targets Sae2 to control DNA-end resection and homologous recombination. Nature, 455(7213): 689-692.

Huertas, P. and Jackson, S. P. (2009). Human CtIP mediates cell cycle control of DNA end resection and double strand break repair. J. Biol. Chem. 284(14): 9558-9565.

Huertas, P. (2010). DNA resection in eukaryotes: deciding how to fix the break. Nat. Struct. Mol. Biol., 17(1): 11-16.

Huyton, T., Bates, P. A., Zhang, X., Sternberg, M. J., and Freemont, P. S. (2000). The BRCA1 C-terminal domain: structure and function. Mutat. Res., 460(3-4): 319-332.

Ira, G., Pellicioli, A., Balijja, A., Wang, X., Fiorani, S., Carotenuto, W., Liberi, G., Bressan, D., Wan, L., Hollingsworth, N. M., Haber, J. E., and Foiani, M. (2004). DNA end resection, homologous recombination and DNA damage checkpoint activation require CDK1. Nature, 431: 1011-1017.

Irminger-Finger, I. and Jefford, C. E. (2006). Is there more to BARD1 than BRCA1? Nature Reviews, 6: 382-391.

Ivanov, E. L., Korolev, V. G., and Fabre, F. (1992). XRS2, a DNA repair gene of Saccharomyces cerevisiae, is needed for meiotic recombination. Genetics, 132: 651-664.

Jackson, S. P. (2002). Sensing and repairing DNA double-strand breaks. Carcinogenesis, 23(5): 687-696.

Jasin, M. (2002). Homologous repair of DNA damage and tumorigenesis: the BRCA connection. Oncogene, 21(58): 8981-8993.

Jazayeri, A., Falck, J., Lukas, C., Bartek, J., Smith, G. C., Lukas, J., and Jackson, S. P. (2006). ATM- and cell cycle-dependent regulation of ATR in response to DNA double-strand breaks. Nat. Cell Biol., 8: 37-45.

Joazeiro, C. A. P. and Weissman, A. M. (2000). RING finger proteins: Mediators of ubiquitin ligase activity. Cell, 102(5): 549-552.

Karran, P. (2000). DNA double strand break repair in mammalian cells. Curr. Opin. Genet. Dev., 10: 144-150.

Khanna, K. K. and Jackson, S. P. (2001). DNA double-strand breaks: signaling, repair and the cancer connection. Nat Genet, 27: 247-254.

Khanna, K. K., Lavin, M. F., Jackson, S. P., and Mulhern, T. D. (2001). ATM, a central controller of cellular responses to DNA damage. Cell Death Differ., 8: 1052-1065.

Kim, H., Huang, J., and Chen, J. (2007). CCDC98 is a BRCA1-BRCT domain-binding protein involved in the DNA damage response. Nat. Struct. Mol. Biol., 14(8): 710-715.

Kim, H., Chen, J., and Yu, X. (2007a). Ubiquitin-binding protein RAP80 mediates BRCA1-dependent DNA damage response. Science, 316: 1202-1205.

Knudson, A. G., Jr. (1971). Mutation and cancer: statistical study of retinoblastoma. Proc. Natl. Acad. Sci. USA, 68(4): 820-823.

Koonin, E. V., Altschul, S. F., and Bork, P. (1996). BRCA1 protein products: functional motifs. Nat Genet, 13: 266-267.

Krogh, B. O., Llorente, B., Lam, A., and Symington, L. S. (2005). Mutations in Mre11 phosphoesterase motif I that impair Saccharomyces cerevisiae Mre11-Rad50-Xrs2 complex stability in addition to nuclease activity. Genetics, 171:1561-1570.

Lavin, M. F. and Khanna, K. K. (1999). ATM: the protein encoded by the gene mutated in the radiosensitive syndrome ataxia-telangiectasia. Int. J. Radiat. Biol., 75(10): 1201-1214.

Lee, J.-H. and Paull, T. T. (2004). Direct activation of the ATM protein kinase by the Mre11/Rad50/Nbs1 complex. Science, 304(5667): 93-96.

Lengsfeld, B. M., Rattray, A. J., Bhaskara, V., Ghirlando, R., and Paull, T. T. (2007). Sae2 is an endonuclease that processes hairpin DNA cooperatively with the Mre11/Rad50/Xrs2 complex. Mol. Cell, 28(4): 638-651.

Levitus, M., Waisfisz, Q., Godthelp, B. C., de Vries, Y., Hussain, S., Wiegant, W. W., Elghalbzouri-Maghrani, E., Steltenpool, J., Rooimans, M. A., et al. (2005). The DNA helicase BRIP1 is defective in Fanconi anemia complementation group J. Nat. Genet., 37(9): 934-935.

Levran, O., Attwooll, C., Henry, R. T., Milton, K. L., Neveling, K., Rio, P., Batish, S. D., Kalb, R., Velleuer, E., Barral, S., Ott, J., Petrini, J., Schindler, D., Hanenberg, H., and Auerbach, A. D. (2005). The BRCA1-interacting helicase BRIP1 is deficient in Fanconi anemia. Nat. Genet, 37(9): 931-933.

Li, S., Ting, N. S., Zheng, L., Chen, P.-L., Ziv, Y., Shiloh, Y., Lee, E. Y., and Lee, W.-H. (2000). Functional link of BRCA1 and ataxia telangiectasia gene product in DNA damage response. Nature, 406: 210-215.

Lieber, M. R., Ma, Y., Pannicke, U., and Schwarz, K. (2003). Mechanism and regulation of human non-homologous DNA end-joining. Nat. Rev. Mol. Cell Biol., 4: 712-720.

Limbo, O., Chahwan, C., Yamada, Y., de Bruin, R. A., Wittenberg, C., and Russell, P. (2007). *Ctp1* is a cell-cycle-regulated protein that functions with *Mre11* complex to control double-strand break repair by homologous recombination. Mol. Cell, 28: 134-146.

Lingle, W. L., Lutz, W. H., Ingle, J. N., Maihle, N. J., and Salisbury, J. L. (1998). Centrosome hypertrophy in human breast tumors: Implications for genomic stability and cell polarity. Proc. Natl. Acad. Sci. USA, 95: 2950-2955.

Lisby, M. and Rothstein, R. (2004). DNA damage checkpoint and repair centers. Curr Opin Cell Biol., 16: 328-334.

Lisby, M., Barlow, J. H., Burgess, R. C., and Rothstein, R. (2004). Choreography of the DNA damage response: Spatiotemporal relationships among checkpoint and repair proteins. Cell, 118: 699-713.

Litman, R., Peng, M., Jin, Z., Zhang, F., Zhang, J., Powell, S., Andreassen, P. R., and Cantor, S. B. (2005). Bach1 is critical for homologous recombination and appears to be the Fanconi anemia gene product FancJ. Cancer Cell, 3: 255-265.

Liu, C.-Y., Flesken-Nikitin, A., Li, S., Zeng, Y., and Lee, W.-H. (1996). Inactivation of the mouse Brca1 gene leads to failure in the morphogenesis of the egg cylinder in early postimplantation development. Genes Dev, 10: 1835-1843.

Liu, F. and Lee, W.-H. (2006). CtIP activates its own and cyclin D1 promoters via the E2F/Rb pathway during G1/S progression. Mol. Cell Biol. 26(8): 3124-3134.

Liu, X., Holstege, H., van der Gulden, H., Treur-Mulder, M., Zevenhoven, J., Velds, A., Kerkhoven, R. M., van Vliet, M. H., Wessels, L. F. A., Peterse, J. L., Berns, A., and Jonkers, J. (2007). Somatic loss of BRCA1 and p53 in mice induces mammary tumors with features of human BRCA1-mutated basal-like breast cancer. PNAS, 104(29): 12111-12116.

Liu, Z., Wu, J., and Yu, X. (2007). CCDC98 targets BRCA1 to DNA damage sites. Nat. Struct. Mol. Biol., 14(8): 716-720.

Ludwig, T., Chapman, D. L., Papaioannou, V. E., and Efstratiadis, A. (1997). Targeted mutations of breast cancer susceptibility gene homologs in mice: lethal phenotypes of Brca1, Brca2, Brca1/Brca2, Brca1/p53, and Brca2/p53 nullizygous embryos. Genes Dev., 11: 1226-1241.

Ludwig, T., Fisher, P., Ganesan, S., and Efstratiadis, A. (2001). Tumorigenesis in mice carrying a truncating Brca1 mutation. Genes Dev., 15: 1188-1193.

Ludwig, T., Fisher, P., Murty, V., and Efstratiadis, A. (2001a). Development of mammary adenocarcinomas by tissue-specific knockout of *Brca2* in mice. Oncogene, 20: 3937-3948.

Magnard, C., Bachelier, R., Vincent, A., Jaquinod, M., Kieffer, S., Lenoir, G. M. and Venezia, N. D. (2002). BRCA1 interacts with acetyl-CoA carboxylase through its tandem of BRCT domains. Oncogene, 21(44): 6729-6739.

Manke, I. A., Lowery, D. M., Nguyen, A., and Yaffe, M. B. (2003). BRCT repeats as phosphopeptide-binding modules involved in protein targeting. Science, 302: 636-639.

McCarthy, A., Savage, K., Gabriel, A., Naceur, C., Reis-Filho, J. S., and Ashworth, A. (2007). A mouse model of basal-like breast carcinoma with metaplastic elements. J. Pathol., 211: 389-398.

McCarthy, E. E., Celebi, J. T., Baer, R., and Ludwig, T. (2003). Loss of Bard1, the heterodimeric partner of the Brca1 tumor suppressor, results in early embryonic lethality and chromosomal instability. Mol Cell Biol, 23(14): 5056-5063.

McVey, M. and Lee, S. E. (2008). MMEJ repair of double-strand breaks (director's cut): deleted sequences and alternative endings. Trends in Genetics, 24(11): 529-538.

Meloni, A. R., Smith, E. J., and Nevins, J. R. (1999). A mechanism for Rb/p130-mediated transcription repression involving recruitment of the CtBP corepressor. PNAS, 96: 9574-9579.

Miki, Y., Swensen, J., Shattuck-Eidens, D., Futreal, P. A., Harshman, K., Tavtigian, S., Liu, Q., Cochran, C., Bennett, L. M., Ding, W. and et al. (1994). A strong candidate for the breast and ovarian cancer susceptibility gene BRCA1. Science, 266: 66-71.

Mimitou, E. P. and Symington, L. S. (2008). Sae2, Exo1, and Sgs1 collaborate in DNA double-strand break processing. Nature, 455(7214): 770-774.

Mimitou, E. P. and Symington, L. S. (2010). Ku prevents Exo1 and Sgs1-dependent resection of DNA ends in the absence of a functional MRX complex or Sae2. EMBO J., 29: 3358-3369.

Mimitou, E. P. and Symington, L. S. (2011). DNA end resection-unraveling the tail. DNA Repair (Amst), 10(3): 344-348.

Mirzoeva, O. K. and Petrini, J. H. (2001). DNA damage-dependent nuclear dynamics of the Mre11 complex. Mol. and Cell Biol., 21(1): 281-288.

Miyake, T., Hu, Y.-F., Yu, D. S., and Li, R. (2000). A functional comparison of BRCA1 C-terminal domains in transcription activation and chromatin remodeling. J. Biol. Chem., 275(51): 40169-40173.

Moreau, S., Morgan, E. A., and Symington, L. S. (2001). Overlapping functions of the Saccharomyces cerevisiae Mre11, Exo1 and Rad27 nucleases in DNA metabolism. Genetics, 159: 1423-1433.

Mosavi, L. K., Cammett, T. J., Desrosiers, D. C., and Peng, Z. (2004). The ankyrin repeat as molecular architecture for protein recognition. Protein Sci., 13(6): 1435-1448.

Moynahan, M. E., Chiu, J. W., Koller, B. H., and Jasin, M. (1999). Brca1 controls homology-directed DNA repair. Mol. Cell, 4: 511-518.

Moynahan, M. E., Cui, T. Y., and Jasin, M. (2001). Homology-directed DNA repair, mitomycin-c resistance, and chromosome stability is restored with correction of a Brca1 mutation. Cancer Res, 61: 4842-4850.

Moynahan, M. E., Pierce, A. J., and Jasin, M. (2001a). BRCA2 is required for homology-directed repair of chromosomal breaks. Mol. Cell., 7: 263-272.

Moynahan, M. E. (2002). The cancer connection: BRCA1 and BRCA2 tumor suppression in mice and humans. Oncogene, 21: 8994-9007.

Moynahan, M. E. and Jasin, M. (2010). Mitotic homologous recombination maintains genomic stability and suppresses tumorigenesis. Nat. Rev. Mol. Cell Biol., 11: 196-207.

Nagaraju, G. and Scully, R. (2007). Minding the gap: The underground functions of BRCA1 and BRCA2 at stalled replication forks. DNA Repair, 6(7): 1018-1031.

Nakamura, K., Kogame, T., Oshiumi, H., Shinohara, A., Sumitomo, Y., Agama, K., Pommier, Y., Tsutsui, K. M., Tsutsui, K., Hartsuiker, E., Ogi, T., Takeda, S., and Taniguchi, Y. (2010). Collaborative action of BRCA1 and CtIP in elimination of covalent modifications from double-strand breaks to facilitate subsequent break repair. PLoS Genet., 6(1): e1000828.

Nicolette, M. L., Lee, K., Guo, Z., Rani, M., Chow, J. M., Lee, S. E., and Paull, T. T. (2010). Mre11-Rad50-Xrs2 and Sae2 promote 5' strand resection of DNA double-strand breaks. Nat. Struct. Mol. Biol., 17(12): 1478-1485.

Nishikawa, H., Ooka, S., Sato, K., Arima, K., Okamoto, J., Klevit, R. E., Fukuda, M., and Ohta, T. Mass spectrometric and mutational analyses reveal Lys-6-linked polyubiquitin chains catalyzed by BRCA1-BARD1 ubiquitin ligase. J. Biol. Chem., 279(6): 3916-3924.

Nitiss, J. L. (2009). Targeting DNA topoisomerase II in cancer chemotherapy. Nat. Rev. Cancer, 9: 338-350.

Niu, H., Chung, W. H., Zhu, Z., Kwon, Y., Zhao, W., Chi, P., Prakash, R., Seong, C., Liu, D., Lu, L., Ira, G., and Sung, P. Mechanism of the ATP-dependent DNA end-resection machinery from Saccharomyces cerevisiae. Nature, 467(7311): 108-11.

Olive, K. P., Tuveson, D. A., Ruhe, Z. C., Yin, B., Willis, N. A., Bronson, R. T., Crowley, D., and Jacks, T. (2004). Mutant p53 gain of function in two mouse models of Li-Fraumeni syndrome. Cell, 119: 847-860.

Oliver, E. R., Saunders, T. L., Tarle, S. A., and Glaser, T. (2004). Ribosomal protein L24 defect in Belly spot and tail (*Bst*), a mouse *Minute*. Development, 131: 3907-3920.

Pathania, S., Nguyen, J., Hill, S. J., Scully, R., Adelmant, G. O., Marto, J. A., Feunteun, J., and Livingston, D. M. (2011). BRCA1 is required for postreplication repair after UV-induced DNA damage. Mol. Cell, 44: 235-251.

Paull, T. T. and Gellert, M. (1998). The 3' to 5' exonuclease activity of Mre11 facilitates repair of DNA double-strand breaks. Mol. Cell, 1: 969-979.

Paull, T. T. (2010). Making the best of the loose ends: Mre11/Rad50 complexes and Sae2 promote DNA double-strand break resection. DNA Repair (Amst), 9(12): 1283-1291.

Penkner, A., Portik-Dobos, Z., Tang, L., Schnabel, R., Novatchkova, M., Jantsch, V., and Loidl, J. (2007). A conserved function for a Caenorhabditis elegans Com1/Sae2/CtIP protein homolog in meiotic recombination. EMBO J., 26: 5071-5082.

Peterson, S. E., Li, Y., Chait, B. T., Gottesman, M. E., Baer, R., and Gautier, J. (2011). Cdk1 uncouples CtIP-dependent resection and Rad51 filament formation during M-phase double-strand break repair. J. Cell Biol., 194(5): 705-720.

Pierce, A. J., Hu, P., Han, M., Ellis, N., and Jasin, M. (2001). Ku DNA end-binding protein modulates homologous repair of double-strand breaks in mammalian cells. Genes & Dev., 15: 3237-3242.

Pihan, G. A., Purohit, A., Wallace, J., Knecht, H., Woda, B., Quesenberry, P., and Doxsey, S. J. (1998). Centrosome defects and genetic instability in malignant tumors. Cancer Res, 58(17): 3974-3985.

Pommier, Y. (2006). Topoisomerase I inhibitors: camptothecins and beyond. Nat. Rev. Cancer, 6: 789-802.

Ratajska, M., Antoszewska, E., Piskorz, A., Brozek, I., Borg, A., Kusmierek, H., Biernat, W., and Limon, J. (2012). Cancer predisposing BARD1 mutations in breast-ovarian cancer families. Breast Cancer Res. Treat., 131(1): 89-97.

Ray, H., Moreau, K., Dizin, E., Callebaut, I., and Venezia, N. D. (2006). ACCA phosphopeptide recognition by the BRCT repeats of BRCA1. J. Mol. Biol. 359: 973-982.

Raynard, S., Niu, H., and Sung, P. (2008). DNA double-strand break processing: the beginning of the end. Genes & Devel., 22: 2903-2907.

Reid, L. J., Shakya, R., Modi, A. P., Lokshin, M., Cheng, J.-T., Jasin, M., Baer, R., and Ludwig, T. (2008). E3 ligase activity of BRCA1 is not essential for mammalian cell viability or homology-directed repair of double-strand DNA breaks. PNAS, 105(52): 20876-20881.

Robinson, G. W., McKnight, R. A., Smith, G. H., and Hennighausen, L. (1995). Mammary epithelial cells undergo secretory differentiation in cycling virgins but require pregnancy for the establishment of terminal differentiation. Development, 121: 2079-2090.

Rodriguez, M., Yu, X., Chen, J., and Songyang, Z. (2003). Phosphopeptide binding specificities of BRCA1 COOH-terminal (BRCT) domains. J Biol Chem., 278(52): 52914-52918.

Rong, S., Donehower, L. A., Hansen, M. F., Strong, L., Tainsky, M., Jeffers, M., Resau, J. H., Hudson, E., Tsarfaty, I., and Vande Woude, G. F. (1995). Met proto-oncogene product is overexpressed in tumors of p53-deficient mice and tumors of Li-Fraumeni patients. Cancer Res., 55: 1963-1970.

Rouet, P., Smih, F., and Jasin, M. (1994). Introduction of double-strand breaks into the genome of mouse cells by expression of a rare-cutting endonuclease. Mol Cell Biol., 14(12): 8096-8106.

Roy, R., Chun, J., and Powell, S. N. (2011). BRCA1 and BRCA2: different roles in a common pathway of genome protection. Nature Reviews Cancer, 12(1): 68-78.

Ruffner, H., Joazeiro, C. A. P., Hemmati, D., Hunter, T., and Verma, I. M. (2001). Cancer-predisposing mutations within the RING domain of BRCA1: Loss of ubiquitin protein ligase activity and protection from radiation hypersensitivity. PNAS, 98(9): 5134-5139.

Sabatier, R., Adelaide, J., Finetti, P., Ferrari, A., Huiart, L., Sobol, H., Chaffanet, M., Birnbaum, D., and Bertucci, F. (2010). BARD1 homozygous deletion, a possible alternative to BRCA1 mutation in basal breast cancer. Genes, Chrom., & Cancer., 49(12): 1143-1151.

Sartori, A. A., Lukas, C., Coates, J., Mistrik, M., Fu, S., Bartek, J., Baer, R., Lukas, J., and Jackson, S. P. (2007). Human CtIP promotes DNA end resection. Nature, 450: 509-514.

Schaeper, U., Subramanian, T., Lim, L., Boyd, J. M., and Chinnadurai, G. (1998). Interaction between a cellular protein that binds to the C-terminal region of the adenovirus E1A (CtBP) and a novel cellular protein is disrupted by E1A through a conserved PLDLS motif. J. Biol. Chem., 273(15): 8549-8552.

Schuermann, M. (1990). An expression vector system for stable expression of oncogenes. Nucleic Acids Res., 18: 4945-4946.

Scully, R., Chen, J., Plug, A., Xiao, Y., Weaver, D., Feunteun, J., Ashley, T., and Livingston, D. M. (1997a). Association of BRCA1 with Rad51 in mitotic and meiotic cells. Cell, 88: 265-275.

Scully, R., Chen, J., Ochs, R. L., Keegan, K., Hoekstra, M., Feunteun, J., and Livingston, D. M. (1997b). Dynamic changes of BRCA1 subnuclear location and phosphorylation state are initiated by DNA damage. Cell, 90: 425-435.

Scully, R. and Livingston, D. M. (2000). In search of the tumour-suppressor functions of BRCA1 and BRCA2. Nature, 408: 429-432.

Shakya, R., Szabolcs, M., McCarthy, E., Ospina, E., Basso, K., Nandula, S., Murty, V., Baer, R., and Ludwig, T. (2008). The basal-like mammary carcinomas induced by Brca1 or Bard1 inactivation implicate the BRCA1/BARD1 heterodimer in tumor suppression. PNAS, 105(19): 7040-7045.

Shakya, R., Reid, L. J., Reczek, C. R., Cole, F., Egli, D., Lin, C.-S., deRooij, D. G., Hirsch, S., Ravi, K., Hicks, J. B., Szabolcs, M., Jasin, M., Baer, R., and Ludwig, T. (2011). BRCA1 tumor suppression depends on BRCT phosphoprotein binding, but not its E3 ligase activity. Science, 334: 525-528.

Shen, S.-X., Weaver, Z., Xu, X., Li, C., Weinstein, M., Chen, L., Guan, X.-Y., Ried, T., and Deng, C.-X. (1998). A targeted disruption of the murine Brca1 gene causes γ-irradiation hypersensitivity and genetic instability. Oncogene, 17: 3115-3124.

Shiloh, Y. (2001). ATM and ATR: networking cellular responses to DNA damage. Curr. Op. Genet. Devel., 11: 71-77.

Shiloh, Y. and Kastan, M. B. (2001). ATM: genome stability, neuronal development and cancer cross paths. Advances in Cancer Research, 83: 209-254.

Shiozaki, E. N., Gu, L., Yan, N., and Shi, Y. (2004). Structure of the BRCT repeats of BRCA1 bound to a BACH1 phosphopeptide: implications for signaling. Mol Cell, 14: 405-412.

Simon, R. and Zhang, X. (2008). On the dynamics of breast tumor development in women carrying germline BRCA1 and BRCA2 mutations. Int. J. Cancer, 122: 1916-1917.

Snouwaert, J. N., Gowen, L. C., Latour, A. M., Mohn, A. R., Xiao, A., DiBiase, L., and Koller, B. H. (1999). BRCA1 deficient embryonic stem cells display a decreased homologous recombination frequency and an increased frequency of non-homologous recombination that is corrected by expression of a brca1 transgene. Oncogene, 18(55): 7900-7907.

Sobhian, B., Shao, G., Lilli, D. R., Culhane, A. C., Moreau, L. A., Xia, B., Livingston, D. M., and Greenberg, R. A. (2007). RAP80 targets BRCA1 to specific ubiquitin structures at DNA damage sites. Science, 316: 1198-1202.

Stark, J. M., Pierce, A. J., Oh, J., Pastink, A., and Jasin, M. (2004). Genetic steps of mammalian homologous repair with distinct mutagenic consequences. Mol. Cell. Biol., 24(21): 9305-9316.

Stokes, P. H., Thompson, L. S., Marianayagam, N. J., and Matthews, J. M. (2007). Dimerization of CtIP may stabilize in vivo interactions with the Retinoblastoma-pocket domain. Biochem. Biophys. Res. Commun. 354: 197-202.

Symington, L. S. and Gautier, J. (2011). Double-strand break end resection and repair pathway choice. Annual Review of Genetics, 45: 247-271.

te Riele, H., Maandag, E. R., and Berns, A. (1992). Highly efficient gene targeting in embryonic stem cells through homologous recombination with isogenic DNA constructs. PNAS, 89: 5128-5132.

Tibbetts, R. S., Cortez, D., Brumbaugh, K. M., Scully, R., Livingston, D., Elledge, S. J., and Abraham, R. T. (2000). Functional interactions between BRCA1 and the checkpoint kinase ATR during genotoxic stress. Genes & Dev., 14: 2989-3002.

Tomlinson, G. E., Chen, T. T.-L., Stastny, V. A., et al. (1998). Characterization of a breast cancer cell line derived from a germ-line BRCA1 mutation carrier. Cancer Res, 58: 3237-3242.

Tsubouchi, H. and Ogawa, H. (1998). A novel mre11 mutation impairs processing of double-strand breaks of DNA during both mitosis and meiosis. Mol. Cell Biol., 18: 260-268.

Tuveson, D. A., Shaw, A. T., Willis, N. A., Silver, D. P., Jackson, E. L., Chang, S., Mercer, K. L., Grochow, R., Hock, H., Crowley, D., et al. (2004). Endogenous oncogenic K-ras (G12D) stimulates proliferation and widespread neoplastic and developmental defects. Cancer Cell, 5: 375-387.

Uziel, T., Lerenthal, Y., Moyal, L., Andegeko, Y., Mittelman, L., and Shiloh, Y. (2003). Requirement of the MRN complex for ATM activation by DNA damage. EMBO J., 22(20): 5612-5621.

Varma, A. K., Brown, R. S., Birrane, G., and Ladias, J. A. (2005). Structural basis for cell cycle checkpoint control by the BRCA1-CtIP interaction. Biochemistry, 44: 10941-10946.

Vilkki, S., Launonen, V., Karhu, A., Sistonen, P., Vastrik, I., and Aaltonen, L. A. (2002). Screening for microsatellite instability target genes in colorectal cancers. J. Med. Genet., 39: 785-789.

Wang, B. and Elledge, S. J. (2007). Ubc13/Rnf8 ubiquitin ligases control foci formation of the Rap80/Abraxas/Brca1/Brcc36 complex in response to DNA damage. PNAS, 104(52): 20759-20763.

Wang, B., Matsuoka, S., Ballif, B. A., Zhang, D., Smogorzewska, A., Gygi, S. P., and Elledge, S. J. (2007). Abraxas and RAP80 form a BRCA1 protein complex required for the DNA damage response. Science, 316: 1194-1198.

Warren, A. J., Colledge, W. H., Carlton, M. L., Evans, M. J., Smith, A. J., and Rabbitts, T. H. (1994). The oncogenic cysteine-rich LIM domain of protein Rbtn2 is essential for erythroid development. Cell, 78: 45-57.

Wijnhoven, S. W., Zwart, E., Speksnijder, E. N., Beems, R. B., Olive, K. P., Tuveson, D. A., Jonkers, J., Schaap, M. M., van den Berg, J., Jacks, T., van Steeg, H., and de Vries, A. (2005). Mice expressing a mammary gland-specific R270H mutation in the p53 tumor suppressor gene mimic human breast cancer development. Cancer Res., 65(18): 8166-8173.

Williams, R. S., Green, R., and Glover, J. N. (2001). Crystal structure of the BRCT repeat region from the breast cancer-associated protein BRCA1. Nat. Struct. Biol., 8(10): 838-842.

Williams, R. S., Chasman, D. I., Hau, D. D., Hui, B., Lau, A. Y., and Glover, J. N. (2003). Detection of protein folding defects caused by BRCA1-BRCT truncation and missense mutations. J. Biol. Chem., 278 (52): 53007-53016.

Williams, R. S., Lee, M. S., Hau, D. D., and Glover, J. N. (2004). Structural basis of phosphopeptide recognition by the BRCT domain of BRCA1. Nat. Struct. Biol., 11(6): 519-525.

Williams, R. S., Williams, J. S., and Tainer, J. A. (2007). Mre11-Rad50-Nbs1 is a keystone complex connecting DNA repair machinery, double-strand break signaling, and the chromatin template. Biochem. Cell Biol., 85: 509-520.

Wong, A. K. C., Ormonde, P. A., Pero, R., Chen, Y., Lian, L., Salada, G., Berry, S., Lawrence, Q., Dayananth, P., Ha, P., Tavtigian, S. V., Teng, D. H., and Bartel, P. L. (1998). Characterization of a carboxy-terminal BRCA1 interacting protein. Oncogene, 17: 2279-2285.

Wooster, R. and Weber, B. L. (2003). Breast and Ovarian Cancer. N. Engl. J. Med., 348(23): 2339-2347.

Wu, L. C., Wang, Z. W., Tsan, J. T., Spillman, M. A., Phung, A., Xu, X. L., Yang, M.-C. W., Hwang, L.-Y., Bowcock, A. M., and Baer, R. (1996). Identification of a RING protein that can interact in vivo with the BRCA1 gene product. Nature Genet, 14: 430-440.

Wu, W., Koike, A., Takeshita, T., and Ohta, T. (2008). The ubiquitin E3 ligase activity of BRCA1 and its biological functions. Cell Division, 3, 1.

Wu-Baer, F. and Baer, R. (2001). Effect of DNA damage on a BRCA1 complex. Nature, 414: 36.

Wu-Baer, F., Lagrazon, K., Yuan, W., and Baer, R. (2003). The BRCA1/BARD1 heterodimer assembles polyubiquitin chains through an unconventional linkage involving lysine residue K6 of ubiquitin. J. Biol. Chem., 278(37): 34743-34746.

Xu, B., Kim, S.-T., and Kastan, M. B. (2001). Involvement of BRCA1 in S-phase and G2-phase checkpoints after ionizing irradiation. Mol Cell Biol, 21(10): 3445-3450.

Xu, B., Kim, S.-T., Lim, D.-S., and Kastan, M. B. (2002). Two molecularly distinct G_2/M checkpoints are induced by ionizing irradiation. Mol Cell Biol, 22(4): 1049-1059.

Xu, X., Weaver, Z., Linke, S. P., Li, C., Gotay, J., Wang, X.-W., Harris, C. C., Ried, T., and Deng, C.-X. (1999). Centrosome amplification and a defective G_2-M cell cycle checkpoint induce genetic instability in BRCA1 exon 11 isoform-deficient cells. Mol Cell, 3: 389-395.

Xu, X., Wagner, K.-U., Larson, D., Weaver, Z., Li, C., Ried, T., Hennighausen, L., Wynshaw-Boris, A., and Deng, C.-X. (1999a). Conditional mutation of Brca1 in mammary epithelial cells results in blunted ductal morphogenesis and tumour formation. Nature Genetics, 22: 37-43.

Yan, J., Kim, Y. S., Yang, X. P., Li, L. P., Liao, G., Xia, F., and Jetten, A. M. (2007). The ubiquitin-interacting motif containing protein RAP80 interacts with BRCA1 and functions in DNA damage repair response. Cancer Res., 67: 6647-6656.

Yang, H., Li, Q., Fan, J., Holloman, W. K., and Pavletich, N. P. (2005). The BRCA2 homologue Brh2 nucleates RAD51 filament formation at a dsDNA-ssDNA junction. Nature, 433: 653-657.

Yarden, R. I., Pardo-Reoyo, S., Sgagias, M., Cowan, K. H., and Brody, L. C. (2002). BRCA1 regulates the G2/M checkpoint by activating Chk1 kinase upon DNA damage. Nature Genetics, 30: 285-289.

Yata, K. and Esashi, F. (2009). Dual role of CDKs in DNA repair: To be, or not to be. DNA Repair, 8(1): 6-18.

You, Z., Shi, L. Z., Zhu, Q., Wu, P., Zhang, Y.-W., Basilio, A., Tonnu, N., Verma, I. M., Berns, M. W., and Hunter, T. (2009). CtIP links DNA double-strand break sensing to resection. Mol. Cell, 36: 954-969.

Yu, X., Wu, L. C., Bowcock, A. M., Aronheim, A., and Baer, R. (1998). The C-terminal (BRCT) domains of BRCA1 interact *in vivo* with CtIP, a protein implicated in the CtBP pathway of transcriptional repression. J. Biol. Chem. 273(39): 25388-25392.

Yu, X. and Baer, R. (2000). Nuclear localization and cell cycle-specific expression of CtIP, a protein that associates with the BRCA1 tumor suppressor. J. Biol. Chem., 275: 18541-18549.

Yu, X. and Chen, J. (2004). DNA damage-induced cell cycle checkpoint control requires CtIP, a phosphorylation-dependent binding partner of BRCA1 C-terminal domains. Mol Cell Biol, 24(21). 9478-9486.

Yu, X., Chini, C. C., He, M., Mer, G., and Chen, J. (2003). The BRCT domain is a phospho-protein binding domain. Science, 302: 639-642.

Yu, X., Fu, S., Lai, M., Baer, R., and Chen, J. (2006). BRCA1 ubiquitinates its phosphorylation-dependent binding partner CtIP. Genes & Dev., 20: 1721-1726.

Yun, M. and Hiom, K. (2009). CtIP-BRCA1 modulates the choice of DNA double-strand-break repair pathway throughout the cell cycle. Nature, 459: 460-463.

Zhang, Y. and Jasin, M. (2011). An essential role for CtIP in chromosomal translocation formation through an alternative end-joining pathway. Nat. Struct. Mol. Biol., 18(1): 80-84.

Zhao, G. Y., Sonoda, E., Barber, L. J., Oka, H., Murakawa, Y., Yamada, K., Ikura, T., Wang, X., Kobayashi, M., Yamamoto, K., Boulton, S. J., and Takeda, S. (2007). A critical role for the ubiquitin-conjugating enzyme Ubc13 in initiating homologous recombination. Mol. Cell, 25(5): 663-675.

Zhong, Q., Chen, C.-F., Li, S., Chen, Y., Wang, C.-C., Xiao, J., Chen, P.-L., Sharp, Z. D., and Lee, W.-H. (1999). Association of BRCA1 with the hRad50-hMre11-p95 complex and the DNA damage response. Science, 285: 747-750.

Zhong, Q., Chen, C.-F., Chen, P.-L., and Lee, W.-H. (2002). BRCA1 facilitates microhomology-mediated end joining of DNA double strand breaks. J. Biol. Chem., 277(32): 28641-28647.

Zhou, B. B. and Elledge, S. J. (2000). The DNA damage response: putting checkpoints in perspective. Nature, 408: 433-439.

Zhu, Z., Chung, W. H., Shim, E. Y., Lee, S. E, and Ira, G. (2008). Sgs1 helicase and two nucleases Dna2 and Exo1 resect DNA double-strand break ends. Cell, 134(6): 981-994.

Zou, L. and Elledge, S. J. (2003). Sensing DNA damage through ATRIP recognition of RPA-ssDNA complexes. Science, 300: 1542-1548.